Energy and Water system integration in the urban environment

van der Roest, E.

DOI
10.4233/uuid:20b43ccc-67f2-443b-a4da-790ff9bcb5df

Publication date
2023

Document Version
Final published version

Citation (APA)
van der Roest, E. (2023). *Energy and Water system integration in the urban environment*. [Dissertation (TU Delft), Delft University of Technology]. https://doi.org/10.4233/uuid:20b43ccc-67f2-443b-a4da-790ff9bcb5df

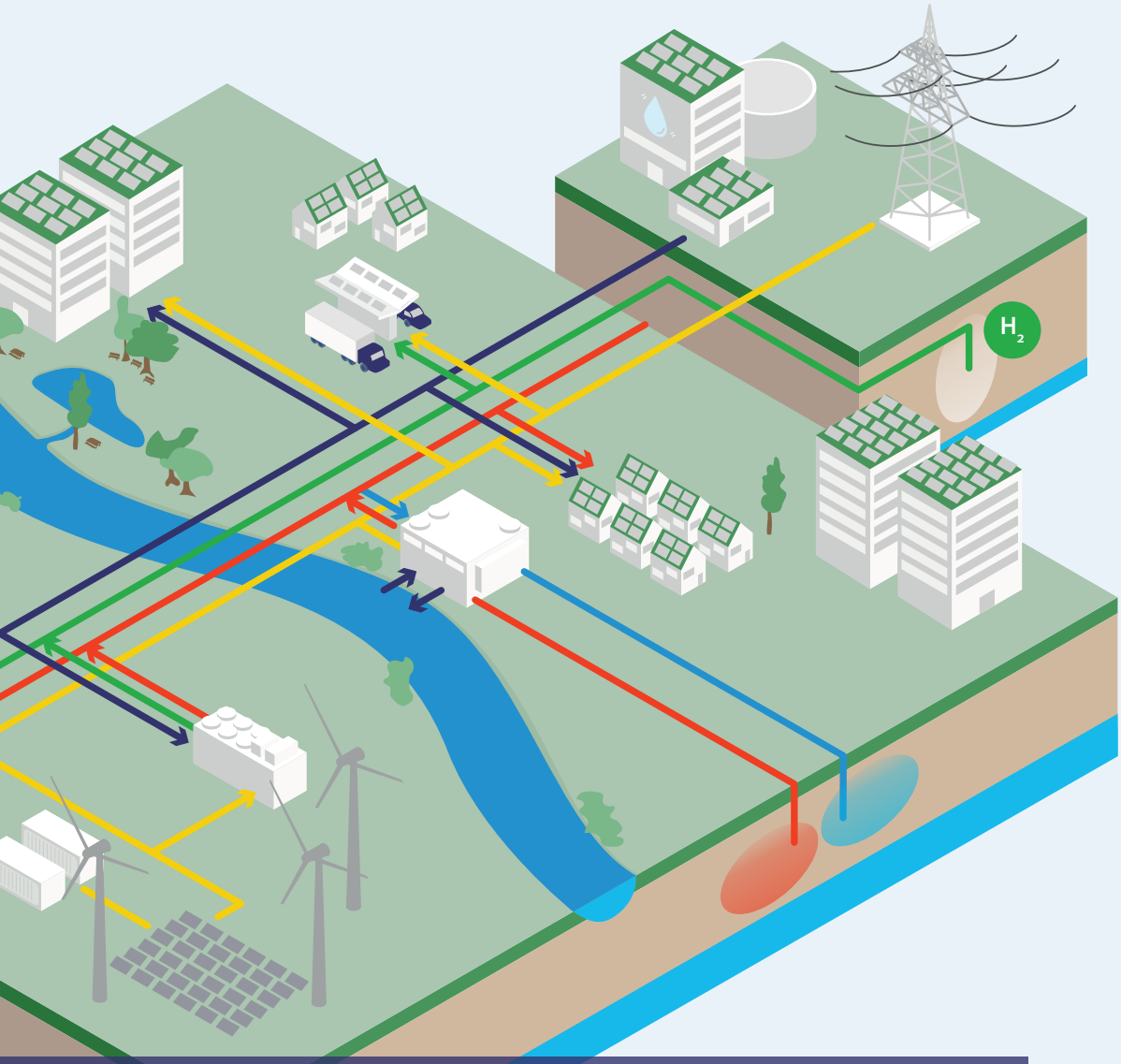

Els van der Roest

Energy and Water system integration in the urban environment

Energy and Water system integration in the urban environment

Energy and Water system integration in the urban environment

Systeemintegratie van energie en water in de gebouwde omgeving
(met een samenvatting in het Nederlands)

Proefschrift

ter verkrijging van de graad van doctor
aan de Technische Universiteit Delft,
op gezag van de Rector Magnificus, Prof.dr.ir. T.H.J.J. van der Hagen,
voorzitter van het College voor Promoties,
in het openbaar te verdedigen op woensdag 15 november 2023 om 10:00

door

Els van der Roest

Master of Science in Energy Science, Universiteit Utrecht, Nederland
geboren te Amsterdam, Nederland

Dit proefschrift is goedgekeurd door de promotoren.

Samenstelling promotiecommissie bestaat uit:

Rector Magnificus,	voorzitter
Prof. dr. A. J. M. van Wijk	Technische Universiteit Delft, promotor
Prof. dr. ir. J. P. van der Hoek	Technische Universiteit Delft, promotor

Onafhankelijke leden:

Prof. dr. B. van der Zwaan	Universiteit van Amsterdam
Dr. ir. E. Abraham	Technische Universiteit Delft
Prof. dr. ir. Z. Lukszo	Technische Universiteit Delft
Prof. dr. ir. L. C. Rietveld	Technische Universiteit Delft

Overig lid:

Dr. T. W. Fens	Technische Universiteit Delft, (voormalig) copromotor

Keywords: system integration, power-to-hydrogen, power-to-heat, high temperature aquifer thermal energy storage (HT-ATES), multi-energy system, waste heat, blue-green roofs
Printed by: Proefschriftspecialist, Zaandam
Cover & design: Ruben Daas

ISBN 978-94-6366-752-4
An electronic version of this dissertation is available at: *http://repository.tudelft.nl/*

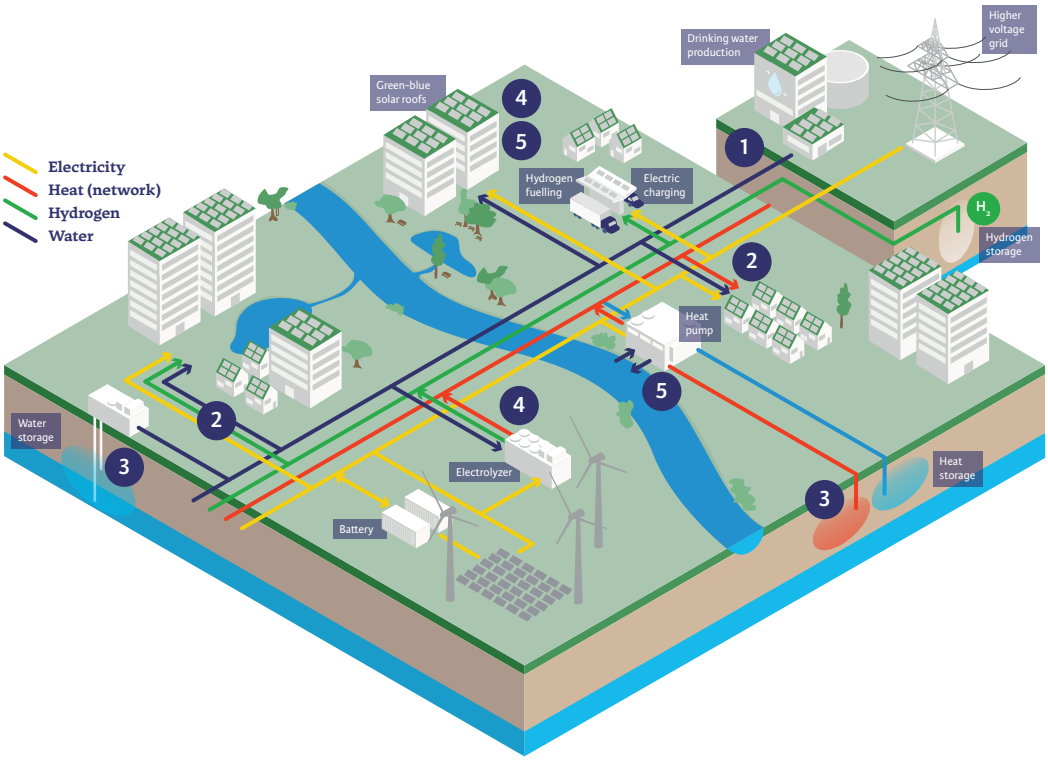

1. Keep the connection with the centralized system, but stay as a neighborhood as much as possible within the boundaries of the current infrastructure connections

2. In existing neighborhoods, explicitly include hybrid options (combinations of energy carriers) in the energy system

3. Include the subsurface as an essential part of the neighborhood design

4. Look for multiple values from both an energy- as well as a water perspective

5. Begin as early as possible with co-designing of both the energy as well as the water system in the neighborhood

Summary

Our energy system is transforming from fossil to renewable sources as a critical component of the global efforts to mitigate climate change. This transition towards a clean energy system is posing several new challenges to keeping energy reliable and affordable. Firstly the costs of renewable energy production are decreasing, yet the availability of materials may emerge as a limiting factor. Secondly, the future energy system will be largely based on intermittent energy sources (i.e. solar and wind) that are not necessarily tailored to and/or close to demand. Thus, connecting supply and demand both at a temporal and spatial scale becomes a challenge. Thirdly, most renewable energy sources generate electricity, which is more challenging to store and transport than fossil energy carriers, thus we need alternative sustainable energy carriers. Lastly, more decentral production is added to a formerly centrally organized energy system, posing a challenge to the current design and capacity of the energy infrastructure.

Addressing these emerging challenges necessitates an integrated system approach in the design of our future 100% renewable energy system. In such an integrated energy system, different sectors including the power, buildings, transport, and industry sector are coupled and multiple energy carriers (electricity, heat/water, gas or liquid and solid fuels) are exchanged between these sectors, creating a multi-energy system (MES). The utilization of different energy carriers facilitates energy storage and enables the alignment of supply and demand in space and time. The water sector also plays an important role in integrated system designs for two reasons. Firstly, the water and energy sectors are interconnected in many ways, as water is needed for the production, storage and transport of energy and vice versa. Secondly, the water sector faces similar goals and challenges as the energy sector, particularly in the context of climate change. An example is the higher probability of flood and drought events, impacting the reliability, security of supply and possibly safety of the water system.

This research focuses on the integration of the water and energy systems within the built environment, and more specifically the neighborhood is chosen as a relevant unit of analysis. It explores how an integrated approach can contribute to the design of a neighborhood that provides clean (no CO_2 emissions), affordable (costs of energy and water should not exceed regular market prices) and reliable (energy and water have to be available at all times) provision of the system services energy, water and transport. The main research question of this dissertation is:

How can an integrated renewable energy and water system at the neighborhood level be designed to provide energy and water in a clean, affordable, and reliable way?

The results obtained are applicable mainly to EU countries with temperate to cold climates and warm summers, especially for neighborhoods located in villages and small to medium-sized cities. The research involves a combination of conceptual development, modeling and experimental

studies. In **Chapter 2**, a concept for an integrated renewable energy and water system for a neighborhood is presented that should fulfill the neighborhood system services energy, transport and water. Referred to as Power-to-H3 (Hydrogen, Heat, H_2O), the concept comprises the conversion and storage of local energy sources (solar and/or wind) to hydrogen and heat and involves local storage and use of rainwater. Hydrogen is produced through electrolysis and used in the transport sector for fuel cell electric vehicles (FCEV). Heat is produced with a large-scale industrial heat pump which extracts thermal energy from surface water, and is subsequently stored in an aquifer thermal energy storage (ATES) at high temperatures (40-60°C). The stored heat supplies residential buildings and houses during winter via a low-temperature district heating network (DHN) operating at temperatures between 35 and 55°C. Additionally, rainwater is collected from a solar park and/or roofs and utilized for hydrogen production and household uses such as washing machines, dishwashers, and toilet flushing.

To assess the energy balance (reliability) and costs (affordability) of the proposed concept, an hourly techno-economic simulation model is developed. This model is applied to a case in Nieuwegein (The Netherlands) with an 8.7 MWp solar park, a 2 MW_{el} electrolyzer, a 2.5 MW_{el} heat pump, and 900 houses. The simulation results demonstrate that the system effectively meets the heat demand of the houses throughout the year, as well as the specified water demands, and provides hydrogen for 540 FCEVs. The costs for production, storage and fueling of hydrogen are 8.7 €/kg and for production, storage, transport, distribution and delivery of heat they are 26 €/GJ. Notably, both are lower than the user selling price of 10 €/kg for hydrogen and 34 €/GJ for heat in the Netherlands (based on 2018 price levels, excluding VAT). A further finding is that incorporating avoided costs associated with grid reinforcement and CO_2 emissions could lead to a decrease in the price of 20% for hydrogen and 26% for heat. Consequently, the system is thus both reliable and affordable as well as clean (based on only renewable sources).

In **Chapter 3**, the model is expanded with electricity demand and supply within the neighborhood, enhanced heat storage modeling and the inclusion of battery electric vehicles (BEV), collective battery systems, fuel cells and heat recovery from both electrolyzers and fuel cells. Moreover, the neighborhood size and demands are adjusted to resemble an average European neighborhood with 2000 households, divided evenly over terraced houses and apartments. Four 100% renewable neighborhood designs are compared with varying modes of system integration, including all-electric, power-to-heat and power-to-hydrogen, starting from an existing neighborhood (with energy label D). The study shows that the system costs are lowest in a system that combines power-to-heat, seasonal heat storage and power-to-hydrogen (Power-to-X), amounting to 2070 €/household/year. This scenario also shows a most evenly distributed energy demand pattern over the course of the year. A slightly more expensive alternative is the scenario that combines hydrogen boilers and heat pumps (H_2-hybrid) with 2175 €/household/year. Scenarios with electricity as the main energy carrier exhibit the highest system costs (All-electric/All-electric H_2 with 2320-2370 €/household/year). These higher costs are mainly attributed to higher retrofitting costs for buildings for insulation to energy label A standards and the costs for a (relatively large) heat pump. On the other hand, the costs for grid reinforcement in the all-electric scenarios are found to be a minor factor in the yearly household costs (50 €/household/year). Another significant finding

is that the local renewable energy supply in this neighborhood can fulfill up to 30-40% of the total energy demand (heat, electricity and transport). Thus, for existing neighborhoods, maintaining a connection with the larger energy system will still be important to fulfill energy demand in the future. In summary, this chapter shows that diversification in energy carriers at the household level can facilitate a fast transition to a clean energy system for existing neighborhoods while ensuring the reliability and affordability of the energy system.

Where **Chapter 2 and 3** give an overall perspective on a water- and energy system for a neighborhood, **Chapters 4-6** focus on specific aspects of the concept. In **Chapter 4** seasonal heat storage is examined, as it is an important aspect of the Power-to-H3 concept which has received limited attention in other MES studies. In this chapter, a high-temperature ATES system is considered (HT-ATES) with 50-65°C infiltration temperature. The size of the neighborhood and its heat demand are aligned with the parameters established in **Chapter 3** and heat is delivered by a low-temperature district heating network (DHN) with a minimum temperature of 40°C. This chapter outlines the expansion and integration of the multi-energy system model from **Chapter 2** with a numerical hydro-thermal model. By combining these two models, insights are obtained on how a HT-ATES system can be coupled to the heat pump of the neighborhood energy system. Several heat pump sizes (1/1.5/2 MW_{el}), storage temperatures (50/65°C) and threshold temperatures of the HT-ATES (30/43°C) are compared in terms of their energetic and financial performance. To lower the threshold temperature of the HT-ATES system, an additional mode of operation is introduced, where the HT-ATES feeds the heat pump instead of the DHN. This mode of operation allows for prolonged heat delivery when the HT-ATES temperature drops below the temperature of the DHN (43°C). Furthermore, this extra mode of operation with a lower threshold temperature (30°C) is effective in delivering 6-12% extra heat compared to a normal threshold temperature (43°C) at limited additional costs. Consequently, it reduces the levelized costs of heat delivery, enhances the recovery efficiency of the HT-ATES and improves the overall MES efficiency. A lower condenser temperature (50°C vs 65°C) contributes as well to a 11-18% lower LCOE (levelized cost of energy, in this case heat) compared to a 65°C condenser temperature. Overall, the scenario with the most optimal balance between reliable (90% of the heat demand fulfilled in the first 10 years of operation) and affordable (13.8 €/GJ_{heat}) features a 1.5 MW_{el} heat pump, 50°C condenser temperature and 30°C threshold temperature. Moreover, the research shows that the integration of HT-ATES with power-to-heat allows for a heat pump that is up to 25% smaller compared to a system without HT-ATES, reducing both space requirements on the surface level as well as costs. Additionally, the integration of HT-ATES results in a more distributed electricity demand over the year. In conclusion, the results show that the integration of HT-ATES in MES contributes to the design of a reliable (matching annual heat demand and supply) and clean energy system for a neighborhood.

Chapter 5 delves into another system integration aspect touched upon in **Chapter 3**, namely the utilization of waste heat from electrolysis. By focusing on this aspect, this chapter contributes to the further integration of different energy carriers (electricity, hydrogen and heat) within a multi-energy system. Initially, a potential design for a polymer electrolyte membrane (PEM) electrolyzer with heat recovery is presented, followed by a calculation of the waste heat potential, the efficiency of the electrolyzer system, and a cost calculation. The method is applied to three use

cases: (1) direct use of the waste heat by a heat consumer; (2) installation of a heat pump at the heat consumer to raise the waste heat temperature; and (3) delivery of the waste heat to a low-temperature district heating network (40-60°C). The analysis reveals that waste heat can be recovered by installing a tie-in on the cooling system of the electrolyzer. With this tie-in, a redundant system is established that secures a continuation of processes at both the electrolyzer and heat consumer regardless of heat delivery and demand fluctuations. The waste heat generated by the PEM electrolyzer is expected to have a temperature of circa 57°C. For a 2.5 MW_{el} PEM electrolyzer, a heat exchanger of 400 kW_{th} would be sufficient to recover the majority of the heat. The recovery of heat from the electrolyzer leads to an increase in stack efficiency of 76% to 90-91%. Furthermore, 14-15% of the electricity input to the electrolyzer stack can be utilized as heat, equivalent to approximately 16% of the heat demand of the neighborhood with 2000 houses from **Chapters 3 and 4**. In terms of environmental impact, the waste heat from the electrolyzer contributes to CO_2 savings. If the waste heat replaces heat in the district heating network generated by a heat pump operating on grid electricity, the savings amount to 0.08 €/tonne of CO_2. Alternatively, if the waste heat replaces natural gas, the savings range from 0.18 to 0.28 €/tonne of CO_2. Economically, the recovery of waste heat from the electrolyzer demonstrates high feasibility when the waste heat can be utilized directly without the need for a heat pump (8.4-8.9 €/MWh_{heat}). This cost range is at the low end of the range when compared to other industrial waste heat sources (6-46 €/MWh_{heat}). When a heat pump is needed to increase the waste heat temperature to 100°C, the margin between costs for waste heat recovery and saved costs for natural gas is 2.9 k€/year, indicating a relatively small margin for a viable business case. However, if CO_2 costs (of 60 €/tonne) are taken into account, the margin increases to 34.4 k€/year, thereby enhancing the feasibility. From a sensitivity analysis, it is clear that the heat transport distance between the electrolyzer and heat consumer is a very important factor in the economic feasibility. The critical threshold will vary per use case, and in this study, the distance is max. 1 km for heat delivery to the district heating network and up to 3 km for direct heat delivery to a heat consumer. In conclusion, this chapter highlights how electrolyzer waste heat adds value to an integrated energy and water system and further integrates the energy carriers electricity, heat and hydrogen.

Besides the integration of different energy carriers, another important aspect of the Power-to-H3 concept is the combination of water and energy within one system. This is particularly important in dense urban environments facing challenges such as air pollution, climate-change-induced drought, flooding and heat stress while having targets for renewable energy production as well. To most effectively utilize the available space, multifunctional buildings and roofs are necessary. **Chapter 6** investigates a practical example of an integrated energy and water concept for a building through an experimental study. This chapter introduces a roof concept that combines a green roof with capillary irrigation, rainwater storage, shower water suppletion, a constructed wetroof for shower water purification and a solar PV system. Previous research has shown that the evaporation of plants can cool the air beneath solar panels, thereby increasing solar PV output. However, the availability of water is essential for this evaporation process. Conventional green roofs have no water storage, and thus water is only available in rainy periods, resulting in a halt of the evapotranspiration process during dry periods unless (drinking) water is supplied. By combining rainwater storage on the roof with shower water purified by a constructed wetroof on the roof itself, a more

continuous water supply is ensured for vegetation, potentially enhancing the cooling effect, especially in dry (and warm) periods. To test this hypothesis, the blue-green solar PV system setup is compared to a bitumen roof with a solar PV system, on two identical rental apartment blocks in Amsterdam. The temperature of the roof, air and solar panels were monitored with sensors, as well as the humidity and electricity output of the system during 5 warmer months (June-October 2022). The results show a maximum temperature difference on the roof surface of 12°C (in the shadow), and 2.39°C on average (during daytime). Additionally, a difference in PV panel temperature is measured as well, yet only when the roof surface temperature is at least 4.64°C. Moreover, the findings indicate that, under similar irradiation, a solar panel on a blue-green roof is expected to produce 4.4% more electricity than a solar panel on a bitumen roof when air temperatures exceed 10°C. Thus, this chapter not only shows that water and energy functions can be combined within one building, but that they do enhance each other as well.

In **Chapter 7**, concluding remarks are given as well as recommendations for policymakers and future research based on the findings from the different chapters. Overall, the research has shown that it is possible to design an integrated energy and water system for a neighborhood in a clean, affordable and reliable way. The Power-to-H3 concept, which involves the integration of different energy carriers (electricity, heat, hydrogen), seasonal heat storage, integration of waste heat sources as well as combined energy and water elements, will contribute to a clean, affordable and reliable neighborhood design.

Five design principles are proposed to address the 'how' aspect of the research question:

1. *Keep the connection with the centralized system, but stay as a neighborhood as much as possible within the boundaries of the current infrastructure connections.*
2. *In existing neighborhoods, explicitly include hybrid options (combinations of energy carriers) in the energy system.*
3. *Include the subsurface as an essential part of the neighborhood design.*
4. *Look for multiple values from both an energy- as well as a water perspective.*
5. *Begin as early as possible with co-designing of both the energy as well as the water system in the neighborhood.*

These design principles are intended for policymakers, researchers, (local) government officials and city planners and can be applied to the design or improvement of new as well as existing neighborhoods. Furthermore, the policy recommendations are offered based on the research findings and the parallel implementation process of the Power-to-H3 concept in Nieuwegein:

1. *Create more low-regulation zones for testing and demonstrating new technologies.*
2. *Acknowledge that a transition is not incremental, and sometimes a step back is necessary to leap forward later on.*
3. *The societal business case should be leading in decision-making, not the individual business cases of stakeholders.*

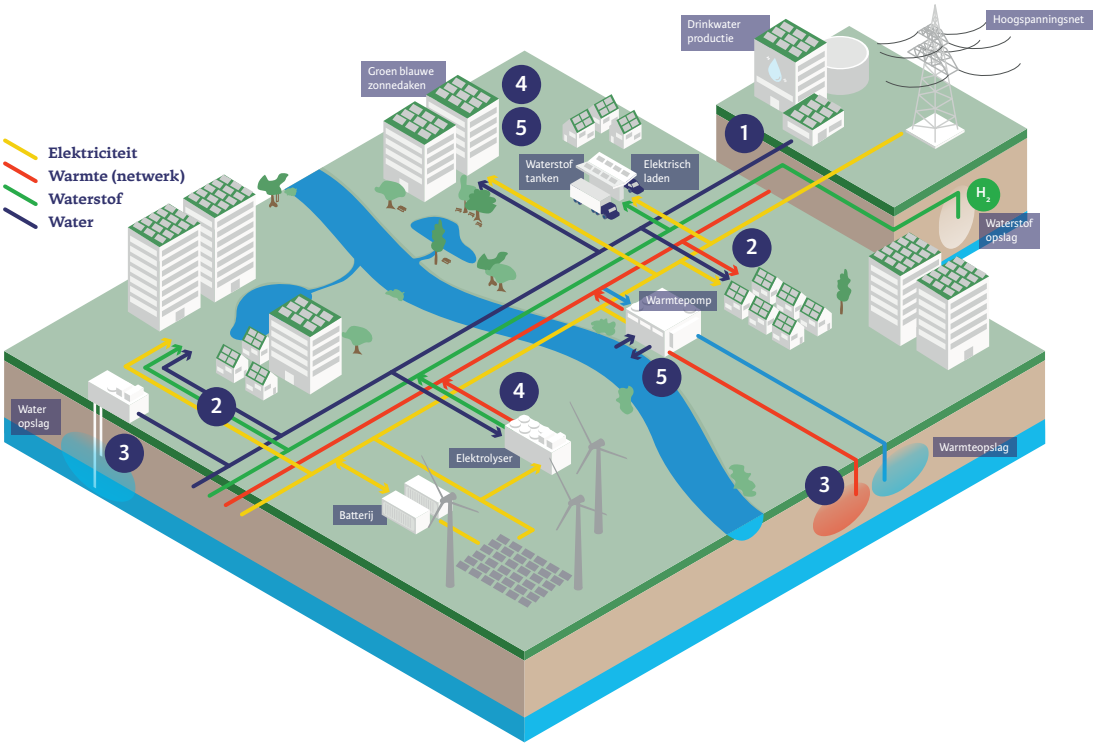

1. Behoud de verbinding met het centrale systeem, maar blijf als wijk zoveel mogelijk binnen de grenzen van de huidige infrastructuur

2. Neem in bestaande wijken expliciet hybride opties (combinaties van energiedragers) op in het energiesysteem

3. Neem de ondergrond mee als essentieel onderdeel van het wijkontwerp

4. Zoek naar meervoudige waarden vanuit zowel energie- als waterperspectief

5. Begin zo vroeg mogelijk met het gezamenlijk ontwerpen van zowel het energie- als het watersysteem in de wijk

Samenvatting

Ons energiesysteem transformeert van fossiele naar hernieuwbare bronnen als essentieel onderdeel van de mondiale inspanningen om klimaatverandering tegen te gaan. Deze overgang naar een schoon energiesysteem brengt verschillende nieuwe uitdagingen met zich mee om energie betrouwbaar en betaalbaar te houden. Ten eerste dalen de kosten voor de productie van hernieuwbare energie, maar de beschikbaarheid van materialen kan een beperkende factor worden. Ten tweede zal het toekomstige energiesysteem grotendeels gebaseerd zijn op intermitterende energiebronnen (d.w.z. zon en wind) die niet altijd afgestemd zijn op de vraag en/of dicht bij de vraag zijn gelegen. Het wordt dus een uitdaging om vraag en aanbod op zowel temporele als ruimtelijke schaal op elkaar af te stemmen. Ten derde genereren de meeste hernieuwbare energiebronnen elektriciteit, die moeilijker op te slaan en te vervoeren is dan fossiele energiedragers, dus zijn er alternatieve duurzame energiedragers nodig. Ten slotte wordt meer decentrale productie toegevoegd aan een voorheen centraal georganiseerd energiesysteem, wat een uitdaging vormt voor de huidige opzet en capaciteit van de energie-infrastructuur.

Om deze nieuwe uitdagingen aan te pakken is een geïntegreerde systeembenadering nodig bij het ontwerp van ons toekomstige 100% hernieuwbare energiesysteem. In een dergelijk geïntegreerd energiesysteem worden verschillende sectoren, waaronder de elektriciteits-, gebouwde omgeving-, vervoers- en industriesector, gekoppeld en worden meerdere energiedragers (elektriciteit, warmte/water, gas of vloeibare en vaste brandstoffen) tussen deze sectoren uitgewisseld, waardoor een multi-energiesysteem (MES) ontstaat. Het gebruik van verschillende energiedragers maakt energieopslag makkelijker en maakt het mogelijk vraag en aanbod in ruimte en tijd op elkaar af te stemmen. De watersector speelt ook een belangrijke rol in een geïntegreerd systeemontwerp om twee redenen. Ten eerste zijn de water- en de energiesector op vele manieren met elkaar verbonden, aangezien water nodig is voor de productie, de opslag en het transport van energie en omgekeerd. Ten tweede staat de watersector voor soortgelijke doelstellingen en uitdagingen als de energiesector, met name in het kader van klimaatverandering. Een voorbeeld is de grotere kans op overstromingen en droogte, met gevolgen voor de betrouwbaarheid, de leveringszekerheid en mogelijk de veiligheid van het watersysteem.

Dit onderzoek richt zich daarom op de integratie van water- en energiesystemen binnen de gebouwde omgeving, en meer specifiek wordt de wijk gekozen als relevante systeemgrens. Er wordt onderzocht hoe een geïntegreerde aanpak kan bijdragen aan het ontwerp van een wijk die voorziet in een schone (geen CO_2-uitstoot), betaalbare (kosten van energie en water mogen niet hoger zijn dan reguliere marktprijzen) en betrouwbare (energie en water moeten te allen tijde beschikbaar zijn) voorziening van de systeemdiensten energie, transport en water.

De hoofdvraag van dit proefschrift luidt:

Hoe kan een geïntegreerd duurzaam energie- en watersysteem op wijkniveau worden ontworpen om op een schone, betaalbare en betrouwbare manier energie en water te leveren?

De verkregen resultaten zijn voornamelijk van toepassing op EU-landen met een gematigd tot koud klimaat en warme zomers, met name voor wijken in dorpen en kleine tot middelgrote steden. Het onderzoek bestaat uit een combinatie van conceptuele ontwikkeling, modellering en experimentele studies. In **Hoofdstuk 2** wordt een concept voor een geïntegreerd hernieuwbaar energie- en watersysteem voor een wijk gepresenteerd dat moet voorzien in de systeemdiensten energie, vervoer en water. Het concept, dat Power-to-H3 (Waterstof – H_2, Warmte - Heat, Water - H_2O) wordt genoemd, omvat de omzetting en opslag van lokale energiebronnen (zon en/of wind) in waterstof en warmte, evenals lokale opslag en gebruik van regenwater. Waterstof wordt geproduceerd via elektrolyse en gebruikt in de transportsector voor brandstofcel-elektrische voertuigen (FCEV). Warmte wordt geproduceerd met een grootschalige industriële warmtepomp die thermische energie onttrekt aan oppervlaktewater die vervolgens bij hoge temperatuur (40-60°C) wordt opgeslagen in een bodemenergiesysteem. De opgeslagen warmte wordt in de winter aan woongebouwen en huizen geleverd via een warmtenet op lage temperatuur dat werkt bij temperaturen tussen 35 en 55°C. Daarnaast wordt regenwater opgevangen van een zonnepark en/of daken en gebruikt voor de productie van waterstof en huishoudelijk gebruik zoals wasmachines, vaatwasmachines en toiletspoeling.

Om de energiebalans (betrouwbaarheid) en de kosten (betaalbaarheid) van het voorgestelde concept te beoordelen, is een uurlijks technisch-economisch simulatiemodel ontwikkeld. Dit model is toegepast op een casus in Nieuwegein (Nederland) met een 8,7 MWp zonnepark, een 2 MW_{el} elektrolyser, een 2,5 MW_{el} warmtepomp en 900 woningen. De simulatieresultaten tonen aan dat het systeem het hele jaar voldoet aan de warmtebehoefte van de huizen, evenals aan de gespecificeerde waterbehoefte, en waterstof levert voor 540 FCEV's. De kosten voor productie, opslag en tanken van waterstof bedragen 8,7 €/kg en voor productie, opslag, transport, distributie en levering van warmte 26 €/GJ. Beide zijn lager dan de verkoopprijs voor de gebruiker van 10 €/kg voor waterstof en 34 €/GJ voor warmte in Nederland (op basis van de prijsniveaus van 2018, zonder BTW). Een andere bevinding is dat het meenemen van vermeden kosten zoals netverzwaring en CO_2-emissies kan leiden tot een prijsdaling van 20% voor waterstof en 26% voor warmte. Het systeem is dus zowel betrouwbaar en betaalbaar als schoon (uitsluitend gebaseerd op hernieuwbare bronnen).

In **Hoofdstuk 3** wordt het model uitgebreid met elektriciteitsvraag en -aanbod binnen de wijk, verbeterde modellering van warmteopslag en de opname van batterij-elektrische voertuigen (BEV), collectieve batterijen, brandstofcellen en restwarmtegebruik uit zowel elektrolyzers als brandstofcellen. Bovendien zijn de omvang en de vraag van de wijk aangepast aan een gemiddelde Europese wijk met 2000 huishoudens, gelijk verdeeld over rijtjeshuizen en appartementen. Vier 100% hernieuwbare ontwerpen voor wijken worden met elkaar vergeleken met ieder verschillende

niveaus van systeemintegratie, waaronder all-electric, power-to-heat en power-to-hydrogen, uitgaande van een bestaande wijk (met energielabel D). Uit de studie blijkt dat de systeemkosten het laagst zijn in een systeem dat power-to-heat, seizoenswarmteopslag en power-to-hydrogen (Power-to-X) combineert, namelijk 2070 €/huishouden/jaar. In dit scenario is de energievraag ook het meest gelijkmatig verdeeld over het jaar. Een iets duurder alternatief is het scenario dat waterstofketels en warmtepompen combineert (H_2-hybride) met 2175 €/huishouden/jaar. Scenario's met elektriciteit als belangrijkste energiedrager blijken de hoogste systeemkosten te hebben (All-electric/All-electric H_2 met 2320-2370 €/huishouden/jaar). Deze hogere kosten zijn voornamelijk te verklaren door de hogere renovatiekosten voor gebouwen voor isolatie tot energielabel A-normen en de kosten voor een (relatief grote) warmtepomp. Anderzijds blijkt dat de kosten voor netverzwaring in de all-electric scenario's een kleine factor zijn (50 €/huishouden/jaar) in de jaarlijkse kosten voor huishoudens. Een andere belangrijke bevinding is dat de lokale hernieuwbare energievoorziening in de wijk maximaal 30-40% van de totale energievraag (warmte, elektriciteit en transport) kan invullen. Voor bestaande buurten blijft het dus belangrijk om een verbinding met het grotere energiesysteem te houden om aan de energievraag te kunnen voldoen. Samengevat laat dit hoofdstuk zien dat diversificatie van energiedragers op huishoudniveau een snellere transitie naar een schoon energiesysteem voor bestaande buurten kan faciliteren, terwijl de betrouwbaarheid en betaalbaarheid van het energiesysteem gewaarborgd blijft.

Waar **Hoofdstuk 2 en 3** een breed perspectief geven op een water- en energiesysteem voor een wijk, richten **Hoofdstuk 4 t/m 6** zich op specifieke aspecten van het concept. **Hoofdstuk 4** gaat in op seizoensgebonden warmteopslag, aangezien dit een belangrijk onderdeel is van het Power-to-H3 concept dat in andere energiesysteemstudies beperkte aandacht heeft gekregen. In dit hoofdstuk wordt een hoge temperatuur bodemenergiesysteem beschouwd (HT-ATES) met een infiltratietemperatuur van 50-65°C. De grootte van de wijk en de warmtevraag zijn afgestemd op de in **hoofdstuk 3** vastgestelde parameters en de warmte wordt geleverd door een lage temperatuur warmtenetwerk met een minimumtemperatuur van 40°C. Dit hoofdstuk beschrijft de uitbreiding en integratie van het multi-energiesysteemmodel uit **hoofdstuk 2** met een numeriek hydrothermisch model. Door deze twee modellen te combineren worden inzichten verkregen over hoe een HT-ATES systeem kan worden gekoppeld aan de warmtepomp van het multi-energiesysteem. Verschillende groottes van de warmtepomp (1/1,5/2 MW_{el}), opslagtemperaturen (50/65°C) en drempelwaarden van de HT-ATES (30/43°C) worden vergeleken in termen van hun energetische en financiële prestaties. Om de drempeltemperatuur van het HT-ATES-systeem te verlagen, wordt een extra bedrijfssituatie toegevoegd, waarbij de HT-ATES de warmtepomp voedt in plaats van het warmtenet. Deze bedrijfssituatie maakt een verlenging van de warmtelevering mogelijk wanneer de HT-ATES-temperatuur onder de leveringstemperatuur van het warmtenet (43°C) zakt. Verder is deze extra bedrijfssituatie met lagere drempelwaarde (30°C) effectief in het leveren van 6-12% extra warmte in vergelijking met een normale drempelwaarde (43°C) tegen beperkte extra kosten. Daarmee leidt dit tot een verlaging van de genivelleerde kosten van de warmtelevering (de levelized cost of energy of LCOE, hier specifiek voor warmte), een verhoging van de terugwinningsefficiëntie van de HT-ATES en een verbetering van de algehele systeemefficiëntie. Een lagere condensortemperatuur (50°C vs. 65°C) draagt ook bij aan een 11-18% lagere LCOE in vergelijking met een condensortemperatuur van 65°C. Het scenario met de meest optimale balans tussen betrouw-

baarheid (90% van de warmtevraag vervuld in de eerste 10 bedrijfsjaren) en betaalbaarheid (13,8 €/GJ_{warmte}) bestaat uit een warmtepomp van 1,5 MW_{el}, een condensortemperatuur van 50°C en een drempeltemperatuur van 30°C. Bovendien laat het onderzoek zien dat de integratie van HT-ATES met power-to-heat een tot 25% kleinere warmtepomp mogelijk maakt in vergelijking met een systeem zonder HT-ATES, waardoor zowel het bovengrondse ruimtebeslag als de kosten dalen. Daarnaast resulteert de integratie van HT-ATES in een meer gespreide elektriciteitsvraag over het jaar. Concluderend tonen de resultaten aan dat de integratie van HT-ATES in een multi-energiesysteem bijdraagt tot het ontwerp van een betrouwbaar (afstemming van jaarlijkse warmtevraag en -aanbod) en schoon energiesysteem voor een wijk.

Hoofdstuk 5 gaat in op een ander aspect van systeemintegratie dat in **Hoofdstuk 3** aan de orde kwam, namelijk het gebruik van restwarmte uit waterstofproductie met elektrolyse. Door de toespitsing op dit aspect draagt dit hoofdstuk bij aan de verdere integratie van verschillende energiedragers binnen een multi-energiesysteem (elektriciteit, waterstof en warmte). In eerste instantie wordt een potentieel ontwerp voor een polymeer elektrolyt membraan (PEM) elektrolyzer met warmteterugwinning gepresenteerd, gevolgd door een berekening van het potentieel aan restwarmte, het rendement van het elektrolyse systeem en een kostenberekening. De methode wordt toegepast op drie gebruikscases; (1) direct gebruik van de restwarmte door een warmteafnemer, (2) installatie van een warmtepomp bij de warmteafnemer om de temperatuur van de restwarmte te verhogen en (3) levering van de restwarmte aan een lage temperatuur warmtenet (40-60°C). Uit de analyse blijkt dat de restwarmte kan worden teruggewonnen door een afkoppeling te installeren in het koelsysteem van de elektrolyzer. Met deze koppeling wordt een redundant systeem opgezet dat de continuïteit van de processen bij zowel de elektrolyser als de warmteafnemer waarborgt, ongeacht de fluctuaties in de warmtelevering en -vraag. De door de PEM-elektrolyzer gegenereerde restwarmte heeft naar verwachting een temperatuur van circa 57°C. Voor een 2,5 MW_{el} PEM electrolyzer zou een warmtewisselaar van 400 kW_{th} voldoende zijn om het merendeel van de warmte terug te winnen. De terugwinning van warmte uit de elektrolyse leidt tot een verhoging van het stack-rendement van 76% tot 90-91%. Bovendien kan 14-15% van de elektriciteit die in de elektrolytische stack wordt gebracht, als warmte worden gebruikt, wat overeenkomt met ongeveer 16% van de warmtebehoefte van de wijk met 2000 huizen uit **Hoofdstuk 3 en 4**. Wat de milieu-impact betreft, draagt de restwarmte van de elektrolyse bij aan CO_2-besparing. Als de restwarmte de warmte in het warmtenet vervangt die wordt geproduceerd door een warmtepomp die op netstroom werkt, bedraagt de besparing 0,08 €/ton CO_2. Als de restwarmte aardgas vervangt, varieert de besparing van 0,18 tot 0,28 euro/ton CO_2. Economisch gezien is de terugwinning van restwarmte uit de elektrolyse financieel gunstig wanneer de restwarmte rechtstreeks kan worden gebruikt zonder dat een warmtepomp nodig is (8,4-8,9 €/MWh_{warmte}). Deze kosten liggen aan de lage kant in vergelijking met andere industriële bronnen van restwarmte (6-46 €/ MWh_{warmte}). Wanneer een warmtepomp nodig is om de temperatuur van de restwarmte te verhogen tot 100°C, bedraagt de marge tussen de kosten voor restwarmte-terugwinning en de bespaarde kosten voor aardgas 2,9 k€/jaar, wat wijst op een relatief kleine marge voor een levensvatbare business case. Als echter met een CO_2-prijs (van 60 €/ton) wordt gerekend, stijgt de marge tot 34,4 k€/jaar, waardoor de haalbaarheid toeneemt. Uit een gevoeligheidsanalyse blijkt dat de afstand tussen de elektrolyse en de warmteverbruiker een zeer belangrijke factor is voor de economische

haalbaarheid. De drempelwaarde verschilt per casus, en bedroeg in deze studie maximaal 1 km voor warmtelevering aan het warmtenet en maximaal 3 km voor directe warmtelevering aan een warmteafnemer. Samenvattend laat dit hoofdstuk zien hoe restwarmte van elektrolyzers waarde toevoegt aan een multi-energie- en watersysteem en de energiedragers elektriciteit, warmte en waterstof verder integreert.

Naast de integratie van verschillende energiedragers is een ander belangrijk aspect van het Power-to-H3-concept de combinatie van water en energie in één systeem. Dit is met name van belang in dichtbevolkte stedelijke omgevingen die te maken hebben met problemen als luchtverontreiniging, door klimaatverandering veroorzaakte droogte, overstromingen en hittestress, terwijl er ook doelstellingen zijn voor de productie van hernieuwbare energie. Om de beschikbare ruimte zo effectief mogelijk te benutten, zijn multifunctionele gebouwen en daken nodig. **Hoofdstuk 6** onderzoekt een praktisch voorbeeld van een geïntegreerd energie- en waterconcept voor een gebouw door middel van een experimentele studie. In dit hoofdstuk wordt een dakconcept geïntroduceerd dat een groen dak combineert met capillaire irrigatie, regenwateropslag, douchewatersuppletie, een helofytenfilter voor de zuivering van douchewater en zonnepanelen. Eerder onderzoek heeft aangetoond dat de verdamping van planten de lucht onder de zonnepanelen kan koelen, waardoor de opbrengst van zonnepanelen toeneemt. De beschikbaarheid van water is echter essentieel voor dit verdampingsproces. Conventionele groendaken hebben geen wateropslag, en dus is water alleen beschikbaar in regenachtige periodes, waardoor het evapotranspiratieproces in droge periodes stopt, tenzij (drink)water wordt aangevoerd. Door regenwateropslag op het dak te combineren met douchewater dat door een helofytenfilter op het dak zelf wordt gezuiverd, wordt een meer continue watertoevoer voor de beplanting gecreëerd, waardoor het verkoelende effect, vooral in droge (en warme) perioden, kan worden versterkt. Om deze hypothese te testen is het blauw-groene dak met zonnepanelen vergeleken met een bitumen dak met zonnepanelen, op twee naastgelegen identieke appartementencomplexen in Amsterdam. De temperatuur van het dak, de lucht en de zonnepanelen werden gemonitord met sensoren, evenals de vochtigheid en de elektriciteitsopbrengst van het systeem gedurende 5 warmere maanden (juni-oktober 2022). De resultaten tonen een maximaal temperatuurverschil op het dakoppervlak (in de schaduw) van 12°C, en gemiddeld 2,39°C (overdag). Daarnaast werd ook een verschil in PV-paneeltemperatuur gemeten, maar alleen wanneer de dakoppervlaktetemperatuur minstens 4,64°C bedraagt. Bovendien geven de bevindingen aan dat, bij gelijke instraling, een zonnepaneel op een blauwgroen dak naar verwachting 4,4% meer elektriciteit produceert dan een zonnepaneel op een bitumendak wanneer de luchttemperatuur hoger is dan 10°C. Dit hoofdstuk toont dus niet alleen aan dat water- en energiefuncties in één gebouw kunnen worden gecombineerd, maar dat ze elkaar ook kunnen versterken.

In **Hoofdstuk 7** worden conclusies geformuleerd en aanbevelingen gedaan voor beleidsmakers en vervolgonderzoek op basis van de bevindingen uit de verschillende hoofdstukken. In het kort heeft het onderzoek aangetoond dat het mogelijk is een geïntegreerd energie- en watersysteem voor een wijk te ontwerpen op een schone, betaalbare en betrouwbare manier. Het Power-to-H3-concept, dat de integratie van verschillende energiedragers (elektriciteit, warmte, waterstof), seizoenswarmteopslag, integratie van restwarmtebronnen en gecombineerde energie- en waterelementen omvat, draagt bij aan een schoon, betaalbaar en betrouwbaar systeemontwerp voor een wijk.

Er worden vijf ontwerpprincipes gepresenteerd die samen het “hoe”-aspect van de onderzoeksvraag beantwoorden:

1. *Behoud de verbinding met het centrale systeem, maar blijf als wijk zoveel mogelijk binnen de grenzen van de huidige infrastructuur.*
2. *Neem in bestaande wijken expliciet hybride opties (combinaties van energiedragers) op in het energiesysteem.*
3. *Neem de ondergrond mee als essentieel onderdeel van het wijkontwerp.*
4. *Zoek naar meervoudige waarden vanuit zowel energie- als waterperspectief.*
5. *Begin zo vroeg mogelijk met het gezamenlijk ontwerpen van zowel het energie- als het watersysteem in de wijk.*

Deze ontwerpprincipes zijn bedoeld voor beleidsmakers, onderzoekers, (lokale) overheidsambtenaren en stedenbouwkundigen en kunnen worden toegepast op het ontwerp of de verbetering van zowel nieuwe als bestaande wijken.

Daarnaast worden drie beleidsaanbevelingen gedaan op basis van de onderzoeksresultaten en het parallelle implementatieproces van het Power-to-H3 concept in Nieuwegein:

1. *Creëer meer regelluwe zones voor het testen en demonstreren van nieuwe technologieën.*
2. *Onderken dat een transitie geen incrementeel proces is, en dat soms een stap terug nodig is om later een grote stap vooruit te kunnen maken.*
3. *De maatschappelijke business case zou leidend moeten zijn bij het nemen van beslissingen, en niet de individuele business cases van stakeholders.*

Nomenclature

Abbreviations

AC	Alternating current
AEC	Alkaline electrolysis cell
APX	Amsterdam power exchange
ATES	Aquifer thermal energy storage
BEV	Battery electric vehicle
BGR	Blue green roof
BiR	Bitumen roof
BOP	Balance of Plant
CAPEX	Capital expenditure
CEDI	Continuous electro de-ionization
CHP	Combined heat and power
COP	Coefficient of Performance
DC	Direct current
DHN	District heating network
DOD	Depth of discharge
EU	European Union
FCEV	Fuel cell electric vehicle
GHG	Greenhouse gas
GW	Gigawatt
HHV	Higher heating value
HP	Heat Pump
HT-ATES	High-temperature aquifer thermal energy storage
kW	Kilowatt
LCOE	Levelized cost of energy
LHV	Lower heating value
MES	Multi-energy system
MILP	Mixed-integer linear programming model
MWh	Megawatthour
OM	Operation and maintenance
OPEX	Operating expenditures
PEM	Proton exchange/elektrolyte membrane
PPA	Power Purchase Agreement

PtH	Power-to-Heat
PV	Photovoltaic
RES	Renewable energy systems
RO	Reversed osmosis
SOEC	Solid oxide electrolysis cell
TJ	Terajoule

Symbols

α	Capital recovery factor	-
αp	Solar cell temperature coefficient of power	%/°C
η	(recovery) Efficiency	%
η_{MES}	MES efficiency	%
η_{mp}	Efficiency of a solar cell	%
$\eta_{mp,STC}$	Efficiency of a solar cell at standard test conditions	%
ρ	Density of water	kg/m³
ρ_0	Density of water at ambient groundwater temperature	kg/m³
$CAPEX_i$	Capital expenditures for a unit i	€/unit
c_{CO_2}	CO_2 price	€/tonne
$c_{electricity}$	Cost of electricity	€/kWh
c_{gas}	Cost of natural gas	€/kWh
C_{Margin}	Margin between potential savings and costs for heat	€/year
$C_{Margin\ with\ CO_2}$	Margin between potential savings and costs for heat with CO_2 pricing taken into account	€/year
$CO_{2\ savings}$	Saved costs by CO_2-pricing of CO_2 emission reduction	€/year
$CO_{2,reduction,heat}$	CO_2 emission reduction potential of replacing a fossil energy source with waste heat	kg
COP_{HP}	Coefficient of performance of a heat pump	-
$COP_{10y\ avg}$	Average COP of the heat pump over the run time (10 year average)	-
$C_{savings}$	Costs savings at the heat consumer	€/year
c_w	Specific volumetric heat capacity of water	kJ/K/m³
$E_{cost,i}$	Costs of energy (in this case electricity) for system component i	€/unit/year
E_{Elec}	Electricity consumption of the electrolyzer	kWh
$E_{electrolyzer\ stack,eff}$	Stack efficiency of the electrolyzer	%
$E_{heat,used}$	Heat from the electrolyzer used by a consumer	kWh_{th}
$El_{dem,10y\ avg}$	Average electricity demand of the total heat system over the run time (10 year average)	TJ/y
$En_{del,10y\ avg}$	Average amount of delivered heat to the neighbourhood (10 year average)	TJ/y

E_{pump}	Pumping energy	kWh
$E_{spaceheat,total}$	Total space heat demand over a run period	MJ
H	Sensible heat	J/m²
$H_{2,produced}$	Amount of hydrogen produced	kg
h_c	Convective heat transfer coefficient	W/m²/K
$\sum HDH$	Sum of heat degree hours over a run period	-
h_{DH_i}	Number of degree hours at hour t	-
I	Cell current	A
Irr	Irradiance	W/m²
kWp	kilowattpeak	
LC_i	Levelized yearly costs for a specific system component i	€/unit/year
$LCOE_{heat}$	Levelized cost of heat production	€/GJ
$LCtotal$	Total levelized yearly costs for the heat recovery installation	€/year
LE	Latent heat	J/m²
L_i	Lifetime of a system component i	years
$Load_{electrolyzer}$	Fraction of the full load of the electrolyzer	-
N_u	Number of units	-
$OPEX_i$	Operational expenditures and maintenance of system component i	€/year
P	Precipitation	mm
P_{HE}	Heat exchanger capacity	kW_{th}
QH	sensible heat flux	W/m²
$Q_{heat,delivered}$	Part of the heat demand delivered by MES (HT-ATES + heat pump)	GJ/year
$Q_{produced}$	Total amount of heat produced	Watt
$Q_{spaceheat,i}$	Heat demand at time t	MJ
r	Discount rate	%
RH	Relative humidity	%
Rn	Net radiation	J/m²
Rs	Incoming short wave radiation	J/m²
r_{VB}	Volume balance ratio	-
T	Water temperature	°C
T_a	Air temperature underneath the solar panel	°C
$T_{air,i}$	Outside air temperature at time t	°C
T_{amb}	Ambient air temperature	°C
$T_{ambient}$	Background temperature of the aquifer	°C
T_{base}	Base temperature for heating	°C
T_c	Cell temperature	°C
T_{hot}	Temperature of the hot well of the HT-ATES	°C

$T_{HP,cond}$	Outgoing temperature heat pump condenser	°C
$T_{HP,evap}$	Ingoing temperature heat pump evaporator	°C
T_{inj}	Injected storage temperature	°C
T_{P}	Back of panel temperature	°C
T_{S}	Roof surface temperature	°C
T_{warm}	Temperature of the warm well of the HT-ATES	°C
$U_{operating}$	Operating voltage of the electrolysis cell	Volt
$U_{thermoneutral}$	Thermoneutral voltage	Volt
v	Wind velocity	m/s
$V_{heatproduction}$	Yearly total extraction volume	m^3
$V_{heatstorage}$	Yearly total storage volume	m^3
v_{in}	Flow of water into the hot well	m^3/hr
v_{out}	Flow of water out of the warm well	m^3/hr
W	Watt	J/s

Subscripts

el	Electric power
EL	Electrolyzer
evap	Evaporator
hd	Heat demand
i	System component
j	Product type
th	Thermal power

Contents

Summary		VII
Samenvatting		XIII
Nomenclature		XIX
1	Introduction	27
2	Introducing Power-to-H3: combining renewable electricity with heat, water and hydrogen production and storage in a neighborhood	45
3	The impact of system integration on system costs of a neighborhood energy and water system	83
4	Towards sustainable heat supply with decentralized multi-energy systems by integration of subsurface seasonal heat storage	125
5	Utilization of waste heat from PEM electrolyzers – Unlocking local optimization	165
6	Increasing solar panel output with blue-green roofs in water-circular and nature inclusive urban development	197
7	Concluding remarks and recommendations	223
Bibliography		239
Acknowledgements/Dankwoord		265
About the author		268
List of publications		269

1 Introduction

"We cannot solve problems with the same thinking we used when we created them"

Albert Einstein

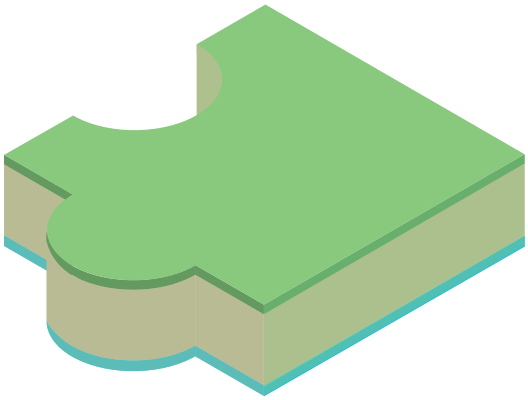

1.1 Motivation

To mitigate climate change, our energy system is transitioning from fossil fuels to clean energy sources without greenhouse gas emissions. This energy transition has multifaceted impacts at various levels, ranging from international arrangements such as the Paris Agreement [1] and European legislation [2] to national [3], [4] and local government plans [5], as well as changes on the level of individual households. Recent developments such as the war in Ukraine have only emphasized the need to reduce our energy consumption and switch to renewable energy sources, driven by geopolitical and cost considerations [6], [7]. In the EU, these developments have resulted in increased ambitions from 9% to 13% for energy consumption reduction in 2030 compared to the baseline projection from 2020, along with an increased 2030 target from 40% to 42.5%, aiming for 45% for renewable energy sources in the gross final energy consumption [8], [9].

The mainly fossil energy system fulfilled certain goals, it had to be 1) affordable, 2) reliable, 3) safe and 4) should have security of supply (in terms of i.e. geopolitics) [10]. To create a sustainable energy system, van Wijk et al. (2023) [10] argue that we need four additional goals, namely 5) clean (no greenhouse gas emissions and other emissions to the air, water, and soil), 6) fair (equitable distribution of benefits and burdens), 7) circular (regarding material use) and 8) security of materials. Thus, a sustainable energy system has eight goals to fulfill. Consequently, a sustainable energy system needs to have some radically different characteristics compared to a fossil-based energy system, which creates both opportunities and challenges, summarized in Table 1.1. Firstly, the transition entails a shift from a fuel cost-centered system to a material (cost) centered system. Therefore, energy efficiency is no longer a core value for an affordable energy system. In a fossil-based energy system with a continuous need for (increasingly scarce) fossil fuels that mainly determine the energy price, efficiency is important. Conversely, in a renewable energy system, the investment costs (and thus material costs) associated with technologies like wind turbines or geothermal wells become predominant, while the marginal costs for production are low as no 'fuel' is needed, leading to low energy prices [11], [12] (Figure 1.1). However, the material use in a renewable energy system increases compared to a fossil-based system [13] and instead of fuel scarcity, material scarcity becomes more important and thus the goals of security of materials and circularity. Additionally, renewable sources such as solar and wind in general require more space than fossil energy sources, which can become scarce as well.

Secondly, there is a shift from an energy system where supply is easily adaptable to demand, to an energy system predominantly reliant on intermittent energy sources where spatial and temporal mismatches need to be solved. In a fossil-based energy system, the availability of power plants is reliable and there is a high security of supply due to large amounts of (seasonal and strategic) reserves. For instance, Europe has a gas reserve equivalent to 25% of its annual consumption [14]. Moreover, a system has been created with flexible power plants (such as gas power plants) that can quickly ramp up and down depending on demand. In contrast, renewable energy systems rely more on sources like solar and wind, which are subject to weather conditions and intermittent production patterns. Furthermore, variations in production costs (as depicted in Figure 1.1) are influenced by geographical factors such as irradiance, wind speed, and land costs. Solar energy, for example, will

be the cheapest to produce in a desert area, with high irradiation and low land costs. Offshore wind energy on the other hand is cheap to produce on the ocean, with high wind speed. In both cases, these favorable production locations are far away from the locations with high energy use, mostly at places with a high population density (i.e. cities). Hence, it is essential to address the temporal and spatial mismatch between energy supply and energy demand in the most reliable and affordable manner, while maintaining security of supply by i.e. means of storage.

Thirdly, fossil energy sources such as oil, coal, and gas offer a wide range of applications, including fuel, electricity generation, and feedstock, whereas renewable sources exhibit less diversity at the point of production. While bioenergy can take various forms, geothermal energy primarily produces heat and, in some cases, electricity. Other main renewable sources (solar, wind), as illustrated in Figure 1.1, predominantly generate electricity. However, storing and transporting electricity is more challenging and costly compared to fossil fuels, which exist in the form of molecules [10]. Consequently, there is a need to convert renewable energy sources into alternative energy carriers, preferably in molecular form, to enable long-distance transportation, and for use as feedstock and for i.e. in industry and aviation [12], [15], [16]. Only through this transformation, a fully clean and affordable energy system can be established.

Lastly, there is a transition from a centrally organized energy supply to a hybrid system that combines large-scale central production with decentral production closer to consumers, such as local biogas production or photovoltaic (PV) systems on buildings [17], [18]. Potentially, this can lead to a more fair energy system if people can cheaply produce their own energy. In countries all over the world (Japan, Brazil, Australia, Germany, China, and India) consumer-owned PV systems are or can be more affordable than grid electricity [19], whereby the exact potential will depend on available space, thus will i.e. not be possible in large and densely populated cities like Dubai, Singapore or New York. Yet, this comparison between local electricity production and grid electricity is flawed because a local PV system is not as reliable as grid electricity and the system costs for reliable supply are not included in a local PV system. In many cases, a local PV system owner also has a connection with an electricity grid which should solve the temporal mismatches in demand and supply. Thus, higher shares of local electricity production can pose challenges to the capacity and structure of our current electricity grid, impacting its reliability and safety, particularly in countries like The Netherlands, Germany, the UK or Australia [19]–[21] and leading to an increase in grid system costs [22].

Considering the above, the way we look at our energy system has to change to fulfill all eight energy system goals; affordable, reliable, safe, security of supply, clean, fair, circular, and security of materials.

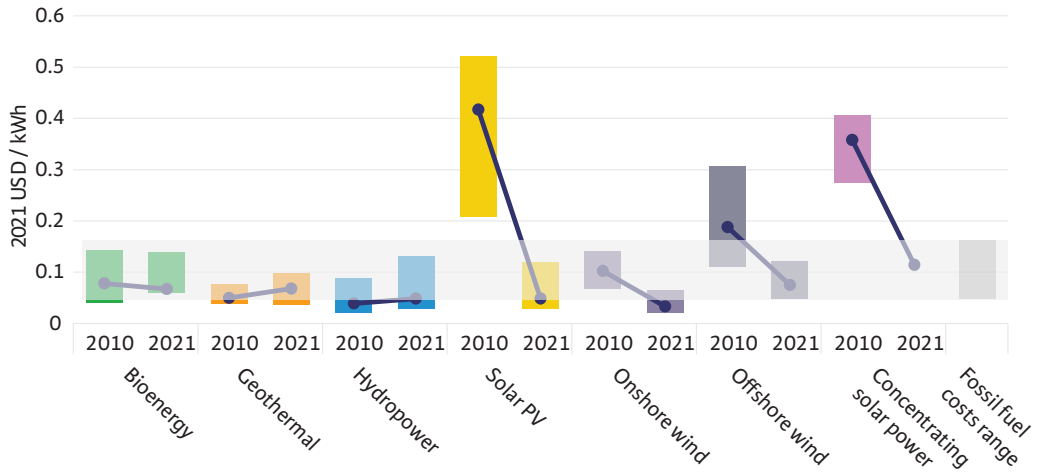

Figure 1.1 Global weighted average levelized costs of energy (LCOEs) – a way to show the average costs of energy generation over the lifetime of the production asset – shown as dots from newly commissioned, utility-scale renewable power generation technologies. The bars show the 5% percentile (lowest value) and 95% percentile (highest value), and the fossil fuel costs range in light grey. Adapted from IRENA [11].

Table 1.1 Main differences between a fossil and sustainable energy system, including the challenge relating to the transition to a sustainable energy system and the energy system goals to which these challenges are related.

Fossil energy system	Sustainable energy system	Transition challenges	Goals
Fuel-based (fossil fuels), focus on energy efficiency	Material-based (no fuel needed), focus on costs	Shortage of materials and space can become a limitation	Security of materials, circular, safe
Demand-oriented (supply can be quite easily adapted to demand), quickly responding power plants and large storage capacity	Intermittent supply, cheaper at good i.e. solar/wind locations, not tailored and/or close to demand	Connecting supply and demand in space and at all times, including day, week, and seasonal timescales	Reliable, security of supply, affordable
Multiple energy sources and carriers (gas, coal, oil, electricity)	Natural energy sources (sun, wind, geothermal, biomass) produce mainly electricity and heat at the point of production	Transport and storage of electricity (and heat) is more difficult than for fossil carriers, thus other carriers are needed	Clean, affordable
Centralized production, one-directional (source to consumer)	Decentralized as well as centralized production, multi-directional (multiple sources, consumers become prosumers)	The current design and capacity of the energy infrastructure are not yet suited to connect local renewable energy sources	Reliable, fair, safe, affordable

1.2 An integrated approach

To deal with these transition challenges (Table 1.1), an integrated system approach could help to design our future 100% renewable energy system whereby energy supply and demand are matched both on a spatial and temporal scale. The need for an integrated view is expressed by the EU in its strategy on energy system integration and is defined as "... the coordinated planning and operation of the energy system 'as a whole', across multiple energy carriers, infrastructures, and consumption sectors" [23]. Related to the concept of system integration is sector coupling, which entails the coupling of i.e. the power sector, built environment, industry and transport, with energy carriers (electricity, heat/water, gas or liquid and solid fuels) moving between these sectors. Sector coupling assists in solving the transition challenges introduced in the previous section (Table 1.1), by diversifying energy carriers and energy demand. This diversification makes it easier to connect supply and demand in space and time by conversion and storage, and potentially to better distribute energy carriers over different infrastructures. Water has a role to play as well in this integrated approach, as water and energy are to a large extent interrelated [24]–[26]. This water-energy nexus is further explained and explored in section 1.4.

The system integration approach is necessary at all energy system levels. Yet, this research will focus on the built environment, and more specifically neighborhoods. The built environment covers 30% of the global final energy consumption [27] and even 40% of Europe's final energy consumption [28]. This research covers not all EU countries, but countries with higher heating than cooling demand, in a temperate or cold climate with a warm summer (Cfb & Dfb climatic zones in the Köppen-Geiger classifications [29]) such as Germany, Belgium, the UK, The Netherlands, Luxembourg, Northern France, Austria, Poland and Denmark. Additionally, the focus is not on very high-density cities like capitals, but more on neighborhoods in villages and small to medium cities. The system integration approach including sector coupling could be very useful here, to balance the system as much as possible on the local scale, before moving on to a higher geographical level in the energy system. Moreover, the challenges defined for the renewable energy system as a whole (Table 1.1) do to a large extent apply to a neighborhood as well.

One specific example is the challenge of integrating a share of decentralized renewable capacity in centrally (source-to-consumer) organized grids. Especially in neighborhoods, decentralized production of mainly solar PV is increasing, and 28% of global installed solar PV capacity was residential in 2021 [30], and by 2030 it is expected that almost 100 million households will have PV panels [19]. These solar PV installations can cause supply peaks in summer, creating pressure on the (local) electricity grid or leading to power quality issues [30]–[32]. In contrast, in our research focus area (temperate or cold climate) there is a high demand for heat during winter in neighborhoods (Figure 1.2), and when all this heat would be produced with i.e. a heat pump, this means a significant rise in electricity demand at times when solar energy from roofs is not widely available. On the one hand, this could lead to high costs for the extension of the electricity grid, and on the other hand, grid extension does still not solve the mismatch between demand and supply. From a system integration approach, conversion of electricity to other energy carriers could be considered, complemented by diversification of energy demand, to reduce the pressure on the electricity grid.

A possible way to diversify energy carriers would be the production and storage of heat (power-to-heat) at times of oversupply of electricity, to be used for heating buildings or in industry [33]–[36]. In buildings, the focus is mostly on renewable electricity (i.e. solar panels), while heat demand in the form of space heating and hot water comprises 79% of the final energy demands of EU households [37]. The seasonal pattern of the gas demand of the North-West European countries indicates the need for longer-term storage as well (Figure 1.2). Another possible energy carrier is hydrogen, for example, produced via electrolysis (power-to-hydrogen), used for industry, transport, long-term energy storage, or buildings [38]–[41]. System integration will thus include sector-coupling, partly through conversion of electricity at times of oversupply, as well as storage for continuous supply [18], [42]–[45]. Combined with the decentralization of part of our energy production, this leads to local energy systems, also called integrated, decentralized, or multi-energy systems (MES). MES have been subject of study for about 20 years now [46]. In a MES the (local) use of renewable energy increases [47]–[50], less pressure is imposed on the electricity grid [36], [42], [51], supply and demand become better connected [42], [49], [52], and a MES could even lead to cost reductions [50]. Thereby, system integration on the neighborhood level is helping to solve the challenges of our future renewable energy system (Table 1.1).

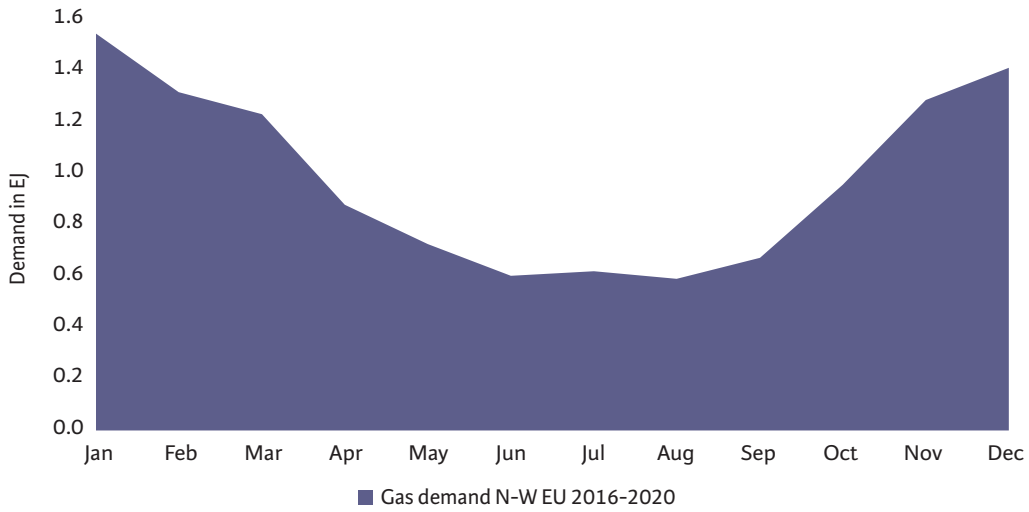

Figure 1.2 The North-West European gas demand per month, average values for the years 2016-2020 [53]. Countries included: Austria, Belgium, Denmark, Germany, France, Luxembourg, The Netherlands, Poland, UK. The difference between the lowest and highest demand is a factor 2.5 on average, yet can differ per country and within a month as well.

Additionally, the neighborhood is a relevant unit of analysis within the concept of system integration. A neighborhood in this research is focused on houses only and has a size varying between 900-2000 households. Within one household, it is hard to scale up solutions and connect different sectors. Studies on household multi-energy systems show they are in general not economically feasible, as opposed to the neighborhood level [54], [55]. Less storage capacity is needed on a neighborhood level as opposed to a household level because energy demand and supply can be

better balanced between households. For example, a community battery instead of home batteries reduces material needs and costs, making the system more affordable. Additionally, the amount of locally produced and consumed renewable energy is higher on a neighborhood level than on a house level because production and consumption patterns can be matched over multiple buildings, contributing to a cleaner system. Three important system services are defined that have to be supplied to the residents in the neighborhood a clean, reliable and affordable way: energy (both electricity and heat), transport and water, which will be discussed in the next two sections.

1.3 Insights on local energy system integration

A multi-energy system (MES) could be a possible solution to enhance a better balance between energy supply and demand in neighborhoods while being clean, reliable and affordable. How can such a neighborhood be designed to fulfill electricity, heat and transport demands? A complete off-grid system would be the most extreme example, but requires large amounts of storage of limited use and makes the system unnecessarily expensive, except for i.e. remote or island areas [55], [56]. Thus, a balance has to be found between affordability and reliability for a local system within the larger geographical (energy) system.

From the available body of literature on MES, a distinction can be made between studies that mostly focus on power-to-gas [47], [57]–[62], on power-to-heat [34], [63]–[66], or both power-to-gas and power-to-heat [51], [67]–[73]. The power-to-gas studies have hydrogen production with electrolysis as a starting point. They mostly use hydrogen directly and couple the transport and power sectors by focusing on fuel cell electric vehicles (FCEV) [57]–[62], or include power-to-fuel by combining hydrogen with CO_2 for methanation [47]. The work of Robinius shows the economic possibility of a dedicated hydrogen pipeline grid for Germany coupled with FCEV and seasonal hydrogen storage, as well the importance of a high spatial resolution in their calculations [57]. Additionally, the potential of coupling the power and transport sector to deal with surpluses of electricity over short time periods (days) is demonstrated in literature [58].

Several other studies focus on power-to-heat in neighborhoods, thus coupling the power and the building sector. In such a power-to-heat system, a combination of retrofitting measures and local energy sources and storage could lower the electricity demand peak with 73-79%, which contributes to more reliability and less material cost for electricity grids [63]. Another study shows that more interconnections between heat and electricity lead to better economic and environmental performance [66]. However, most of these studies include combined heat and power (CHP) systems that use natural gas [51], [63], [64], [66], [67], or gas boilers in houses [65], so they do not consider 100% renewable (clean) systems.

Another group of studies combine both power-to-heat and power-to-gas with a focus on the built environment, thus providing heat and electricity to neighborhoods [51], [67]–[70]. Bartolini shows that a neighborhood energy system with multiple conversion technologies (batteries, heat pumps,

thermal storage, and hydrogen) is cheaper than a system relying on batteries only [51]. Gabrielli et al. [67] applied the concept of multi-energy systems, including both power-to-heat and power-to-gas, with a focus on minimizing total annual costs and total annual emissions. They included seasonal storage for hydrogen and short-term sensible heat storage on a yearly time horizon with hourly resolution. In a later publication, it was shown that power-to-gas (in this case hydrogen) is important to achieve zero operational CO_2 emissions in a neighborhood and maximize renewable self-consumption [68], thus helps to realize a cleaner energy system. Petkov & Gabrielli mention that the seasonal shift (especially heat demand) is a relevant factor for MES design [70], and power-to-hydrogen as seasonal storage is a 'last-mile' technology to reach zero emissions.

Lastly, there is a group of studies that include power, buildings and transport [59]–[62], [71]–[73]. Studies by Oldenbroek et al. [59]–[62] show the potential of FCEV to balance the energy system via vehicle to grid with FCEV, in combination with seasonal hydrogen storage. These studies thus combine the supply of electricity, heat (via heat pumps) and transport in a neighborhood. They indicate that 50% of the car fleet at 10% of its maximum capacity is enough to act as a storage medium in a neighborhood, even at extreme peaks in demand [61], [62]. Murray et al. [69] have made an extensive model, including building data, building retrofit rates and included both hydrogen and thermal storage for heating and electricity demand. In a later publication, transport was added to the model as well [71]. Optimization with pareto fronts was done both on CO_2 emissions and costs, while always fulfilling the demands. Their results pointed out that both building retrofitting and renewable energy integration are necessary to meet the energy targets for buildings. This is one of the few publications on MES for neighborhoods that model heat storage, although it is modeled simplified with 1% heat loss per hour. The publication including the transport sector [71] showed that battery electric vehicles will be most important for transport in terms of costs and CO_2 emissions, which is also what Mittelviefhaus et al. [72] concluded. Lastly, Maroufmashat et al. [73] considered an energy network in Canada with four hubs, including a school, a food distribution center, a residential house complex and a hydrogen refueling station, concluding that local hydrogen production is more beneficial than hydrogen import.

Considering the literature on MES systems for neighborhoods, it is clear that combining multiple energy carriers (electricity, heat/water, gas/hydrogen) can have both costs and environmental benefits, also compared to fully electric systems. Hydrogen is mentioned in these studies both as energy storage medium as well as employed in the transport sector. In power-to-heat studies, it is remarkable that seasonal heat storage is never really included, while other studies indicate that it can be an economically favorable option for heat storage [74]–[76]. When heat storage is mentioned in energy system publications, it is modeled over a short period or with simplified loss factors. These studies then merely conclude that heat storage is only an option for short periods (up to a week). This conclusion is related to the specific heat storage solutions that are considered, which are mostly hot water storage tanks with high loss factors [34], [69], [70], [77], [78]. Yet, there are other options for heat storage as well, such as aquifer thermal energy storage (ATES), phase-change materials or thermo-chemical storage (i.e. metal oxides) [79]. Especially ATES and thermo-chemical energy storage are feasible to store heat for longer periods of time (i.e. months). ATES is a proven technology, with lower levelized cost of storage than tank storage [80], but its potential appears to

have not been explored before in MES studies. Thus, in the current literature on power-to-heat and integrated energy systems for neighborhoods, seasonal thermal energy storage has been underexposed.

1.4 The role of water in local energy systems

Next to the system services energy and transport, water is another essential system service in the daily lives of people, and the planet as a whole. It is connected to many sustainable development goals and has its own challenges; water availability, water pollution and flood risk [81]. At first sight, water and energy sometimes seem to be separate worlds, while there are many interlinkages. This interdependence is defined as the water-energy nexus [24]–[26], which is part of the water-energy-food nexus. On the one hand, to produce and distribute clean water and transport and treat wastewater, energy is needed. The water sector accounted for 4% of the global electricity consumption in 2020 (972 TWh) [82], and this amount is in absolute terms expected to double by 2040 because of more energy-intensive water production technologies (such as desalination), an increasing drinking water demand and higher level of wastewater treatment [24], [83]. On the other hand, to produce, store and transport energy, water is needed, either as cooling water or for the production of fuels (i.e. biofuels or hydrogen). The energy sector was responsible for 10% of the global water withdrawals in 2021 [84]. Depending on the energy transition pathway chosen, water withdrawals by the energy sector will probably decrease as PV and wind need no cooling water. The water use for energy, mainly cooling water, could be reduced by 38% by 2050 in the EU [25]. Conversely, water consumption could rise, for i.e. biofuels, concentrated solar power, carbon capture and storage or nuclear power [24], [25].

The studies mentioned above focus on the water-energy nexus on the global or continental level. When zooming in from the global and general interlinkages between the water and energy system to the neighborhood, connections between water and energy are found as well (Figure 1.3):

- *Water as an energy carrier in the form of heat or cold*
  Although this water is not consumed, water is essential to distribute heat or cold from heat/cold sources to consumers via district heating/cooling networks [85].
- *Water as a source for hydrogen*
  To produce green hydrogen via electrolysis, stoichiometrically 9 liters (kg) of water are necessary to produce 1 kg of hydrogen. Yet, hydrogen can also be seen as a water carrier, because when hydrogen is converted back to electricity (and air/oxygen is added), this water is released again [86].
- *Water as a means for energy storage*
  Next to a transport medium, water is an important medium for heat and cold storage in the built environment [87]. Different forms of heat and cold storage exist, yet water is an often used and inexpensive medium for thermal energy storage (TES) [79], [88] in i.e. a tank, or underground storage (pit, borehole or aquifer) [87], [89].

- *Energy recovery from water*
  In neighborhood energy systems, energy can be recovered from different sources of water. Energy can be recovered from surface water, wastewater or drinking water, for both cooling [90] and heating purposes (mainly with a heat pump to increase the temperature) [91], [92]. Energy can be recovered directly in a house from shower water [93] as well. Lastly, sludge from a wastewater treatment plant is a form of energy [91], [94].
- *Energy to operate the water system*
  To operate the water system, energy is needed for drinking water extraction, treatment and transport, wastewater treatment and transport, drainage and surface water management [24]. The largest part of the energy demand is related to water heating in houses ('Demand/consumption' in Figure 1.3), accounting for 80% of the energy balance, with all other treatment and transport steps representing 20% of the energy use in the water cycle [95].

Besides the physical interlinkages, the goals for a sustainable future water system are similar to a sustainable future energy system. Just as the energy system, the water system should provide water in a reliable (always available), affordable, clean (based on renewable energy), circular (reuse of waste materials from water treatment), safe (public health) and fair (distribution of benefits and burdens) way, with security of supply (available water sources, water storage) and security of materials (technology and consumables). Moreover, there are similar challenges within both the water and energy sector. Firstly, due to climate change, periods of drought as well as more intense precipitation and flooding will occur more often [81], [96], affecting both the reliability, security of supply and potentially safety (water quality). To solve problems of inundation and droughts, similar to energy storage, aquifer (water) storage and recovery could be an option [94], [97]–[99], making blue-green open spaces in cities very important [81], [99]. Secondly, there are trends toward integrated and decentralized water systems that depend more on local water supplies [94], [100], related to the system services safety (water quality), circularity and reliability. Thirdly, within such a decentralized water system, rainwater could be a form of water supply. The availability of rainwater is intermittent, like the production of renewable energy; and again it is a matter of balancing supply and demand in time and space (and thus reliability).

In conclusion, we have seen that water plays a critical role in local energy systems, and there are quite some parallels between the water and energy sectors. This stresses the importance of not only focusing on the integration of the energy and transport within a neighborhood in a MES, but including water as well as an essential element of the neighborhood design [94].

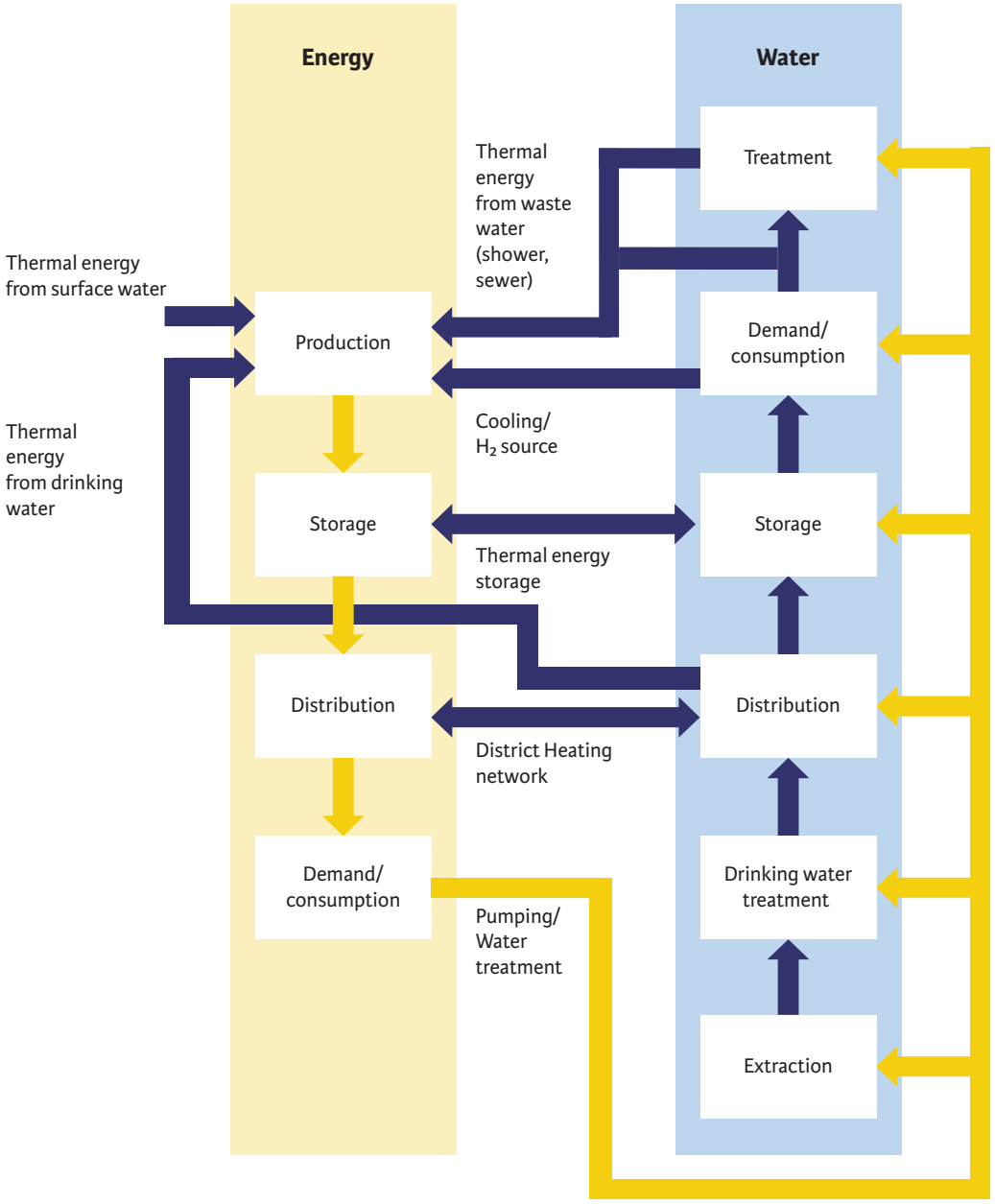

Figure 1.3 Possible Interlinkages between energy and water in a neighborhood.

1.5 Research question

In the existing literature on integrated systems for neighborhood system services (energy, transport and water) some areas of research are underexplored and can be considered as knowledge gaps, based on the insights from 1.3 & 1.4.

1. *A lack of focus on 100% renewable systems*
   Not many studies focus on 100% renewable energy systems for neighborhoods. Although it seems more of a future prospect, it is necessary to get a better grip on how 100% renewable (but not autarkic) neighborhoods could be designed, given the EU targets to be climate neutral in 2050 [2], as well as the Paris Agreement [1].

2. *Seasonal heat storage in MES is unexamined*
   The role of seasonal heat storage in MES is largely unexamined, despite the role it could play in increasing the reliability of heat supply and its potential economic and environmental benefits [74]–[76]. Mavromatidis et al. (2019) asked themselves ten questions regarding MES modeling and stated that more methods have to be developed that bridge models focusing on specific sub-dimensions; "As scientists ... [we] have to integrate and represent knowledge extending beyond the bounds of our own scientific disciplines" [101].

3. *Limited attention for a combination of multiple energy carriers (electricity, heat, gas) in one neighborhood desig*n
   Most studies focus on electricity and heat, or electricity and (a form of) gas, but studies integrating electricity, heat and (a form of) gas within a neighborhood are less common [71]–[73]. Nevertheless, more connections between these energy carriers reduce emissions and can increase reliability and affordability [51], [66]. Additionally, connections with industry near neighborhoods could be interesting as well for the utilization of waste heat [102], [103].

4. *Lack of an integrated approach to water and energy*
   There is a lack of an integrated view on both water and energy within a neighborhood system, despite the many interlinkages. Furthermore, both sectors face similar challenges, such as connecting demand and supply and more decentralization [94], and have to fulfill similar system goals (clean, reliable, affordable, circular, security of supply, security of materials, safe and fair). Knowledge exchange could therefore be useful to work towards a common perspective on future neighborhood design.

Given the challenges for the transition to a sustainable energy system (Table 1.1) and the identified knowledge gaps, this research aims to contribute to the design of more integrated renewable energy and water systems for the urban environment. It was mentioned that there are eight system goals to fulfill (see 1.1), yet the focus of this dissertation lies mainly on the goals clean (no CO_2 emissions), affordable (energy and water are basic needs that have to be delivered at an affordable price to consumers, not exceeding current market prices) and reliable (energy and water have to be available at all times). Thus, the overarching research question is:

How can an integrated renewable energy and water system at the neighborhood level be designed to provide energy and water in a clean, affordable, and reliable way?

By addressing this question, the research will provide valuable insights into how integrated systems can be designed to meet the needs of urban communities while contributing to a sustainable future. Through the course of this research, various aspects of system integration are explored, including different conversion and storage technologies, with a focus on energy and water. The objective is to assess more decentralized and integrated technologies that can enhance the reliability and affordability of the system on the boundary condition of having zero greenhouse gas (GHG) emissions (and are thus clean). Meanwhile, the identified knowledge gaps will be addressed.

To achieve this, a combined energy- and water system for a neighborhood will be analyzed using modeling techniques from a techno-economic perspective. A simulation modeling approach was chosen as it allows to more accurately model physical processes [101] such as thermal energy storage. The approach is called the Power-to-H3 concept: involving power-to-Hydrogen, power-to-Heat, water (H_2O) and storage technologies to provide all neighborhood system services (energy, transport and water). The energy and water balances, economic viability and greenhouse gas emissions of this system will be investigated. Next to modeling the overall system, attention is given to specific system components that address the identified knowledge gaps on (high temperature) heat storage, further integration of power-to-gas and power-to-heat and the integration of water and energy within one system. The research will primarily concentrate on the Netherlands and a temperate to cold climate with warm summers (Cfb & Dfb climatic zones [29]) for data collection and case study selection.

1.6 Outline

In order to answer the research question, this dissertation is divided into different parts, see Figure 1.4 for a graphical representation including the connection of the different chapters to the defined research gaps. **Chapters 2 and 3** provide an introduction to the concept and modeling of an integrated water and energy system for a neighborhood and thereby contribute to all four knowledge gaps. **Chapter 2** introduces the Power-to-H3 concept, which combines the production of renewable energy with the conversion and storage of both Heat and Hydrogen, and includes water (H_2O). Via a techno-economic analysis of a Dutch neighborhood, it is investigated to which extent the proposed concept is reliable, affordable and clean. In **Chapter 3**, the dynamic simulation model for energy and water balances based on the Power-to-H3 concept is elaborated upon and applied to an existing neighborhood case by working out different energy system choices. Comparison between different scenarios is done based on the share of local energy use, peaks in demand and supply and (energy) system costs.

Apart from conceptual and modeling studies with an integrative approach, in **Chapters 4-6** zoom in on different aspects of the Power-to-H3 concept, namely heat (**Chapter 4**), hydrogen (**Chapter 5**) and water (**Chapter 6**) which all contribute to one of the identified knowledge gaps. In **Chapter 4** the focus lies on heat storage with high-temperature aquifer thermal energy storage (HT-ATES), thereby contributing to the knowledge gap 2 on seasonal heat storage within MES. In HT-ATES systems, groundwater is the energy storage medium. HT-ATES systems are relatively new and most of the modeling done merely looks at seasonal effects. By combining the subsurface modeling of HT-ATES systems with the hourly dynamics of the 'ground-level' Power-to-H3 model, new insights on the working mechanism of a HT-ATES system coupled to a MES are gained. The study described in **Chapter 5** zooms in on hydrogen production with electrolysis, whereby the aspect of waste heat utilization is further explored, thus further integrating different energy carriers (electricity, hydrogen and heat, knowledge gap 3). Two use cases for the applications of electrolyzer heat are analyzed to gain insight on how and how much waste heat can be used to further enhance local system optimization. In **Chapter 6**, knowledge gap 4 on the integration of energy and water within a neighborhood is addressed by exploring the combination of energy production and water (re) use within a building. The importance of blue-green spaces in cities increasingly and seemingly competes with energy production (i.e. PV panels on buildings). However, it could also be an option to combine green-blue roofs with solar PV systems, as part of a Power-to-H3 concept. It is investigated how different water and energy functions work together in one building, and whether the solar PV system benefits from the evaporation of the vegetation of the blue-green roof in terms of output power. The results of this thesis are synthesized in **Chapter 7**, including an answer to the overarching research question in the form of design principles, policy recommendations and subjects for future research.

Chapters 2-6 have been written and can be read as independent work, and are based on different journal publications, slightly adapted for this dissertation. The work can thus be read as a complete text, but selective readers could go to the chapter of interest without missing essential information. Nevertheless, it is recommended to read **Chapter 2** as an introduction to the overall concept.

Setting the scene: System integration in local energy and water systems

1. Introduction

Integrated system designs and modelling

2. Introduction to the Power-to-H3 concept

Introducing Power-to-H3: Combining renewable electricity with heat, water and hydrogen production and storage in a neighborhood

Knowledge gap 1,2,3,4

3. Comparing different integrated system designs for an existing neigbhorhood

The Impact of System Integration on System Costs of a Neighborhood Energy and Water System

Knowledge gap 1,2,3

Zooming in on specific aspects of integrated energy and water systems

4. Zooming in on heat storage

Towards Sustainable Heat Supply with Decentralized Multi-Energy Systems by Integration of Subsurface Seasonal Heat Storage

Knowledge gap 2

5. Zooming in on hydrogen

Utilization of waste heat from electrolyzers – Unlocking local optimization

Knowledge gap 3

6. Zooming in on buildings

Increasing solar panel output with blue-green roofs in water-circular and nature inclusive urban development

Knowledge gap 4

Conclusions and reflections

7. Concluding remarks and recommendations addressing the main question:

How can an integrated renewable energy and water system at the neighborhood level be designed to provide energy and water in clean, affordable, and reliable way?

Figure 1.4 Outline of the dissertation.

2 Introducing Power-to-H3: combining renewable electricity with heat, water and hydrogen production and storage in a neighborhood

" The future we want needs to be invented, otherwise we will get one we don't want "

Joseph Beus

Abstract: In the transition from fossil to renewable energy, the energy system should become clean, while remaining reliable and affordable. Because of the intermittent nature of both renewable energy production and energy demand, an integrated system approach is required that includes energy conversion and storage. We propose a concept for a neighborhood where locally produced renewable energy is partly converted and stored in the form of heat and hydrogen, accompanied by rainwater collection, storage, purification and use (Power-to-H3). A model is developed to create an energy balance and perform a techno-economic analysis, including an analysis of the avoided costs within the concept. The results show that a solar park of 8.7 MWp combined with rainwater collection and solar panels on roofs, can supply 900 houses over the year with heat (20 TJ) via an underground heat storage system as well as with almost half of their water demand (36,000 m^3) and 540 hydrogen electric vehicles can be supplied with hydrogen (90 tonnes). The production costs for both hydrogen (8.7 €/kg) and heat (26 €/GJ) are below the current end user selling price in the Netherlands (10 €/kg and 34 €/GJ), making the system affordable. When taking avoided costs into account, the prices could decrease with 20-26%, while at the same time avoiding 3600 tonnes of CO_2 a year. These results make clear that it is possible to provide a neighborhood with all these different system services, completely based on solar power and rainwater in a reliable, affordable and clean way.

This chapter is based on the publication:
E. van der Roest, L. Snip, T. Fens, and A. van Wijk, "Introducing Power-to-H3: Combining renewable electricity with heat, water and hydrogen production and storage in a neighbourhood," Appl. Energy, vol. 257, Jan. 2020, doi: 10.1016/j.apenergy.2019.114024.

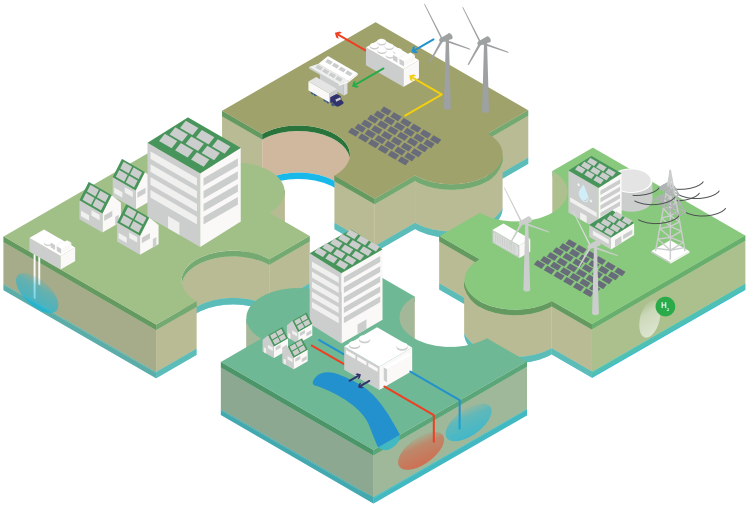

2.1 Introduction

Over the past century, the energy system has been focused on centralized fossil-based energy production and distribution. In the coming decades, this energy system will transform into a renewable-based system, in order to limit the effects of climate change and due to the fact that fossil resources are exhaustive [1], [104]. In this renewable-based energy system, energy will be abundant [105] as prices for solar and wind based electricity are rapidly decreasing over the last few years [106]. The prices for solar and wind energy are the lowest at places with high solar irradiation or high wind speeds, such as in the middle of the Atlantic ocean, or in deserts, which are not necessarily places where most people live. Thus, we will need to find ways to convert and store this renewable energy in some form that we can transport it to the place where the energy is actually needed. A suitable energy carrier could be hydrogen [105], [107], either compressed, liquefied, or converted to ammonia.

In addition to large scale centralized renewable energy production at mostly remote locations, there will be local, decentralized production of renewable energy, such as photovoltaic (PV) on roofs, PV parks or small wind parks. These decentralized forms of energy production will mainly be situated in or closeby urban areas, where space is scarce. Yet, there is a need to fulfil different services next to electricity, such as heat, water and transport. In these urban decentralized energy systems, there is an opportunity to utilize as much local energy as possible by applying different conversion and storage mechanisms to overcome the temporal mismatch in supply and demand. At the same time, these conversion and storage mechanisms should make optimal use of the limited space available.

How could decentralized renewable energy production combined with conversion and storage fulfil most of the neighborhood-system services? Solar or wind energy can fulfil the energy demand in a neighborhood and (partly) the transport service when electric cars are used. Currently, the energy used for transport is mainly based on gasoline or diesel, but electric driving is rapidly increasing [108]. The electric motor of an electric car can either be provided with electricity via a battery (BEV, battery electric vehicles) or via a fuel cell, which converts hydrogen to electricity within the car (FCEV, fuel cell electric vehicle). The batteries of electric cars could certainly be involved in day-night storage, but are less suitable for seasonal storage [109]. Additionally, when transport is electrified, this could lead to increased pressure on the electricity grid and again demand will not always match supply.

Another part of the energy system service in neighbourhouds, next to electricity, is heat. In general, most neighborhoods will have a surplus of (mainly solar) energy in the summer, while the largest part of their energy demand consists in the form of heat during winter. This heat demand will increasingly be electrified [110], [111], which results in a large unbalance between the surplus energy from roofs that is fed to the electricity grid in summer, and the high electricity demand of the heat pumps in electrified houses in winter. Moreover, a solar or wind park near an urban area needs a strong grid connection to feed its excess electricity to the grid in summer. Within a neighborhood, both effects could lead to inefficient systems and could cause problems at the connection with the high voltage grid, which results in a less reliable energy system [112].

In addition to these three energy-related services, water is very important in the urban environment. Coastal area's worldwide will face challenges regarding salinization, because of increasing water demand, climate change and relative sea level rise [104], [113]. Even in a country with as much water as the Netherlands, the availability of freshwater can be limited, mostly in the western part of the Netherlands. Freshwater shortages should be prevented, which points out the need for a more robust freshwater provision. On a yearly basis, there is no freshwater shortage, but mainly a lack of storage capacity. Underground freshwater storage could contribute to large scale freshwater storage [97], [98]. In addition, water storage systems could help to reduce inundation by storage of excess water. This stresses the importance of not only focusing on electricity but to integrate the different services (energy in the form of electricity and heat, transport and water) into one system within a neighborhood.

The concept we propose is an integrated system for a neighborhood combining different system services. The system utilizes solar or wind energy to produce heat in summer or to produce hydrogen as an energy carrier and is thus an example of a Power-to-X system. The produced heat is stored in the subsurface, and during winter this stored heat is used to heat houses directly. The hydrogen is produced from peaks in the renewable electricity production and utilized as a transport fuel. Furthermore, rainwater is collected from solar panels, stored in the subsurface and used for hydrogen production and for a part of the water supply in houses. The system hereby fulfils the system services energy (Heat), transport (Hydrogen), and (partly) water (H_2O) in a neighborhood. The concept is summarized by the term Power-to-H3, were the H stands either for heat, hydrogen or water (H_2O).

Besides being reliable, the purpose of this system is to be affordable and clean. For the system to be affordable, the production costs for each product should not exceed the regular market prices. As the market prices are influenced by the investment costs of the applied technologies, it is important to note that most of the technologies applied in the concept are still influenced by economies of scale and learning. This means that in the near future, the system costs will decrease. Nevertheless, in this study the current costs of these technologies will be used to calculate the affordability. In order to be clean, the system should minimize environmental impacts, such as CO_2-emissions. This means for example that the hydrogen production should avoid CO2 emissions, which means that only green hydrogen is part of the concept, which can be produced by using renewable energy to split ultrapure water into hydrogen and oxygen with an electrolyzer.

The combination of system services as described in the Power-to-H3 concept, especially of energy and water, is not often found in literature. It is highlighted that energy storage is necessary and therefore we should not only look to electricity storage, but integrate different sectors and energy storage technologies to create a smart energy system [114]. Different types of smart energy systems that focus on neighborhoods exist [59], [63], [67], [69], [115]–[118], but only few include hydrogen [59], [67], [69] and even less include hydrogen as a transport fuel [59]. Furthermore, water is never included in these studies. Heat production and storage for buildings or neighborhoods in aquifers are well-known techniques [119]–[121], and the heat system from Power-to-H3 is comparable to a low or ultra-low temperature district heating [122], [123]. However, in this concept the storage

temperatures (40-60°C) are high compared to the state of the art heat storage temperatures for seasonal storage (max. 25°C) that are mentioned in literature. Thus, the combination of fulfilling all neighborhood system services in addition to the high temperature seasonal heat storage make the Power-to-H3 concept an unique and innovative system.

The objective of this chapter is to introduce a reliable, clean and affordable integrated energy and water system for a neighborhood. In the next sections we will further explain the general Power-to-H3 concept (Section 2.2). The concept will be evaluated with a techno-economic analysis based on a simulation model (Section 2.3), to determine whether the concept can fulfil its goals to be reliable, affordable and clean. In the economic analysis, we include avoided (social) costs, as the concept illustrates the importance to think about urban energy supply and demand at a system level. The concept will be applied on an existing case of a neighborhood in the Netherlands (Section 2.4). Here, the first steps towards realization of a first Power-to-H3 system are taken, based on a 8.7 MWp solar park and a neighborhood of 900 houses. The concept will thus be applied on an existing neighborhood with the final aim to realize as many Power-to-H3 elements as possible. Results will be shown in Section 2.5. Finally, we will discuss the findings and draw conclusions (Section 2.6 & 2.7).

2.2 System description

To be able to match demand and supply during every moment of the year in a reliable, affordable and clean way, Power-to-H3 focuses on a novel energy and water system for a neighborhood. This proposed system can be divided into the energy source, conversion, storage and consumption. Within consumption, there are demands for demi water, heat, electricity and transport (see the left side of Figure 2.1). The sources consist of wind turbines, PV panels that include rainwater collection and a source for heat production, represented here as surface water, but air could be an option too. In order to connect the sources with the consumption, different conversion and storage techniques are proposed (see Figure 2.1).

The heat demand is met by storing heat (water) with a heat pump in a warm aquifer (40-60 °C), while the return flow of the heat grid is stored in a medium temperature aquifer (15-30°C). The electricity supplied by the wind turbines and PV panels is converted from DC to AC in order to be used within households. In addition, this electricity is converted to hydrogen in order to fulfil the transport service and cover short term fluctuations within supply and demand of electricity. The production of hydrogen requires water which is supplied by the rain water collection after purification in a reverse osmosis system. As the rain water is in excess compared to the hydrogen demand, the remainder of water fulfils part of the demi water demand in the neighborhood. The subsystems are described in more detail in the following paragraphs.

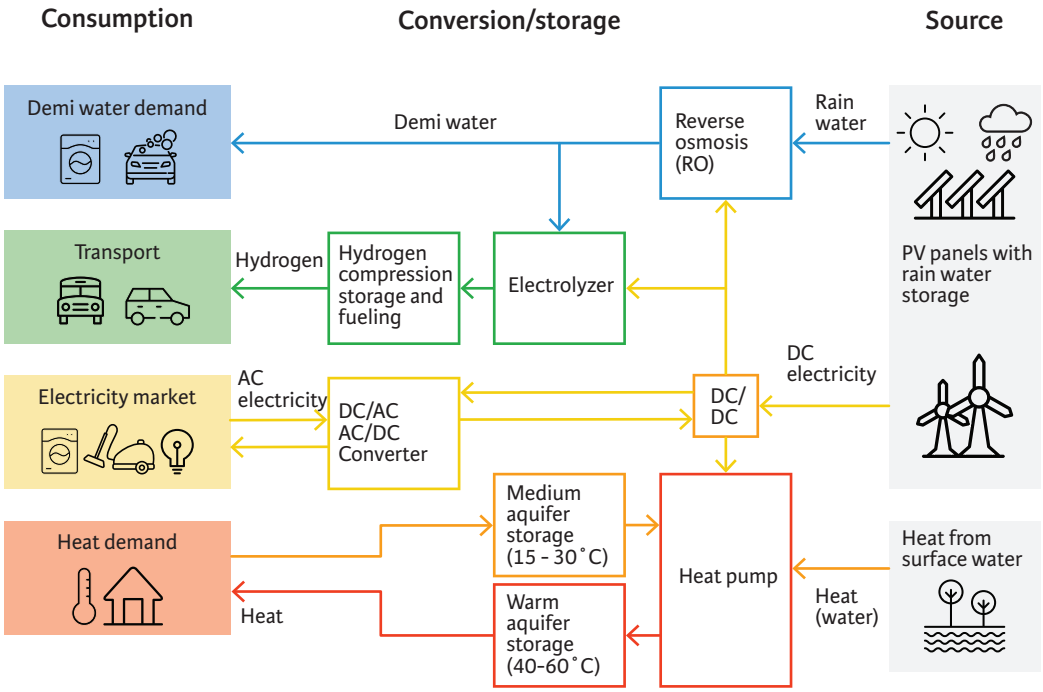

Figure 2.1 Overview of the Power-to-H3 concept with neighborhood system services as consumption the left, conversion and storage technology in the middle and renewable energy and water sources on the right side of the figure.

When proposing this integrated concept, we do not advocate that neighborhoods should be autark systems. When supply and demand do not match within the neighborhood, the local system will communicate with the large scale energy system via the electricity grid, or via the energy carriers produced from large scale wind and solar parks at other places in the world to resolve the unbalance. This communication increases the reliability of the system. Thus, in the current system design, we assume that the electricity demand from houses is fulfilled with solar PV on roofs and a grid connection and any excess electricity from houses is sold to the electricity grid. This means that the electricity demand of households is not included in the concept at this moment, but the heat, water and transport demand are.

2.2.1 Electricity to heat

During summer, when there is an abundance of solar power that cannot be used directly, electricity is converted to heat by a large scale heat pump. The heat pump produces heat with an output (condenser) temperature of 40-60 ˚C. The heat source for the heat pump is surface water. As the heat pump mainly runs during summer when the surface water temperature is relatively high, the operation results in a high coefficient of performance (COP) of the heat pump. When surface water is not available, an air-source heat pump could be used as well.

The produced heat is stored in an Aquifer Thermal Storage (ATES)-system with two or three wells, also called a (high temperature) geothermal doublet/triplet [124]. One warm well is used for the storage of the 40-60 ˚C heat. The medium well is used to store the return flow from the district heating network that connects the houses to the ATES-system as shown in Figure 2.2. Additionally, the system could be extended with a third cold well for cooling purposes, but this aspect is not covered in this study.

Storage of heat at this temperature is a relatively new concept, as the standard storage temperature in the Netherlands is around 25 ˚C [125]. Yet, storage of heat at higher temperatures can increase both energy storage capacity and overall energy efficiency [126], [127]. Firstly, by eliminating heat pumps in households and saving space. Secondly, by enabling the use of the energy in a more balanced way as this approach eliminates the use of electricity in the winter for heating, when the power output of the solar panels is low.

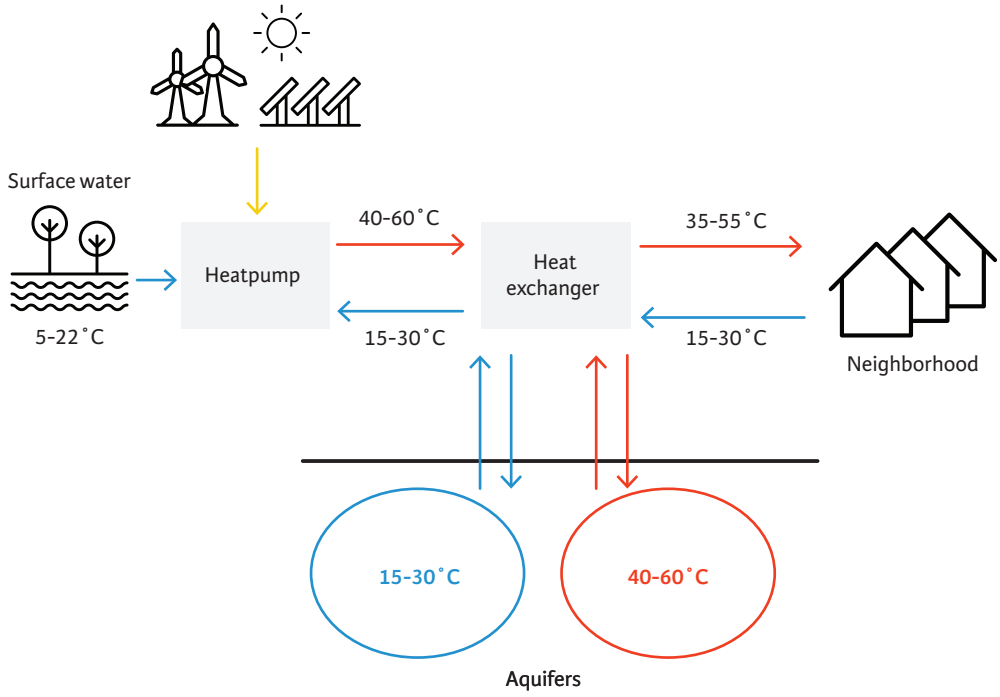

Figure 2.2 Overview of the heat system in the Power-to-H3-concept, with a large-scale heat pump, aquifer thermal storage and a district heating network.

2.2.2 Electricity to hydrogen

Electricity can also be stored as hydrogen which acts as an energy carrier. This carrier can fulfil different functionalities in the future energy system, as means of energy storage, high temperature heat, transport, feedstock for industry or even use in households [107]. In the Power-to-H3 concept, hydrogen will be used for transport as well as storage of energy. In this study, we mainly consider the utilization of hydrogen as a transport fuel for cars as they are mainly used by the inhabitants of the neighborhood. Earlier research has shown the role that hydrogen could play within a neighborhood, with the car as power plant concept [59]. Fuel cell electric vehicles (FCEV) are seen as an important trend in the automotive industry and are expected to have similar shares to electric, hybrid and internal combustion cars by 2040 [128]. Furthermore, prices will decrease rapidly when mass production starts, similar to the current trend of electric vehicles [107].

Figure 2.3 gives an overview of the hydrogen production in the Power-to-H3 system. Hydrogen is produced at 30 bar in the PEM electrolyzer and subsequently compressed to 200 bar, to allow more efficient transportation to a fueling station by a tube trailer, as shown in Figure 2.3. In this study, the PEM electrolyzer is chosen for the concept, because its characteristics seem to fit best when converting intermittent solar power, in a system that should fit within a neighborhood and with hydrogen that needs to be pressurized for transport [129]. After arrival at the fueling station, the hydrogen is compressed further to 900 bar. Cars can tank around 5-6 kg of hydrogen at 700 bar via hydrogen dispensers, which gives them a driving range of 500-600 km.

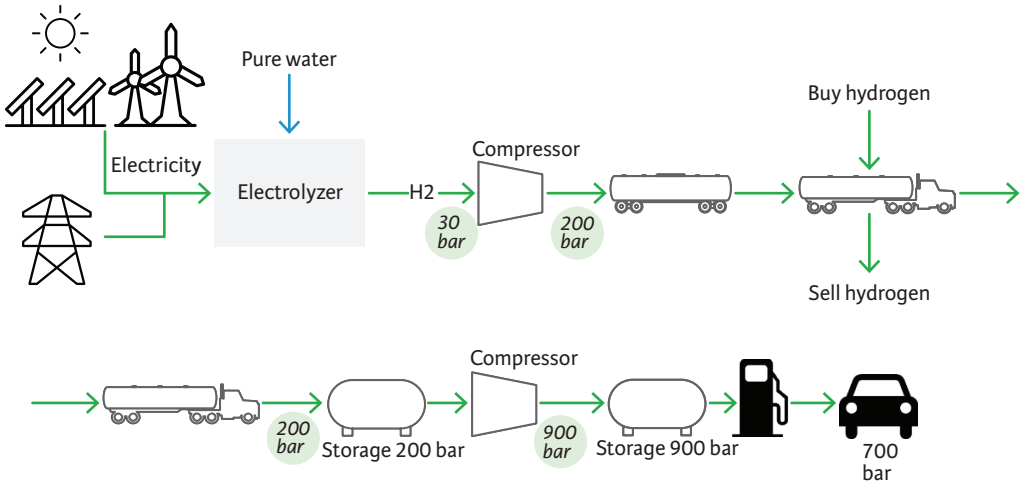

Figure 2.3 Overview of the hydrogen system in the Power-to-H3 concept, including hydrogen production by electrolysis, compression, transport and fuelling infrastructure.

2.2.3 From rain and electricity to demi water production

The production of hydrogen requires very pure water (or demi water), that will be produced from rainwater captured from solar panels. In general, the amount of water captured from solar panels is abundant in comparison with the water necessary to produce hydrogen. One solar panel of 270 Wp in the Netherlands could produce around 230-240 kWh/year [130], enough for the production of around 4 kg of hydrogen. For 4 kg of hydrogen, about 36 L of demi water is needed, which requires with conversion and losses no more than 80 L of rainwater. However, this same solar panel could capture about 1,300 L of rainwater a year, based on average precipitation of 880 mm per year in the Netherlands [131], leaving a substantial amount of demi- or rainwater available for other purposes. This demi water could be stored and used in the neighborhood, for specific applications such as the dishwasher and washing machine, to save on detergent use and to prolong the lifetime of the appliances. Other possible uses are watering of green areas within the neighborhood in the dry summer season with stored rainwater.

The design of the (demi)-water system in the Power-to-H3 concept is shown in Figure 2.4. Rainwater is caught from roofs (via the gutter) or solar panels with a draining-off system. The rainwater is filtered and then stored in an aquifer as freshwater buffer [97], [98]. When there is a demiwater demand, water is taken from the buffer and purified to demi water quality by a reversed osmosis installation. A ground level tank serves as a demi water buffer for the neighborhood and as a basis for Continuous Electro De-Ionization (CEDI). During this process, ions in the water are removed under influence of an electric field in combination with cation and anion membranes [132]. Furthermore, ionic resins are used to accelerate the process. After this step, the water has a conductivity of less than 0.1 µS/cm, which is suitable as input for the electrolyzer.

The demiwater demand of households is fulfilled via a separate water network and used in, for example, washing machines and dishwashers. The water from aquifer storage could also be utilized directly for watering of green areas in the neighborhood.

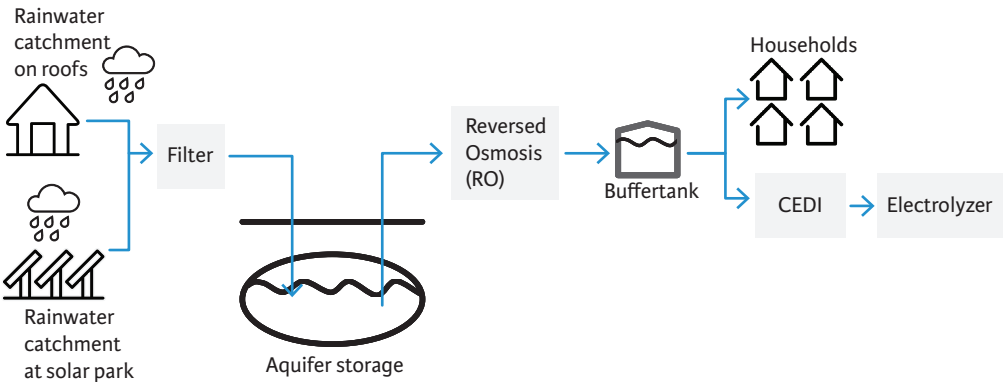

Figure 2.4 Overview of the water system within the Power-to-H3 concept, which consists of rainwater catchment, aquifer storage, purifying by reversed osmosis and continuous electro de-ionization for an extra purification step in case the water is used as a source for hydrogen production.

2.3 Methodology

In order to analyze whether the Power-to-H3 concept could result in a reliable, affordable and clean energy and water system for a neighborhood, we developed a simulation model. This model is able to perform hourly calculations for at least one year or a multitude of years. It provides the energy- and water balance (reliable), economic (affordable) and environmental calculations (clean).

Figure 2.5 shows the model structure, with the model input on the left side, which is specified per case and is further described in Section 2.3. The calculations section of the model (in the middle of Figure 2.5) include the calculations for conversion and storage of electricity, heat, water and hydrogen. Between those systems, there is interaction on an hourly basis. This interaction is partly determined by a scheduling strategy that distributes the available renewable energy over the different system components, which is further explained in section 3.1.3. All calculations and inputs from the different parts of the model are integrated within hourly time-steps, which results in the model output shown at the right hand side of Figure 2.5. The energy and water balance are monitored and adjusted every hour, while the economic and environmental calculations are carried out at the end of a run.

The most important input for the energy and water balance is explained in the next paragraph, followed by the environmental analysis and finally the economic calculations. Lastly, we zoom in on the avoided costs that are an integral part of the Power-to-H3 concept, and how those could partly be included in the business case.

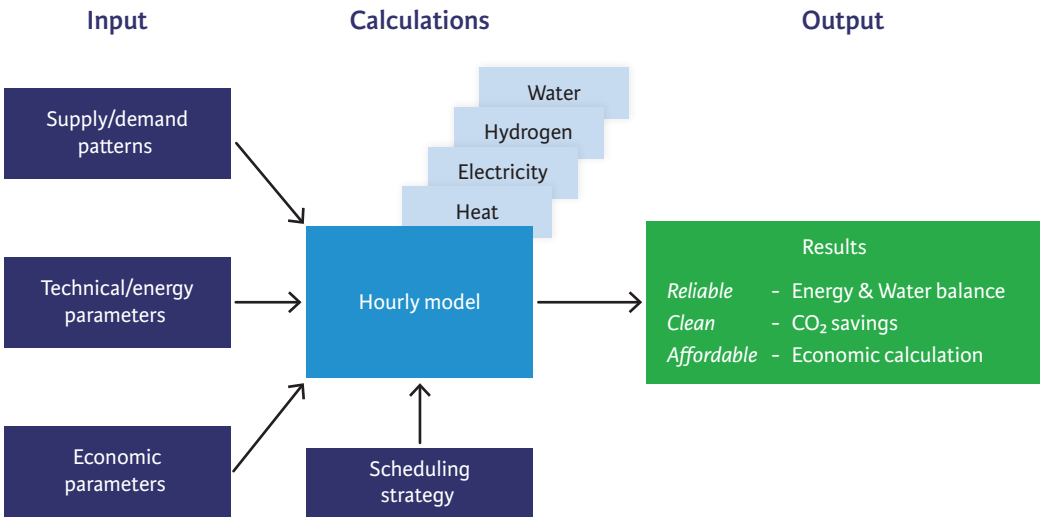

Figure 2.5 Overview of Power-to-H3 model structure with the model input, calculations with for the different system services (water, hydrogen, electricity and heat) as well as the model outputs.

2.3.1 Reliable, the system components

2.3.1.1 Input

Within the Power-to-H3 concept, the balance between supply and demand of both water and energy is checked every hour during the simulation. Therefore, the model has input in the form of external supply and demand patterns. The supply patterns include weather data about solar irradiation, temperature and rain, as well as the surface water temperature. The energy demand includes parameters such as the heat demand per house, amount of houses, yearly hydrogen demand or size of equipment. Those patterns and parameters depend on a specific case and are therefore specified in Section 2.3. The economic parameters are further explained in Section 2.2.2.

2.3.1.2 Conversion and storage calculations

For energy supply and conversion, the most important energy parameters are summarized in Table 2.1. To balance supply and demand, there are options for 1) heat storage in the subsurface, 2) water storage in the subsurface and buffer tanks, and 3) hydrogen storage in high- pressure tanks. The buffers should always be able to fulfil a minimum demand for hydrogen, heat or water. In addition, all storage media have a specified maximum storage capacity. The main objective of the storage systems is to distribute the available energy in such a way that the storage levels are kept on a predetermined acceptable level.

Table 2.1 Important technical and energy parameters within the Power-to-H3 model.

System element	Energy consumption/efficiency
PV system	17%[a]
Heat pump	$COP = 7.5 - 0.07\ (T_{cond\ (out)} - T_{evap\ (in)})$[b]
Infiltration temperature warm aquifer ($T_{cond\ (out)}$)	65 °C[c]
Electrolyzer (PEM)	50 kWh/kg[d]
RO system	90%[e]
Electricity conversion (AC/DC and DC/AC)	95%[f]

[a] Report from IRENA [106]
[b] Based on Dorin software [133]
[c] Bases on different configurations for the heat system [134]
[d] Combined number for electrolysis, gas cleaning and compression to 200 bar, based on literature [107] and commercially available information from Thyssenkrup [135] and Hydrogenics [136]
[e] On water basis, based on expert knowledge (Hans Huiting & Emile Cornelissen, KWR, 21-02-2017)
[f] Assumption, based on [63]

Heat

A maximum heat storage capacity is defined that varies over the year. The purpose of the heat storage is to balance the seasonal difference in supply and demand of energy. Therefore, most heat will be produced in summer, while the largest heat demand occurs in winter. In addition, there should be a sufficient amount of heat stored to fulfil the demand, without creating an oversupply

of heat. An oversupply of stored heat will degrade over time resulting in efficiency losses for the heat system. If at any moment in time the heat storage system has not enough heat stored to fulfil the heat demand, heat is produced directly with the heat pump based on grid electricity while utilizing surface water as a heat source. This ensures a reliable system operation.

In order to comply with these requirements, a heat storage pattern is developed whereby the total heat demand is divided over the year. Each week a certain percentage of the total heat demand is added to the maximum amount of heat that is allowed to be present in the aquifer at that moment. Every hourly step a check is performed of how much heat can be stored at that hour based on the available produced energy and if this agrees with the amount of heat that can be stored in that week. If the weekly value is already reached, the storage of heat is paused until the next week.

The amount of heat stored needs to exceed the heat demand to take the losses during heat storage into account. Therefore, the weekly heat storage values are multiplied with a certain factor. In equation 2.1, the relationship between the weekly maximum storage values and total heat demand is shown.

$$HD_{week,max\ i} = \frac{HD_{week,\%\ i}}{100} \cdot HD_{sum} \cdot f_{hd} \tag{2.1}$$

Where $HD_{week,max\ i}$ (kWh) is the maximum amount of heat stored in a certain week, $HD_{week,\%\ i}$ (%) the percentage of the total heat demand that can be stored in that week. With surface water and electricity from PV as a heat source, the heat storage can only be filled in the summer period. Therefore, the weekly storage value is set to 0 from November up until the end of February. From March to October, the surface water temperature is expected to be high enough to extract heat, with a peak in late summer. Solar irradiation is expected to peak in June and July. Based on this knowledge, a storage pattern was created that starts ascending from around 1% in March to 4,6% in July and August, and starts decreasing again to 1% in October. HD_{sum} (kWh) is the total annual heat demand and f_{hd} is a factor that takes the heat losses during storage into account. In this study, the factor is 1.2, as a heat loss in the subsurface of approximately 20% is assumed. This factor is determined by an iterative process and will change depending on the size and temperature range of the system and can therefore not be generalised.

Hydrogen

Hydrogen is stored at a pressure of 200 bar in tanks on tube trailers. At the hydrogen fuelling station, there is a 200 bar buffer tank installed as well. If the volume in this storage tank comes below a certain minimum, while there is not enough hydrogen produced yet to refill the tank, hydrogen can either be produced with electricity from the grid or be bought from an external source, again ensuring a reliable system. When the maximum hydrogen storage capacity is reached, a full hydrogen tank is transported to the hydrogen fuelling station or a third party. Meanwhile, the system starts filling a new tank or tube trailer with hydrogen.

Water

Water is stored in the subsurface and partly in buffer tanks. If the buffer tanks reach a certain minimum level, they are filled with water from the aquifer. If there is not enough rainwater stored at that time, ground water can be used as a source for (pure) demiwater production, as long as the system is in balance over a period of a number of years.

Another option to fulfil a shortage of pure water would be to buy pure water from an external source. For water storage in the subsurface, there is no real maximum, but the difference between the infiltrated volume and restrained volume is provided. If over a number of years, the infiltrated volume is significantly larger than the restrained volume, it is possible to withdraw some extra water for irrigation in summer months, while at the same time creating a balanced water storage system.

2.3.1.3 Scheduling strategy

The available energy in the form of solar or wind electricity can be distributed over at least three different alternatives; producing hydrogen, producing heat or feeding electricity into the grid. The model thus needs an energy distribution strategy and we decided to design two distribution scenarios. The first one is to ensure reliable heat production where the use of locally produced energy is maximized, while hydrogen can be imported from external sources. With this scenario, priority is given to heat production, whereby the generated electricity is in principle allocated to the heat pump. If the amount of available renewable electricity is larger than the capacity of the heat pump, or when the warm aquifer if full enough for that moment in time, the electricity is available for the electrolyzer. When there is still renewable electricity left after usage by the electrolyzer, this is fed into the electricity grid. However, if the demand for hydrogen is higher than the production by the electrolyzer with the available energy, this means that hydrogen has to be imported from elsewhere.

The other option is to produce all heat and hydrogen on-site in a reliable way. In this scenario, there is a priority for hydrogen production, which means the electricity from the solar panels and wind turbines is first available for the electrolyzer. When the electrolyzer runs at full capacity, the remainder of the generated electricity is allocated to the heat pump. Whether this electricity is used to produce heat by the heat pump depends (as before) on the capacity of the heat pump and on the amount of heat already stored in the aquifer. If there is still renewable electricity available, it is fed into the electricity grid.

When hydrogen is set as a priority, there should always be enough hydrogen to fulfil the hydrogen demand at the fuelling station. Therefore, electricity is bought from the grid if the level of the hydrogen buffer tank comes below a certain level ensuring the production of hydrogen on site. Furthermore, there is an obligation to fulfil the heat demand of the neighborhood at any time, because heat cannot be easily imported. Hence, it is possible to buy electricity from the grid to fill the heat storage, whereby the user sets the maximum price for electricity. Moreover, if the warm aquifer should become empty at any moment, the system switches over to direct heat production with electricity from the grid, with surface water as a heat source.

2.3.2 Affordable, the system economics

The Power-to-H3 system aims to be affordable, which means that the costs should not be higher than regular market prices. Table 2.2 shows the current market prices used for the different products, based on the Dutch prices for heat, hydrogen and drinking water. The heat price consists of a fixed charge per year and price per GJ, to have a fair comparison with the price for heat from a Power-to-H3 system, we have chosen to combine this two cost factors in one price per GJ based on an average heat demand of a well isolated Dutch house. To check whether the Power-to-H3 system is affordable, we then calculated the production costs for the different products and check whether the production cost exceeds the current market price for this product. If needed, these market prices can easily be adjusted to match prices in other areas.

Table 2.2 Product market prices used to calculate the affordability of the Power-to-H3 system.

Product		Price (VAT excluded)
Hydrogen		10 €/kg[a]
Heat – price per unit	22.5 €/GJ[b]	34 €/GJ[c]
Heat – fixed charges	252 €/year[b]	
Heat – connection costs (one occurrence)		821 €[b]
Demiwater		1.4€/m³ [d]

[a] This value is not market driven, but currently used as hydrogen price because the costs per km driven are on the same level as gasoline.
[b] Based on the regulations for heat delivery by the Dutch authority for consumers and market (ACM) [137].
[c] Based on an average heat demand of 22 GJ/year for a well isolated Dutch house [138], [139]
[d] Approximate price for drinking water in the Netherlands [140]

The production cost per product is calculated according to equation 2.2:

$$Production\ cost_j = \frac{\sum(\alpha \cdot CAPEX_i + OM_i + Ecost_i)}{\sum N_{product,year}} \quad (2.2)$$

Where $Production\ cost_j$ (€ per GJ, kg or m³) represents the production costs for a certain product j, being either hydrogen, heat or water. The right-hand side of the equation represents the sum of the yearly costs of the components i that are part of a certain system, divided by the total yearly production in kilos of hydrogen, gigajoules (GJ) of heat or cubic meters (m³) of pure water. Here the $CAPEX_i$ (€) covers the capital expenditures for a particular system component i (i.e. the electrolyzer, compressor or storage tank) and OM_i (€/year) represent the operational expenditures for a particular system component. $Ecost_i$ (€/year) are the electricity costs for a system component i and lastly $\sum N_{product,year}$ (in GJ, kg or m³) is the amount of heat, hydrogen or water sold during a year. The capital recovery factor (α, no unit) in equation 2.2 is calculated according to equation 2.3.

$$\alpha = \frac{r}{1 - (1+r)^{-L_i}} \quad (2.3)$$

With α the capital recovery factor (no unit), r the discount rate (in %) and L_i (year) the lifetime of a particular system component i.

The most relevant economic parameters for the calculations from equations 2.2 & 2.3 are shown in Table 2.3, based on current technology costs. All those parameters could be adjusted to adapt the model to different locations, scales or new developments.

Table 2.3 Relevant economic parameters in the Power-to-H3 model, based on current costs of technology.

	Cost(function) for CAPEX	Operation and maintenance (OM)	Lifetime in years
System elements			
Solar Park	900 €/kWp[a]	1%	20
Heat pump	1,400€/kW_{el}[b]	1% [141]	20 [142]
District heating network	(214 + 1,725 * d_{pipe})*$L_{network}$[c] in € with d_{pipe} de pipe diameter in m and $L_{network}$ the length of the network in m	1% [142]	50 [143]
Electrolyzer	1,100€/kW[d]	2%[e]	20 [59]
Hydrogen fuelling station	1.3M€[e]	70,000€/j[e]	15[f]
RO system	15,000 + 8,000*VRO in € with V_{RO} in m^3/hr[f]	2.5%[f]	15[f]
CEDI system	30,000 * V_{CEDI}/18 + 1,000 * V_{CEDI}[f]	2,5%[f]	7,5[f]
Aquifer thermal storage	1.5M€[g]	1.5%[g]	40[g]
Water storage	0.55M€[h]	0.5%[h]	40[h]
Other economic parameters			
Purchase grid electricity	On average 6.5 €¢/kWh [i]		
Discount rate	3%[j]		

[a] Based on the investment price for solar PV larger than 1 MW in the Netherlands [144]
[b] Based on different quotations from heat pump suppliers, and validated with expert knowledge.
[c] The pipe diameter is a model parameter, and the formula is valid for outer city areas based on an IEA document on District Heating [142]
[d] Costs based on literature [107] combined with expert knowledge from (Ekinetix, November 2017).
[e] Based on literature [59], [145] and quotation from a Dutch-based green fuel company (PitPoint).
[f] Based on calculations with a membrane that produces 20 L/m^2/hour for RO, and based on data from Pure Water Group for CEDI (Hans Huiting, KWR, 09-10-2017).

[g] Costs are a sum of investments in boreholes, casting, pipes, pumps, injection valves, heat exchanger, technical room and preliminary design, exact formulas can be found in the project report [134].
[h] Costs for water storage in the subsurface [146], including rainwater collection, self-cleaning filters and pumps [134]
[i] For electricity purchase from the grid, APX prices from 2016 were used. On top of the APX, a network price of 1.7€₵/kWh plus taxes (VAT excluded, 1.6€₵/kWh) are added, together 3.3 €₵/kWh in 2016, based on CBS data for wholesale users in the 200-200,000 MWh/year category. Fixed charges are not taken into account, these are paid by the company that builds the solar park.
[j] The average recommended discount rate by the study group discount rate [147]

2.3.3 Clean

Besides being a balanced and affordable system, the Power-to-H3 system has the objective to provide a clean and safe living environment. It fulfils this objective in many different ways: (1) it is only based on renewable energy, which reduces CO_2 emissions, (2) the risk of CO related deaths [148], [149] by the central heating boiler is avoided when applying a district heating network instead of natural gas, (3) there is less air (and noise) pollution by cars when driving fuel-cell/electric instead of on gasoline or diesel. In this study, we do not go further into detail on all those effects, but instead, we have taken the avoided CO_2-emissions in the system as a measuring unit for a clean system. In order to calculate the avoided emissions, the current conventional situation with heat delivery via a gas boiler, a gasoline car and the emissions of the electricity mix in the Dutch electricity grid are used for comparison with the Power-to-H3 system. These emissions are summarized in Table 2.4. As with the economic parameters, these parameters can easily be adjusted to reflect different situations.

Table 2.4 CO2 emission factors for heat, transport and electricity applied in the Power-to-H3 model.

	Amount	Unit	Reference
CO_2 emission heat	59.7[a]	kg CO_2/GJ	Boiler on natural gas (December 2017)
CO_2 emission car	0.22[a]	kg CO_2/km	Average car and fuel use (2014)
CO_2 emission electricity	0.413[a]	kg CO_2/kWh	Representative Dutch electricity mix (December 2017)

[a] Data are taken from the CO_2-emission factors database [150]

To monetize avoided CO_2 emissions, a price of 60€/tonne CO_2 is taken as a reasonable value. This CO_2 price corresponds to the price projected necessary to achieve the goals as set in the 2015 Paris Agreement [151]. The $CO_{2_{emission\ factor}}$ in € are calculated according to Eq 2.4.

$$CO_{2_{cost\ savings}} = CO_{2_{emission\ factor}} \cdot Product_{delivered} \cdot CO_{2_{price}} \quad (2.4)$$

Where $CO_{2_{emission\ factor}}$ (in kg CO_2 per GJ, km or kWh) are the factors as shown in Table 2.4, $Product_{delivered}$ is the amount of electricity (in kWh), heat (in GJ) or hydrogen (in kg) that are sold to the grid, house owner or car driver and $CO_{2_{price}}$ (€/tonne) the price of a tonne CO_2.

2.3.4 Avoided costs

In an integrated concept such as Power-to-H3, there is a need for alignment between technology and institutional arrangements. When a Power-to-H3 system is realized, there is an impact on different aspects of society. Examples of possible impacts are already mentioned in section 2.3.3, however there are more possible impacts. A large impact can be realized if extension of the electricity grid is avoided when part of the energy is converted and stored locally. Moreover, a decreased risk of water inundation and less water scarcity during droughts will occur when rainwater is stored in the neighborhood. All those effects are expected to have a contribution to a cleaner, quieter, safer and greener living environment from a societal perspective, yet are hard to quantify and do not directly improve the business case.

In this research, two possible effects of a Power-to-H3 system in a neighborhood are quantified. The first one concerns CO_2 savings, which are monetized by a CO_2 price as explained in Section 2.3.3. The second element of the avoided cost calculations are the savings on electricity grid extension. In a standard situation, the installation of a solar or wind park will require reinforcement or extension of the electricity grid in order to dispatch the electricity peaks in the summer. By converting the electricity peaks in summer to other forms of energy, the required grid connection capacity can be reduced. The cost savings related to this grid connection reduction will vary depending on the situation and can be very hard to quantify as is pointed out by Agora Energiewende [152] as well as KU Leuven [153].

Network costs can be calculated in kWh (transported energy) and kW (peak power). The required investment is generally based on peak power capacity, but both units are used when avoided cost are calculated. For example, the transmission and distribution costs for added wind/solar (land-based) in Germany as reviewed by Agora Energiewende are estimated at approximately 7.5 €/MWh [152]. For Belgium, these costs vary between 2.4-3.1 €/MWh for additional renewable energy capacity [153]. If conversion and storage systems are installed, savings on these grid connections could occur. A recent study about the impacts of a form of high-temperature seasonal heat storage in the Netherlands calculated a saving on the grid extension of 3.3-8.5 €/GJ of heat delivered [154]. From a study focusing on different power-to-hydrogen possibilities, the savings on grid extension costs for an agricultural area are around 1,000 €/kW, while for large scale PV (100 MW) the savings are approximately 280 €/kW [155]. However, these cases are not applicable to the urban environment where the Power-to-H3 system will be situated and therefore the savings on grid extension will most likely be lower.

Next to savings on the grid connection of the solar or wind park, there is an additional advantage for the neighborhood. Because of the relatively high temperature at which heat is delivered, no heat pumps need to be installed in the houses which have an approximate capacity of 6 $kW_{electric}$ each. In the Power-to-H3 concept, either no heat pumps at all or only small booster heat pumps of 0.5 $kW_{electric}$ for tap water are installed in each house, saving at least 5.5 $kW_{electric}$ per household [156]. This saving in electrical connection is quantified by van Melle et al. [156] at a value of 204-700 €/kW. However, as mentioned before this saving is highly depended on the location and the capacity of the already existing grid.

In this study, we assume the lower value of 200 €/kW for avoided grid connection costs for both the solar and wind park as well as the neighborhood, since the Power-to-H3 system is located in an urban area. This means that there is already a grid connection available and the costs for reinforcement are not as high as in a remote or agricultural area. The costs for grid reinforcement are calculated according to Equation 2.5

$$C_{grid} = P_{additional} \cdot C_{reinf} \tag{2.5}$$

With C_{grid} are the costs for grid reinforcement in €, $P_{additional}$ the additional grid capacity needed in kW and C_{reinf} the cost for grid reinforcement in €/kW, in this study this value is set to 200 €/kW.

2.4 Case study of Power-to-H3 in Nieuwegein, the Netherlands

The Power-to-H3 system is applied to an existing neighborhood in Nieuwegein, the Netherlands to investigate the reliability, affordability and cleanness of the system. The final aim will be to realize as many elements from the Power-to-H3 concept as possible.

In Nieuwegein, a solar park of 8.7 MWp is installed for the production of heat and hydrogen in order to fulfil the demands for heat and transport of a neighborhood of 900 houses, which are situated about 2 km from the solar park (Figure 2.6). There is no direct physical electrical connection between the houses and the solar park, so both the neighborhood and the solar park have their own grid connection.

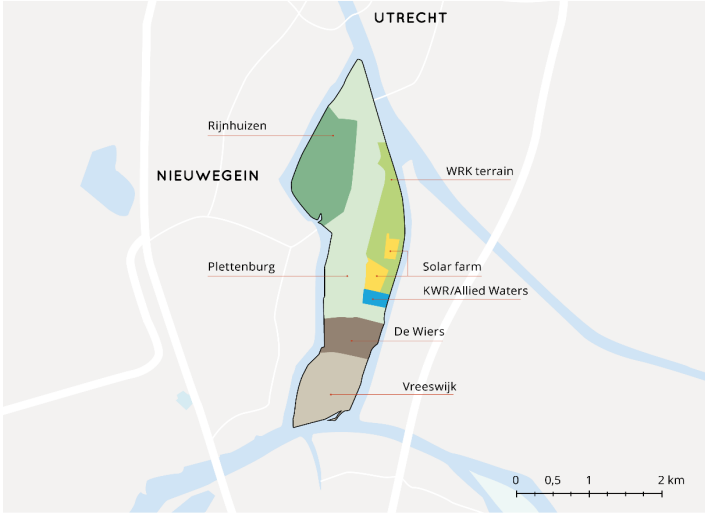

Figure 2.6 Overview of the first Power-to-H3 project location, the colours show different locations in the project-area, including the solar farm (yellow) and the Neighborhood Rijnhuizen (dark green) [105].

The main parameters that describe the Nieuwegein case are depicted in Figure 2.7. The solar electricity production will be 8.7 MWp and the current electricity connection is 4MW (MVA). To prevent grid extension, the heat pump and electrolyzer are scaled at 2.5MW. Probably, this capacity is more than necessary to just fulfil heat and hydrogen demand, but here we have chosen to relate the size of the conversion technology to the supply side instead of the demand side, which is a consequence of taking a system approach. In the neighborhood of 900 houses, we expect that in the near future approximately half of the households will have a fuel cell electric vehicle, while the other households have an electric car [128]. More background information about the system size, years simulated, weather conditions and supply and demand in the case study can be found in the supplementary information (***SI-A***).

For the economic analysis, it is important to note that Waternet, the water company for the Amsterdam region, will install the solar park and sell the produced electricity to the Power-to-H3 system at a price of 3.9 €¢/kWh, which is comparable to the fossil-based electricity price. Waternet can afford this selling price as the solar park is subsidized. Therefore, the investments for the solar park are thus outside of the system boundary and instead an electricity purchase price is included in the energy costs of the system. This electricity price is part of the sensitivity analysis that is carried out for a total of ten parameters in the Nieuwegein case. The values and ranges chosen are further explained in SI Table A.4.

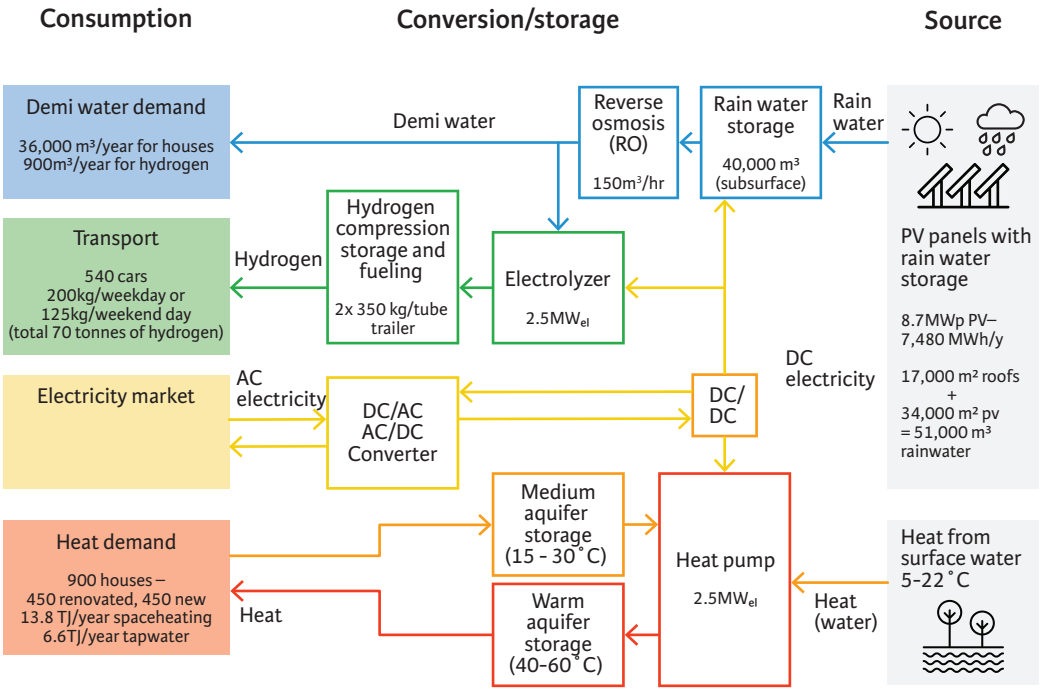

Figure 2.7 Schematic overview of the Power-to-H3 system with supply, demand and system component sizes for the case of Nieuwegein, the Netherlands.

2.5 Results

This section is based on the results of the case study as described in Section 2.3, whereby heat production is set as a first priority. Results of the hydrogen scenario are shown in the ***SI-B***.

2.5.1 Renewable energy distribution

When the Power-to-H3 system is applied to a neighborhood in Nieuwegein with a nearby solar park, the yearly electricity production is 7,480 MWh. The monthly distribution pattern of the solar electricity for the complete 5 year period is shown in Figure 2.8. There is a clear production peak in June and July, as the electricity production in July is almost 10 times higher than in December. The average energy distribution per year is summarized in Table 2.5.

In this scenario, 60% of the yearly electricity output is utilized for hydrogen production, 25% for heat and the surplus (15%) is fed back into the grid. The electricity consumption for pure water production is so little (0.1% of the total energy production) that it is seen as negligible. In the period from November – February, almost all electricity is used for hydrogen production, while the rest of the year there is a combination of heat and hydrogen production and some surplus electricity which is fed into the grid.

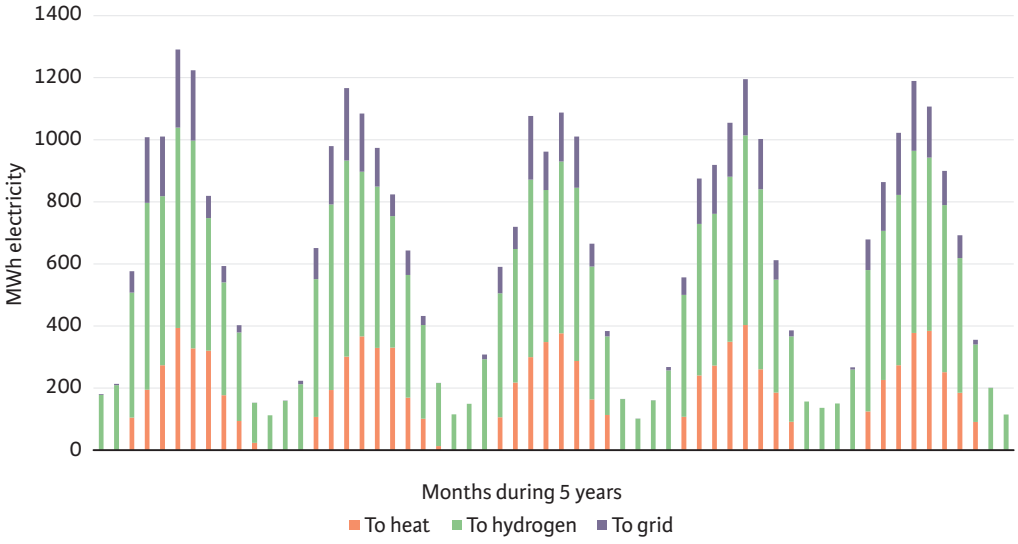

Figure 2.8 Monthly energy distribution for the heat as priority system, period shown here is 2010-2014, with monthly values.

Table 2.5 Distribution of energy over the different Power-to-H3 products on a yearly basis (5-year average).

In MWh/year	Heat priority
Renewable electricity to heat	1,910
Renewable electricity to hydrogen	4,500
Renewable electricity to grid	1,070
Total renewable electricity production	7,480

2.5.2 Reliability of the system

2.5.2.1 Heat

Figure 2.9 shows the heat production with electricity from the solar park, the heat demand from the neighborhood and the surface water temperature, which is heat source for the heat pump. With heat as a priority (see Figure 2.9), heat is produced in the warmer months when the temperature of the surface water is at least 7 °C. The Fig. clearly shows the idea of the seasonal storage; heat is produced and stored in summer while being supplied during the winter. All heat is produced with electricity from the solar park, with an average COP of 4.2. With this average COP, the total heat production is 28.8 TJ, while the total heat demand is 20.4 TJ, resulting in an overall efficiency of 70% for the heat system. The efficiency does include heat losses during storage in the aquifers, during transport in the district heating network up until the delivery of heat in the houses. The heat demand of the neighborhood is fulfilled at any time, resulting in a reliable heat system.

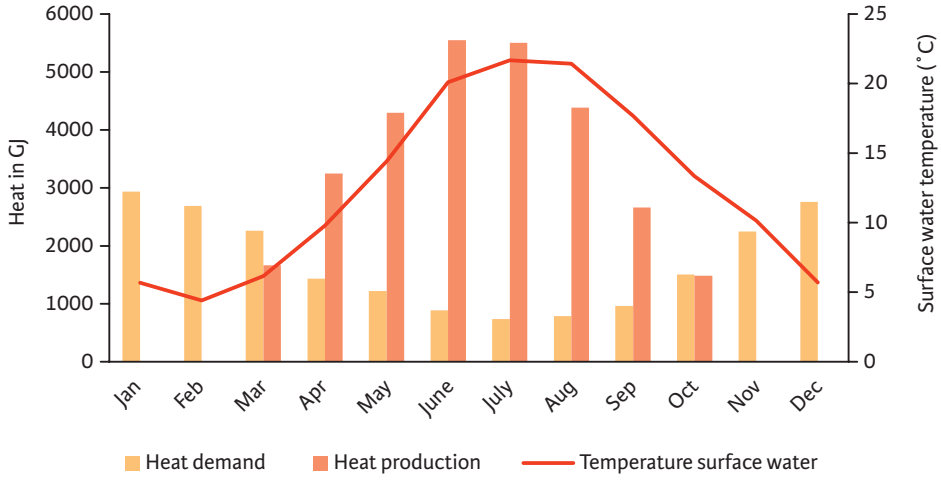

Figure 2.9 Heat demand and supply in a Power-to-H3 system for a neighborhood of 900 houses, monthly average over five years.

2.5.2.2 *Hydrogen*

How hydrogen demand and production are matched over the year is shown with monthly averages in Fig. 2.10. The electrolyzer uses 4500 MWh of solar power and produces 90 tonnes of hydrogen per year compressed to 200 bar. The yearly hydrogen demand based on 540 hydrogen cars is around 70 tonnes, which means there is a surplus of 20 tonnes of hydrogen each year, mainly produced during the summer months. However, while the (monthly) demand is more or less constant, the production peaks in summer while during winter there is a shortage of 9.1 tonne of hydrogen, which corresponds to 13% of the total yearly hydrogen demand. One solution would be to store the surplus hydrogen in summer, to be able to use it in winter, in a similar way as the heat storage system. However, hydrogen storage in pressurised tanks is expensive, and therefore the best option at this point in time would be to sell the surplus hydrogen in the summer and import hydrogen in the winter when production falls short. In the mid-term future, the gas grid and/or salt caverns could serve as a hydrogen buffer.

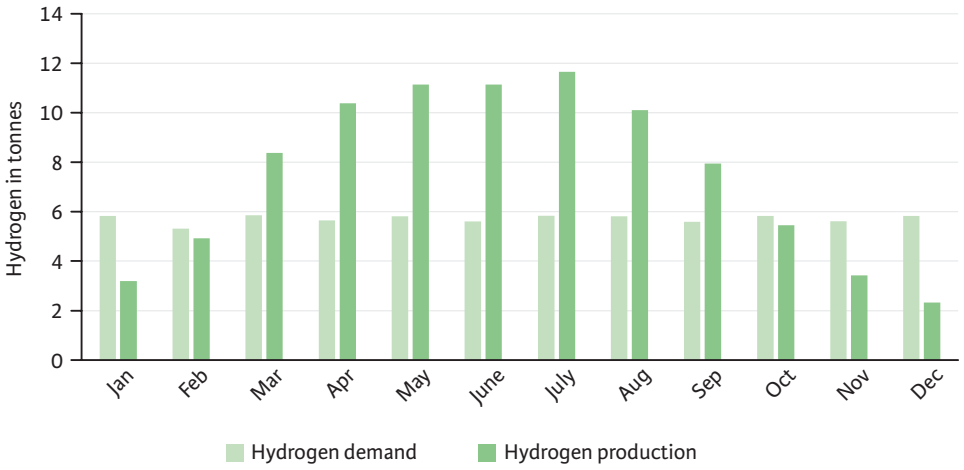

Fig. 2.10 Hydrogen demand and supply over a year for a Power-to-H3 system with a supply of 540 cars, monthly average over five years.

2.5.2.3 *Pure water*

For the hydrogen production as discussed in 2.5.2.2, 900 m^3 pure water is needed. The pure water demand for hydrogen is only a fraction of the total yearly (rain)water supply of 51,000 m^3/year, of which 17,000 m^3 is captured from the solar park, and 34,000 m^3/year from roofs. The pure water demand in the neighborhood is 40,000 m^3, including loss factors during purification steps. This leads to a surplus of 10,000 m^3/year that could be used for irrigation purposes in the summer months. Over the year, the water storage ensures a reliable water supply, even in months where the water supply is lower than the demand. This situation merely happens during spring, as can be seen in Figure 2.11.

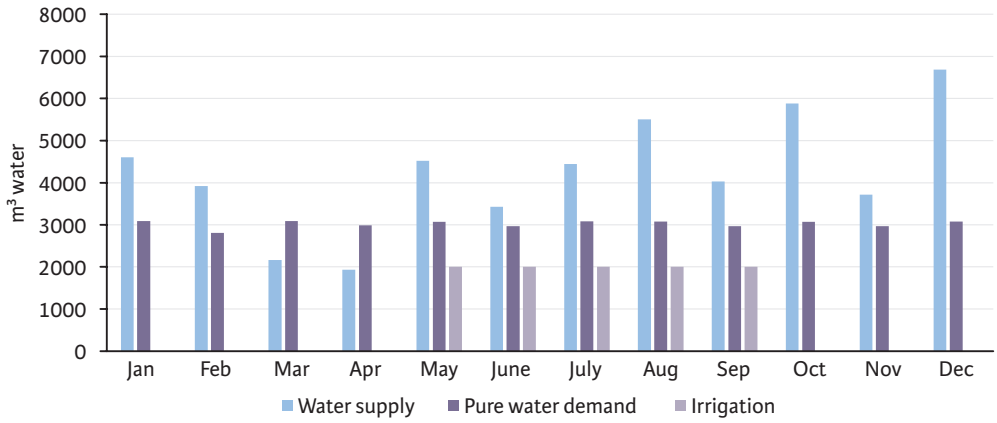

Figure 2.11 Rainwater supply and (pure)water demand, monthly average over five years.

2.5.3 Sustainability, a clean system

The total CO_2 savings would be 3090 tonnes per year if the renewable electricity from the solar park would be completely sold to the grid and replace electricity needs elsewhere. When operating the Power-to-H3 system, the CO_2-reduction is 3620 tonnes per year (see Fig. 2.12), based on CO_2 reduction factors as given Section 2.3.3. The Power-to-H3 system is thus saving more CO_2 because of the conversion of electricity to other products.

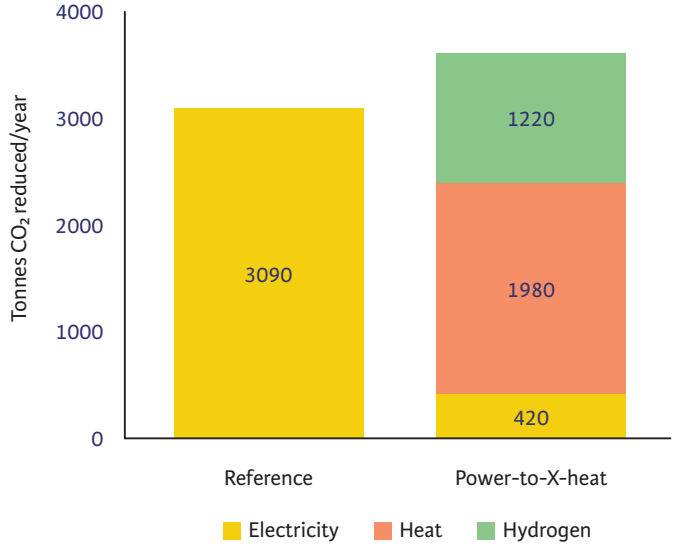

Fig. 2.12 Reduction of CO_2 emissions in a reference scenario where all electricity would be sold to the grid versus the reduced CO_2 emissions in a Power-to-H3 system, split in electricity, heat and hydrogen.

2.5.4 Affordability of the system

2.5.4.1 System costs

The Power-to-H3 system produces four different products; heat, hydrogen, water and electricity. The costs for the system are shown in Table 2.6. These costs include the investments (CAPEX or Capital Expenditure) and the operation and maintenance (OM or OPEX, Operational Expenditure) costs, which also cover the transport of hydrogen and costs for buying electricity from the solar park. The investments in the solar park are excluded from the CAPEX of the Power-to-H3 system because the solar park will be installed independently of the realization of the Power-to-H3 system (as mentioned in section 2.4).

The total CAPEX is 13.7 million euro (M€), of which the heat system represents 53%. Another 33% of the total CAPEX consists of investments in the hydrogen system, and 10% of the CAPEX corresponds to the water system. The OM costs are on average 2% of the total CAPEX, at 280 k€/year. In the breakdown of the OM and transport costs, almost 50% is related to the hydrogen system, mainly because of hydrogen transport. The fuel costs are the cost made for buying electricity from the solar park which add up to 260 k€/year.

Table 2.6 CAPEX and OM of the Power-to-H3 system for a neighborhood.

	Total CAPEX (M€)	OM and Transport (k€/year)	Fuel Cost (k€/year)
Heat production, storage, transport, distribution and delivery	7.4	80	75
Hydrogen production, storage and fuelling	3.2	70	175
Hydrogen fuelling	1.3	110	10[a]
Rainwater capture, storage, pure water production, transport and distribution.	1.3	10	1
Electricity infrastructure within the system	0.5	5	-
Total investments Power-to-H3-system	13.7		
Operation and maintenance per year		280	260

[a] The electricity for the hydrogen fuelling station is bought from the grid at a price of 8 €¢/kWh.

2.5.4.2 Product production costs

In Table 2.6 the total costs as shown in Table 2.7 are broken down per system service. For heat and water, the costs per household are shown based on a neighborhood with 900 households. The current maximum end-user price for heat in the Netherlands is 22.5 €/GJ [157], plus a fixed charge of 252 €/year [137], leading to a selling price of 34 €/GJ based on the yearly heat demand of an average household. The calculated heat price for Power-to-H3 heat is 26 €/GJ, which indicates that heat can be delivered at an affordable price.

For pure water production, the end-user price is set at the average price of around 1.4 € per m^3 drinking water [140]. The actual production cost for pure water 50% higher than the end-user price, as can be seen in Table 2.7. This specific part of the Power-to-H3 system is thus not affordable as an independent system, but within the total system costs, these costs are almost negligible.

For hydrogen, costs per household are not calculated, because the household will not invest in the production of hydrogen and the hydrogen fuelling station directly, but via the hydrogen price. Producing green hydrogen with electrolysis on a 2.5 MW scale leads to production costs of 5.4 €/kg, and transport and fuelling infrastructure add another 3.3 €/kg to the hydrogen costs. The end-user price is currently 10 €/kg, leaving a margin of 1.3 €/kg, which shows that hydrogen can be produced for an affordable price.

A household that has a district heating connection, only drinking water instead of partly demi water and drives a hydrogen car would spend approximately a total of 2,100 €/year on heat (€ 750), water (€ 56) and hydrogen (€ 1,300). A household that is part of a Power-to-H3 system would pay 315 €/year less on system services, as the total costs in Power-to-H3 are 1,785 €/year. Thus, overall the Power-to-H3 system is more affordable than a house with similar facilities without an integrated system approach.

Table 2.7 Cost break-down per production unit for heat, pure water and hydrogen, as well as the total costs per household per year.

Costs are shown per house, except for the production cost	Heat	Pure water	Hydrogen production + Hydrogen transport & fuelling station[a]
Investment costs	8,290 €	1,500 €	-[b]
Operation & Maintenance per year	90 €	10 €	-[b]
Costs for electricity from solar park per year	85 €	1 €	-[b]
Production cost	26 €/GJ	2.1 €/m^3	5.4 €/kg + 3.3 €/ kg = 8.7 €/ kg
Cost per household per year[c]	570 €/y	85 €/y	1,130 €/y

[a] The '+' sign between the values in the columns shows the values for hydrogen production (above the '+') and transport & fuelling (under the '+').
[b] Costs are not shown per house, as the households pay for the hydrogen, and not for the infrastructure itself. Total investment costs for hydrogen are shown in Table 2.6.
[c] Based on the demand of an average household for heat (22 GJ/year), demiwater (40m^3/year) hydrogen (130 kg/year), see also 2.4.

2.5.5 Avoided costs, the economics

As stated before, avoided costs are an essential part of the Power-to-H3 system. In this analysis, we have considered two types of avoided costs; one related to network reinforcement and the other to avoided CO_2 emissions.

The current connection of the site in Nieuwegein where the solar park will be installed is 4 MVA, and with the addition of 8.7 MWp of solar PV, the connection has to be reinforced with an additional 4.7 MVA to assure that all produced solar power can be transported to the grid. By installing the Power-to-H3 system, both the heat pump and the electrolyzer can facilitate peak-shaving at times when the solar output is high. Together, they are able to convert 5 MW of solar power, which results in a lower maximum output power of the solar park (+ Power-to-H3) of 3.7 MVA, see Table 2.8. Thus, the existing connection does not need to be reinforced if a Power-to-H3 system is installed. With average reinforcement costs of 200€/kW (see section 2.3.4) the avoided cost of the Power-to-H3 system at the solar park sum up to € 940,000. This amount is equally divided over hydrogen and heat production and subtracted from the investment cost of the electrolyzer and heat pump respectively.

Table 2.8 Overview of required additional grid connection capacity and costs with Solar PV and with Power-to-H3

Solar Park	Standard situation	With Solar PV	With Power-to-H3
Grid connection – demand (MVA)	4	4	4
Solar PV – supply (MVA)	-	8.7	8.7
Heat pump – demand (MVA)	-	-	-2.5
Electrolyzer – demand (MVA)	-	-	-2.5
Extra connection capacity (MVA)	0	4.7	0
Grid connection costs (k€)	-	940	-
Avoided grid connection costs (k€)	-	-	940

For the neighborhood, a similar grid capacity analysis is shown in Table 2.9. We should either investigate a situation with heat pumps and PV panels on roofs, and compare to a district heating network and PV panels on roofs (which represents PtX). Currently, the average electricity demand of a Dutch household is around 1 kW [156]. When all houses would have enough solar panels to fulfill their electricity demand of 3,000 kWh [158] a household would need approximately 3.4 kWp of solar PV. If all solar PV systems would produce at peak capacity at a time when there is no electricity use, 3.1 MVA of additional grid capacity is required.

If heat pumps with a COP of 1 on a cold winterday [156] would be installed in the neighborhood, this results in an additional 5.4 MVA grid capacity (see Table 2.9). The electricity demand for heat

pumps in winter thus leads to a higher grid load than solar PV would do during summer. Therefore, in a neighborhood without a district heating network (DHN), the additional grid capacity would be around 5.4 MVA. When a Power-to-H3 system is in place, only small booster heat pumps are installed in homes with a maximum capacity of 0.45 MVA. In this situation, the solar PV is the determining factor for grid reinforcement (see section 2.3.4 for an analysis of the grid connection costs). So, in both cases, there is additional capacity required from the grid, but with a Power-to-H3 system including a DHN, about €468,000 is avoided compared to a system with heat pumps installed in homes. This avoided grid reinforcement costs are completely allocated to the heat system of Power-to-H3, because the hydrogen system is of no importance for the grid within the neighborhood.

Table 2.9 Overview of required grid connection capacity and costs in a neighborhood with heat pumps and PV or with a district heating network (DHN) and PV.

Neighborhood	Standard situation	With Heat Pump & PV	With DHN & PV (PtX)
Grid connection – demand (MVA)	0.9	0.9	0.9
Solar PV – supply (MVA)		3.1	3.1
Heat pump – demand (MVA)		5.4	0.45
Extra connection capacity (MVA)	0	5.4	3.1
Grid connection costs (k€)		1,080	612
Avoided grid connection costs (k€)			468

The avoided costs due to reduced CO_2-emissions consist of replacing natural gas with (renewable) heat and gasoline with hydrogen (see section 2.3.3). For both types of avoided costs, the effect on the production cost for heat and hydrogen was investigated, and the results are presented in Table 2.10. If avoided costs could be part of the business case of the Power-to-H3 system, the heat production cost would decrease with 26%, while hydrogen production costs decrease by 20%.

Table 2.10 Results of avoided cost analysis of a Power-to-H3 system in a neighborhood.

	Production cost without avoided costs	Avoided grid reinforce-ment costs	Monetized CO_2 emission reduction	Production cost with all avoided costs	Total reduction of production cost by avoided costs (%)
Heat (€/GJ)	26.0	3.1	3.6	19.3	26
Hydrogen (€/kg)	8.7	0.4	1.3	7.0	20

In addition to the more elaborated sensitivity analysis below, we carried out a sensitivity analysis on the CO_2-price to investigate the effect of a changing CO_2-price on the avoided costs calculati-

ons. The sensitivity of both the heat and hydrogen price is about 2.5% for a change in CO_2-price of 10€/kg. This means that in case the CO_2-price would be 20€/tonne instead of 60€/tonne, the reduction in production costs of heat would be 16% instead of 10%, and for hydrogen 10% instead of 20%.

2.5.6 Sensitivity analysis

For some important parameters, a local sensitivity analysis was carried out. The sensitivity of a certain parameter is shown for three outputs; the production cost of heat, hydrogen or water. In the graphs, the range of effect on the output is cut off at -40% and +40%, which has the implication that the full variation for the discount rate (see ***SI-A*** Table A.4) is not always shown. For every product, the three parameters for which the product price is most sensitive are discussed.

Figure 2.13 shows the sensitivity analysis of the heat production costs. The heat production cost is most sensitive to the number of houses in the neighborhood, as can be seen by the high slope at smaller numbers of houses. The figure also demonstrates that the influence decreases as the number of houses increases. However, even at a higher number of households this parameter has the highest impact on the heat production costs of all evaluated parameters. The space heat demand of a household has the second-largest impact on the heat production price, which indicates that a more exact knowledge of household heat demand is necessary. Thirdly, the heat pump costs influence the heat production cost significantly and therefore it is important to learn more about the cost developments for heat pumps.

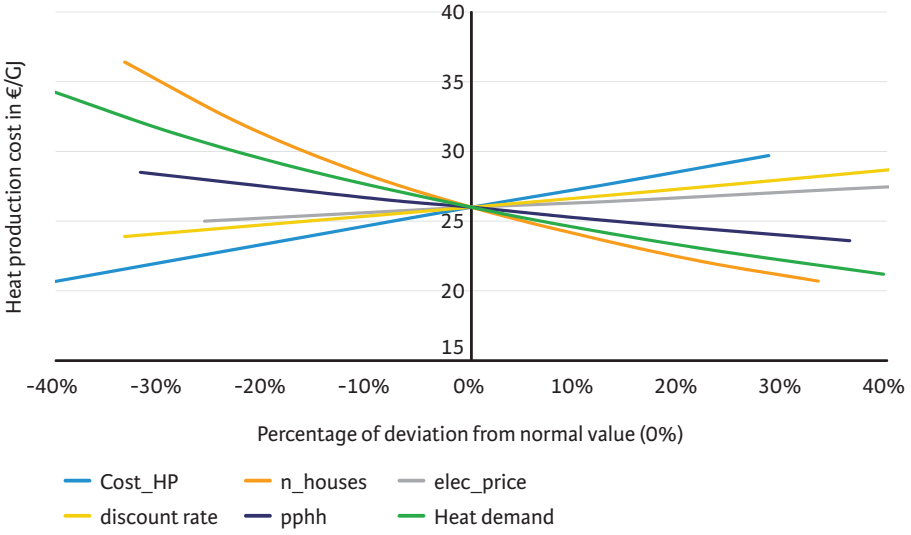

Figure 2.13 Sensitivity analysis on the heat production costs. Cost_HP are the heat pump investment costs, n_houses the number of houses in the neighborhood, elec_price the electricity purchase price from PV and pphh the number of people per household.

For the hydrogen production cost, the sensitivity analysis is shown in Figure 2.14. Based on the slope of the lines in this figure, the energy use of the electrolyzer, which in essence reflects the efficiency, is an important factor that influences the hydrogen production cost. The electrolyzer investment costs are the second most important factor with respect to sensitivity on the hydrogen production price. It is therefore valuable to have more information about learning curves, which will be further discussed in Section 2.6. The electricity price has a significant influence on the hydrogen production costs as well and is clearly more important for hydrogen than for heat. Probably this difference exists because the investment costs for the heat production system are more than 50% higher. This implies that the electricity costs, which are part of the OPEX, have a smaller influence on the heat price than the investment costs.

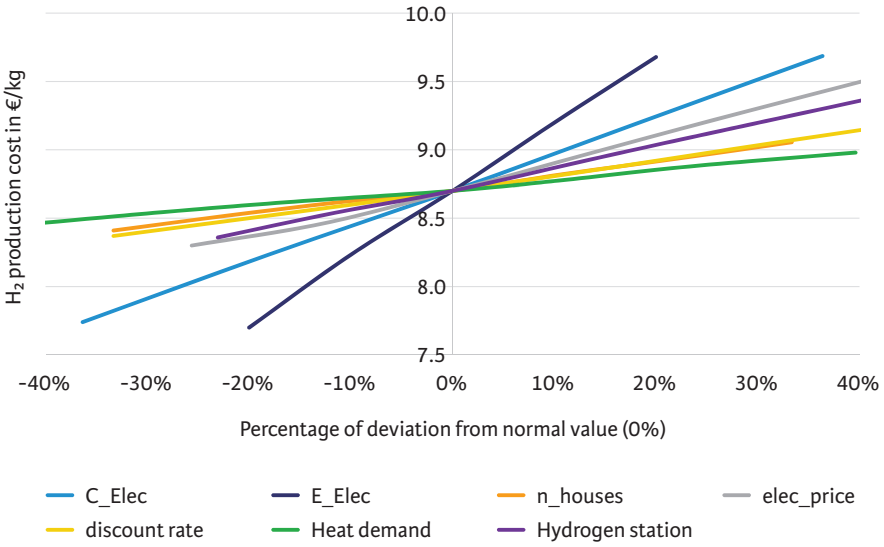

Figure 2.14 Sensitivity analysis on the hydrogen production costs, C_Elec are the investment costs of the electrolyzer, E_Elec the energy use of the electrolyzer, n_houses the number of houses in the neighborhood and elec_price the electricity purchase price from PV.

The most substantial changes in the pure water production price occur due to changes in the number of people per household (pphh), which is shown in Figure 2.15. The number of houses have a considerable effect on the price as well. The discount rate has a moderate influence on the pure water production cost. However, not the complete curve is shown which means the uncertainty is high. To decrease the uncertainty in the pure water production cost, it will be necessary to get more insight into the number of people per household, the number of houses and the discount rate.

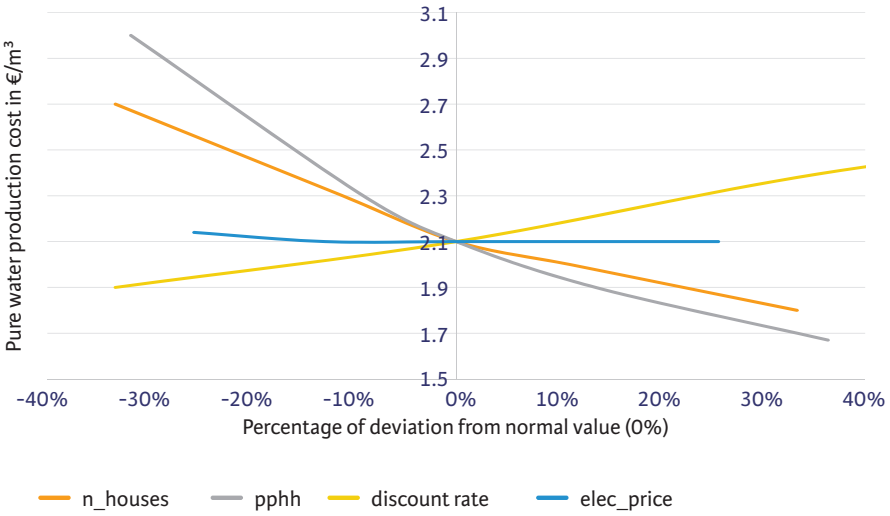

Fig. 2.15 Sensitivity analysis on pure water production costs, with n_houses the number of houses in the neighborhood and pphh the number of people per household.

Overall, most of the chosen parameters seem to have a moderate to large effect on the production cost of heat, hydrogen or water. This means it is important to obtain more information about the exact values of these parameters in further research. Based on the results, below we suggest the priority list in order of importance:

1. Number of houses
2. Energy use electrolyzer
3. Electrolyzer costs
4. Heat pump costs
5. Space heating demand per household
6. People per household
7. Electricity price
8. Hydrogen fuelling station cost
9. Discount rate

2.6 Discussion

2.6.1 The subsurface as a storage medium

Conversion and storage mechanisms are key elements of the proposed Power-to-H3 system. For both heat and (rain)water, the subsurface is chosen as a storage medium. This means that when Power-to-H3 concepts are to be applied in urban areas, multi-purpose use of the subsurface will become increasingly important. On ground level, there is a lot of pressure on the available space and storage applications need a lot of space in general. By utilizing the subsurface, there is almost no impact of the storage system on street level, while still making energy conversion and storage in urban energy areas possible. However, the subsurface is not an empty space. Therefore, there is a need for collaboration with other stakeholders that have an interest in the subsurface, such as drinking water companies that rely on groundwater in the subsurface as a source for drinking water production. Using the subsurface as a way of energy storage thus requires more collaboration between different stakeholders with an interest in the subsurface.

2.6.2 Scenario comparison

Switching priority from heat to hydrogen has a significant effect on the energy balance of the system, as can be seen in Figure 2.16 (full results of the system with hydrogen as a priority can be seen in SI-B). Because the hydrogen demand in the hydrogen priority scenario should always be fulfilled with local hydrogen production, there is a small amount of import from the grid at times when PV generation is low to ensure continuous hydrogen production. This does not occur in the heat as priority scenario, because here hydrogen is bought from third parties when demand cannot be fulfilled with own production. An alternative solution would be long-term hydrogen storage, for which salt caverns are the most feasible option [107]. Currently, a Power-to-H3 neighborhood would rely on small-scale high-pressure hydrogen storage, which is too expensive for seasonal storage. However, when in the coming decades a hydrogen infrastructure is developed, long-term hydrogen storage would become an option.

The production cost for heat will increase from 26 to 27 €/GJ in the hydrogen priority scenario, while the cost for hydrogen production decrease (from 8.7 to 7.9 €/kg) and electricity from the grid is required to fulfil both heat demand and hydrogen demand. The heat production price increases because the heat system has a lower overall efficiency as not enough heat is stored during summer and electricity from the grid is imported at a higher price. The hydrogen production price decreases mainly because of increased hydrogen production, both with electricity from the solar park and (more expensive) electricity from the grid. An increase in the capacity factor of the electrolyzer thus leads to lower costs, even when the electricity price for buying electricity from the grid is higher than from the solar park.

To lower the hydrogen production price and the system costs, it could be an option to install a smaller electrolyzer, so the capacity factor increases while still producing enough hydrogen. Here some optimization could still be done in further research. In addition, there will be different stakeholders involved in both heat and hydrogen production and sales, who will aim at the lowest production cost for their product. This analysis has shown there can be a significant price difference when switching priority from heat to hydrogen. Therefore, a sophisticated control system needs to be developed that is able to control both the heat and hydrogen production in order to optimize the production costs.

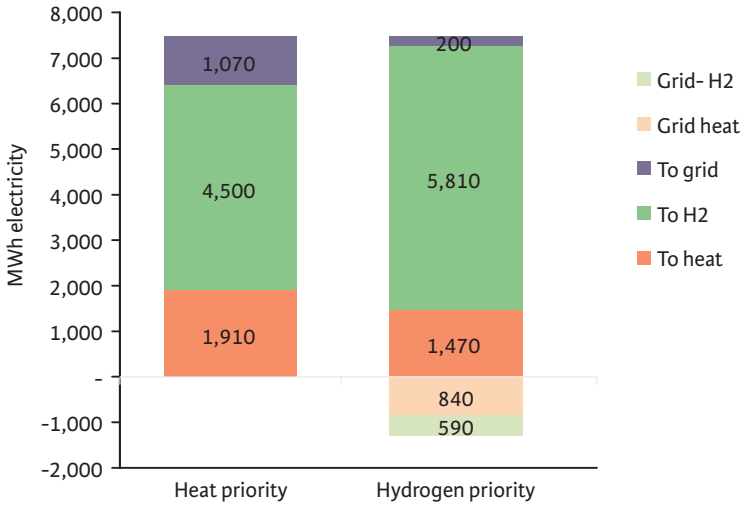

Figure 2.16 Aggregated yearly energy distribution of the Power-to-H3 system with heat and hydrogen as priority, whereby the negative values represent purchase of electricity from the grid.

2.6.3 System size

A sensitivity analysis on the production costs of heat, hydrogen and pure water was carried out, which shows that the number of houses and therefore the heat and water demand have a large impact on the heat price and pure water price. Economies of scale are important for a system like Power-to-H3. A district-heating network requires a large investment, which implies that a certain minimum amount of houses is necessary to obtain a feasible business case.

Next to an economic perspective, from a technical point of view a small heat storage system will be difficult to manage in an optimal way. The relative heat loss will increase with decreasing storage volume, because the surface area of a spherical volume of warm water increases in relation to the volume of the sphere. With small storage volumes, these conduction effects become more apparent [125]. Both from an economic and technical point of view, 900 houses are close to the minimum amount necessary to create a reliable and affordable heat system.

2.6.4 Learning curves and their effects

From the results of the sensitivity analysis, we have seen that the production costs for heat and hydrogen are sensitive to changes in the heat pump and electrolyzer costs, as well as the energy use of the electrolyzer. In the analysis, both higher and lower values were chosen. However, it is expected that investment costs of heat pumps and electrolyzers will mainly decrease because of further development in technology, manufacturing and economies of scale, which will have a positive effect on the business case of both hydrogen and heat. Schmidt et al. stated in an overview paper that the learning rate of alkaline electrolysis for different forms of electrical energy storage is 18% ± 6% [159]. The technology for PEM electrolysis has a higher development rate than alkaline and an expert elicitation study that included different electrolyzer types estimated 8 – 24% decrease in production costs for PEM electrolysis based on R&D funding [160]. Another paper by Saba et al. investigates costs projections over the last thirty years and concludes that the projections for PEM electrolyzer cost are within a range of 397 – 955 €/kW_{el} (HHV) in 2030 [161]. Those projections and calculations clearly show a high level of confidence towards significant price reductions. Besides, developments in hydrogen infrastructure and storage in salt caverns [107] will likely lead to a higher reduction in hydrogen production prices because the costs of storage will decrease.

Data about learning effects of industrial heat pumps are scarce, despite the expected large role of heat pumps in the energy system. There is a twenty-year-old study that focused on household appliances including heat pumps that found a learning curve of 25-42% based on Swiss data [162], but this does not seem to apply for the large scale industrial heat pumps in the Power-to-H3 concept. Recently, another Dutch report estimated a 10% learning rate for heat pumps [163], although they also report a lack of data for a good discussion. A report from the European Heat Pump Association from 2014 pointed out a cost reduction of around 20% in 10 years based on a doubling of the heat pump market, which means a learning rate of 20% [164]. From these studies, it can be concluded that more data is needed to get insight into heat pump learning curves. However, the estimated learning rates lie between 10 and 20%, which indicates a significant potential for a reduction of the heat pump cost.

Learning effects are valid for solar PV as well, with prices decreasing by 80% over the period 2010-2016 and an average learning rate of 35% [106]. The solar electricity price adopted in this chapter is still subsidized, but this will probably change because solar PV will become inexpensive without subsidy. In conclusion, all learning effects are expected to have a positive effect on the affordability of a Power-to-H3 system.

2.6.5 Avoided costs

The analysis of the avoided costs (see section 2.5.5) has shown that avoided costs can have an important role in a Power-to-H3 system with savings on the production cost of heat and hydrogen between 20 and 26%. Currently, only network reinforcement and CO_2 savings were included in the analysis, but other factors such as reduction of air-pollution and reduced risk of CO-poisoning

would be interesting to include in future research. However, even when these effects would be quantified, these avoided costs can not be allocated to the business case.

Even the saved costs on electricity grid extension, which are relatively simple to quantify, can be difficult to include in the business case. In the current Dutch institutional model, the internal costs associated with gas and electricity transport, hence the networks, are fully regulated and allocated to the grid operators (transmission and distribution) but funded by the end users as these services are socialised into the energy tariffs. A Power-to-H3 system will contribute in solving the unbalance between supply and demand on a more local scale and therefore avoids grid extension or redispatch, which means costs are reduced for the grid operators. However, these costs were not planned to be spent yet, and therefore are not easily incorporated in a business case.

The other part of the analysis was on CO_2-emission reduction. There is a market for CO_2-emission allowances, but only for power & heat companies and energy-intensive industry and not (yet) for small scale systems or neighborhoods. Furthermore, the current CO_2 price is not at the level necessary to achieve the goals from the 2015 Paris agreement, which are calculated to be 60€/tonne, which is the value used in this chapter [151]. Therefore, a sensitivity analysis was done which shows that if the CO_2 price would stay at 20 €/tonne, the production costs decrease of heat and hydrogen will still be 10-16%.

To be able to solve the suboptimal allocation of costs and benefits within a Power-to-H3 system, institutional interventions are needed in the form of legal measures like fiscal arrangements, changes in policy and legislation and financial compensation schemes.

2.6.6 Future research and steps to realization

The concept presented in this chapter was verified by a simulation model. As the purpose of this chapter is merely to introduce the concept, the model presently has some simplifications. For example the high-temperature heat storage in this chapter does not include a groundwater flow model. However, the model has a flexible structure and can easily be extended with a more sophisticated groundwater flow model that includes the hydrological dynamics within the subsurface to gain more insight into the subsurface dynamics and heat losses. At the moment, cooling demands have not been included in HT-ATES modeling, but with rising cooling demand due to climate change [165], in future research this could be a relevant addition. Regarding the HT-ATES, field test are carried out to get more insight into the chemical and microbiological changes as well as storage efficiency when heat is stored in aquifers at 40-60 ˚C. The results can lead to a better design of the HT-ATES system as proposed in this chapter. Lastly, this chapter has focused on the conversion and storage system and its costs, but in future research, the concept could be extended by taking into account the PV production by households, as well as investment costs in households for (booster) heat pumps and cars.

Besides model improvements and experiments, the first steps to realization of a Power-to-H3 system are carried out in Nieuwegein, the Netherlands. The first phase of the solar park (3.8 MWp) has been built, a small hydrogen refuelling point is installed, there are ongoing discussions with the local government about the heat storage system and we work towards a more detailed system design. Many of the challenges of the Power-to-H3 system will not be technical but more related to governance and social aspects, such as investigating an organisational form for producing and selling the different products, informing project developers in the neighborhood and try to incorporate the avoided costs in the business case. From our perspective we argue that actual practice is the proof of the socio-economic importance of this research project.

2.7 Conclusions

In this chapter, we present an energy and water system for a neighborhood based on the conversion and storage of heat, hydrogen and water, called 'Power-to-H3'. The results of our modeling have shown that Power-to-H3 is capable of fulfilling the demand for heat, hydrogen and (pure) water in a neighborhood of 900 houses at every hour of the year. The heat storage makes it possible to produce heat (at 65 °C) in summer with solar power and surface water, and deliver it directly to houses (at 50-55 °C) in winter with an overall efficiency of 70%. By capturing rainwater on the solar park and on the roofs, it is possible to fulfil the pure water demand of the households during the year (almost 40,000 m^3), with the aquifer serving as a buffer. On a yearly basis, there is enough hydrogen production to fulfil the demand of 540 fuel cell electric vehicles. Costs for heat production will be 26 €/GJ and 8.7 €/kg for hydrogen under the heat priority scenario and 27 €/GJ for heat and 7.9 €/kg for hydrogen with the hydrogen priority scenario. In both cases, demi water production costs are 2.1 €/m^3. Based on this concept, the modeling results and the discussion, we conclude the following:

- For a case of a neighborhood in Nieuwegein, it is shown that the Power-to-H3 concept is
  - Reliable – demands for heat, transport and (pure) water are fulfilled at every hour of the year.
  - Affordable – Households connected to a Power-to-H3 system spend on average 1300 €/year on heat, transport and water, in comparison to 1785 €/year for household in a neighborhood without an integrated system approach.
  - Clean – completely based on renewable energy, thereby saving 3600 tonnes of CO_2 per year compared to a conventional system and 500 tonnes compared to a system where all renewable electricity would be used as electricity directly.
- In a renewable-based energy system the subsurface will become increasingly important, as a means for energy and water storage to balance demand and supply of intermittent renewable energy sources.

- Future renewable energy systems should focus increasingly on system costs, instead of system efficiency. The economic analysis of the Power-to-H3 system has illustrated that despite the energy losses that belong to the conversion and storage methods described, the system is still affordable.
- The analysis shows the importance of a sophisticated control mechanism for integrated systems as Power-to-H3, because a priority within the distribution of renewable energy for either heat or hydrogen has a significant impact on the business case of these products.
- Further investigation of how avoided costs can be allocated is important. A Power-to-H3 system has impacts on different parts of society and when those effects would be an integral part of the business case, the concept becomes even stronger and more convincing. In this case, it could lead to a 26% in heat production costs and a 20% decrease in hydrogen production costs.

Supplementary information

More background information about the system size, years simulated, weather conditions and supply and demand in the case study can be found in the supplementary information (SI-A). Results of the hydrogen scenario are shown in the SI-B. Both are available via:
https://ars.els-cdn.com/content/image/1-s2.0-S0306261919317118-mmc1.docx

Data

Raw data of the modeling results from the scenarios described in this chapter can be accessed via
https://doi.org/10.4121/22096307

Funding

This activity is co-financed with PPS-funding from the Topconsortia for Knowledge & Innovation (TKI's) of the Ministry of Economic Affairs and Climate. The authors would like to thank the TKI Watertechnology (2016KWR019 or RVO5289) and TKI Urban Energy (TEUE117059) in the Netherlands for their financial contribution to the research projects that form the basis of this publication.

3 The impact of system integration on system costs of a neighborhood energy and water system

" All models are wrong, but some are useful "

George E.P. Box

Abstract: The fossil-based energy system is transitioning towards a renewable energy system. One important aspect is the spatial and temporal mismatch between intermitted supply and continuous demand. To ensure a reliable and affordable energy system, we propose an integrated system approach that integrates electricity production, transport, heating of buildings and water management with a major role for storage and conversion. The minimization of energy transport in such an integrated system indicates the need for local optimization. This study focuses on a comparison between different novel system designs for neighborhood energy and water systems with varying modes of system integration, including all-electric, power-to-heat and power-to-hydrogen. A simulation model is developed to determine the energy and water balance and carry out economic analysis to calculate the system costs of various scenarios. We show that system costs are the lowest in a power-to-X system that combines power-to-heat, seasonal heat storage, and power-to-hydrogen (2070 €/household/year), followed by a scenario that combines a hydrogen boiler and heat pumps for household heating (2175 €/household/year). Scenarios with electricity as the main energy carrier have higher retrofitting costs for buildings (insulation + heat pump), which leads to higher system costs (2320–2370 €/household/year) than more integrated systems. We conclude that diversification in energy carriers can contribute to a smooth transition of existing residential areas.

This chapter is based on the publication:
E. van der Roest, T. Fens, M. Bloemendal, S. Beernink, J. P. van der Hoek, and A. J. M. van Wijk, "The Impact of System Integration on System Costs of a Neighborhood Energy and Water System," Energies, vol. 14, no. 9, p. 2616, May 2021, doi: 10.3390/en14092616.

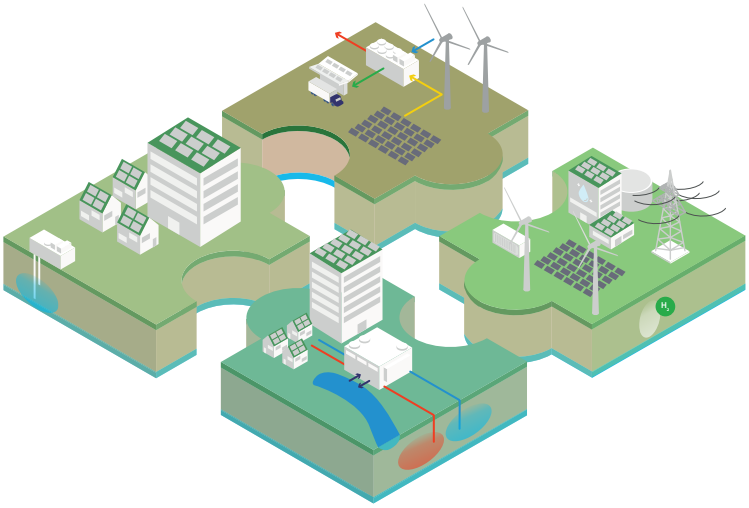

3.1 Introduction

In 2018, modern renewable energy production accounted for 11% of the total world energy consumption [166]; in Europe, it was 18% [167]. The European ambition is to strive towards climate neutrality in 2050 [2]. Our future energy systems will thus be very different from current systems, with clear shifts to intermittent renewable resources [168]. Furthermore, energy systems will become more decentralized and multidirectional, with energy production closer to the energy consumers, especially in the urban environment [169], [170]. More local production reduces the transport of energy and thus reduces the need for reinforcement of the energy infrastructure. These changes come with challenges to keep the system reliable and affordable while increasing the share of clean energy. Energy conversion and storage will be essential to overcome the temporal and spatial mismatch between demand and supply. Hence, there is a need for an integrated energy system. The focus of this chapter is on different designs for integrated energy and water systems for neighborhoods. There is ongoing research into integrated neighborhood energy systems with sector-coupling and decentralized energy production.

The studies from the literature review in **Chapter 1.3** show the potential benefits of integrated systems with various forms sector coupling to overcome the supply and demand mismatches and provide energy in a reliable and affordable way. However, some aspects show potential for further enabling, or better performance, of system integration. We focus on the followings aspects of integrated energy and water systems, based on the knowledge gaps as defined in **Chapter 1.5**:

- Consider 100% renewable systems, so excluding fossil sources, such as natural gas;
- Seasonal heat storage can contribute considerably to the large seasonal, temporal mismatch.
- Taking into account multiple system services in a neighborhood (energy for electricity and heat, transport and water);
- Hydrogen can be used for more purposes than electricity only, as it can also be applied in both the transport sector and for buildings (heating and electricity purposes);

The novelty of our work is thus to consider integrated energy and water systems for existing neighborhoods based on 100% renewable energy, taking into account multiple neighborhood system services and different conversion and storage mechanisms (hydrogen and heat). It is yet to be identified to what extent these aspects contribute to a better performance of the energy- and water system in a neighborhood, both from a technical and economic perspective. This brings us to the central research question:

What is the impact of different modes of system integration on the local energy and water use, energy imports and exports, peaks in demand and supply and system costs for a neighborhood energy and water system?

In this chapter, we evaluate the potential of integrated energy systems by comparing four scenarios with different modes of system integration in an existing neighborhood. Thereby we take into account the aspects mentioned above related to the identified knowledge gaps. One of the main

interests is to assess the impact of these different designs on the local energy use, imports and exports, peak demand and supply and (energy) system costs of the neighborhood. To answer the research question, the simulation model from **Chapter 2** is further developed to allow for systematic assessment of the different modes of system integration. The focus of this chapter is on the energy system, while the contribution of water is done as a first-level approach of supply, demand and storage based on rainwater in the neighborhood.

The modeling methodology is outlined in Section 3.2. In Section 3.3, different modes of neighborhood system integration are described in four scenarios. The scenarios cover a range, starting from one energy carrier (all-electric) towards systems that allow for conversion between electricity, heat and hydrogen. However, this is not an exhaustive list of possibilities; other renewable energy systems are also possible. In Section 3.4 the results of the simulated scenarios are presented and analyzed, followed by a discussion in Section 3.5. Finally, the conclusions are presented in Section 3.6.

3.2 Modeling Methodology

The model described here is an extended version of the Power-to-H3 model that was introduced together with the Power-to-H3 concept in **Chapter 2** [171]. In the current chapter, the different calculations are described in more detail and extended with the energy demands and PV installations of households, electric transport, electricity storage in batteries and fuel cells. Moreover, numerical groundwater modeling for accurate modeling of an HT-ATES system was added. In **Chapter 2**, the temperatures of the HT-ATES were kept constant during the runtime, whereas now they are recalculated on a daily basis, including a decrease in temperature over time. In Figure 3.1, an overview of the different model components and their interactions is shown. On the supply side, rainwater, surface water (for the heat pump), solar PV, wind turbines and the electricity grid are included in the model. Conversion and storage technologies comprise rain water storage and purification, electrolysis, hydrogen storage (tank and salt cavern), fuel cell, industrial heat pump, HT-ATES and a battery. We have chosen to only model central hydrogen storage as it is much cheaper than local (pressurized) hydrogen storage. Heat storage should be done locally, as heat transport over long distances leads to high losses and high costs for heat transport. The HT-ATES system includes a hot and a warm well to supply heat. It could also deliver cold when a third aquifer would be added to the system to create a triplet [124], [172], but this is not covered in this chapter. The neighborhood demands exist of water, transport (either FCEV or BEV), heat (electric, district heating network or hydrogen) and electricity demand for appliances and lighting. Furthermore, the households partially supply themselves with electricity via solar PV on roofs. For the water demand, no specific design choices are made yet on how the water will be used. Some options are elaborated in the discussion. The specific technologies and component sizes that are combined in one system are chosen by the modeler.

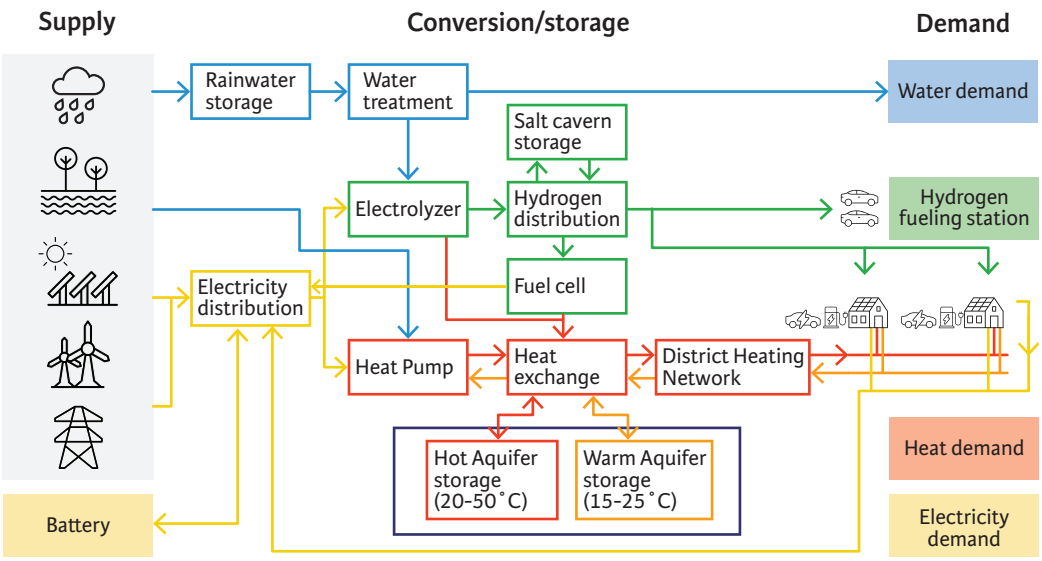

Figure 3.1 Schematic overview of the Power-to-H3 model with all components and interactions. We distinguish a water (blue), electricity (yellow), hydrogen (green) and heat (red/orange) part in the system, with multiple connections between, i.e., water and hydrogen, water and heat, hydrogen and heat and electricity and heat. The demands are focused on the built environment, in which different houses with multiple demands are considered. Energy demands can be fulfilled locally by PV on roofs or a local PV or wind park, but remaining demands can be fulfilled by the grid as well. All model components shown in the figure are described in more detail in the ***supplementary information***.

The model is created in Python and calculates the energy balance hourly for many years of varying weather data (to be chosen by the modeler). The first model step is to distribute the given (yearly) energy demands over time. Then, the supply of rainwater and renewable energy (wind/PV/surface water) are calculated based on geographical weather data. Next, the model tries to match energy supply and demand for every hour during the runtime by applying the different conversion and storage technologies. The different energy flows for supply, demand, conversion and storage result in an energy balance. Lastly, we perform an economic evaluation combining costs data of all technologies with the relevant parameters from the model run, such as the total volume of hydrogen produced and/or the amount of electricity that is exported or imported to/from the electricity grid.

Some important system elements for which a fixed efficiency or factor is used are summarized in Table 3.1. The numbers mentioned are targeted at a near-future scenario (2030) when we expect these types of systems to be economically feasible and mature. In the ***Supplementary Information***, the different model components are described in more detail. This includes system elements not mentioned in Table 3.1 because there is no fixed efficiency to mention (such as rainwater catchment or demand patterns for electricity and heat of households). The economic parameters, such as the investment costs (capital expense or CAPEX), operation and maintenance (OM) and lifetime, are presented in Table 3.2.

Table 3.1 Overview of fixed efficiency parameters in the model. A more elaborate description per system element is included in the Supplementary Information.

System Element	Energy Consumption/Efficiency
Solar PV	Hourly calculation within the model based on HOMER formulas [173], with irradiation and temperature as inputs fixed 10% loss factor (shadow, dust, waste, cables) fixed linear derating factor to 81% of original efficiency over 25 years
Electrolyzer	78.8% efficiency (HHV, 50 kWh/kg, on AC) [107] at 90% load
Industrial heat pump	$COP_{HP} = 0.0028\ (T_{HP,cond} - T_{HP,evap})^2 - 0.3276\ \ T_{HP,cond} - T_{HP,evap} + 13.021$ [133]
House heat pump	Air sourced: $COP_{ASHP} = 6.08 - 0.09 \cdot \ T_{out} - T_{in}\ + 0.0005\ \ T_{out} - T_{in}{}^2$ [174] Water sourced: $COP_{WSHP} = 9.97 - 0.02 \cdot (T_{out} - T_{in}) + 0.0012\ (T_{out} - T_{in})^2$ [174]
H_2 boiler	98% efficiency (HHV)
Heat exchanger	Fixed heat loss of 1.5 °C
Fuel cell	60% efficiency—(HHV)
Rainwater storage	70% recovery efficiency [175]
HT ATES	Input temperature warm well 50 °C Hydrological model (see *Supplementary information Section 3.3*) to determine the efficiency
District heating network (DHN)	2% energy use for pumping, heat loss determined per hour (see *Supplementary Information Section 4.2*)
Battery	95% one-way efficiency [109], [176] 25% (4C) charge/discharge rate [176] max 90% depth of discharge (DOD)
Electricity grid	98% AC/DC conversion
BEV charging	90.7% charging efficiency [177]

Table 3.2 Economic component parameters used in the model.

	CAPEX	Lifetime	OM Cost (% of Investment Cost Unless Stated Otherwise)
Neighborhood systems			
PV panels (park)	600 €/kWp [178]–[180]	25	1.5%
Battery storage	300.000 €/MWh [a] [109], [176]	12 (4000 cycles) [109]	1%
Electrolyzer	500 €/kW [177], [181], [182]	20 [177]	2% [177]
Fuel cell (stationary)	500 €/kW [b] [107], [181], [183]	15 [183], [184]	2%
Heat pump	400 €/kW_{th} [c] [183], [185], [186]	20 [183]	1% [183]
Heat storage system	0.1 €/kWh_{th} [76]	40 [171]	1.5% [171]
District heating network [d]	6000 €/house [187]	40	2% [142]
Grid reinforcement [e]	862 €/kW [188]	40	1%
Household systems			
PV panels (roof)	870 €/kWp [183]	25	1.2% [183]
Air-sourced heat pump [f]	6000 €/house [188]	15	2%
Booster heat pump [g]	1000 €/house [189]	15	2%
Hybrid heat pump, including boiler	4300 €/house [188]	15	2%
Adjustments gas network for hydrogen + new gas meter	373 €/house [190]	40	274 €/y/house [h] [191], [192]
Electricity grid costs			308 €/y/house [i] [191]
Renovation costs—D-C [j] (13% energy savings) Apartment/terraced	2940/4680 €/house [188]	40	-
Renovation costs—D-B [j] (20% energy savings) Apartment/terraced	4560/9600 €/house [188]	40	-
Renovation costs—D-A [j] (34% energy savings) Apartment/terraced	7320/19,200 €/house [188]	40	-

[a] Projected battery costs by IRENA for 2030 are 150 €/kWh, but it is unclear if this includes power conversion and balance of plant. Therefore, the IRENA value was used as capital costs for energy capacity, while on top of that, data from Mongird et al. [176] were used to make sure to include power conversion, the balance of plant and construction and commissioning. As Mongird et al. only give values for 2025, we have used the lower range values to estimate the costs for 2030. [b] sources range from 425–1500 €/kW for stationary systems, but fuel cell systems for cars have much

lower price expectations (250–300 €/kW [193]). We expect that developments in the transport sector will also reduce the costs for stationary systems and have used lower range value here. [c] The cost for the heat pump is based on multiple sources and supplier data. The heat pump capacity in kW_{th} is calculated by multiplying the electric capacity (in kW_{el}) with the average COP of the heat pump over a run time. The costs include installation costs (which are approximately 50% of the investment cost). [d] Costs for the DNH itself plus household installations for an outer city area. The OM costs mentioned in the source are actually 1%, but in this chapter, we look specifically at a low-temperature DHN with insulated pipes that probably needs more maintenance, and therefore, we have multiplied this value by a factor of two. [e] This includes costs for the low voltage grid (= distribution grid) up until the transformer station to the high voltage grid (=transmission grid), but no costs for the transmission grid itself because this study focuses on local optimization and makes no concrete assumptions for the changes in the transmission grid. [f] Currently these costs are around 8000€/house, but we expect a cost decrease of 25% due to learning effects by upscaling in production. [g] Included a 50% cost reduction to extrapolate to 2030 because, in 2020, it is still relatively new technology, so a large economy of scale effect is expected. [h] These costs are based on the current fixed yearly costs for gas consumers, about 68 + 186 = 254 €/y [191] + extra costs concerning the expected changes in the inspection regime when switching to a hydrogen of 20 €/y [190]. [i] Fixed costs for an electricity grid connection for consumers per year. [j] Costs for insulation are based on gas demand related to energy labels for apartments and terraced houses in the Netherlands (2018) [194]. The gas demand is converted to space heating energy demand through a correction for cooking gas, domestic hot water and the average efficiency of the boiler [195] (p. 52/53) and finally the% of gas savings when renovating to a higher energy label (Dutch terminology for savings on building energy use). An A-label house is comparable to what many European countries would classify a nearly zero energy building with an energy consumption between 45 and 70 kWh/m^2 [196]. The costs for retrofitting are calculated based on the average surface area of the house [188] (p. 71). Insulation requires no maintenance, so no OM percentage is included.

3.2.1 Rule-Based Scheduling Strategy

The size of system components is not set by an algorithm within the model but is defined by the user. For the calculations and scenarios in this chapter, the following scheduling strategy is in place to decide how supply and demand are connected within the model. If certain system components are not part of a scenario, they are skipped in the scheduling strategy.

Electricity supply from PV on houses is first used within the house itself (for appliances, lighting, heat pump and/or BEV), then it is evaluated whether an excess of PV electricity in some houses (i.e., a terraced house) could be used to fulfill the demand in others (i.e., in a multi-apartment building with a shared roof). The next evaluation is whether the industrial heat pump (coupled with the HT-ATES) could take up electricity, followed by the electrolyzer. The heat pump is prioritized in the scheduling strategy because it needs to produce enough heat for the heat storage system to provide heat in winter. There is a cap on the amount of heat stored based on the yearly heat demand plus a loss factor, explained in ***Supplementary Information Section 3.3***. Hydrogen can also be imported from outside the system and thus has less priority. If after the houses, industrial heat pump and electrolyzer, any electricity are left, it is stored in the (collective) battery, and when this is not possible, the electricity is exported to the grid.

The electricity supply from local RES production (PV park or wind turbines) is first used by the industrial heat pump coupled to the heat storage system, followed by the electrolyzer. For this part of the supply, the collective installations are prioritized in the scheduling strategy because it is assumed that those installations will be placed close to the local RES production and can, therefore, reduce peaks in that part of the grid. Subsequently, it is evaluated whether the households still have an electricity need, followed by storage in the battery. Lastly, any surplus electricity is exported to the grid.

To fulfill an electricity demand, the prioritization is reversed. Hence, a household electricity demand is first fulfilled by their own PV system, followed by local RES production, then the battery and the fuel cell. Finally, when the electricity demand is not yet fulfilled, electricity is imported from the grid. The modeler can choose if the fuel cell functions as a peak shaver (only when the grid has not enough capacity) or more as a baseload, always fulfilling any leftover electricity needs up until its full capacity. The heat from the electrolyzer and fuel cell is only reused when a district heating network (DHN) is in place. In that case, the heat is first used to fulfill any direct heat demand. Any heat that cannot be used directly is stored in the HT-ATES system. In system designs without a DHN or HT-ATES, the heat is denoted as heat loss.

If a heat pump is installed and needs the energy to heat up water from the hot well of the heat storage system during winter (see ***Supplementary Information Section 3.3***), it is first evaluated whether it could be fulfilled by the local RES production, followed by a possible surplus of the PV systems on the households. If energy demand is still not fulfilled, it is evaluated whether electricity is still stored in the battery or if electricity can be produced by the fuel cell. Any leftover demand is fulfilled by import from the electricity grid. Hydrogen production is always exported to the hydrogen gas grid, and hydrogen supply is fulfilled by the hydrogen gas grid. If a DHN is in place, heat demand is fulfilled first with heat from the electrolyzer or fuel cell (if available), then by direct production from the heat pump (if available) and otherwise from the HT-ATES.

3.2.2 Economic Calculations

Costs are defined here as system costs, represented as the costs per household per year that include costs for electricity, heat and transport. In the cost calculations, the levelized costs per system component (LC) are determined according to equation 3.1:

$$LC_i = \alpha \cdot CAPEX_i + OM_i + \sum_{0}^{8760} Ecost_i \tag{3.1}$$

here LC_i represents the annual levelized costs for a certain system component in (€/year). Here the $CAPEX_i$ (€) covers the capital expenditures for a particular system component I (i.e., the PV panels, the electrolyzer, compressor or storage tank) and OM_i (€/year) represent the operational expenditures for a particular system component. $Ecost_i$ (€/year) are the electricity costs for a system component i. The capital recovery factor (α, no unit) in equation 3.2 represents a fraction of the total CAPEX cost. In this way, a constant yearly value of depreciation is calculated based on the lifetime of the system component and the discount rate.

$$\alpha = \frac{r}{1 - (1+r)^{-L_i}} \tag{3.2}$$

With *r* the discount rate (as a fraction of 1) and L_i (year), the lifetime of a particular system component *i*.

The costs per household per year (HC) are then calculated according to equation 3.3 by dividing the sum of the yearly cost of all system components by the number of households in the neighborhood:

$$HC = \frac{\sum_{i=1}^{n} LC_i}{N_{households}} \tag{3.3}$$

A complete overview of all economic parameters per system component and some general economic parameters are given in Table 3.2 an Table 3.3. All costs mentioned here are for the near future (2030). We have excluded investment costs in vehicles (BEV/FCEV) as we expect these costs to become similar to fossil-fuel cars [107] and will be similar for all scenarios.

Table 3.3 Other relevant economic parameters.

Parameter	Value
Discount Rate [a]	3% [147]
Grid electricity costs 2030 (100% renewable) [b]	115 (70–145) €/MWh [197]
Feed-in tariff [c]	57 €/MWh [198]
Extra infrastructure for peak capacity in all-electric scenario [d]	All electric: 5 €/MWh [197]
Hydrogen import costs [e]	Production: 2.5 €/kg (1.5–3.5 €/kg) [107], [182], [192], [199] Storage: 0.2 €/kg [200] Transport: 0.39 €/kg for 3000 km (0.09–0.17 €/kg for 1000 km) [199] Total: 3.09 €/kg (1.8–4.55 €/kg)

[a] We assume one discount rate for the total system, while in reality, the discount rate will differ depending on if the investment is done by a household (i.e., household PV system) or a company (i.e., a district heating network). Here we look at the societal costs, and therefore, we have used a social discount rate. [b] The assumption made here is that the electricity used in the system is climate neutral. It includes costs for production, transport, distribution and extra grid cost (due to more complex balancing in a 100% renewable energy system). The range chosen by PBL is 70–145 €/MWh for 2030, with an average of 115 €/MWh for smaller users (<50 MWh/year). [c] Cuts on feed-in tariffs have occurred globally for utility-scale systems [201], and with still decreasing costs for PV, feed-in tariffs for individual home power systems are being reduced as well, at least in western countries. We expect a phase-out of the feed-in tariff, and therefore, we have chosen a feed-in tariff equivalent to the expected market price for renewable electricity in 2030 [198]. [d] Due to more complex system balancing in an all-electric system, extra overhead costs (for balancing the grid) are estimated at 5 €/MWh [197]. [e] The hydrogen storage costs are a calculation for ten storage cycles (so closer to seasonal storage than daily storage), based on the cost numbers given in Roobeek et al. (2020) [200]. We do not know exactly where the imported hydrogen will come from, but assuming a distance of 3000 km allows for import by pipeline from North Africa, Ukraine [182] or southern Europe, regions with favorable climates for wind and solar power and low hydrogen production costs.

3.3 Neighborhood Scenarios

The neighborhood presented here is based on an actual neighborhood in Nieuwegein, the Netherlands, but modified for generalization. The amount of houses (2000) corresponds to an average European neighborhood as defined in earlier research into a transport and energy system for a neighborhood [59] and is close to an average Dutch neighborhood as well [202]. The neighborhood has an electricity infrastructure, water and wastewater distribution network and a natural gas network. Because 95% of the Dutch households are heated by natural gas [203], we assume that a district heating network is not yet in place in this neighborhood, but the density of the housing stock is high enough to install one. We only consider the energy use of houses in the neighborhood and not nonresidential energy use. Furthermore, it is assumed that every household owns a car.

The reference situation of the neighborhood is shown in Figure 3.2. The buildings were built during 1975–1991 with 50% apartment buildings and 50% terraced houses. The annual gas demand is calculated with 31.65 MJ/m^3 natural gas, which is the average value for the low-caloric gas used in the Netherlands. For an apartment, the annual gas demand is 1020 m^3 (9 GWh for 1000 apartments) and 1350 m^3 (11.9 GWh for 1000 terraced houses) for a terraced house, including space heating, tap water and cooking [158]. We have used data on average gas use to determine the peak in gas demand [204] and used a boiler efficiency of 1.0 based on the house types [195, p. 53]. For 2000 houses, this results in average hourly peak demand for gas of 980 m^3 or 9.8 $MW_{p,-gas}$ with an average peak demand per household of 4.9 $kW_{p,-gas}$. The electricity demand is set at 3000 kWh/household/year for a terraced home and 2400 kWh for an apartment, based on various data on Dutch house types and building years [158], [191]. Average electricity demand patterns were used to divide the electricity demand over the year (see ***Supplementary Information Section 5.3.1*** and [204]). By using these patterns, the average peak demand for electricity per household is 0.66 $kW_{p\text{-}elec}$.

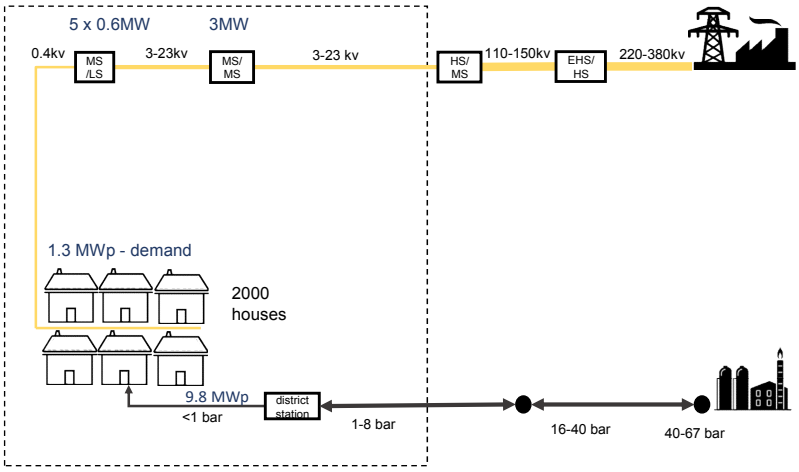

Figure 3.2 Schematic overview of the reference scenario without local renewable production, conversion and storage and with a gas grid for heating demand. This reference scenario has non-renewable electricity and natural gas as their energy sources. The energy demands are based on an existing neighborhood with 50% terraced houses and 50% apartments without solar PV. The houses have not yet been retrofitted and/or insulated.

The average peak capacity that the grid operators use for existing neighborhoods is 1.2 kW per household [188], [205]. This means that when considering the simultaneity factor for a neighborhood of more than 1000 households, the average peak capacity available per household in a low-medium voltage grid station is 1.2 kW. We assume that some extra capacity is available in a substation that connects the low voltage grid to the medium voltage grid. Therefore, we have assumed that for a neighborhood of 2000 households, 3 MW of capacity is available at the station (1.5 kW average peak capacity per household). The electricity peak demand that we calculated for the reference situation (0.66 $kW_{p\text{-}elec}$) of the neighborhood is almost a factor two lower than the value used by the grid operators. A possible explanation is using hourly (average) data, which means that peaks that occur on a shorter time interval within are flattened out. This flattening effect is more apparent for the electricity demand patterns than for gas, as electrical appliances have a more intermittent use pattern (water cooker, vacuum cleaner) than a gas boiler. It is important to be aware of this in the further analysis as the peaks in electricity demand and supply will probably be a conservative estimation.

With the reference situation of the neighborhood (Figure 3.2) as a starting point, we created four scenarios based on 100% renewable energy sources. Renewable energy is supplied by own decentralized PV on roofs, a small PV park, or via the electricity grid. We have summarized the most important data about the neighborhood in Table 3.4. In the reference situation, the houses have energy label D, but retrofitting to a higher energy label is possible to reduce the energy demand for space heating, as specified in Table 3.4. Energy demand for domestic hot water is set at 920 kWh/person/year (=3.3 GJ), which is based on different building types and domestic hot water demands [195]. Because electric cooking is not a common practice yet in the Netherlands, we included 175 kWh/household/year for electric cooking on top of the average electricity demand for appliances and lighting [206]. All roofs are equipped with solar panels of 400 Wp, 12 panels on a terraced home (S-W, 45° inclination) and two panels (S, 36° inclination) per household on an apartment building. Additionally, there is a PV park near the neighborhood of 2 MWp, again with 400 Wp panels (S, 15° inclination). Wind turbines are not included in the scenarios as wind turbines are not likely to be placed in or very close to existing neighborhoods. For transport, we assume that 70% of the houses have an electric car and 30% a hydrogen car. A BEV or FCEV drives 13,000 km per year [207] (average NL). With an energy consumption of 20 kWh/100 km, the energy consumption is 2600 kWh/BEV/year [208]–[210], or 110 kg of hydrogen for an FCEV with 60% fuel cell efficiency. For the BEV, we assume they charge 60% of the time at home.

Table 3.4 Energy demands and supply in the neighborhood.

	Terraced	Apartment	Total
Number of houses	1000	1000	2000
Surface area per house	120 m^2	60 m^2	-
People per household	2.4	2	-
Solar panels on the roof	4.8 kWp	0.8 kWp (shared roof)	5.6 MWp roof PV
Local PV park	-	-	2 MWp
Energy demand domestic hot water	2200 kWh/year	1840 kWh/year	4 GWh/year
Space heat demand [a]	A—5590 kWh/year B—6770 kWh/year C—7365 kWh/year D—8465 kWh/year	A—4045 kWh/year B—4900 kWh/year C—5330 kWh/year D—6130 kWh/year	A—9.6 GWh/year B—11.7 GWh/year C—12.7 GWh/year D—14.6 GWh/year
Electricity demand (including electric cooking)	3000 kWh/year + 175 kWh/year cooking	2400 kWh/year + 175 kWh/year cooking	5.4 GWh/year
Transport	BEV—2600 kWh/year FCEV—110 kg/year (4.333 kWh/year—HHV based)	BEV—2600 kWh/year FCEV—110 kg/year (4.333 kWh/year—HHV based)	BEV: FCEV = 70/30: Electric cars—3.6 GWh/year (of, which 2.2 GWh/year at home charging) Hydrogen cars—66 tons H_2–2.6 GWh/year

[a] The letters refer to a specific energy label (A–D). An A-label house is comparable to what many European countries would classify a nearly zero energy building with an energy consumption between 45 and 70 kWh/m^2 [196]. The space heat demand is based on a gas demand for a terraced house or apartment build between 1975 and 1991 in the Netherlands with energy label D [194]. From this number, the energy demand for space heating is derived with a correction for cooking gas, and domestic hot water and the average boiler efficiency [195] and then the energy demand is reduced by a certain percentage [188] related to insulating a house to obtain a higher energy label.

For weather data, such as irradiation, wind speed, precipitation and temperature, we consider a northwest European climate. Data from the central weather station De Bilt of the Dutch Meteorological Institute (KNMI) is used [211]. Simulation time is five years (2010–2015) to consider yearly variation in weather conditions. This period is representative in terms of average temperature (with both warmer and colder years than average). A representative point for a peak in heat demand by households was the especially cold period in February 2012 when the temperature decreased to −18 °C. There is enough variation between dry, wet and normal years for precipitation. The period was sunnier than the long-term average, leading to a slight overestimation of the produced solar energy. However, every year since 1999 has been sunnier than the long-term average, which points in the direction of a trend to a sunnier climate in the Netherlands for the future and as we look at the year 2030, we do think the irradiation data are representative.

For surface water temperatures, 10-min data from Rijkswaterstaat [212] are available for the Lekkanaal (in Nieuwegein) and averaged to produce hourly values. If data are missing, data from the last hour are repeatedly used until data appear again. In general, this period is no longer than a couple of 10-min time intervals.

3.3.1 Design Choices

The focus of this chapter is to analyze different designs with varying modes of system integration within a neighborhood, which leads to a different choice and sizing of conversion and storage technologies. We strive to use as much energy locally as possible while there still is a connection to the electricity and/or gas grid. We have chosen four scenarios that represent different modes of system integration, yet other scenarios would be possible as well. The designs presented here are either a well-known option (all-electric) or designs including techniques that we have identified as gaps in the literature (see Section 3.1) and/or integrate more different energy carriers. A high-temperature district heating network (>70 °C) is not considered because it is not yet in place and high-temperature heat sources are not locally available. Low-temperature ATES systems (15–20 °C) are not considered here as well, as these houses have no cold demand. For thermal heat storage, we have chosen an HT-ATES system. We did not include hot water tank storage, which has been done in other literature [34], [69], [77], because tanks do not provide enough storage volume for seasonal storage. Pit thermal energy storage could have been another option, but free space is needed to install the structure in the subsurface, which is not easily available in existing neighborhoods. If the PV park is installed close to the neighborhood (<2 km, to avoid heat losses) on a free space, such as a meadow, it could be possible to install a pit thermal energy storage system under the PV park. With an HT-ATES system, the necessary above-ground space to drill, install and operate the wells is relatively small, while the system has a sufficient size to function as a seasonal energy storage system, and the investment costs are relatively low. A completely hydrogen-based system for space heating and tap water or fuel cells in houses are other possible options to include in the design, but for now, we have chosen to have one scenario with partly hydrogen-based heating demand. Thus, the scenarios chosen are mainly an illustration of a line of reasoning and do not show results for all possible 100% renewable energy system designs.

Another aspect is that the storage and conversion of renewable energy outside the neighborhood will not be modeled (outside highlighted area in Figure 3.3-Figure 3.6). These storage mechanisms are larger than necessary for a neighborhood and generally used by a whole region or country. They are placed at central locations outside the neighborhood and are, therefore, outside the scope of this research. We do not know yet how storage and conversion in the system on an (inter)national scale will be designed. Instead of modeling the (inter)national energy system with many assumptions and high uncertainties, we have chosen to represent the possible options by including a range of prices for the import of electricity and/or hydrogen. In this way, we will be able to get insights on when system integration on a local level can be beneficial concerning the price developments in the overall energy system. We do, however, assume a 100% renewable-based energy system, which does also imply that only green hydrogen is imported.

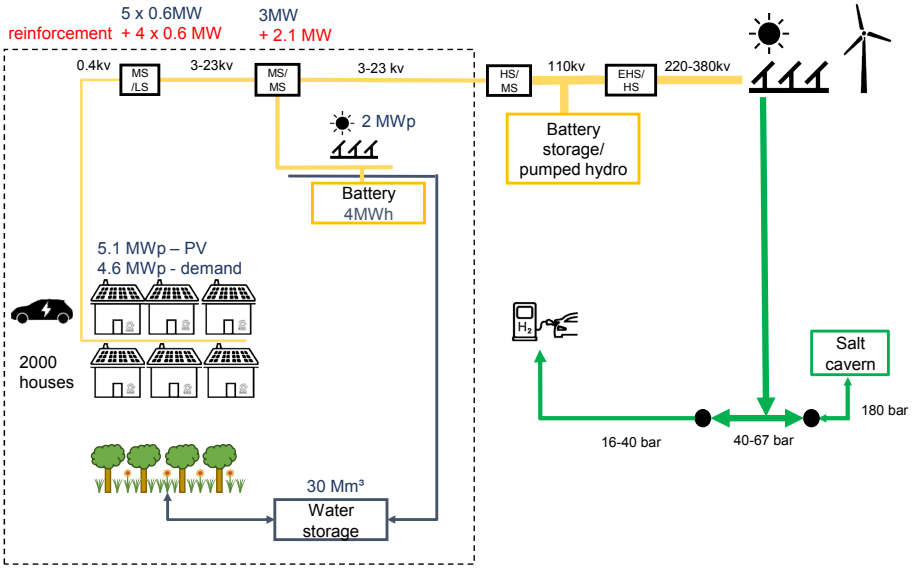

Figure 3.3 Schematic overview of the all-electric scenario with the respective supply and storage capacities. This scenario is based on 100% renewable electricity, either from local PV production on roofs or the local solar park or imported from large-scale renewable capacity via the electricity grid. The houses are retrofitted from label D to label A. The system boundary is shown with a dotted line. Outside of the system boundary, we do not model the electricity production, conversion and storage. However, we assume both electricity storage (in the form of batteries or pumped hydro) and hydrogen storage (via electrolysis) in salt caverns are included in the larger energy system. Because of the local PV production and electricity demands for, i.e., heat pumps, the original grid capacity of 3 MW is not sufficient anymore for this neighborhood. The red numbers with the plus sign represent the grid reinforcement that is necessary for this scenario. Inverters are not shown in this picture but are necessary for the transformation of DC to AC electricity.

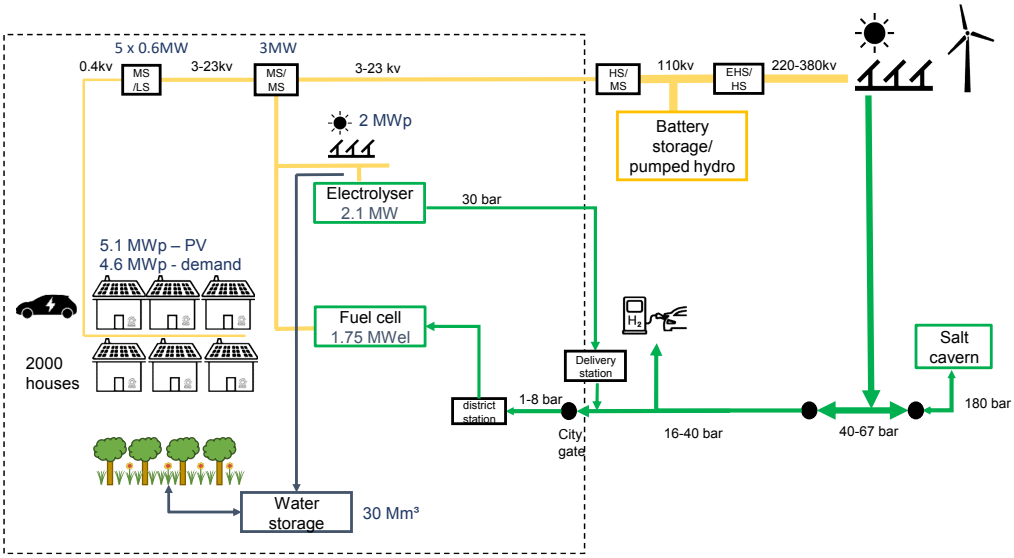

Figure 3.4 Schematic overview of the all-electric H_2 scenario that includes both an electrolyzer and fuel cell for local hydrogen production and uses while preventing grid reinforcement. The electricity supply by PV and electricity

demand is the same as in the all-electric scenario (Figure 3), but instead of grid reinforcement, an electrolyzer (2.1 MW_{el}) shaves peaks in electricity export. On the other hand, the fuel cell has a sufficient capacity (1.75 MW_{el}) to shave demand peaks, thereby avoiding grid reinforcement. The houses are retrofitted from label D to label A. The fuel cell is utilized as a baseload installation in the system. The fuel cell would have a very low usage otherwise (0.3% of the year). This scenario will import more hydrogen than electricity, so the effect of large amounts of hydrogen import can be assessed.

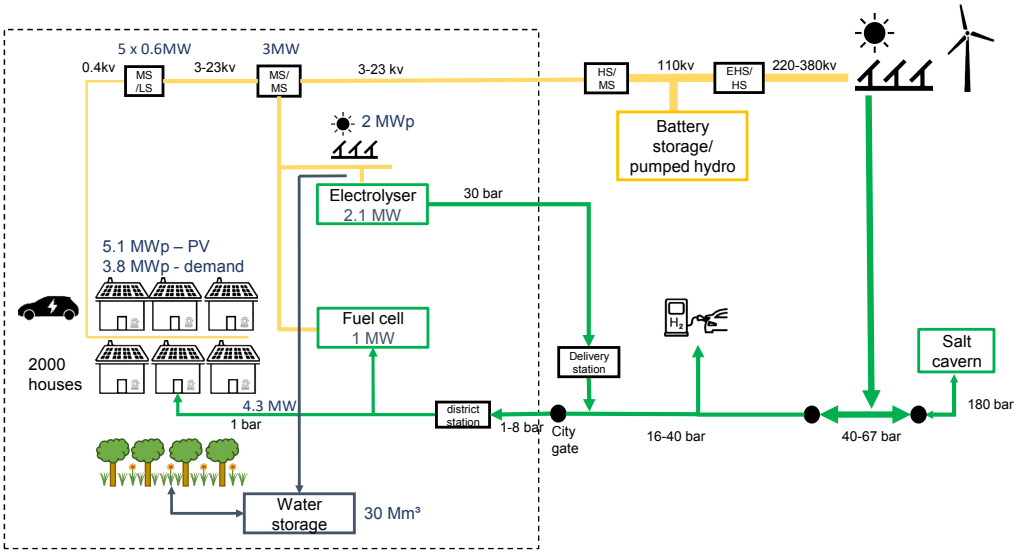

Figure 3.5 Schematic overview of the H_2 hybrid scenario with power-to-hydrogen and using hydrogen for household heating demand. The electrolyzer (2.1 MW_{el}) is utilized for peak shaving on the supply side (PV on roofs and the local PV park). The houses are retrofitted to a lesser extend (label C) than in the all-electric scenarios (see Table 3.4), which results in higher heating demands. In this scenario, we have chosen to fulfill the heating demand with hybrid heat pumps with hydrogen boilers. The hydrogen boilers assist the heat pump at cold periods (< - 5 °C), and for tap water production, so the houses are heated comfortably while demand peaks are reduced. The remainder of the electricity demand peak (3.8 MW_{el}) is shaved by the 1 MW_{el} fuel cell, preventing grid reinforcement.

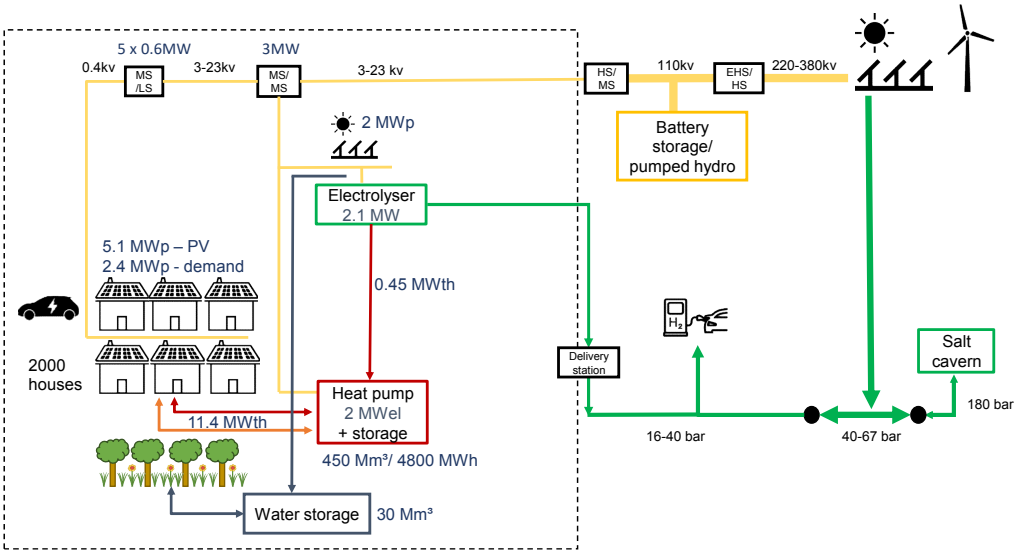

Figure 3.6 Schematic overview of the power-to-X scenario with both power-to-heat and power-to-hydrogen combined, including using heat from the electrolyzer for the heat storage system. The houses are retrofitted from label D to label B. The electricity supply peaks are shaved by the electrolyzer (2.1 MW_{el}) and the heat pump (2 MW_{el}). The heat pump produces heat in summer with surface water as a heat source and stores heat locally in aquifers (HT-ATES). The heating demand of the houses is fulfilled by a low-temperature district heating network (40 °C), with booster heat pumps for tap water production.

We now discuss the differences between the system designs of the scenarios. The general scheduling strategy is applied to all scenarios (see 3.2.1), and only deviations are mentioned. Energy demand and supply parameters are mentioned if they are not yet included in Table 3.4.

3.3.2 All-Electric

The first scenario takes an all-electric approach and has no local conversion techniques in place (Figure 3.2). It represents a reference model for a renewable energy system in a neighborhood based on complete electrification, so with one energy carrier and limited system integration. It does have a local battery of 4 MWh to increase the amount of locally used energy within the neighborhood. In this scenario, the houses need to be retrofitted thoroughly (from label D to label A) to provide both space heating and domestic hot water with air sourced heat pumps. The maximum peak demand in this scenario will be 4.6 MWp, and the supply peak is 5.1 MWp, which means there is a need for grid reinforcement because the electricity demand and supply peak are higher than the current grid capacity (3 MW), mainly due to the heat pumps and PV systems. The battery will not be able to reduce this peak capacity because it is empty when the demand peak occurs (in the early morning hours during winter) and full when the supply peak occurs (in summer at the middle of the day).

3.3.3 All-Electric H_2

In this mode of system integration, we introduce power-to-hydrogen for peak shaving of locally produced electricity. Simultaneously, there is the option to produce electricity from hydrogen with a fuel cell to provide a part of the electricity demand. Concerning the scheduling strategy, we have chosen to deploy the fuel cell as a baseload in the system. This means that the fuel cell is first used to produce electricity before electricity is imported from the grid. Hydrogen import is thus favored over electricity import here because only installing a fuel cell as a demand peak shave unit results in a very low usage (ca. 0.3% of the year), resulting in high OPEX costs that could be reduced by increasing the number of full load hours. Therefore, we will be able to investigate the effect of importing large amounts of hydrogen in a neighborhood on system costs. The battery is removed in this scenario because the electrolyzer and fuel cell takes over its function. The size of both the electrolyzer (2.1 MW) and fuel cell (1.75 MW_{el}) are chosen such that grid reinforcement is no longer necessary. The houses still need to be very well insulated (label A).

3.3.4 H_2 Hybrid

In 95% of the (existing) neighborhoods in the Netherlands, there is a natural gas network [188]. It could be an option to reuse the existing gas infrastructure for hydrogen [192], [213], further explored in this scenario. It is thus again a form of power-to-hydrogen, like the all-electric H_2 scenario. In this mode, we use hydrogen directly as an energy carrier in the house itself. We look at a combination of a hybrid heat pump with hydrogen as a backup for cold periods (< −5 °C) when the heat pump has a low-efficiency, and for domestic hot water production. This hybrid design benefits from the high-efficiency of the heat pump, without the need for electricity grid reinforcement because the hydrogen boiler can take over at times of peak demand. Because the hydrogen boiler can assist the heat pump in creating the necessary heat at a higher temperature, the houses are retrofitted to a lesser extent than the all-electric scenarios (label C). This does however mean that the total heat demand is higher than for the all-electric and all-electric H_2 scenario (see Table 3.4).

Similar to the all-electric H_2 scenario, we have included local hydrogen production with an electrolyzer (2.1 MW) to reduce the supply peaks and a fuel cell (1 MW_{el}) for reduction of the demand peaks (max. 3.8 MWp). The fuel cell is again used as baseload; see in Section 3.3.3 for a justification.

3.3.5 Power-to-X

In this mode, we include both power-to-heat and power-to-hydrogen. There is a synergy between those two conversion mechanisms as the heat from the electrolyzer can be used for the district heating system and heat storage. The houses are retrofitted from label D to label B. Household heating is provided with a low-temperature district heating network (40 °C). Moreover, small booster heat pumps are installed with a capacity of about 0.5 kW_{el}/2 kW_{th} to produce domestic hot water with 40 °C as input temperature. Water in the DHN is a closed-loop, and the tap water is

produced directly from drinking water and at a higher temperature (60 °C) at the other side of the heat exchanger [214], [215]. Therefore, the risk of growth of Legionella, an opportunistic pathogenic bacteria, in water between 20 and 45 °C is minimized.

Because heat is now merely provided via the DHN, the electricity peak demand of the neighborhood (2.4 MWp) is reduced compared to the other scenarios. As the electricity demand peak is lower than the grid capacity, there is no need to install a fuel cell in this scenario. The heat pump (2 MW_{el}) size is chosen so that enough heat can be provided to the neighborhood in winter. Although the heat pump is 2 MW_{el} and should be able to reduce electricity production peaks, we still need a 2.1 MW_{el} electrolyzer. Because at a cold but sunny day in February or the beginning of April, the heat pump is switched off (surface water temperature is too low), while there is still an excess of electricity production from households. The heat pump is thus not suitable to deliver peak shaving capacity throughout the year. Hence, as solar production peaks do happen outside the summer months as well, the electrolyzer is necessary for year-round peak shaving capacity.

3.4 Results

Based on the scenarios described in 3.3, model simulations were performed to determine the energy balance and system costs for each scenario. In this section, we compare the scenarios on their local energy and water use, monthly and yearly energy imports and exports and peaks in demands and supply. As longer-term seasonal subsurface storage is often not included in energy system designs for neighborhoods, we elaborate on the functioning of the HT-ATES system within the power-to-X scenario. Subsequently, a comparison of system costs is presented, including a cost breakdown for different system elements and a sensitivity analysis on hydrogen and electricity costs.

Sankey diagrams of all scenarios are presented in Figure 3.7-Figure 3.10. The figures visualize the yearly energy and water flows of the different scenarios based on five-year averages. The Sankey diagrams show that the different scenarios vary in their mode of integration. The all-electric scenario has three separate flows for electricity, hydrogen and water and only uses electricity in households. In the other scenarios, the number of interconnections for conversion increases as well as the different energy carriers used. All-electric H_2 and H_2 hybrid show integrating power-to-hydrogen in different ways. In the fourth mode (power-to-X), power-to-heat is added as well. Moreover, as Figure 3.10 shows, a connection between power-to-heat and power-to-hydrogen is made by using heat from the electrolyzer for the DHN.

All-electric

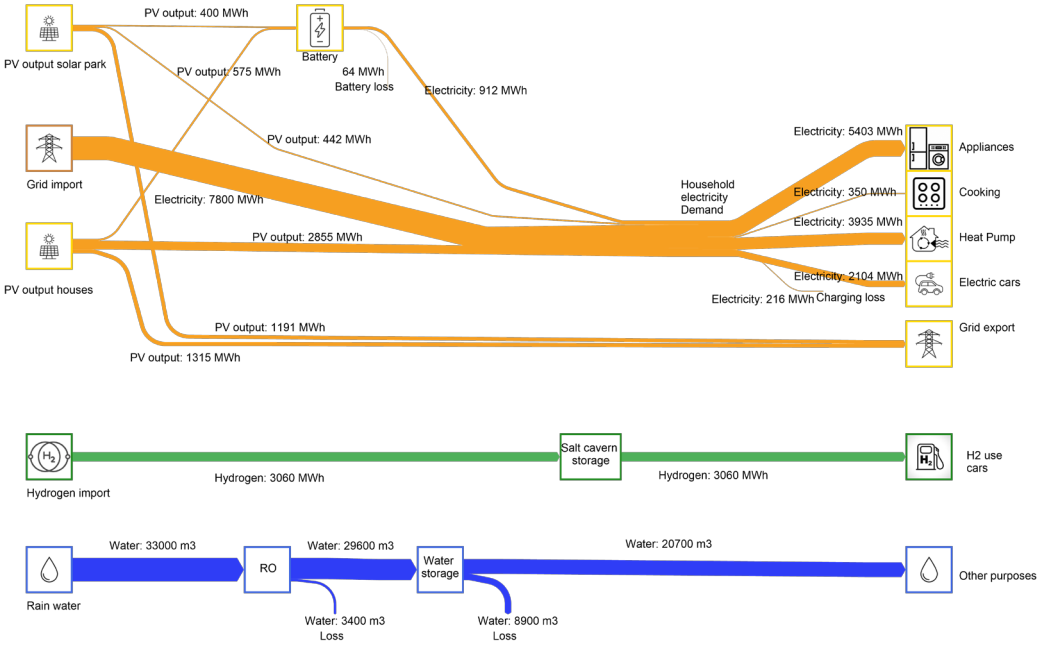

Figure 3.7 Sankey diagram of the yearly energy and water flows in the all-electric system. Electricity, hydrogen and water are three separate flows without integration. The households solely use electricity as their energy source. Part of their electricity demand (3297 MWh or 27%) is fulfilled by local PV, 7800 MWh or 65% by import from the grid and 912 MWh or 8% by local battery storage. Not all locally produced electricity can be stored in the battery or used directly, which results in 2506 MWh of electricity export to the grid. Losses for electricity conversion will be a few percentage points and are not shown in the Sankey diagrams. This will be done in a later stage of the system design and need to include DC/DC conversion as well.

All-electric H_2

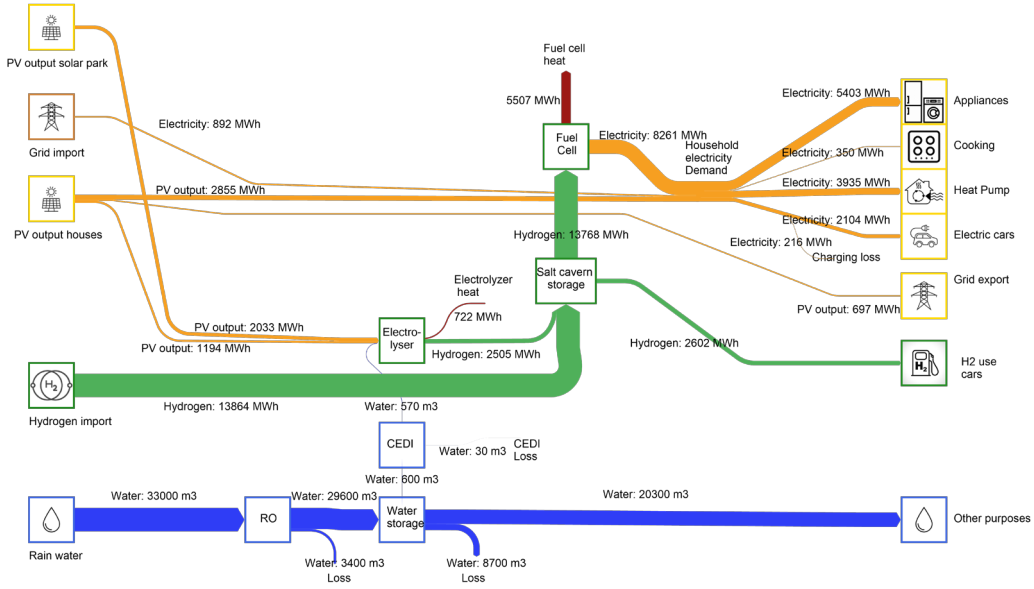

Figure 3.8 Sankey diagram of the yearly energy and water flows in the all-electric H_2 system. Connections between water and hydrogen (for hydrogen production) and hydrogen and electricity (electrolyzer and fuel cell) create a more integrated system in this scenario. The houses have electricity as their only direct energy source. 2885 MWh or 24% of their electricity demand is fulfilled by direct use of local PV production, and 892 MWh or 7% is imported from the electricity grid. The remainder of the electricity demand is fulfilled by the import of hydrogen and local conversion of hydrogen to electricity by a fuel cell (8261 MWh or 69%). Local electricity production that could not be used directly is first converted to hydrogen (3227 MWh), and if the electrolyzer is working at full capacity, the remainder is exported to the grid (697 MWh).

H_2 hybrid

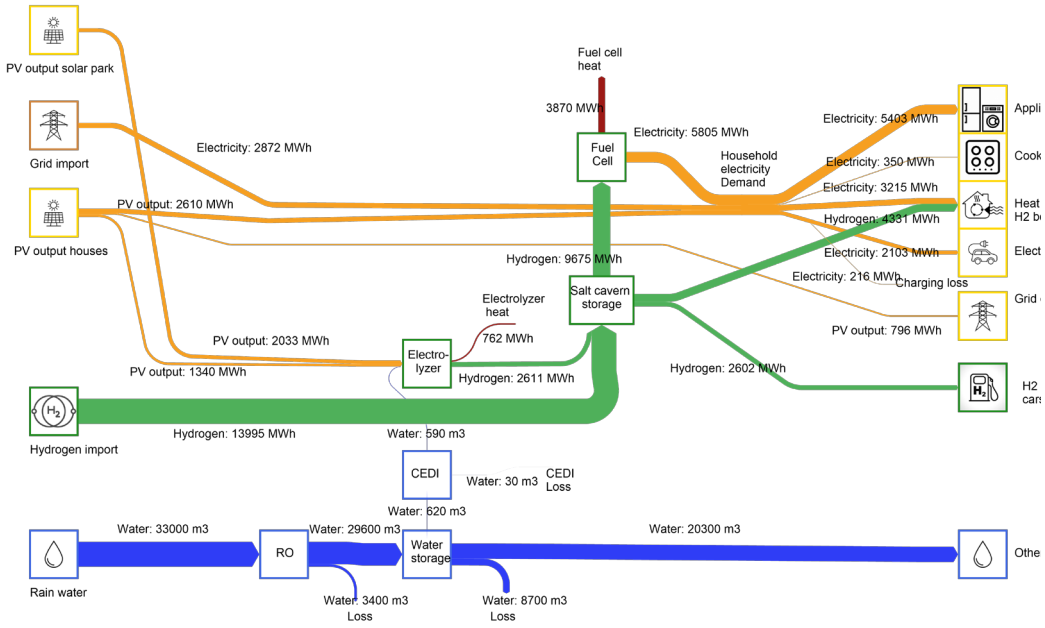

Figure 3.9 Sankey diagram of the yearly energy and water flows in the H_2 -hybrid system. The total heat demand (4794 MWh) is higher than in the all-electric scenarios (3935 MWh) because the houses are retrofitted to a lesser extent. Instead, one extra flow is added as hydrogen is now used in households directly for tap water and space heating in cold periods (< −5 °C), still maintaining a sufficient comfort level. Local PV production fulfills 23% (2.610 MWh) of the electricity demand, and the 1 MW_{el} fuel cell provides 52% (5.803 MWh). As the fuel cell is smaller than in the all-electric H_2 scenario, 2.872 MWh (26%) of the electricity demand is imported from the grid. Local electricity production that could not be used directly is first converted to hydrogen (3373 MWh), and if the electrolyzer is working at full capacity, the remainder is exported to the grid (796 MWh).

Power-to-X

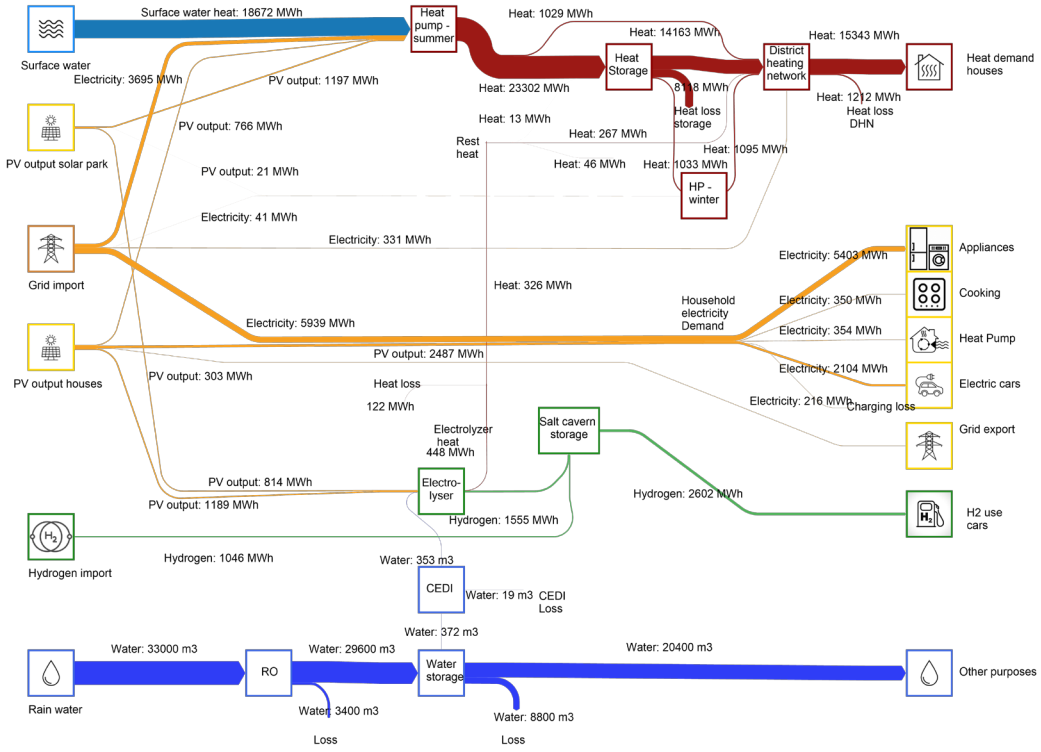

Figure 3.10 Sankey diagram of the yearly energy and water flows in the power-to-X system. An extra flow is added to the Sankey diagram to show the heat production, storage, and houses' heat demand when a low-temperature district heating system is installed in the neighborhood. The electricity demand of the houses is reduced compared to the other scenarios, as only 354 MWh of electricity is used by the booster heat pumps for tap water production. The district heating network makes a fuel cell for demand peak shaving redundant. The heat pump is shown twice in the Sankey diagram, although only one large-scale heat pump is installed. This large-scale heat pump is used in summer to produce heat (Heat pump summer) and partly in winter as well (HP-winter) to increase the temperature of the heat storage system to a sufficient temperature.

3.4.1 Local Energy and water use

The local energy supply (PV on roofs plus a solar park) in the neighborhood can fulfill 23–30% of its electricity demands (see Table 3.5). As the battery provides storage of locally produced energy, the amount of locally used electricity is the highest in the all-electric scenario (27% + 8% = 35%), followed by the power-to-X scenario (30%). The other two scenarios have just under 25% direct local electricity use.

Table 3.5 Percentages of the electricity, hydrogen and heat demand arranged per energy carrier (electricity, heat, hydrogen) and scenario.

		Electricity		
	All-electric	All-electric H_2	H_2 hybrid	Power-to-X
Direct from RES	27%	24%	23%	30%
From grid	65%	7%	26%	70%
From H_2 storage	0%	69%	51%	0%
From battery	8%	0%	0%	0%
		Hydrogen		
	All-electric	All-electric H_2	H_2 hybrid	Power-to-X
Direct from RES	-	15%	16%	60%
From H_2 storage	-	85%	84%	40%
		Heat		
	All-electric	All-electric H_2	H_2 hybrid	Power-to-X
From electricity (grid/RES)	100%	100%	43%	10%
From hydrogen	-	-	57%	-
From heat storage	-	-	-	90%

Next to electricity, there is local hydrogen production as well. The electrolyzer functions mainly as a peak shaver and only works on local RES supply. The hydrogen demand for transport can be fulfilled for max. 60% (power-to-X) to around 100% (all-electric H_2 and H_2 hybrid) by local hydrogen production.

However, despite the local energy production, a considerable amount of energy import is necessary for all scenarios. This shows that even in a neighborhood with a high potential for PV plus some extra local production, there is still a high dependence on energy imports if all energy system services are considered.

From the roofs and PV-park, a total of 33,000 m^3 of rainwater can be collected each year (see Sankey diagrams). The amount of pure water needed for the electrolyzer is about 340 m^3/year, about 1%. If the entire water supply stream would be treated by an RO installation, 30,000 m^3 of water is available (after first treatment) for other water demands. If this excess water would be stored in a subsurface storage system, on average, 20,500 m^3 of water would be available—after recovery—for other purposes in the neighborhood.

3.4.2 Import and Export of Energy

In terms of total energy import, the all-electric scenario has the lowest amount of total import (10.9 GWh/year, electricity and hydrogen import combined), followed by the power-to-X scenario (11.2 GWh/year). The other scenarios have more hydrogen imports, which reduces the import from the grid but increases the total energy imported in the system to around 15 GWh/year in total. As expected, most energy exports and conversion of energy to hydrogen and heat occur during the summer months. In an all-electric scenario, 37% of the locally produced electricity is exported to the grid. This decreases to 10% (hydrogen scenarios) and 5% for the power-to-X scenario.

The role of conversion and storage on the import and export varies highly per scenario. The battery of 4 MWh in the all-electric scenario can provide 8% of the total electricity demand (see Table 3.5), whereas 65% of the energy demand is imported from the grid. In contrast, the all-electric H_2 scenario imports 70% of its energy from (central) hydrogen storage, and the H_2 hybrid system 50%. The power-to-X system has the highest percentage of electricity demand fulfilled by the grid (70%). In contrast, the heat demand in the power-to-X scenario is fulfilled for 85% by the HT-ATES. The H_2 hybrid scenario has its heat demand fulfilled by a combination of electricity (43%) and hydrogen (57%), while the all-electric scenarios completely fulfill their heat demand with electricity. This variation in heat sources and retrofitting level leads to a difference in energy use for heat pumps, as shown in the Sankey diagrams.

More insight into yearly variations can be obtained from Figure 3.11, where each monthly bar shows the amount of energy import (positive value) and export/storage (negative value). Again, we see a pattern where scenarios with a (baseload) fuel cell have more hydrogen import and higher energy demand. The power-to-X scenario has the most balanced energy demand profile over the year because a significant amount of energy is imported during summer to produce and store heat, which is used during winter.

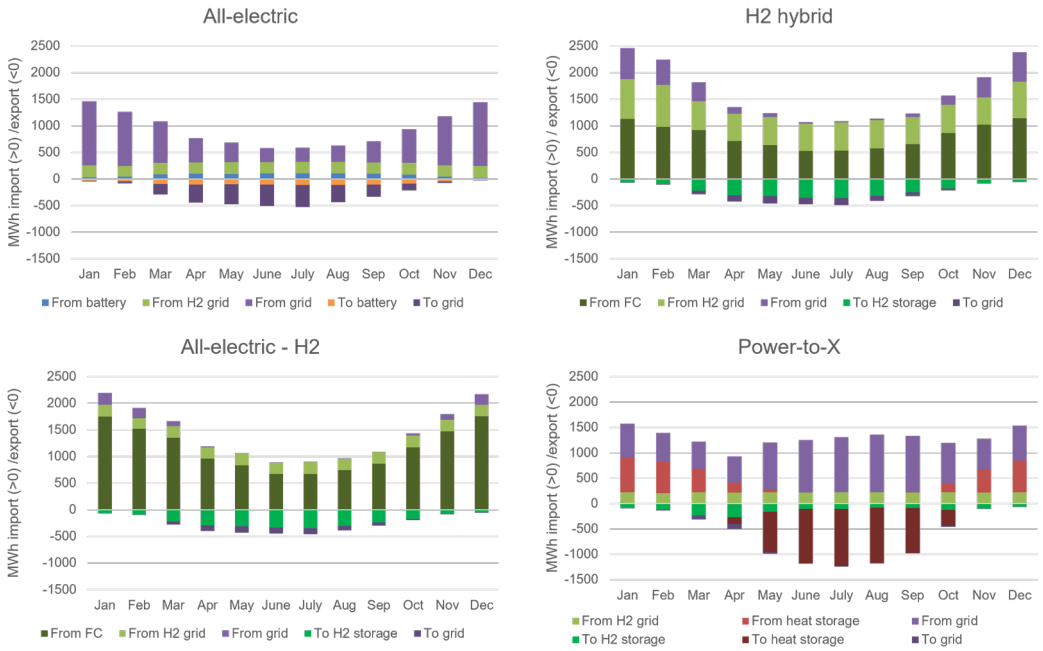

Figure 3.11 Monthly energy balance of the four scenarios, positive values represent energy use, while negative values show the energy that is stored or exported. The all-electric scenario has the lowest overall energy demand because it has the least conversion losses. The all-electric, all-electric H_2 and H_2 hybrid systems all show a seasonal pattern of lower energy demand and more export in summer, and higher energy demand and less export in winter. The power-to-X scenario has a more distributed energy demand pattern, as in summer, heat is produced with the large-scale heat pump (with surface water as a source), and heat is stored for use in winter.

3.4.3 Peaks in Energy Demand and Supply

The scenarios have different peaks in demand and supply. An example is shown in Figure 3.12, visualizing the net electricity demand of the neighborhood on a (very) cold day in February 2012. Although cold, this day was sunny with enough production from the roof solar PV systems to fulfill the electricity demand in the middle of the day. This peak in PV production explains the sharp decline in electricity demand from the grid.

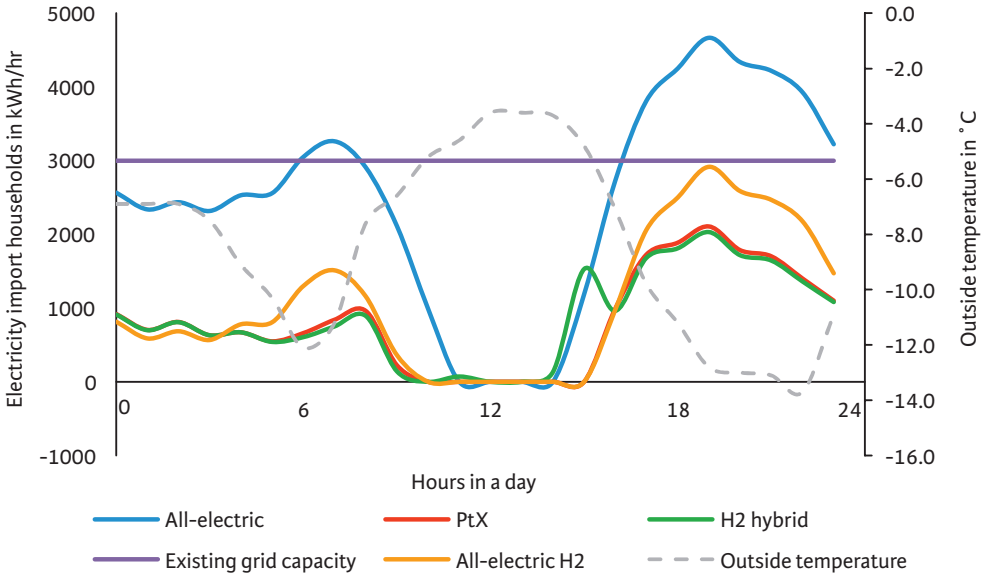

Figure 3.12 Neighborhood peak demands during a very cold day of the simulation period (6 February 2012), with the outside temperature on the second (right) axis. PtX is the power-to-X scenario. The current maximum grid capacity (3 MW) is shown as a purple line. The all-electric scenario exceeds the current maximum grid capacity of the neighborhood due to high electricity demand for heat pumps, combined with other electricity demand (cooking, appliances, electric car) in the evening hours. The other scenarios have different ways to lower the demand peak, either by shaving the peak with a fuel cell (all-electric H_2), using hybrid heat pumps with hydrogen boilers (H_2 hybrid), or a district heating network to fulfill the heat demand (PtX). Another interesting finding is that this cold day was sunny as well, which explains the low electricity import in the middle of the day when the roof PV systems fulfill the electricity demand of the households.

How heat demand is fulfilled is the determining factor that leads to the differences between the graphs. The all-electric scenario fulfills the heat demand completely with electricity, thereby creating a higher peak demand than the current maximum grid capacity (black line). Therefore, the grid capacity in this scenario needs to be increased. The all-electric H_2 has the same electricity demand profile, but in this case, the fuel cell reduces the peak demand in the morning and evening. In the H_2-hybrid scenario, the hydrogen boiler provides most of the heat demand as long as the temperature is below −5 °C. The explanation for the little peak around 3 pm is the heat pump switched on because the temperature is just above −5 °C, while the rooftop PV systems are not fully covering this demand. From 4 pm onwards, the hydrogen boiler provides the heat again as the temperature drops below −5 °C. Lastly, in the power-to-X scenario, the district heating network does provide most of the heat demand plus a little electricity demand for the booster heat pump producing tap water, but overall, the electricity demand stays well below 3 MW for the neighborhood as a whole.

The example given here is, of course, an exceptional situation. Nonetheless, the peak in electricity demand in the all-electric scenario is not an exception. During the runtime analyzed (2010–2014), the electricity demand exceeds the existing grid capacity about a hundred times a year in the all-electric scenario. In the other scenarios, the peak demand never exceeds the current grid capacity due to the deployment of the fuel cell or the existence of a DHN.

At times of peak supply from PV on roofs and the solar park, the all-electric scenario has a battery to shave those peaks, while the other scenarios have a 2.1 MW_{el} electrolyzer. In Figure 3.13 is illustrated how on two sunny days in April, the battery in the all-electric scenario cannot store the PV production peaks. Around noon, the battery is already full and unable to reduce the production peaks between 12 and 2 pm. This is not the case for the other scenarios because they have the electrolyzer and/or heat pump to reduce the peak at every hour of the day.

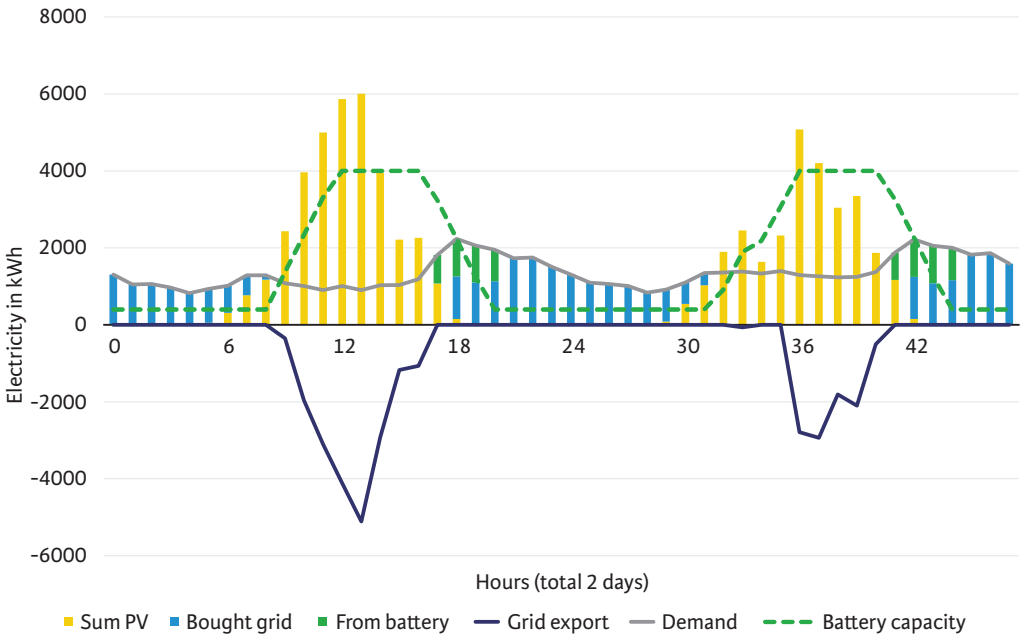

Figure 3.13 Battery dynamics of the all-electric scenario during two days in April 2010. The graph shows how the energy demand (demand) is fulfilled with PV (sum PV), electricity from the grid (bought grid) and from battery (from battery). The surplus energy is first stored in the battery (battery capacity), and when the battery is full (4 MWh), energy is exported to the grid (grid export).

The electrolyzer is used as a peak shaver and runs only on local renewable electricity. This design choice impacts the load factor of the electrolyzer, which is between 14 and 18% (ca. 1200–1800 full load hours); see Table 3.6. The industrial heat pump has a higher load factor (33%) than the electrolyzer because it can import electricity from the grid to store enough heat for the winter. In the three scenarios in which a fuel cell is installed, it has a >50% load factor because it is utilized as a baseload unit. This means that fuel cell capacity is used first to produce electricity before electricity is imported from the grid.

Table 3.6 Load factors of main system components for all scenarios, based on a five-year average.

Load Factors in %	All-Electric	All-Electric H_2	H_2 Hybrid	Power-to-X
Heat pump	-	-	-	33.0
Electrolyzer	-	17.5	18.3	10.9
Fuel cell	-	53.9	66.2	-
PV park	11.4	11.4	11.4	11.4
PV houses	9.5	9.5	9.5	9.5

3.4.4 Zooming in on Long-Term Heat Storage

The power-to-X scenario includes HT-ATES, where heat is stored in aquifers. During heat storage, water is extracted from a warm well, heated, and injected in a hot well. During heat supply, the opposite happens, groundwater is extracted from the hot well, exchanged with the return flow of the DHN via a heat exchanger and reinjected in the warm well. The groundwater temperature at the wells changes during the simulated time of five years and is shown in Figure 3.14. During the first phase of the winter, water from the hot well is used directly to exchange heat with the return flow of DHN. At some point during the winter, the heat storage system has cooled down too much to deliver heat directly to the DHN. At that point, the HT-ATES system starts to use the heat pump to provide heat at the right temperature in the most efficient way (see ***Supplementary Information Section 3.3*** for the details on the exact operating strategies of the heat pump combined with the HT-ATES wells). This also results in a sharp decrease of the warm well temperature as the heat pump allows for further cooling of the flow entering the warm well, see arrow in Figure 3.14. The yearly stored volume during heat supply and storage is 700,000 m^3 on average and changes somewhat over time (see Table 3.7). For the five simulated years, the average heat recovery efficiency is 55%. The recovery efficiency varies per year based on weather circumstances.

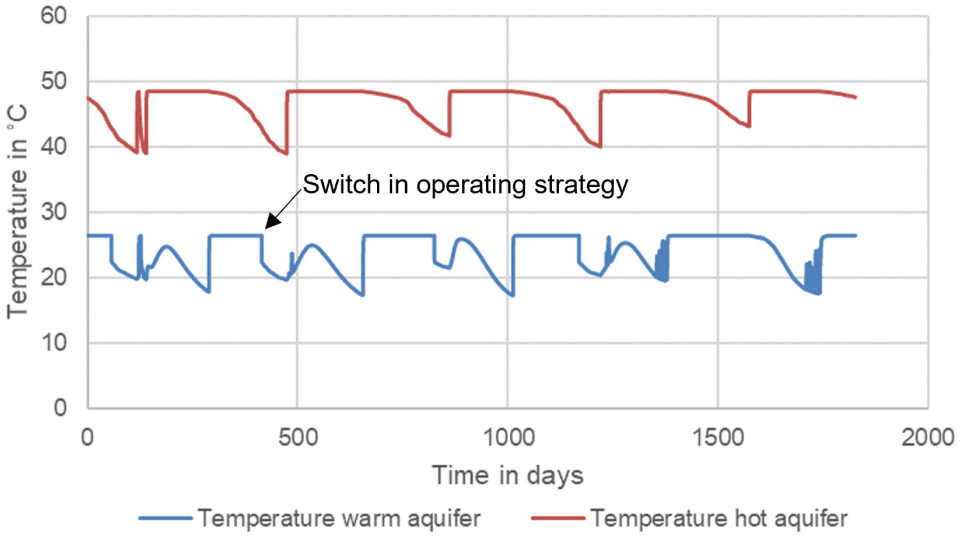

Figure 3.14 Temperature of the hot and warm well over five years (2010–2015). The last five years of ten years of modeling are shown, as the first five years were used to heat up the wells starting from background temperature (12 °C). After five years, the system has reached an equilibrium state. The arrow shows the switch to a different operating strategy (see text) and a decrease in the warm well temperature.

The heat demand of the neighborhood is fulfilled 85.5% of the time from the HT-ATES system. Another 13% of the heat is used directly after production before it could be stored. The heat from the electrolyzer and fuel cell fulfills 1.5% of the heat demand. Lastly, electricity is used to elevate the return temperature of the DHN in winter when the hot well temperature decreases below 43 °C. This electricity use amounts to <1% of the heat demand. To produce the heat, a total of 5720 MWh of electricity is used by the heat pump, of which 1985 MWh came from local RES production and 3735 MWh from the grid (derived from Figure 3.9).

Table 3.7 Overview of the HT-ATES performance over five years, starting from the sixth year that the system is running after it has been warmed up in years 1–5.

	Hot Well Efficiency	Warm Well Efficiency	Yearly System Efficiency	Heat Storage (TJ)	Heat Supply (TJ)	Volume Storage (–1000 m^3)	Volume Supply (–1000 m^3)
Year 6	92%	73%	75%	83.4	62.9	717	747
Year 7	54%	117%	44%	100.0	43.7	788	522
Year 8	69%	91%	55%	92.6	51.0	728	604
Year 9	75%	88%	60%	92.5	56.0	696	666
Year 10	57%	108%	45%	91.9	41.3	689	472
Average	69%	93%	55%	92.1	51.0	724	602

3.4.5 Economic Results

Table 3.8 shows the volumes of electricity and hydrogen bought and sold in each scenario, as well as the CAPEX of the system and the yearly costs per household for electricity, transport and heat (excluding taxes). In Figure 3.15, a breakdown of the costs per household per year is shown. The costs include bars for discounted CAPEX plus OM cost and separate bars for electricity/hydrogen import costs. Some of these costs will most probably be made by, for instance, the grid operator (grid reinforcement) or the heat provider (heat pump). Here we show the discounted costs if the costs made for a certain scenario would be divided over all households, so they represent the societal costs and are mainly meant for a fair comparison between the scenarios.

Table 3.8 Economic results of the four scenarios.

	All-Electric	All-Electric H_2	H_2 Hybrid	Power-to-X
Total electricity bought (MWh/year)	7780	890	2870	9680
Total electricity sold (MWh/year)	2510	700	800	300
Total H_2 used (ton/year)	66	415	420	66
Total H_2 produced (ton/year)	0	64	66	36
Total CAPEX system (M€)	47	46	24	40
OM system (M€/year)	1.0	1.0	1.4	1.0
E_{cost} system (electricity + H_2 in M€/year)	1.0	1.1	1.2	1.2
Discounted investment costs (€/year/household)	1820	1800	1480	1480
Electricity import costs (€/year/household)	400	30	140	550
Hydrogen import costs (€/year/household)	100	540	549	40
Costs per household (€/year)—see Figure 3.15 for breakdown	2320	2370	2175	2070

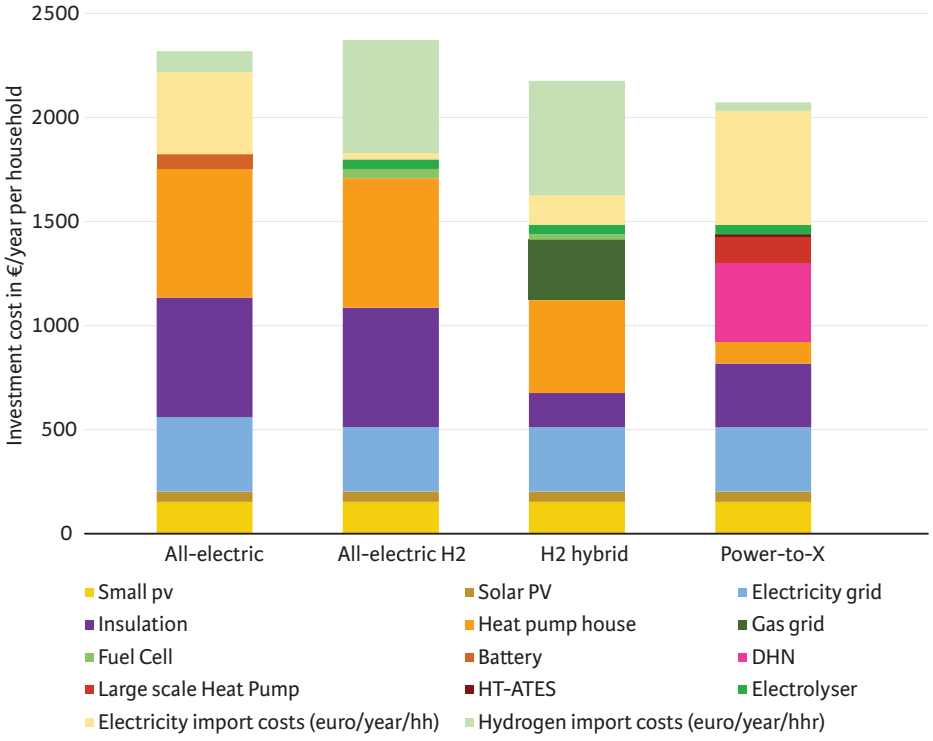

Figure 3.15 Yearly cost breakdown of the different components in the four scenarios. Costs include discounted CAPEX and OPEX (OM and electricity/hydrogen costs) and are divided over the 2000 households. The all-electric H_2 scenario has the highest costs (2370 €/household/year), mainly due to the high investment costs for insulation (retrofitting from label D to label A), the heat pump and the import costs for hydrogen. The insulation and heat pump costs are important cost factors because those are investments for each individual house. The scenarios with less retrofitting (H_2 hybrid and power-to-X) have more costs for conversion, storage and infrastructure (hydrogen and heat), but these costs are shared among all households, resulting in overall lower costs per household.

The total CAPEX costs are the lowest for the integration mode with hybrid hydrogen heat pumps, the H_2 hybrid scenario (24 M€). In this case, the costs for retrofitting are limited, and the gas network is reused for hydrogen, which saves costs for new infrastructure. The power-to-X scenario with both power-to-heat and power-to-hydrogen is about 16 M€ more expensive, mostly due to investments in the district heating network and heat pump. The all-electric and all-electric H_2 scenarios are another 6–7 M€ more expensive than power-to-X. In these scenarios, retrofitting costs (insulation + heat pump) are an important factor in the cost breakdown (Figure 3.15). For an all-electric system with an air-sourced heat pump, extensive insulation measures are necessary to keep the house warm with a low-temperature heat system. As the H_2 hybrid mode needs less insulated buildings, there is a positive impact on the costs because the hydrogen boiler assists the heat pump at times of peak demand and can deliver higher temperature heat. In line with this result Table 3.8 shows a clear distinction between the all-electric and H_2 hybrid/power-to-X scenarios with a yearly cost difference of about 145–300 €/household/year.

If we compare the all-electric scenarios, we observe a similar CAPEX for both, but the OPEX costs of the all-electric H_2 scenario are 100 k€/y higher, mainly because there is relatively more hydrogen import in this scenario.

The scenario with the most different energy carriers (power-to-X) has almost 70% higher system costs than the H_2-hybrid system, but the discounted costs per household are the same. The higher investments in the power-to-X system are mainly due to the heat grid (and the industrial heat pump), as these are long-term investments, the yearly discounted costs are quite low. Additionally, the OPEX of the power-to-X system is 400 k€/y lower than for H_2 hybrid. This is a combined effect of smaller heat pumps, which leads to lower OM costs (as we used a % of CAPEX for OM costs) and lower OM costs for the DHN (as% of CAPEX) versus the fixed yearly OM costs for the maintenance of the gas grid. The DHN is installed locally, while the gas grid should also be maintained outside of the neighborhood to provide gas from central gas storage locations.

The storage and conversion installations have a limited contribution to the yearly costs per household, contrasting with the retrofitting/insulation costs (see Figure 3.15). Although these installations require large investments, when discounted over the lifetime and shared by 2000 households, the contribution to the yearly costs appears to be modest. Infrastructure, on the other hand, has a larger contribution to the cost breakdown, mainly maintenance of the gas infrastructure and the construction and maintenance of a DHN and industrial heat pump. The grid reinforcement costs, however, have a minor contribution to the yearly cost breakdown. In the all-electric scenario, the costs for the electricity grid reinforcement are 50 €/household/year, or 2% of the total costs per household within that scenario. These costs are comparable to the battery (70 €/household/year) or the electrolyzer (50 €/household/year).

Two scenarios rely on hydrogen for 83–94% of their total energy import (all-electric H_2 and H_2 hybrid), while the other two (all-electric and power-to-X) rely on 70–86% electricity import. As there is quite some uncertainty on the prices for both hydrogen as well as climate-neutral electricity, we have done a sensitivity analysis on these two economic parameters. The price ranges found in the literature and mentioned in Table 3.3 are applied. Moreover, we analyzed a low, middle and high price of electricity over a range of hydrogen prices and vice versa. In this way, we get more insight into the combined effect of changes in both prices simultaneously. The results are shown in Figure 3.16.

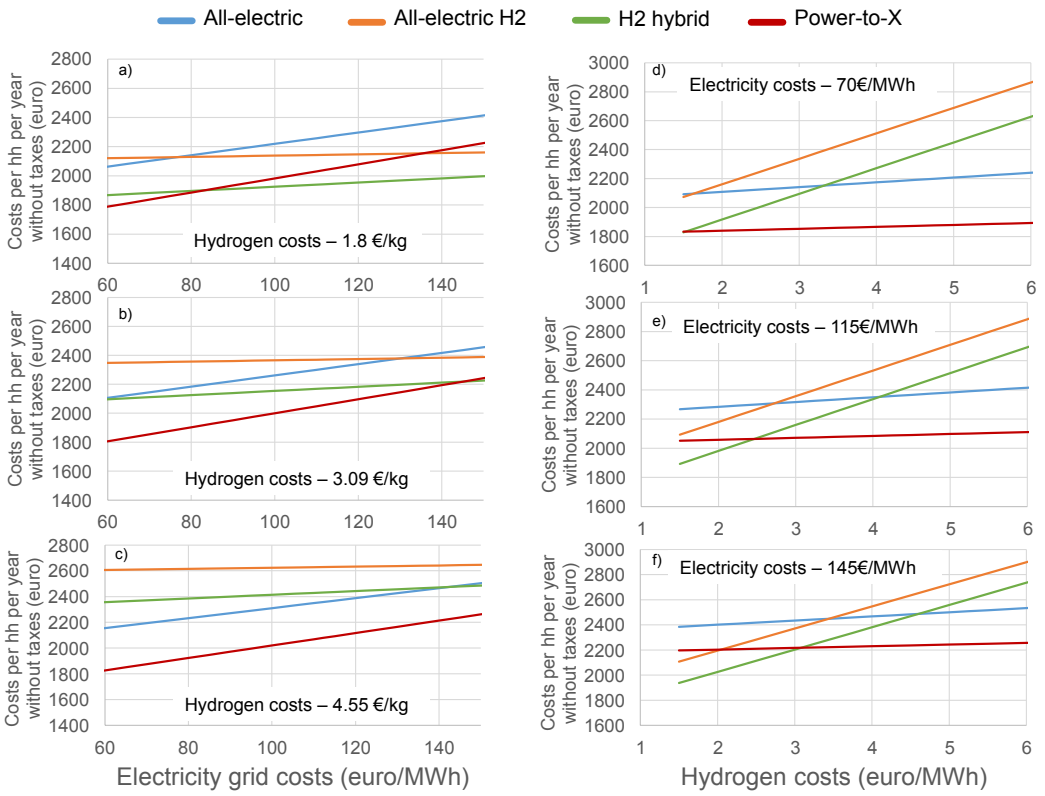

Figure 3.16 Sensitivity analysis on electricity costs (import from the grid) and hydrogen import costs. The left side shows the sensitivity of the yearly costs per household to the electricity price for climate-neutral electricity, with a fixed hydrogen price in the low (**a**), middle (**b**) and high (**c**) range. The right side shows the sensitivity of the yearly costs per household to the hydrogen costs, with a fixed electricity costs price in the low (**d**), middle (**e**) and high (**f**) range. The middle range values are the values used for the economic analysis in this chapter. The analysis shows that the lowest costs option is either the H_2 hybrid system or power-to-X, which are the systems with the most conversion and storage mechanisms and diversification of energy carriers in the households.

In general, we observe that the competition for the lowest cost option is always between the H_2 hybrid and power-to-X scenario. Even with very low electricity prices, especially the costs for retrofitting still make the all-electric scenarios more expensive. First, we look at varying electricity prices (Figure 3.16 a–c). The electricity price should be lower than 140 €/MWh for the power-to-X system to have the lowest system costs (per household) with the average hydrogen price (Figure 3.16 b). If the hydrogen costs turn out to be at the low end of the range (1.8 €/kg), the H_2 hybrid scenario will have the lowest system costs as the electricity price is higher than 83 €/MWh. Moreover, if the hydrogen costs eventually end up at the high end of the range, the power-to-X system will have the lowest costs over the total electricity price range.

Second, we take a closer look at varying hydrogen prices (Figure 3.16 d–f). The intercepts between the system costs for the H_2 hybrid and power-to-X scenario are around 1.5, 2.5, and 3 €/kg of hydrogen, depending on the electricity costs. With a hydrogen price of 3 €/kg, the power-to-X scenario will most certainly be the lowest cost option for all electricity price levels (up until 150 €/MWh).

3.5 Discussion

3.5.1 Energy Balance

3.5.1.1 Local production versus energy import

Creating a more integrated energy system has an impact on the energy balance of a neighborhood. System integration modes with power-to-hydrogen (all-electric H_2 and H_2 hybrid) leads to 30% less export of locally produced electricity than an all-electric scenario because of local conversion (and partly storage). For a scenario with a combination of power-to-heat and power-to-hydrogen, this is even 35%. At the same time, the local hydrogen production can fulfill 60–100% of the hydrogen demand for transport in the neighborhood. On the other hand, every scenario has a high amount of energy import, either in the form of hydrogen or electricity, whereas we already assumed a high potential for solar PV in the neighborhood. Therefore, we expect that the local renewable energy supply can fulfill a maximum of 30–40% of the total energy demand (heat, electricity and transport) with currently available PV technology for existing neighborhoods. The import of energy will thus still be important in future energy systems for existing neighborhoods, according to our analysis. This finding is confirmed by other neighborhood studies [69], [216].

3.5.1.2 More stable energy distribution pattern with HT-ATES

The all-electric, all-electric H_2 and H_2 hybrid scenarios show a seasonal pattern in their energy import due to the higher heating demand in winter (see Figure 3.11) and, therefore, rely on a central energy storage system. An exception is a power-to-X scenario with a more distributed energy import over the year. In this case, the heat storage is filled during summer, reducing the energy demand in winter. The combination of power-to-heat with local seasonal heat storage systems could thus create more stabilized demand patterns.

3.5.1.3 The impact of electrolyzer and fuel cell heat integration on the energy balance

Lastly, we expected the combination of power-to-hydrogen and power-to-heat would benefit the energy balance because the heat from the electrolyzer could be utilized in the DHN or heat storage. However, the results show a modest 1.5% contribution of the heat from the electrolyzer to the total heat demand. In this system design, there is thus no real added value for the recovery of heat (as it would also require extra installations to recover the heat). In earlier research, we have seen that the electrolyzer could fulfill up to 25% of the heat demand if the electrolyzer has a higher capacity factor, which means that there still could be a potential of coupling those two conversion technologies [217].

3.5.1.4 HT-ATES recovery efficiency

The average yearly system efficiency is 55%, and the hot well efficiency is 69%. The literature on different HT-ATES systems gives values of 78–88% system efficiency at 100 °C injection temperature [218], 77–86% for hot well efficiency at 61 °C injection temperature [219] or 54–79% hot well efficiency with a cutoff temperature of 80 °C [220]. Thus, our findings are within the range or at the lower end of the range compared to the literature. One possible explanation is that the stored volume is lower, which negatively impacts the recovery efficiency due to a less optimal area/volume ratio compared to larger systems [125]. Moreover, our system could be further optimized, for example by using a smaller heat pump and/or storing less heat.This study is one of the first to include HT-ATES in analyzing a total neighborhood energy system and shows the potential of this type of seasonal energy storage. Further development and analysis of HT-ATES systems are necessary to get more insight into the potential of this type of seasonal storage within integrated energy systems.

3.5.2 Water Supply and Possible Water Demands

3.5.2.1 Rainwater supply and storage in the neighborhood

In the neighborhood, water could be collected both from roofs as well as from the nearby solar park. In total, 33,000 m^3 rainwater/year is available, of which the electrolyzer only needs a fraction (1%). Hence, after treatment and storage, approximately 20,500 m^3 of water is available for other purposes. To make this water available throughout the year, a local storage system needs to be installed. There are multiple reasons to implement local storage and use of rainwater. Rainwater storage systems help to prevent inundation, increase water availability, and plant evaporation has a cooling effect that helps to reduce the urban heat island effect. An example of a large-scale water storage system is an aquifer storage and recovery (ASR) system [97], [98]. Another smaller scale option is a blue-green roof [221], although such a system is often not combined with solar panels.

3.5.2.2 Possible water demands

The storage of collected rainwater could be deployed for plants in (communal or private) gardens, as well as for irrigation of the vegetation in the public spaces of the neighborhood. Furthermore, rainwater has a very low salt concentration (<20 mg Cl^-/L) [97], even compared to drinking water (50–130 mg Cl^-/L) [222]. This is an advantage for the production of pure water because the recovery factor of the RO increases, and there is a slight reduction in energy demand for desalination. Pure water is the source of hydrogen in the electrolyzer. However, next to that, it could be used for more industrial purposes inside or near the neighborhood, such as a car wash or laundry. Purifying rainwater for household purposes is an option as well. The water demand per household is 102.7 m^3/year, of which the toilet, dishwasher and washing machine appear suitable for applying RO-treated rainwater, which would add up to approximately 46 m^3/household/year [223]. The supply of 20,500 m^3 would then cover about 20% of this water demand. A study on rainwater harvesting in the Netherlands found that if water from pavements would be included as well, about 50% of the water demands of a neighborhood could be covered by rainwater [224]. A more thorough analysis of the possible system layouts, future water demand patterns and costs would be a topic for further research.

3.5.3 Peak Demand and Supply

3.5.3.1 The effect of power-to-hydrogen on peak demand

The results in Section 3.4.3 have shown that integrated system designs that include power-to-hydrogen are better able to deal with peaks in supply and demand than an all-electric scenario. Supply peaks caused by PV production are converted to hydrogen by an electrolyzer, which offers a more continuous capacity for peak shaving than the battery in the all-electric scenario. Moving towards a combination of different energy carriers instead of solely electricity thus has a positive effect on peak demands and supply within the neighborhood. However, we should note here that smart battery use was not thoroughly analyzed, as well as vehicle-to-grid options. If the battery would also be able to import electricity from the grid and provide that at times of high electricity demand, the demand peak in winter could decrease. In combination with the curtailment of PV production peaks in summer, there would probably be less need for grid reinforcement [225]. However, even if smart battery use would be included, we still think our estimation for peak demand in this research is reasonable because of the conservative estimation for peak demand (see Section 3.3). The option of vehicle-to-grid could also offer flexibility during peak times [226] and would be interesting to include in the model in the future. Including BEV as the battery capacity is, however, subjected to more restrictions than stationary batteries.

3.5.3.2 More potential for peak shaving with power-to-heat and power-to-hydrogen

In the power-to-X scenario, there could be more room for peak shaving than was shown in the results. The power-to-X has a similar-sized electrolyzer compared to the other scenarios (2.1 MW_{el}) next to a 2 MW_{el} heat pump. The electrolyzer could probably be of a smaller size if the heat pump would be used more smartly. At times when the surface water temperature is not high enough, the heat pump is now switched off. An alternative is to increase the temperature in the DHN for a short period to reduce peaks in the local electricity grid. This option was not included in this study but could be looked into in future research to further optimize this scenario. Thus, integrating hydrogen or heat could offer even more peak shaving to the energy system than shown in this study.

3.5.3.3 Other flexibility services of power-to-heat and power-to-hydrogen

Besides reducing local peaks in demand and supply, both the heat pump and the electrolyzer could offer flexibility to the grid by buying at moments when there is an oversupply on the grid. The heat pump has a 33% load factor, but if only the hours during summer are considered (when the surface water is warm enough), the load factor would be approximately 70%. By shifting the running hours of the heat pump within the summer season, flexibility to the grid could be offered. The potential for load shifting and peak shaving is even higher for the electrolyzer, which currently has a load factor of 14–20%. The potential of offering flexibility to the grid was not analyzed in this study and could not be calculated because fixed electricity prices were used. Although fixed tariffs for consumers may continue to exist, the actual wholesale prices for electricity will become more volatile with high shares of renewables. Other research has shown that offering flexibility with a heat pump [33], [227] or electrolyzer [155], [228] could be feasible (i.e., targeting low electricity prices) and could be something to apply to these scenarios in future research.

3.5.4 System Costs

3.5.4.1 Diversification of energy carriers lead to lower system costs

The sensitivity analysis has shown (see Figure 3.16) that the "tipping points" for the switch between the H_2 hybrid and power-to-X scenario as the lowest cost option are actually within the possible price range of both electricity and hydrogen prices. Yet, we can conclude that in any case, integration modes with more diverse energy carriers (heat, electricity and hydrogen) do lead to lower system costs (145–300 €/year/household) than the all-electric scenarios with electricity as the main energy carrier.

As explained in Section 3.3.1, this chapter has not shown all different possible system designs for neighborhoods. Eventually, every neighborhood has its specific circumstances and (im)possibilities that need to be considered. However, based on the results, it could be interesting to compare more system designs with hydrogen in future research. For example, a design with fuel cell micro-CHP systems could be interesting as they both produce heat and electricity to be used directly within the house. Developments towards reversible hydrogen systems (combined electrolyzer/fuel–cell in one system) have an even larger potential as they can reduce demand and supply peaks at the household level. In summary, we see that modes of system integration with more diverse energy carriers lead to more complex systems, but because they can provide energy in multiple ways, they are more robust.

3.5.4.2 Retrofitting as an important factor in energy system costs

A factor that is often mentioned as an advantage for integrated systems is the reduction in grid reinforcement costs. However, this analysis shows the grid reinforcement cost within the neighborhood, for the low voltage grid up until the transformer station, is a small factor in relation to the total system costs for end-users, such as households. Alternatively, the costs for insulating existing buildings have shown to be one of the most important cost components that determine the total yearly costs. Because the all-electric modes need a high level of insulation to be compatible with a low-temperature heating system, those scenarios are the most expensive. This is in line with a recent report by the Dutch Environmental Assessment Agency (PBL). The report concluded that the costs for insulation of a house from energy label D to B do not outweigh the energy savings (over 30 years) and are not financially attractive for house owners [229].

3.5.4.3 Local hydrogen production to electricity is more expensive than using electricity directly

The all-electric H_2 scenario is a mode where hydrogen is introduced as an energy carrier besides electricity and thus integrates more energy carriers in one system. We have seen that introducing more energy carriers leads to lower system costs, but in this case, the all-electric H_2 scenario has the highest system costs. Only when the hydrogen costs would be low (1.8 €/kg) and the electricity price above 80 €/MWh, the all-electric H_2 scenario will be cheaper than the all-electric scenario. The determining factor here is not the grid reinforcement versus the installation of the electrolyzer, as the discounted costs per year are both similar (50 €/household/year). As both scenarios assume an all-electric heating system, the retrofitting costs are similar as well. In this case, the import

costs for hydrogen become the determining factor (see Figure 3.15). Because of the conversion loss of hydrogen, it is cheaper to have an all-electric system with grid extension than to have local energy production with a fuel cell and hydrogen import (the all-electric H_2 scenario). Converting an alternative energy carrier (here hydrogen) to electricity in a central place in the neighborhood leads to higher system costs than an all-electric solution. It is thus more useful to bring alternative energy carriers to the house itself, as was analyzed in the other scenarios.

3.5.4.4 The importance of hybrid designs

Our analysis shows that a hybrid design with hydrogen fulfilling part of the heat demand in households is a favorable option to obtain low system costs for existing neighborhoods. Without a need for thorough retrofitting, a start could still be made with less drastic retrofitting measures, including the installation of a hybrid heat pump, while still maintaining the natural gas boiler. As we have shown, about two-thirds of the heating demand could already be electrified. Over time, the gas boiler could be retrofitted or replaced with a hydrogen boiler or hydrogen-ready boiler, and maybe continue the retrofitting process to further reduce the energy demand. Hybrid systems are an important solution in the smooth transition to a renewable energy system in existing neighborhoods.

3.6 Conclusions

In this chapter, we have analyzed four scenarios with different modes of system integration for 100% renewable energy systems for existing neighborhoods. Moreover, we included several system services in a neighborhood (electricity, heat, transport and water). We consider the combination of multiple system services and energy carriers with local conversion and (seasonal) storage leading to integrated energy—and water systems as a novel aspect of this work. We can conclude that integrating different energy carriers at end-users shows a positive impact on the energy system costs. The integrated system designs with local hydrogen production combined with hybrid hydrogen boilers (H_2-hybrid) or a low-temperature district heating network, heat storage and hydrogen production (power-to-X) lead to 145–300 €/household/year decrease in cost compared to an all-electric system. In these two modes of system integration, we utilize other energy carriers, such as heat and hydrogen, in the house itself, besides electricity. This diversification of energy carriers decreases the need for extensive retrofitting measures, which have shown to be an important factor in the total system costs.

In the H_2 hybrid scenario 2,175 €/household/year) houses have installed a heat pump as well as a hydrogen boiler for hot tap water and heat production on cold days. The Power-to-X scenario has local heat production and seasonal heat storage (with a HT-ATES) as well as hydrogen production (2,070 €/household/year). The sensitivity analysis has shown that the Power-to-X system is most likely to have the lowest costs over the sensitivity range, namely if the hydrogen price is above 3 €/kg and the electricity price is < 150 €/MWh.

However, we can conclude that both modes of system integration (power-to-heat and power-to-hydrogen) are important to consider, depending on local circumstances and price developments for hydrogen and electricity.

Furthermore, the results show that integrated neighborhood energy systems with local conversion and storage mechanisms (heat or hydrogen) can lower electricity peak demands. Moreover, they have the potential to flatten peaks from the grid at times of oversupply, and only 5–10% of locally produced energy is exported to the grid. Yet, the percentage of local electricity use is not more than 23–35% of the total demand, so importing electricity will still be important in future neighborhoods. A seasonal heat storage system leads to the most distributed energy import over the year compared to the other scenarios. Lastly, we have shown that a seasonal heat storage facility (in this study HT-ATES) for a neighborhood is a potentially suitable option for large-scale seasonal heat storage.

In conclusion, this research shows the importance of considering more integrated and hybrid options in designs for future clean, affordable and reliable energy systems for existing neighborhoods.

Supplementary Information

The Supplementary Information describing the different model components is available online at *https://www.mdpi.com/article/10.3390/en14092616/s1*

Data

Raw data of the modeling results from the scenarios described in this chapter can be accessed via *https://doi.org/10.4121/14464881*.

Funding

This activity is co-financed with PPS-funding from the Topconsortia for Knowledge and Innovation (TKI's) of the Dutch Ministry of Economic Affairs and Climate. The authors would like to thank TKI Urban Energy (TEUE117059) in the Netherlands for their financial contribution to the research project that was the foundation for this publication.

4 Towards sustainable heat supply with decentralized multi-energy systems by integration of sub-surface seasonal heat storage

" If it's not Here, that means it's out There "

Winnie the Pooh (A.A. Milne)

Abstract: In the energy transition, multi-energy systems are crucial to reduce the temporal, spatial and functional mismatch between sustainable energy supply and demand. Technologies as power-to-heat (PtH) allow flexible and effective utilization of available surplus green electricity when integrated with seasonal heat storage options. However, insights and methods for integration of PtH and seasonal heat storage in multi-energy systems are lacking. Therefore, in this study, we developed methods for improved integration and control of a high temperature aquifer thermal energy storage (HT-ATES) system within a decentralized multi-energy system. To this end, we expanded and integrated a multi-energy system model with a numerical hydro-thermal model to dynamically simulate the functioning of several HT-ATES system designs for a case study of a neighborhood of 2000 houses. Results show that the integration of HT-ATES with PtH allows 100% provision of the yearly heat demand, with a maximum 25% smaller heat pump than without HT-ATES. Success of the system is partly caused by the developed mode of operation whereby the heat pump lowers the threshold temperature of the HT-ATES, as this increases HT-ATES performance and decreases the overall costs of heat production. Overall, this study shows that the integration of HT-ATES in a multi-energy system is suitable to match annual heat demand and supply, and to increase local sustainable energy use.

This chapter is based on the publication:
E. van der Roest, S. Beernink, N. Hartog, J. P. van der Hoek, and M. Bloemendal, "Towards Sustainable Heat Supply with Decentralized Multi-Energy Systems by Integration of Subsurface Seasonal Heat Storage," Energies, vol. 14, no. 23, p. 7958, Nov. 2021, doi: 10.3390/en14237958.

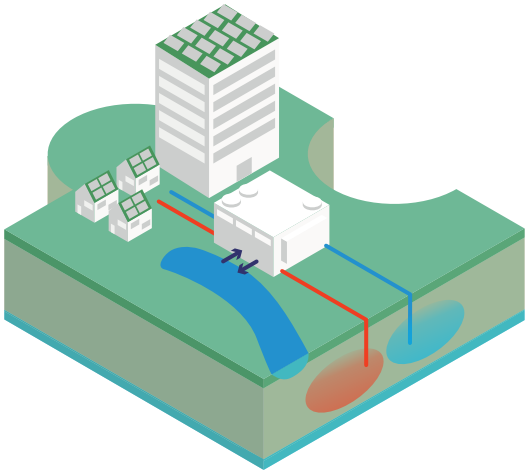

4.1 Introduction

To limit global warming, governments aim to reducing greenhouse gas (GHG) emissions caused by the use of fossil fuels [1], [167]–[169] and transition to renewable energy sources. As a result of the transition to renewable sources, the energy system will, in part, become more decentralized with energy production by e.g., photovoltaic systems (PV) and, on a small scale, wind, brought closer to consumers [168], [169]. These types of renewable energies are intermittent and thus storage facilities are required to overcome the temporal mismatch between availability of and demand for energy [109], [230], [231]. These mismatches can (partly) be overcome by the introduction of multi-energy systems (MES), as they provide possibilities for system integration [23], [48], [52], [232]. In such integrated systems, production of sustainable electricity and heat, as well as storage and conversion of these commodities, are integrated with the goal to efficiently maximize the utilization of available sustainable energy and to balance supply and demand. A MES consists of sustainable energy sources and conversion and storage facilities. Different forms of conversion can be applied in a MES, such as power-to-heat and power-to-gas (i.e., hydrogen). Consequently, traditionally separate operating sectors have become connected, such as the heat, transport and electricity sectors [47], [67], [69], [73], [171], [233].

In order to overcome seasonal mismatches between supply and demand, storage of gas from power-to-gas technologies is often applied. Additionally, great potential is attributed to underground thermal energy storage techniques, like aquifer thermal energy storage (ATES) systems, as these techniques offer efficient and large storage capacities at relatively low costs [234]. Yet, the authors notice that seasonal heat storage is often overlooked in the design and evaluation of sustainable multi-energy systems [34], [67], [69], [77], despite the large potential benefits for overall system efficiency and GHG emission reduction [74]–[76], [171]. Probably, there is a lack of attention for including seasonal storage in MES because methods for the evaluation of integration based on cost-effectiveness and robustness are lacking [34], [67], [69], [77]. In previous work [134], [171] (**Chapter 2**), we evaluated the potential benefit of a high temperature aquifer thermal energy storage (HT-ATES) system that is used for seasonal heat storage in a multi-energy system, and compared four MES designs [235] (**Chapter 3**). Here it was shown that a scenario with HT-ATES led to the most balanced energy demand profile compared to an all-electric and hydrogen scenario, the highest amount of local electricity use, and lower costs for households (250–300 €/year) compared to an all-electric scenario [235]. To further explore the novel application of HT-ATES in a MES, a more detailed description and evaluation of different innovative designs for the combined HT-ATES and heat pump system is necessary. This was not included in earlier chapters. Therefore, in this research, we elaborate on the connection between the HT-ATES and the heat pump of the MES, to provide methods for integration and foster the use of HT-ATES within multi-energy systems.

4.1.1 Goal and Approach

The goal of this study is to develop novel methods for integration and control of a HT-ATES system in an innovative power-to-heat energy system. Moreover, we assess how these methods affect

the costs and provision of sustainable heat year-round. The methods are tested for a case-study neighborhood to assess how conditions and the different components in the integrated HT-ATES system affect the efficiency and ability to sustainably meet the heat demand.

More specifically, three aspects are studied; firstly, the effect of the heat pump design (size, condenser temperature, modes of operation between heat pump and HT-ATES) on the heat delivery by the HT-ATES system is assessed. Secondly, the performance of the HT-ATES system is assessed to evaluate the effectiveness of this storage component. Thirdly, an analysis is done on the levelized costs of the heating system (in €/GJ) as a whole.

To do this, a detailed model of a multi-energy system is expanded and integrated with a numerical hydro-thermal model to simulate the functioning of a HT-ATES system. The integration of the multi-energy system and the HT-ATES system is applied in a case study of a neighborhood in Nieuwegein (the Netherlands) that has been the focus of earlier work on a multi-energy and water system [105], [134], [171], [217], [235] (**Chapter 2 & 3**). In this decentralized multi-energy system, renewable electricity (PV) is converted to high temperature heat and stored in the HT-ATES system during summer. In winter, the HT-ATES system is used to fulfil the heat demand of the neighborhood.

4.1.2 Structure

In this chapter, we first explain the HT-ATES model (4.2.1) and the relevant parts of the multi-energy system model (4.2.2) in the methods, followed by a description of the field case and how the multi-energy system and HT-ATES are integrated (4.2.3). Then, we describe the scenarios for the case where we compare different heat pump designs (4.2.4) and we discuss the assessment framework (4.2.5). In the results, we compare the results of the different scenarios in terms of fulfilment of heat demand by the HT-ATES system (4.3.1), the HT-ATES performance (4.3.2), and the levelized costs of heat production (LCOE, 4.3.3). In Section 4.4, we discuss the results and combine the different aspects from the results to more overarching insights. Finally, in Section 4.5, we draw conclusions on the integration of HT-ATES in a multi-energy system.

4.2 Materials and Methods

4.2.1 HT-ATES Model

Aquifer thermal energy storage (ATES) systems utilize groundwater to store heat (or cold) in water-bearing layers, so-called aquifers, in the subsurface. A conventional ATES system consists of (multiple) cold and warm wells. During heat demand, warm water is extracted from the warm well, heat is released to the system and the cooled water is pumped into the cold well. When cooling is needed, groundwater is extracted from the cold well, heated and stored through the warm well [236].

For this study, a high temperature (HT-)ATES system is studied, which means that storage temperatures are above 25 °C [237], Figure 4.1. In contrast to LT-ATES systems, the temperatures of the warm and the cold well are both above the ambient groundwater temperature. Therefore, we use the terms hot and warm instead of warm and cold for the wells in this study.

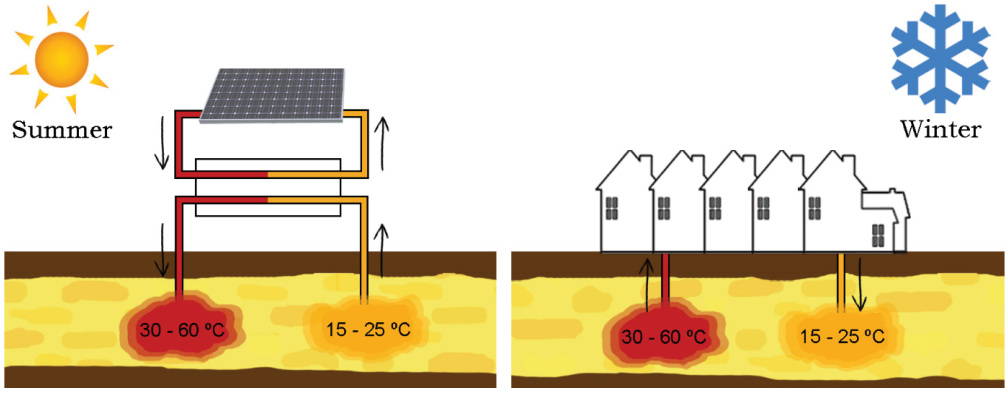

Figure 4.1 High temperature aquifer thermal energy storage (HT-ATES) system working principle. (Left) In summer, available heat from solar + heat pump (PtH) is stored in the HT-ATES system. (Right) In winter, heat is delivered from the HT-ATES hot wells.

Compared to LT-ATES, the higher storage temperatures require consideration of temperature-dependent density and viscosity to simulate the heat transport [126], [238]. Therefore, the simulations for heat injection, storage and extraction are performed using the coupled groundwater flow model MODFLOW and the multi-species transport code MT3DMs in connection with SEAWAT [239]–[241]. In this study, we use Flopy, a software package to operate SEAWAT from within a Python environment [242]. The multi-energy system model is also programmed in Python code to facilitate coupling with the ATES model.

4.2.1.1 Modelling Approach

Depending on the needed maximal capacity of a specific HT-ATES system (e.g., MW_{th}), the productivity of the aquifer and the well screen length (dependent on the aquifer thickness), multiple hot and warm wells could be needed. In practice, these wells should be placed in such a configuration that interaction between wells has a positive effect. Beernink et al. (2020) showed that positive interaction between the hot and warm well(s) of a HT-ATES system causes a relatively small positive effect (< 7%) on overall system performance compared to a situation without interaction [243]. Therefore, to simplify the modelling exercise, we assume that the total thermal volume is stored and recovered from one hot and one warm well which do not interact. Our simulations, compared to a 3D model, thus represents a slight underestimation of actual overall performance. Because of these simplifications, an axisymmetric hydrogeological model could be used, as was done previously [126], [244]. For both the hot and the warm well, a separate axisymmetric model is initialized. From monitoring data, Lopik et al. (2016) [126] established a calibrated axisymmetric model of a

high temperature (80 °C) ATES system. In this study, we therefore use a similar axisymmetric model set-up and parameter values. Several modelling aspects of the model are described below:

- *Spatial discretization.* The spatial discretization in the horizontal direction is 0.5 m close to the well location. Because flow velocity decreases with the radial distance from the well, the cell size may increase outwards. This was done logarithmically to a maximum of 50 m at the model domain boundary. To prevent boundary conditions from influencing simulation results, several test runs were carried out. The test runs showed that outcomes did not change significantly (< 1%) with an increasing grid size of 1500 m around the well. This was therefore set as the outer model boundary distance. To allow for sufficient detail/insight in the vertical (free convection) flow component, the vertical layers are also discretized at high resolution; 0.5 m thickness. Further refining of the modelling grid did not result in different results. The discretization was therefore assessed to be sufficient.
- *Temporal discretization.* Internal time steps of the SEAWAT model are limited because of the courant number that is implemented in the advection package. We use a value of 0.8, meaning that the maximal distance that advection will be allowed in one internal transport time step is 0.8 cell length; the length of the time step is automatically adjusted accordingly. Model input and output is changed and transferred with the multi-energy system model with a daily time step. This means that the flow in/out of the wells is changed once a day and evenly divided for this timespan.
- *Boundary conditions.* The boundary conditions are set as constant head and constant temperature at the outer boundary of the modelling domain. The top and bottom of the model are set as constant temperature and no-flow boundary. The constant temperature is equal to the starting temperature of the aquifer groundwater, T_{amb} = 12 °C. Therefore, water enters the model via the well or via the outer model boundary (at 1500 m distance). Heat can leave the model domain via the top, bottom, and outer model boundaries.
- *Subsurface characterization and hydrogeology.* The characterization of the subsurface parameters follows the subsurface model presented in [24], which is a 30 m thick homogeneous aquifer. The model consists of an aquifer confined by 25 m thick aquitards at the top and bottom. Aquifer horizontal hydraulic conductivity is 35 m/d, aquitard horizontal hydraulic conductivity is 0.05 m/d, and hydraulic conductivity anisotropy was used as $K_h/K_v = 5$ for both the aquifer and the aquitard.
- *Well implementation.* The simulated wells have a fully penetrating well screen (L_{well} = 30 m). The well screen consists of multiple grid cells based on the vertical discretization. The flow for each well screen cell is calculated proportionally to the transmissivity distribution along the layers belonging to the cells. For the modelled homogeneous aquifer, this results in equal flow distribution over the well screen length. The extraction temperature of each well cell is calculated by SEAWAT as the average well temperature at the well screen during extraction or injection.
- *Parameter values.* The parameter values assigned to MODFLOW follow Lopik et al. (2016) [30] and are corrected for axisymmetric flow according to Langevin (2008) [244], and given in Table 4.1.
- *Solvers.* The groundwater flow is solved using the Preconditioned Conjugate Gradient 2 package. The standard finite-difference method with upstream or central-in-space weighting is applied in the advection package.

Table 4.1 MODFLOW, MT3DMs and SEAWAT simulation parameters.

Parameter	Value	Used for Package class [242]
Water heat capacity	4.18 kJ/kg/°C	RCT
Solid heat capacity *	710 kJ/kg °C	RCT
Water reference density	1000 kg/m^3	RCT
Solid density *	2640 kg/m^3	RCT
Water thermal conductivity	0.58 W/m/°C	RCT
Solid thermal conductivity	3 W/m/°C	RCT
Thermal distribution coefficient #	1.7 × 10^{-4} m^3/kg	RCT
Thermal retardation +	2.21	RCT
Porosity	0.3	BTN
Specific storage aquifer	6 × 10−4/m	LPF
Longitudinal dispersion	0.5 m	DSP
Transversal dispersion	0.05 m	DSP
Vertical dispersion	0.005 m	DSP
Effective molecular diffusion heat #	0.157 m^2/day	DSP
Effective molecular diffusion salt	8.6 × 10^{-6} m^2/day	DSP

* quartz, # Calculated following Langevin et al. (2008) [241], + Calculated following Hecht-Mendez et al. (2010) [245]. RCT = MT3DMs Chemical Reaction package, BTN = MT3DMs Basic Transport package, LPF = MODFLOW Layer Property Flow Package, DSP = MT3DMS Dispersion Package.

4.2.1.2 *Implementation of Variable Viscosity and Density*

The viscosity and density of groundwater decrease with increasing temperature. This has an effect on the behavior of the groundwater at elevated temperatures compared to the ambient groundwater. Implementation of this relationship with temperature, therefore, is important for this modelling exercise. In reality, both viscosity and density have a non-linear relationship with temperature. In this study, we use the viscosity and density dependency of water as implemented by Langevin et al. (2008) [241]. Here, the non-linear viscosity–temperature relationship of VOSS (1984) [246] was used to determine the groundwater viscosity accurately. For density, however, a linear relationship was used to calculate the density at different temperatures. This was done because SEAWAT does not simply allow for a non-linear density function. Therefore, we used an approximation based on the injection temperature to include the possible influence of buoyancy flow according to the following linear relationship, similar to previous research [247]:

$$\rho(T) = \rho_0 + \frac{\delta\rho}{\delta T}(T - T_{amb}) \quad (4.1)$$

where T is the water temperature in the aquifer °C and ρ is the density in kg/m^3. Here, the density change gradient per temperature difference ($\delta\rho/\delta T$) is changed according to the maximal injection temperature, resulting in a value of −0.22 for *Tinj* = 50 °C and a value of −0.29 for *Tinj* = 65 °C.

4.2.2 Multi-Energy System Model

To analyze different layouts for future multi-energy systems (in neighborhoods) a simulation model was developed that matches supply and demand on an hourly basis and integrates different renewable energy sources, conversion and storage mechanisms [171], [235] (**Chapter 2 & 3**). In Figure 4.2, an overview of the model components is given, with a highlight on the aspects that are the focus of this study. Most of the modelling methodology has been explained in detail earlier, including both energy and water aspects [134], [171], [235] (**Chapter 2 & 3**); here we focus on the coupling between the multi-energy system model and HT-ATES integration. The Python simulations of different model setups are done with an hourly time step for 10 years. The most important aspects of the model related to heat production and storage are described in the following paragraphs.

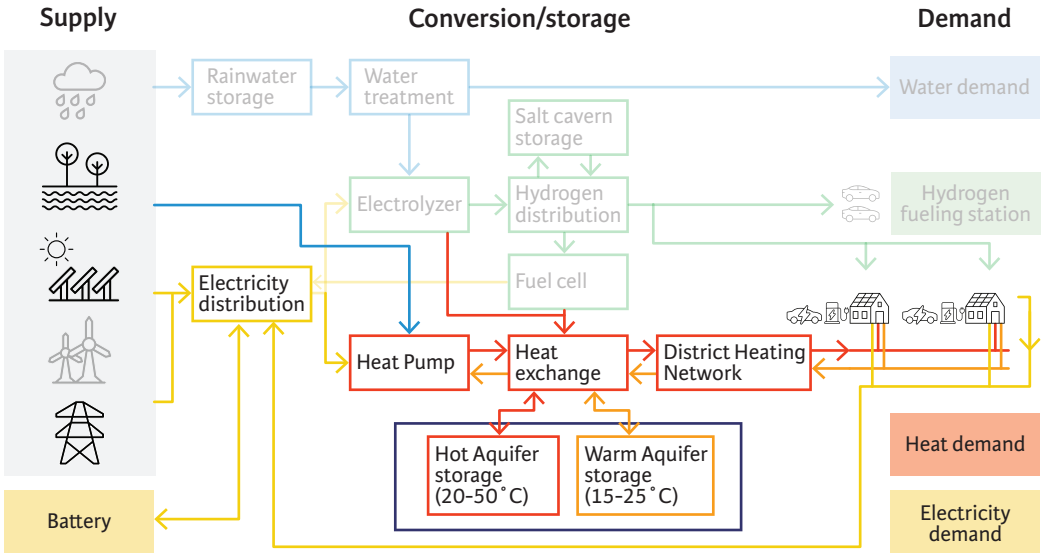

Figure 4.2 Overview of the components in the multi-energy system model, with a highlight on the model parts that are the focus of this chapter.

4.2.2.1 COP Heat Pump

The coefficient of performance (COP) curve of the heat pump (HP) is based on supplier information (GEA: cooling agent R717, extra heat recovery by oil cooling, 1.8 MW_{el} installation at 65 °C and 50 °C condenser temperature) for heat pump condenser temperatures of both 65 °C and 50 °C. From literature [185], we know that the COP of a heat pump (COP_{HP}) is mainly based on the temperature lift and less on the exact condenser temperature (heat sink). Therefore, we can use one equation for different condenser output temperatures ($T_{HP,cond}$) (heat sinks), as long as the temperature lift between condenser and evaporator temperature ($T_{HP,evap}$) is taken into account:

$$COP_{HP} = -0.00007 \cdot (T_{HP,cond} - T_{HP,evap})^3 + 0.0097 \cdot (T_{HP,cond} - T_{HP,evap})^2 - 0.5311 \left(T_{HP,cond} - T_{HP,evap}\right) + 14.68 \quad (4.2)$$

4.2.2.2 Heat Demand Pattern

The model input for heat demand is a fixed yearly heat demand that varies per type of household. Based on the degree-day method [248], the total heat demand is distributed over the runtime with the adaptation of using degree-hours, according to:

$$h_{DH,t} = \frac{T_{base} - T_{air,t}}{24} \; if \; T_{air,t} < T_{base} \quad (4.3)$$

with $h_{DH,t}$ being the number of degree-hours in a certain hour and $T_{air,t}$ being the outside air temperature, based on KNMI data from De Bilt [249]. The base temperature T_{base} is set to be 14 °C to calculate the degree-hours for a certain moment in time. In the degree days method, it is important to choose the right base temperature, which is often set around 18 °C [250]. We have chosen a value of 14 °C because the houses we consider in this case are well isolated and probably have a low-temperature heating system (such as floor heating) and large building inertia, and therefore space heating is not necessary above 14 °C outside air temperature. The heat degree hours are also weighted based on the season. This means $h_{DH,t}$ is multiplied by 1.1 in November–February, by 1.0 in March and October, and by 0.8 in the remainder of the year [250].

The next step is to calculate the heat demand of the neighborhood for every hour of the run period, based on the specific fraction of the total amount of heat degree hours:

$$Q_{spaceheat,t} = \frac{h_{DH,t}}{\sum HDH} \cdot E_{spaceheat,total} \quad (4.4)$$

Here, $Q_{spaceheat,t}$ is the heat demand of the neighborhood in a specific hour (t) in MJ, $\sum HDH$ is the sum of all heat degree hours over the total run period (in this case 10 years), and $E_{spaceheat,total}$ is the total heat demand for the run period in MJ.

Using this method implies that the distribution of the heat demand varies with the run period chosen. On the one hand, this is an advantage as yearly variations in outside air temperature are taken into account. On the other hand, this implies that the space heat demand of a particular

hour can vary slightly for a run period of i.e., 2010–2012 vs. 2017–2019. It is therefore important to only compare scenarios with the same run period; in our case data from 2010–2019 are used for all scenarios.

4.2.2.3 Heat Supply Pattern

To ensure enough heat is stored to cover the heat demand in winter, a certain amount of heat needs to be stored in spring and summer. This should be the heat demand plus the expected loss during storage. The model applies a pattern with weekly values that represent a percentage of the total yearly heat demand that should be stored in the months from March to October, as elaborated upon in an earlier publication [171, p. 6] (**Chapter 2**). To compensate for the heat loss, a factor is applied to the total heat demand. The model will adapt this factor every year based on the difference in volume that is stored either in the hot or warm well. If the difference in volume is more than 15%, the factor is either increased by 0.1 (if the volume stored in the hot well is too small) or decreased by 0.15 (if the volume in the warm well is too small). The starting value of the loss factor is 1.8 for this study, meaning that the heat storage target for the HT-ATES is 1.8 times the yearly heat demand of the neighborhood at the start of the run time. This value of 1.8 is higher than the actual expected heat loss over time, because in the first years of system operation a shell with elevated temperature around the stored volume is developed. After this period, the loss factor will start to decrease and will finally stabilize around the yearly heat loss value of the wells (which is more around 1.1–1.4).

4.2.2.4 Coupling of the HT-ATES Model and the Multi-Energy System-Model

The input of the SEAWAT model (see Section 4.2.1) is adjusted with a daily time step, while the multi-energy system model calculates the energy flows on an hourly basis. To bridge the hourly and the daily models, the hourly data of the multi-energy system is stored and combined into daily input data for the SEAWAT model. This can be interpreted as having an above-ground buffer tank that controls the daily fluctuations of the energy system. From the hourly multi-energy system model, both the weighted average temperature and the corresponding net flow from/to the HT-ATES are used as input for the SEAWAT model. The SEAWAT model subsequently returns the temperature of the extracted groundwater of both the warm and the hot well after simulation. These values are then used for the next 24 h of the overall energy system model calculations.

4.2.3 Application of the Multi-Energy System Model in a Case Study

4.2.3.1 Case Description; Nieuwegein, The Netherlands

In order to apply our multi-energy system with HT-ATES integration, we present a field case located in the eastern part of Nieuwegein (the Netherlands). We assume 2000 houses will be connected to a low-temperature heat grid and the houses will be suitable for low-temperature floor heating. The energy for domestic hot water production is provided with a booster heat pump. Assumptions for heat demand are given in Table 4.2 and are based on the Dutch energy label B, which is not the most efficient building type but is on a European level in the range of a Nearly Zero Energy Building

(40–70 kWh/m²) [196]. Energy demand related to domestic hot water consumption is set at 3.3 GJ/person/year [195]. In this chapter, we use the case study only to determine the heat demand of the neighborhood and the role of heat storage in the fulfilment of heat demand. For exact temporal energy flows (local use, import and export) and comparison of the MES with a HT-ATES with other possible system designs, the reader is referred to an earlier publication focusing on the same neighborhood case [235] (**Chapter 3**).

Table 4.2 Neighborhood energy demand parameters.

	Terraced House	Apartment	Total
Number of houses	1000	1000	2000
People per household	2.4	2	-
Energy demand domestic hot water	7.9 GJ/y	6.6 GJ/y	14.5 TJ/y
Space heat demand	24.4 GJ/y	17.6 GJ/y	42 TJ/y

The main heat source of the neighborhood is heat from surface water (aquathermal energy) provided by the Lekkanaal, a 100 m wide channel located east of the case study area. The surface water heat is extracted in summer (April–September) and the temperature is raised by a large scale heat pump. Part of the heat is used to provide heat directly, and the remainder of the heat is stored in a HT-ATES system to be utilized during winter. A HT-ATES system is chosen as the most suitable heat storage option, because of the large storage size required for 2000 houses, combined with a relatively low amount of space available on the surface level. The large scale heat pump will use excess electricity from local sources such as a solar farm and home solar PV systems on houses, supplemented with electricity from the grid to ensure enough heat is stored to fulfil the total heat demand of the neighborhood in winter. This system layout could assist in peak reduction on the electricity grid by PV systems in summer and prevent high peaks in electricity demand in winter if houses would be heated by i.e., an (air-sourced) heat pump. In this way, it is thus possible to decouple supply and demand, which gives more flexibility in a future energy system based on renewable energy.

Hourly weather data on outside temperature from the period 2010–2019 are used in this analysis, from the weather station De Bilt (closest to the project location) [211].

4.2.3.2 Modes of Operation for the Heat Pump and HT-ATES

The heating system has different modes of operation defined in the model, depending on the situation. In the explanation, we have chosen a heat pump condenser temperature of 50 °C and heat delivery via a district heating network (DHN) with a minimum of 40 °C. Schemes for a heat pump condenser temperature of 65 °C are given in the ***Supplementary Information***.

There are five possible modes of operation:

1. *Heat production and storage in the HT-ATES (no heat demand)*
   In this mode of operation, heat is produced with surface water (14–26 °C) as input during the summer months (see Figure 4.3A). Heat is injected into the hot aquifer at 48.5 °C (assumed 1.5 °C loss over the heat exchanger).

2. *Simultaneous heat production and delivery*
   If there is a heat demand at a time when the heat pump is producing heat (during summer), the heat demand is fulfilled directly from the heat pump (50 °C) via the hot distributor (see Figure 4.3B). After fulfilling the heat demand, the remainder of the heat is injected into the hot aquifer at 48.5 °C.

3. *Heat delivery from the HT-ATES above the inlet temperature of the district heating network (hot well > 43 °C)*
   In the period from October–April (approximately), the heat pump is not able to produce heat with surface water as the surface water temperature is too low (< 14 °C). Heat demand from the multi-energy system is now fulfilled by extracting heat from the hot aquifer of the HT-ATES system (see Figure 4.3C). Water from the hot well (43–48.5 °C) is extracted and exchanged with the return flow from the DHN (25 °C) and subsequently injected into the warm well (at 26.5 °C). The heat supply flow of the DHN is heated to 41.5–47 °C.

4. *HT-ATES is shut off (Hot well under threshold temperature < 43 °C)*
   In this mode of operation, the temperature of the hot aquifer has dropped below the threshold temperature (43 °C) to guarantee heat delivery at 40 °C. The HT-ATES system is now shut off and cannot be used to fulfil the heat demand of the multi-energy system. In this case, heat must be delivered from another (external) source, such as a peak boiler or a sustainable heat source. This is not included in this analysis. For this study, we added an extra mode of operation to prolong the heat delivery from the HT-ATES system and to assess its effect on the efficiency of the heat production system and the heat production costs.

5. *HT-ATES feeds heat pump mode; heat delivery from the HT-ATES with alternative threshold temperature (hot well temperature between 30 °C and 43 °C)*
   To prolong heat delivery from the HT-ATES system, we designed an extra mode of operation for the heat pump and HT-ATES. In this mode of operation, the heat delivery from the HT-ATES continues when the temperature of the hot well is below 43 °C but above 30 °C. This is possible because of additional heat exchange with the HT-ATES in combination with a heat lift by the heat pump (see Figure 4.3D). First, the return flow of the DHN is exchanged with water from the hot well (30–43 °C) and thereby the return flow is heated to 28.5–41.5 °C. This already heated return flow of the DHN is then fed to the condenser side of the heat pump and raised to 50 °C. The flow from the hot aquifer

is thus first exchanged with the return flow of the DHN, which results in a temperature of 26.5 °C. Then, the same flow is led to a second heat exchanger, to extract more heat by a (closed) loop that is connected to the evaporator side of the heat pump (inlet temperature of 25 °C). The return flow from the evaporator side of the heat pump is then finally exchanged with the flow that is injected in the warm well (at 16–22.5 °C). In this way, the heat from the hot well is exchanged in two stages before being injected into the warm well, making the heat exchange more efficient. Moreover, the injection temperature in the warm well is decreased, creating a larger ΔT between the wells which could be beneficial for the HT-ATES efficiency. The electricity demand of the heat pump in this mode is retrieved directly from local RES (renewable energy systems) when possible, or from the grid when no electricity from local RES is available.

A) Mode of operation 1

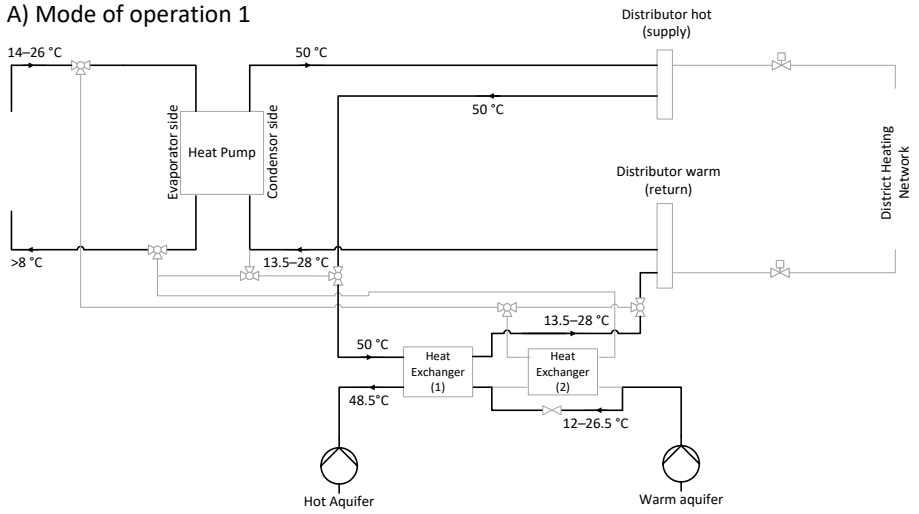

B) Mode of operation 2

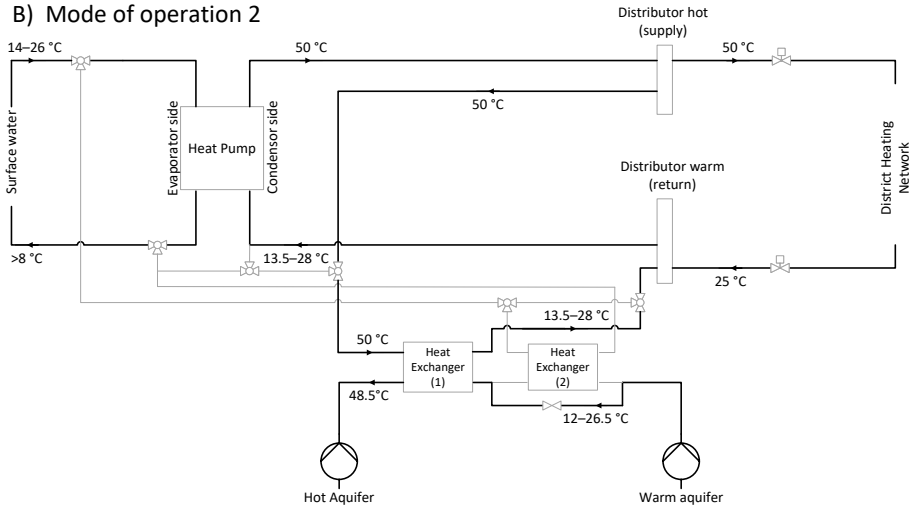

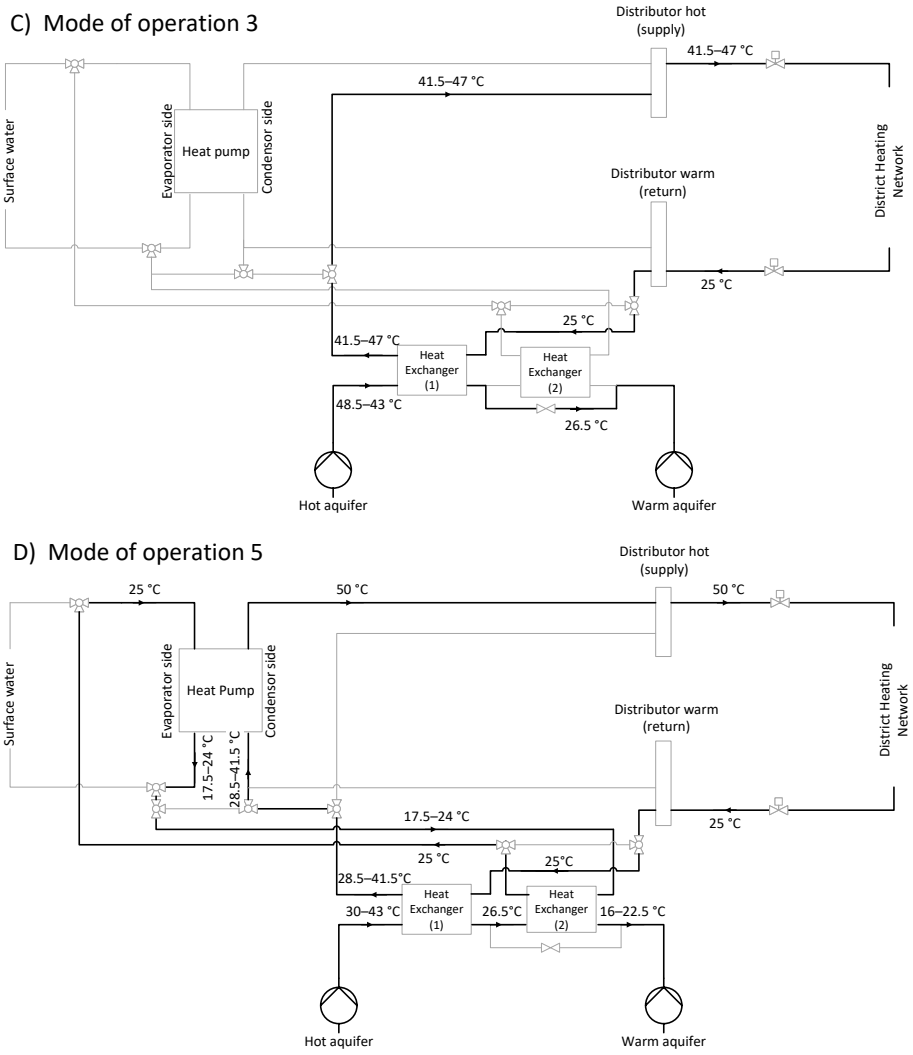

Figure 4.3 Overview of the hydraulic schemes for the different modes of operation. (A) Mode of operation 1: Heat production and storage in the HT-ATES. (B) Mode of operation 2: Simultaneous heat production and delivery. (C) Mode of operation 3: Heat delivery from the HT-ATES above the inlet temperature of the DHN. (D) Mode of operation 5: HT-ATES feeds heat pump mode for charging the HT-ATES with a heat pump condenser temperature of 50 °C. In the mode of operation 4, the HT-ATES is shut-off, therefore no hydraulic scheme is shown. The shaded lines are inactive hydraulic connections, needed for other modes of operation. An indication of the temperature (range) of the different flows is given.

4.2.4 Scenarios

The goal of this study is to identify methods for integration and control of a HT-ATES within a multi-energy system, as well as assess how these methods affect the performance of the energy system. In Section 4.2.3, we have introduced an additional mode of operation for the heat pump/HT-ATES system. We hypothesise that this mode of operation prolongs heat delivery from the hot well and could increase the overall performance of the heat pump/HT-ATES system. Therefore, we have selected ten scenarios (Table 4.3) to examine this hypothesis, as well as obtain general insights on how the HT-ATES system performs within the multi-energy system.

The heat demand and heat delivery temperature are kept constant for all scenarios. The amount of heat that should be provided to the neighborhood houses is 55.2 TJ per year at a temperature of at least 40 °C. We have chosen to vary the condenser temperature, the threshold temperature (HT-ATES feeds heat pump mode) and the size of the heat pump. Table 4.3 gives an overview of the ten scenarios that are investigated in this study. The description code is built up as: condenser temperature|HT-ATES threshold temperature|heat pump size.

We compare two condenser temperatures because we hope to learn more about their actual effects on heat delivery, recovery efficiency and costs. We know that a higher condenser temperature of 65 °C leads to a lower COP of the heat pump compared to 50 °C, decreasing the amount of energy that can be stored with a given heat pump size. Additionally, the heat pump will be more expensive at a higher condenser temperature and more heat loss can occur at a higher storage temperature. On the other hand, storage at 65 °C leads to a smaller storage volume for the HT-ATES system, which saves costs and space. By comparing scenarios with both condenser temperatures, we obtain more insight into the combined result of these contradictory effects on the chosen performance parameters.

To ensure heat delivery at 40 °C, the threshold value for the hot well is set at 43 °C. In Section 4.2.3, we introduced an HT-ATES feeds heat pump mode that allows a lower threshold temperature of the hot well of 30 °C, as the heat pump is then used for an extra temperature lift. Scenarios 65|30|2, 65|30|1.5, 50|30|2 and the 50|30|1.5 will give insight into the effects of including this HT-ATES feeds heat pump mode, and can be compared to their respective twins where the HT-ATES feeds heat pump mode is not used and the threshold temperature is set at 43 °C.

Lastly, we investigate the effect of different heat pump sizes. A smaller heat pump will save costs, but it should be large enough for the HT-ATES system to provide sufficient heat in winter. We hypothesise that the scenarios with an extra heat pump mode lead to a more efficient HT-ATES system, which could imply that the amount of heat stored in the HT-ATES could be reduced. For a good comparison, we included scenarios with a 2 MW_{el}, 1.5 MW_{el} and 1 MW_{el} heat pump. We expect the 1 MW_{el} heat pump to be too small to fulfil the heat demand of the neighborhood in the multi-energy system (55.2 TJ/y). With an average COP of 4 and approximately five months of heat production, a maximum of 51.8 TJ/y could be stored with a 1 MW_{el} heat pump, which is less than the heat demand of the neighborhood (55.2 TJ/y). However, to investigate the effect of a relatively small heat pump

on the HT-ATES system, we included two scenarios with a 1MW_{el} heat pump, both with a lower (30 °C) threshold temperature.

Table 4.3 Overview of scenarios.

	Heat Pump Condenser Temperature	HT-ATES Threshold Temperature	Heat Pump Size
65|43|2	65 °C	43 °C	2 MW_{el}
50|43|2	50 °C	43 °C	2 MW_{el}
65|30|2	65 °C	30 °C	2 MW_{el}
50|30|2	50 °C	30 °C	2 MW_{el}
65|43|1.5	65 °C	43 °C	1.5 MW_{el}
50|43|1.5	50 °C	43 °C	1.5 MW_{el}
65|30|1.5	65 °C	30 °C	1.5 MW_{el}
50|30|1.5	50 °C	30 °C	1.5 MW_{el}
65|30|1	65 °C	30 °C	1 MW_{el}
50|30|1	50 °C	30 °C	1 MW_{el}

4.2.5 Assessment Framework

4.2.5.1 Fulfilment of Heat Demand

The main goal of the combined heat pump and HT-ATES system is to fulfil the heat demand of the neighborhood in the multi-energy system in a reliable and affordable way. To fulfil the heat demand at a certain moment, there are multiple options. In our system, we first check if the heat demand can be fulfilled by direct heat production, which mainly happens during summer. Next, it is checked if the heat demand can be fulfilled by the HT-ATES system, which mostly happens in the winter season. If the HT-ATES feeds heat pump mode (see section 4.2.3.2) is switched on, it is possible to increase the temperature of the HT-ATES with the heat pump, and the heat demand is fulfilled by the HT-ATES system with some additional electricity use. Lastly, if the temperature of the hot aquifer is below the set threshold temperature (43 °C or 30 °C in our case), the HT-ATES system will not be used for heat production. In this case, an external source of heat is necessary. This external source is not defined in this study, but could, for example, be a peak gas boiler, or a renewable option.

In the first few years of operation, it is likely that the HT-ATES system has not yet stored enough heat to ensure continuous heat delivery throughout the year. However, the goal would be to reach continuous operation within a few years, so no external heat source is necessary and the heat pump-HT-ATES system can function independently.

Because the heat pump can work on 100% renewable electricity with surface water as a source, there are no direct GHG emissions of the system if it operates independently from an external source. Energy use during production and recycling of system components is not taken into account here. The GHG emissions of the external heat source are not taken into account in this study as we do not define a particular heat source.

4.2.5.2 HT-ATES Performance

The performance of the HT-ATES system is assessed with two main parameters, the well recovery efficiency of stored energy and the volume balance between the wells.

Regarding the recovery efficiency, we use three different indicators that give insight into the efficiency of the heat system as part of the multi-energy system. The performance of the HT-ATES system is calculated in terms of hot well recovery efficiency, warm well recovery efficiency and system recovery efficiency. For each indicator, a separate ΔT is used, see below. The average recovery efficiency (η) over the total run period (10 years) is calculated and analyzed in the results section.

$$\eta = \frac{\sum_0^{10y} \Delta T \cdot V_{out} \cdot c_w}{\sum_0^{10y} \Delta T \cdot V_{in} \cdot c_w} \tag{4.5}$$

$$\Delta T_{system} = \hat{T}_{hot} - \hat{T}_{warm} \tag{4.6}$$

$$\Delta T_{hot\ well} = \hat{T}_{hot} - T_{amb} \tag{4.7}$$

$$\Delta T_{warm\ well} = \hat{T}_{warm} - T_{amb} \tag{4.8}$$

T_{hot} and T_{warm} are the temperatures of the hot and warm well (in °C) per day, vin and vout are the flows in or out of the hot well (m³/hr), and c_w is the heat capacity of water (4180 kJ/K/m³). T_{amb} is the ambient background temperature of the aquifer (12 °C). Depending on the ΔT applied in formula (4.5), either the system recovery efficiency (4.6), hot well recovery efficiency (4.7), or warm well recovery efficiency (4.8) is calculated.

Secondly, the volume balance ratio (r_{VB}) between the hot and warm wells is calculated as described by Beernink et al. (2019) [251]:

$$r_{VB} = \frac{V_{heat,storage} - V_{heat,production}}{V_{heat,storage} + V_{heat,production}} \tag{4.9}$$

where $V_{heat,storage}$ is the yearly total storage volume (m³) and $V_{heat,production}$ is the yearly total production volume (m³). Here, a positive ratio means that more volume is used to store heat in the hot well. Therefore, this also means that less volume is stored in the warm wells. Oppositely, a negative ratio means that more volume is stored in the warm wells.

4.2.5.3 MES Performance

For improved integration of HT-ATES within a multi-energy system, it is relevant to know the efficiency of the MES as a whole, under varying modes of HT-ATES integration. This indicator gives insight into the final efficiency by which the heat is delivered from the MES to the houses. Thus, this parameter is the amount of total delivered energy (heat) to the neighborhood divided by the used total energy (electricity) for heat production:

$$\eta_{MES} = \frac{En_{del,10y\ avg}}{COP_{10y\ avg} \cdot El_{dem,10y\ avg}} \tag{4.10}$$

With η_{MES} as the MES efficiency, $En_{del,10y\ avg}$ is the average amount of delivered heat to the neighborhood (in TJ/year over the first ten years), which can thus be lower than the actual heat demand. $COP_{10y\ avg}$ is the average COP of the heat pump over the run time (10 years), and $El_{dem,10y\ avg}$ is the average electricity demand of the total heat system over the run time (10 years).

It includes the efficiency of both directly produced as well as stored heat and heat loss in the district heating network. In case a certain system design is not able to provide the total heat demand, this is corrected for by only taking the delivered heat into account and not the total heat demand of the neighborhood. The part of the heat that must be delivered from an external source is thus not taken into account by this parameter. The MES efficiency purely gives the efficiency of heat delivery of the MES including a heat pump and HT-ATES system, without other sources.

4.2.5.4 Economic Analysis/Levelized Cost of Energy

We determine the levelized costs of heat production (LCOE) in €/GJ, including the costs for heat storage, and excluding the heat delivery (district heating network), according to:

$$LCOE_{heat} = \frac{\sum \alpha \cdot CAPEX_i + OPEX_i + E_{cost_i}}{Q_{heat,delivered}} \tag{4.11}$$

in which:

$$\alpha = \frac{r}{1 - (1+r)^{-L_i}} \tag{4.12}$$

where α is the capital recovery factor (no unit), representing a fraction of the total CAPEX costs depending on the yearly depreciation. r is the discount rate (as a fraction of 1) and L_i is the lifetime of a system component i. The $CAPEX_i$ are the total capital expenditures for a particular system component i, such as the heat pump, heat exchanger or HT-ATES wells. $OPEX_i$ are the operational expenditures and maintenance in €/year for a system component i, expressed as a percentage of the CAPEX. E_{cost_i} are the average (in this study, for 10 years) electricity costs for the heat system (in €/year). These costs are thus only for the modelled heat system, and not for any external source that might be necessary to fulfil the total heat demand. $Q_{heat,delivered}$ is the part of the heat demand delivered by the multi-energy system with HT-ATES in GJ/year. We thus only take into account

the heat that can actually be delivered by the multi-energy system with HT-ATES and not by an external source. This ensures a fair LCOE comparison between different scenarios.

Cost data is given in Table 4.4. A discount rate (*r*) of 6% (0.06) is applied, and electricity costs are set at 60 €/MWh_e based on CBS data for non-households with an electricity demand of > 70,000 MWh_e in 2019 [252], and is similar to Wesselink et al. 2018[75]. Lastly, the electricity use of the heat pump is calculated, averaged over the run period (here 10 years).

Table 4.4 Investment and operational costs for HT-ATES components.

System Component	CAPEX (in €)	OPEX (%)	Lifetime (in y)
Aquifers and equipment[a]	$(75{,}860 \times \ln(kW_{th}/6.69) - 115{,}000) \times 1.25$	4%	30
Heat exchanger[b]	$1500 \times \sqrt{kW_{th}} \times 1.1$	2%	20
Heat pump—65 °C condenser temp.[c]	600 €/kW_{th}	1%	20
Heat pump—50 °C condenser temp.[c]	400 €/kW_{th}	1%	20

[a] Formula was originally for ATES systems [253], and is adapted for HT-ATES by multiplying with 1.25, because at higher temperatures more expensive materials have to be used. [b] Costs data based on supplier data for ATES systems, multiplied by 1.1 for higher temperatures (HT-ATES). [c] Costs estimation based on different sources [185], [186] in combination with supplier data. Heat pump size in MW_{th} is calculated by multiplying the electrical power (MW_{el}) with the average COP of the heat pump in that scenario.

4.3 Results

In the previous section, we described the models, the coupling of the models and the scenarios that are used as input for the coupled model infrastructure. In this section, we describe the results of the scenario model runs assessed on the heat fulfilment by the (HT-ATES) system to the neighborhood, the performance of the HT-ATES, the differences in costs (LCOE) between scenarios, and finally we combine these results in an overall analysis of the performance.

4.3.1 Fulfillment of Heat Demand with HT-ATES

Simulation results show that in all cases, 12–14% of the heat demand in summer is delivered to the neighborhood directly by the heat pump for all scenarios (Figure 4.4) during the ten-year simulation (A) and the last five years of the simulation (B). This percentage is the same for each scenario because the net demand is the same and in all cases, the heat pump capacity is much larger than the heat demand in summer, when the heat pump produces heat that otherwise would be stored in the HT-ATES.

The simulation results show that at the heat delivered from the HT-ATES, a distinction is made between scenarios that are able to reach heat delivery by the HT-ATES system within five years, and scenarios that take longer to reach 100% delivery of demand by the heat pump and HT-ATES system. In scenarios that take longer than five years to reach 100% delivery, the HT-ATES system is shut off for > 20% of the time, which negatively influences the amount of heat delivered from the HT-ATES system (40–65%). The other scenarios that reach a stable heat supply within five years have 70–80% of the heat demand delivered from the HT-ATES system. In Figure 4.4B, the origin of the heat delivered during the last five years of operation of the heat pump-HT-ATES system are shown. Five scenarios can operate independently of an external source after an initial start-up period.

For this case study, we show that the addition of a HT-ATES to a multi-energy system with power-to-heat results in > 90% fulfilment of the heat demand during the first 10 years of operation, while after 3–5 years, the combined system can supply the full heat demand of the neighborhood in the multi-energy system sustainably.

The HT-ATES feeds heat pump mode of operation allows a lower threshold temperature. As a result, the HT-ATES system can be operated longer during winter. Hence, with a 2 MW_{el} heat pump, the amount of heat provided from the HT-ATES is increased by 6–7% when using the HT-ATES feeds heat pump mode (see Figure 4.4A). When specifically comparing the scenarios at 50 °C condenser temperature (see 50|43|2 and 50|30|2 in Figure 4.4A), the HT-ATES feeds heat pump mode decreases the time needed to reach 100% heat delivery from 5 to 3 years. This positive effect of the HT-ATES feeds heat pump mode is even more pronounced with a 1.5 MW_{el} heat pump and leads to 9–11% more heat delivery from the HT-ATES system.

For the 65 °C and the 1 MW_{el} and 1.5 MW_{el} heat pump scenarios, it is not possible to reach 100% heat delivery in 10 years. Without the HT-ATES feeds heat pump mode, an external heat source is still necessary after 10 years of operation (see 65|43|1.5 and 65|30|1.5 in Figure 4.4A). At 50 °C, the HT-ATES feeds heat pump mode is able to reduce the time it takes to reach stable operation to five years, compared to nine years for a scenario without the HT-ATES feeds heat pump mode (see 50|43|1.5 and 50|30|1.5 in Figure 4.4A). Thus, the HT-ATES feeds heat pump mode makes it possible to create a reliable HT-ATES system with a smaller heat pump (1.5 MW_{el} vs. 2 MW_{el}) at 50 °C condenser temperature.

The amount of electricity necessary for this mode comes from local RES when possible, or from the grid otherwise. In Figure 4.5, the electricity demand for heat production is shown over time in relation to the heat demand. This graph makes it clear that the electricity demand for the extra mode of operation is small in relation to the total electricity demand of the HT-ATES system. In all scenarios, it is never more than 2–6% of the total electricity demand of the HT-ATES system (6% for the 65|30|1.5 scenario in Figure 4.5). This small amount of electricity used in winter decreases the utilization of an external heat source for fulfilment of heat demand by 6–12%, depending on the scenario (12% for the 65|30|1.5 scenario). Furthermore, Figure 4.5 clearly shows the temporal decoupling of heat production and demand made possible by the integration of HT-ATES in the MES.

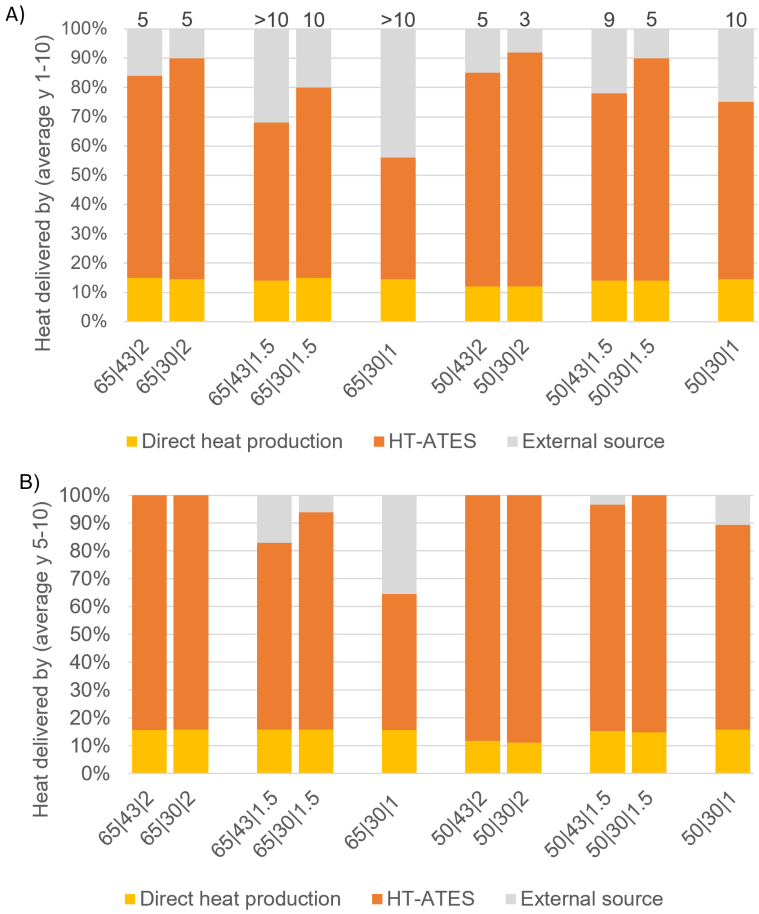

Figure 4.4 Stacked bar plots of the distribution of heat delivery from direct production of heat and from the HT-ATES system. In grey, the amount of heat that cannot be fulfilled by the heat pump and HT-ATES system is shown. The left plot (A) shows the distribution for the first ten years of operation. The numbers on top of the bars indicate the number of years when full heat delivery from the heat pump-HT-ATES system is reached, with no external source requirement. The right plot (B) shows the distribution of heat delivery for the last five years of operation, with five scenarios fully able to fulfil the heat demand.

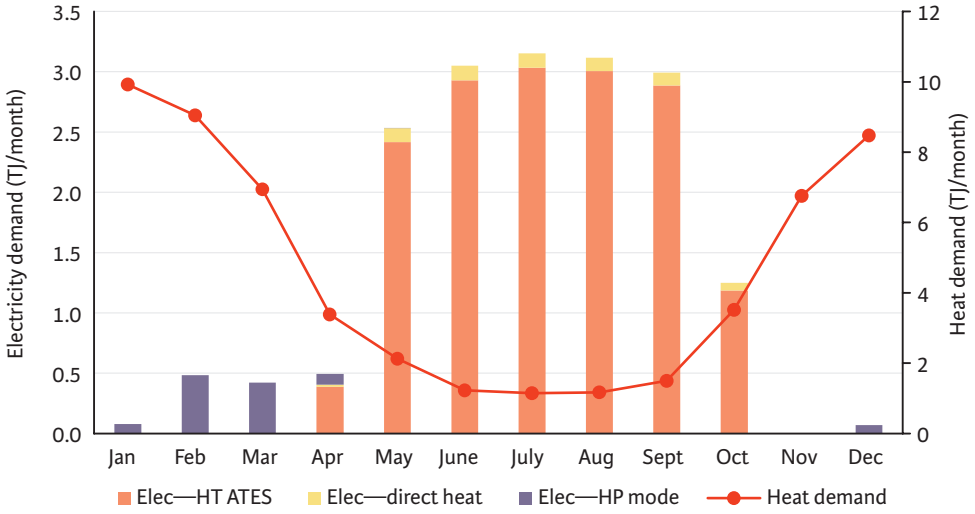

Figure 4.5 Electricity demand (left axis) for heat production is shown together with the heat demand (right axis) for the 65|30|1.5 scenario, which is the scenario with the highest utilization of the HT-ATES feeds heat pump mode. The electricity demand is divided into heat production for the HT-ATES (Elec—HT-ATES), the direct production of heat for the MES (Elec—direct heat) and the electricity for the HT-ATES feeds HP mode (Elec—HP mode).

4.3.2 HT-ATES Performance

4.3.2.1 Well Temperature Development

Results show that the fulfilment of the heating demand by the HT-ATES system varied significantly between the 10 scenarios (Figure 4.4), to a large extent as a result of the varying performance of the HT-ATES system. The HT-ATES system cannot supply the entire demand if the threshold temperature is reached during heat extraction from the hot well. Figure 4.6 shows the well temperature over time of the relatively large 2 MW_{el} heat pump size scenarios. The hot well temperature drops below the threshold temperature during recovery in the first years. After year 4, the hot well temperature always stays above the threshold temperature, both for the Tthreshold = 43 °C and the HT-ATES feeds heat pump mode (Tthreshold = 30 °C). The effect of the HT-ATES feeds heat pump mode is visible as a sharp drop in warm well temperature when the hot well temperature drops below the first threshold of T = 43 °C. For the 65 °C storage temperature, the HT-ATES feeds heat pump mode is no longer activated after the system has sufficiently warmed up after the first years, as shown in Figure 4.6A. For the 50 °C storage scenarios (Figure 4.6B), the HT-ATES feeds heat pump mode is active for most of the modelled years, because the hot well temperature often drops below the threshold of 43 °C at the end of extraction season. This is also visible in the warm well temperature of this scenario in Figure 4.6B; the warm well temperature drops once the HT-ATES feeds heat pump mode becomes active, which results in a very irregular warm well temperature pattern.

For the smaller heat pump scenarios (1.5 and 1 MW_{el}), the temperature in the hot and warm wells is presented in Figure 4.7. Here we observe the same behaviour, but the temperature drops in both the hot and the warm wells are stronger. Hence, for these smaller heat pump capacity scenarios, less heat is stored compared to a 2 MW_{el} heat pump, resulting in a more depleted heat storage at the end of the extraction season. As a result, the threshold temperature of 43 °C is reached for both the 65 °C scenarios and the 50 °C scenarios in almost all years. However, at the end of the simulated period, we see that higher temperatures are maintained and the threshold temperature is reached less often. This indicates that the losses of previous years have created a shell with elevated temperature around the stored volume over time. As a consequence, the heat loss decreases and the system moves towards an equilibrium situation.

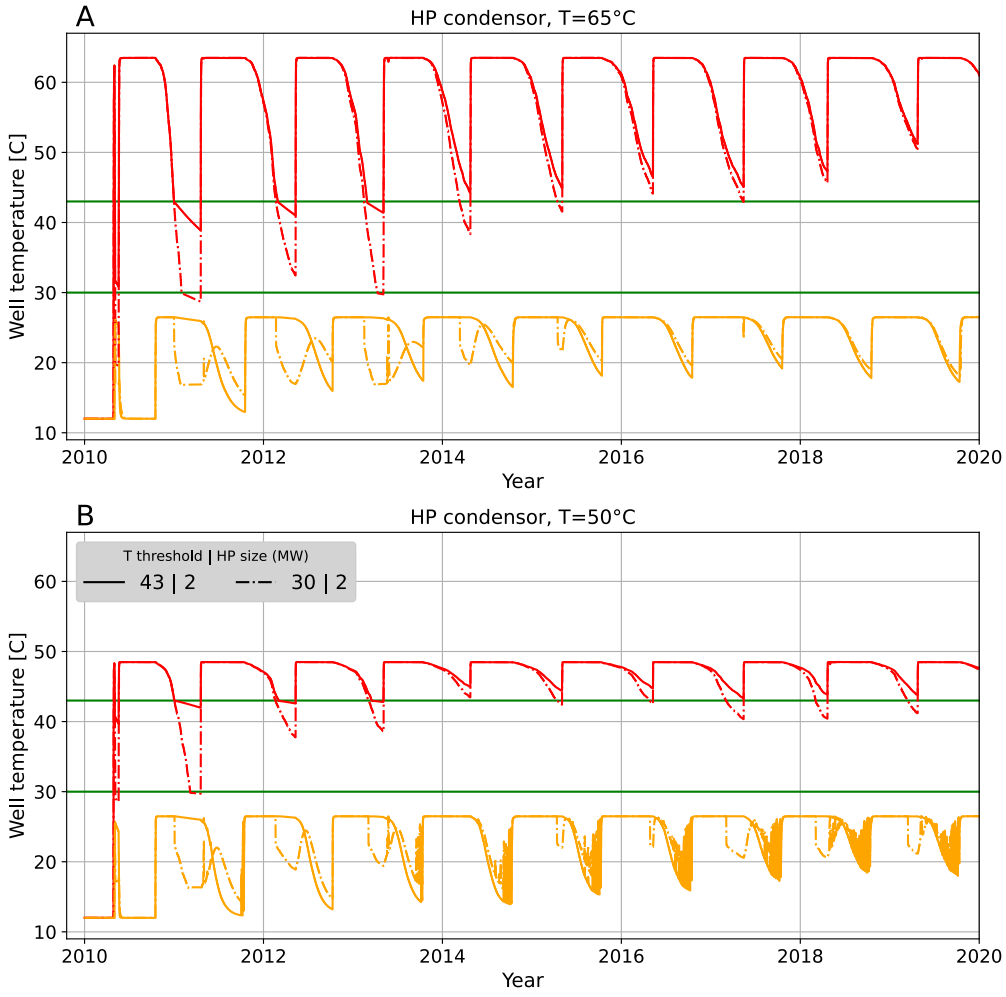

Figure 4.6 Overview of the temperature variations of the hot well and warm well for a 65 °C condenser temperature (A) and 50 °C condenser temperature (B). Scenarios with a 2 MW_{el} heat pump are shown, both with (65|30|2 or 50|30|2) and without (65|43|2 and 50|43|2) the HT-ATES feeds heat pump mode. The green lines show the threshold

temperatures at 43 °C and 30 °C (with the HT-ATES feeds heat pump mode). With the HT-ATES feeds heat pump mode (threshold temperature of 30 °C), a sharp drop in the temperature of the warm well is visible when the 43 °C threshold temperature in the hot well is reached. The HT-ATES feeds heat pump mode is utilized mostly during the first four years of operation at the 65 °C condenser temperature and during most of the run period at the 50 °C condenser temperature. The legend in (B) is valid for (A) as well.

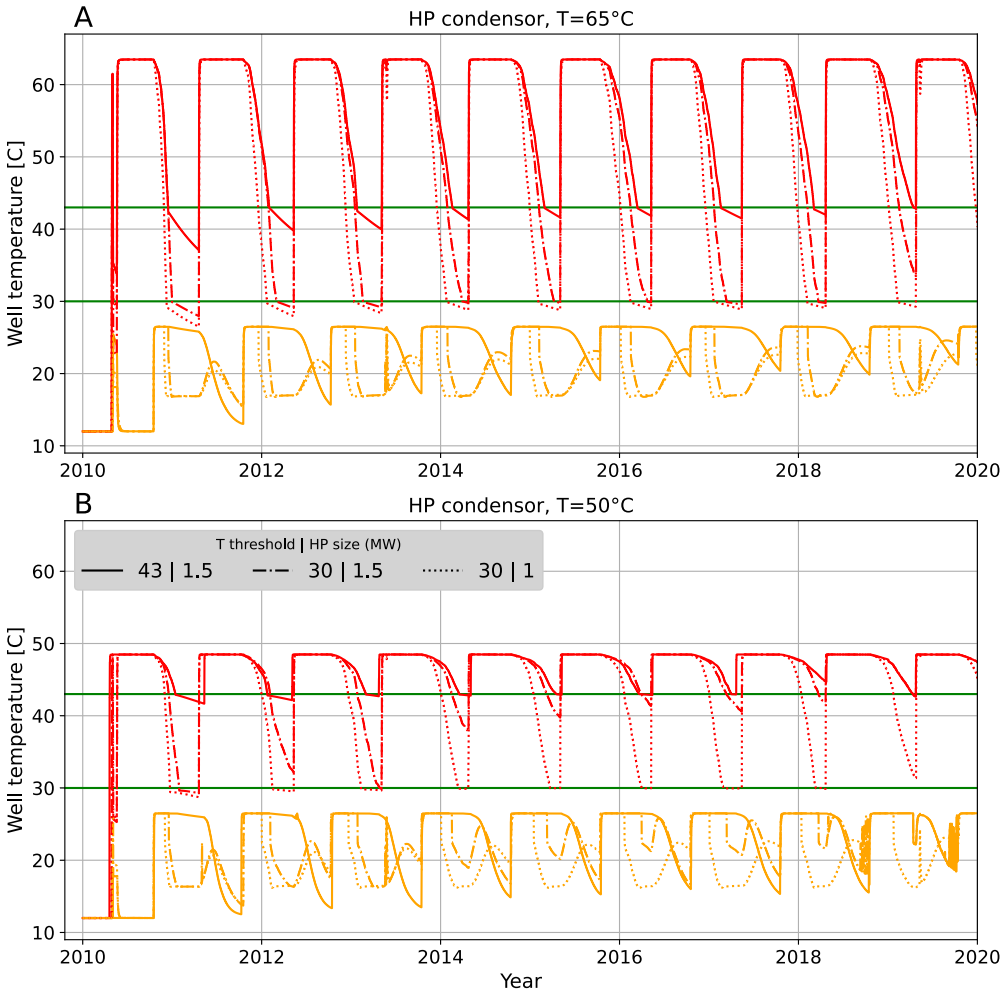

Figure 4.7 Overview of the temperature variations of the hot well and warm well for a 65 °C condenser temperature (A) and 50 °C condenser temperature (B). Scenarios with a 1.5 MW_{el} heat pump are shown, both with (65|30|1.5 or 50|30|1.5) and without (65|42|1.5 and 50|43|1.5) the HT-ATES feeds heat pump mode. Furthermore, scenarios with a 1 MW_{el} heat pump are included (65|30|1 and 50|30|1). The green lines show the threshold temperatures at 43 °C and 30 °C (with the HT-ATES feeds heat pump mode). The legend in (B) is valid for (A) as well.

4.3.2.2 HT-ATES Performance Results

The hot well, warm well and system recovery efficiency are presented in Table 4.5. In the previous section, we showed that the heat that is delivered by the multi-energy system is influenced strongly by the size of the heat pump. With a large heat pump size, more energy is stored in the subsurface in summer, which results in more energy that is recovered in winter. Table 4.5 shows that, while this might feel counter-intuitive, the system recovery efficiency is lowest (50–55%) for the scenario where most heat is provided to the multi-energy system (largest heat pump scenarios) and vice versa. Because the amount of stored energy varies between the scenarios, the delivery of heat from the HT-ATES system cannot be directly coupled to the recovery efficiency of the HT-ATES system.

In the large heat pump scenarios, more volume is stored in summer than required (and thus recovered) in winter, resulting in low recovery efficiencies. Oppositely, for the small heat pump scenarios, more volume is extracted in winter compared to what was stored in summer. The balance between these two volume flows, the volume balance ratio (rVB) varies from −0.15 for small heat pump scenarios to 0.21 for the large heat pump scenarios (Table 4.5).

In Figure 4.8, the recovery efficiency and rVB during the last five years of simulation are shown. The rVB has an opposite effect on the hot and the warm well efficiency. For the hot well, a negative rVB means that relatively large amounts of water is extracted, compared to what was initially injected, resulting in high recovery efficiency. The opposite is true for positive rVB.

The system recovery efficiency is a result of the recovery efficiency of the hot and the warm well. However, the hot well has a stronger influence, compared to the warm well, because relatively more heat is stored in this side of the system. Consequently, the highest system recovery efficiency is observed for the highest hot well recovery efficiencies at negative rVB. However, for the lowest rVB ratios, the system recovery efficiency stops increasing because the warm well recovery decrease has a stronger effect compared to the hot well recovery efficiency increase. It thus seems that maximal system recovery is obtained at slightly negative rVB.

The recovery efficiency is not only influenced by the volume balance ratio; the storage temperature affects the recovery efficiency as well. For higher storage temperature, more losses due to buoyancy flow occur, resulting in lower recovery efficiency. This is clearly visible for the scenario operating in volume balance (last five years) in Figure 4.8. Here, the warm well recovery efficiency is higher compared to the hot well recovery efficiency. Moreover, we observe two linear relationships for the hot well efficiencies, corresponding to the two varied storage temperatures, which is due to higher energy losses during storage for the 65 °C storage scenarios. Due to the limited difference in storage temperatures (65 °C vs. 50 °C) and the strong effect of volume balance, the recovery efficiency is dominated by the volume balance ratio for the simulated scenarios.

Table 4.5 Ten-year average HT-ATES performance results. The amount of stored energy is mainly determined by the size of the heat pump and the temperature levels. This subsequently results in different amounts of stored volumes and recovery efficiencies. The scenario name abbreviation consists of: condenser temperature|HT-ATES threshold temperature|heat pump size.

Scenario	Vhot Injection 10y Average (10^3 m^3/y)	Vhot Extraction 10y Average (10^3 m^3/y)	Volume Balance Ratio (rVB)	Hot Well Recovery Efficiency 10y Average (-)	Warm Well Recovery Efficiency 10y Average (-)	HT-ATES Heat Delivered 10 y Total ($En_{del,10y\ avg}$ in TJ)	HT-ATES Heat Stored 10 y Total (TJ)	HT-ATES System Recovery Efficiency 10y Average (-)	MES Efficiency 10y Average (ηMES)
65|43|2	446	339	0.14	0.64	0.88	413	778	0.53	0.53
65|30|2	450	397	0.06	0.69	0.85	445	780	0.57	0.56
65|43|1.5	330	282	0.08	0.70	0.82	322	569	0.57	0.57
65|30|1.5	315	389	-0.10	0.83	0.59	377	568	0.66	0.63
65|30|1	193	259	-0.15	0.86	0.51	239	354	0.68	0.64
50|43|2	774	509	0.21	0.63	0.92	436	900	0.48	0.48
50|30|2	736	570	0.13	0.71	0.89	480	838	0.57	0.55
50|43|1.5	692	450	0.21	0.62	0.90	381	810	0.47	0.48
50|30|1.5	680	540	0.11	0.71	0.87	448	785	0.57	0.55
50|30|1	432	441	-0.01	0.83	0.69	351	522	0.67	0.61

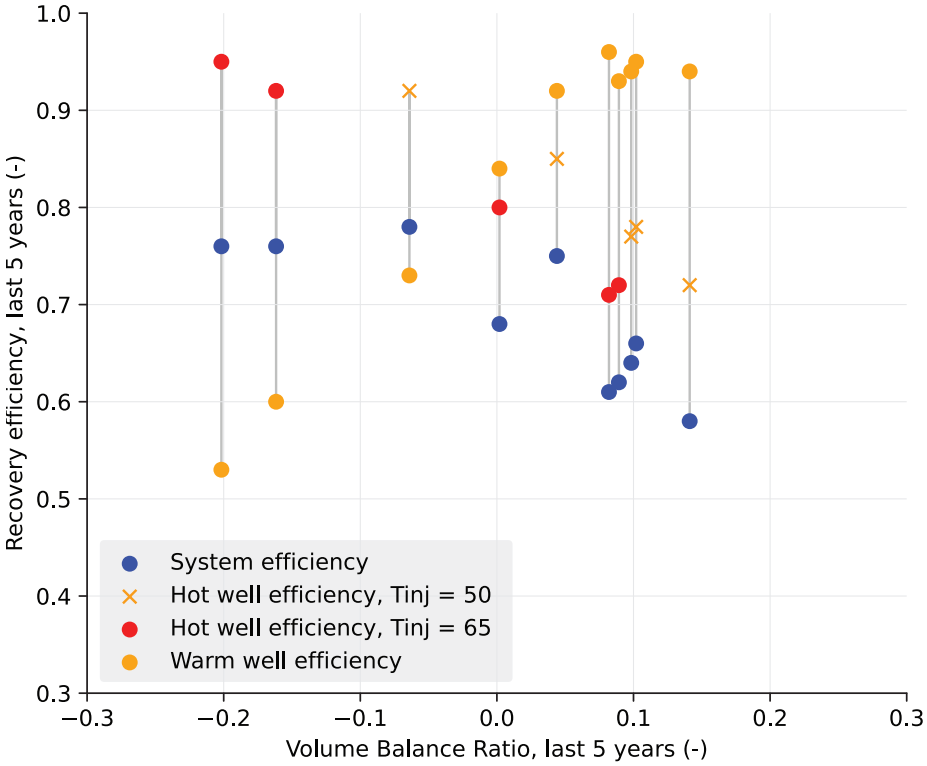

Figure 4.8 HT-ATES System, hot well and warm well recovery efficiency (last five years) (y-axis) vs. the volume balance ratio (rVB) during the last five years (x-axis) for the ten modelled scenarios. The average recovery efficiency during the last five years of simulation is shown to take out any effects of the first start-up years of HT-ATES operation.

The system recovery efficiency of the HT-ATES only indirectly provides insight into the amount of heat that is delivered to the multi-energy system, because this depends on the absolute amount of energy that is actually stored in the HT-ATES system. The largest heat pump scenarios can store and deliver most heat, but they do this with a relatively small system recovery efficiency, shown in Figure 4.9. Consequently, this means that a relatively high amount of the stored heat is lost to the subsurface. Additionally, we observe here that for equal heat pump size, the 50 °C scenarios can provide more heat, with a lower system recovery efficiency. This is caused by the fact that more heat is stored for the 50 °C scenario (higher COP of heat pump) and that less heat is lost during storage due to the lower storage temperature and larger storage volume.

To get more direct insight into the actual efficiency of the delivered heat within the MES, we have included the system delivery efficiency in the calculations (see Table 4.5). The system delivery efficiency of the MES is similar (1–2% lower) to the system recovery efficiency of the HT-ATES for most scenarios. This outcome indicates that heat loss in the district heating network and the direct heat production and delivery more or less outweigh each other in these scenarios. Three scenarios that take longer than eight years to reach 100% delivery and have a negative rVB (65|30|1.5, 65|30|1 and 50|30|1) have a slightly lower MES efficiency (3–6%) than HT-ATES system recovery efficiency.

Still, the same trend is observed that scenarios with a small heat pump have a high MES efficiency, but a relatively low amount of heat delivered, and vice versa.

The influence of the HT-ATES feeds heat pump mode when recovery temperatures reach the threshold is observed in Figure 4.9. For the four scenarios for which both the normal and the extra mode of operation were simulated, we observe that both the absolute amount of energy that can be delivered to the multi-energy system and the system recovery efficiency strongly increase. The HT-ATES feeds heat pump mode thus has a positive impact on the performance of the HT-ATES, resulting in a higher recovery efficiency of the system (4–10% depending on the scenario) which increases the amount of heat delivered (in TJ) to the houses (7–15% depending on the scenario). In Figure 4.9, the optimal scenario regarding heat delivery is the 50|30|2 scenario, because most heat is delivered (difference of 25 TJ), while the same system recovery efficiency is observed as the 50|30|1.5 and 65|30|2 scenarios.

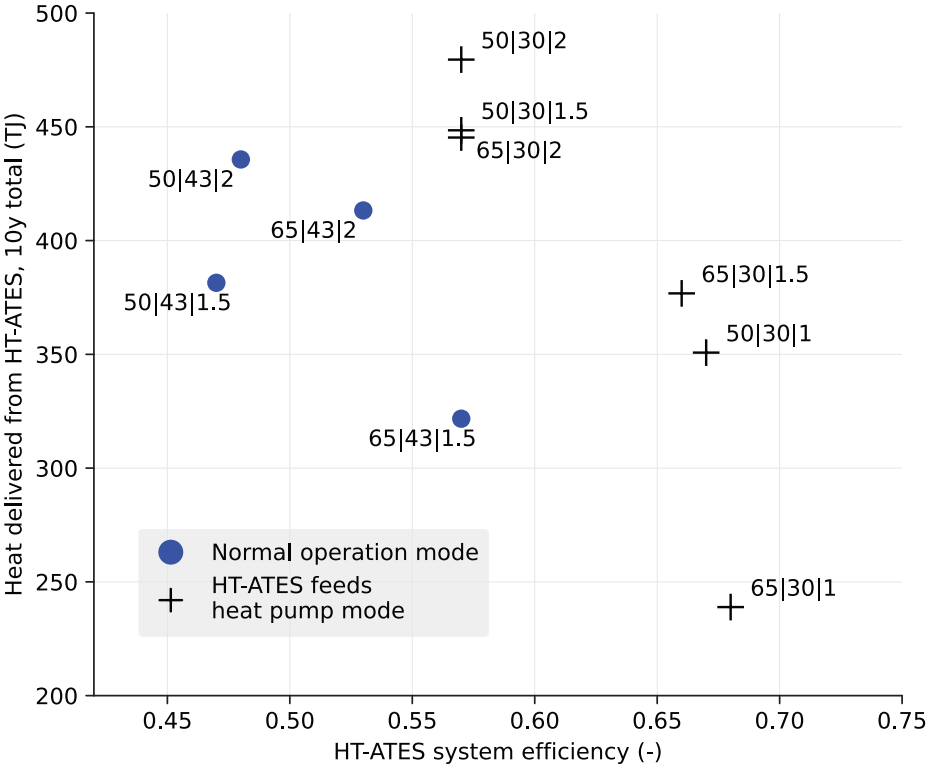

Figure 4.9 The absolute amounts of delivered heat (y-axis) vs. the HT-ATES system efficiency (x-axis) for the ten modelled scenarios. An optimal system would have both a high amount of delivered heat (TJ) and a high HT-ATES system efficiency. The HT-ATES feeds heat pump mode provides a more efficient HT-ATES system for all scenarios.

4.3.3 LCOE of Heat Production and Storage

The levelized costs of energy (in this case heat) in €/GJ are shown in Table 4.6. All scenarios with a 50 °C condenser temperature have a higher LCOE (2.5–4.5 €/GJ or 11–18%) than at 65 °C condenser temperature with the same heat pump size. An important reason is the higher COP for the 50 °C scenarios, which results in more heat injection in the HT-ATES with the same heat pump size. The difference in COP is proportional to the difference in Carnot efficiency based on the extra temperature lift when the heat pump condenser temperature is raised to 65 °C instead of 50 °C. This means that it is 30% more efficient to produce heat from surface water at 50 °C (average COP = 5.5) than at 65 °C (average COP = 4). Moreover, the heat pump investment costs per kW_{th} are higher for 65 °C (600 €/kW_{th}) than for 50 °C condenser temperature (400 €/kW_{th}). On the other hand, this cost difference is almost cancelled out as the COP is higher at 50 °C, resulting in a higher thermal heat pump capacity for the same electrical heat pump capacity. Eventually, the investment costs for the heat pump are slightly lower (around 6%) with 50 °C condenser temperature. The investments for the HT-ATES depend on the required capacity and with that the number of doublets (shown in Table 4.6). There is an increase of one doublet required at 50 °C vs. 65 °C condenser temperature, as the capacity delivered from the HT-ATES is quite similar over all scenarios, resulting in limited variations in the HT-ATES investment costs across the scenarios. The main decrease in costs between 50 °C and 65 °C condenser temperature is caused by the lower electricity demand (because of higher COP) at 50 °C vs. 65 °C.

Next to the condenser temperature, the HT-ATES feeds heat pump mode has an impact on the LCOE. The differences in results between 65|43|2 and 65|30|2, as well as the 50|43|2 and 50|30|2 scenarios illustrate this, as the only difference here is the extra mode of operation. In both cases with the additional mode of operation, there is an increase in costs for an additional heat exchanger, but a decrease in electricity costs while the amount of delivered heat increases. For the 65 °C condenser temperature, the electricity costs increase by 2%, while 6% more heat is delivered from the heat pump/HT-ATES system, which leads to a reduction of 1.0 €/GJ for the LCOE; while at 50 °C condenser temperature, the HT-ATES feeds heat pump mode leads to a decrease in electricity costs of 5%, and 7% more heat delivered, resulting in a total LCOE decrease of 1.4 €/GJ.

The HT-ATES feeds heat pump mode thus results in extra heat delivered at limited extra costs, hence the low LCOE for these scenarios. With a smaller heat pump size of 1.5 MW_{el}, the LCOE decreases further. For the 65 °C scenarios, the electricity demand does significantly decrease as well, although the % of heat demand delivered decreases with a smaller heat pump. Still, a reduction of 1.1 €/GJ is realized compared to a 2 MW_{el} heat pump with an LCOE of 18.5 €/GJ. The cost reduction is further enhanced by the HT-ATES feeds heat pump mode with 12% more heat delivery resulting in an LCOE of 16.6 €/GJ. For a 50 °C condenser temperature, the same effects are visible, although in this case, the HT-ATES feeds heat pump mode does not lead to an increase in electricity demand, but raises the heat demand delivered to 90%, which is almost similar to the 50|30|2 scenario, but with a smaller heat pump (1.5 MW_{el} vs. 2 MW_{el}). In this scenario (50|30|1.5), the LCOE is 13.8 €/GJ, which is 1.7 €/GJ lower than without the HT-ATES feeds heat pump mode.

A 1 MW_{el} heat pump with a 65 °C condenser temperature (65|30|1) does not lead to a further decrease in LCOE compared to a similar scenario with a 1.5 MW_{el} heat pump (65|30|1.5). The savings on heat pump investment and electricity costs thus do not compensate for the decrease in heat delivery (56% vs. 80%) by the heat pump/HT-ATES system.

Overall, the 50|30|1 scenario with a 1 MW_{el} heat pump has the lowest LCOE, with 75% of the heat demand delivered from the heat pump/HT-ATES system. The lower investment costs for the heat pump do make this scenario the most feasible. Furthermore, these results show that by installing a HT-ATES system, the heat pump size is not the determining factor for heat delivery anymore. As the HT-ATES is the main source of heat delivery during winter, the capacity of the HT-ATES system is more important than the size of the heat pump. HT-ATES systems thus help to reduce the size of the heat pump.

These results indicate a tipping point in heat pump size in relation to the amount of heat that can be delivered from the HT-ATES system to the multi-energy system. In the cases where the heat pump size is becoming a limiting factor, the positive effect of the extra mode of operation is most pronounced. The actual heat pump size tipping point will depend on the local conditions (maximum required heating power, temperature level) and thus vary per project. This analysis showed that for identifying the lowest LCOE scenario, it is worthwhile to identify this tipping point when a HT-ATES system in a multi-energy system is realized.

Table 4.6 Energetic and financial performance of the heat production and storage system as part of a multi-energy system. The % of heat delivered by the HT-ATES/heat pump is the sum of the yellow and orange bars in Figure 4.4. The scenario name abbreviation consists of: condenser temperature|HT-ATES threshold temperature|heat pump size.

Scenario	Average COP Heat Pump ($COP_{10y\ avg}$)	Max. Capacity Infiltrated (MW_{th})	Max. Capacity Delivered (MW_{th})	Amount of Doublets	Average Electricity Demand—10y Average ($En_{del,10y\ avg}$ in TJ/y)	% of Heat Demand Delivered by the HT-ATES/Heat Pump	Heat Production Costs (LCOE in €/GJ)
65|43|2 *	4	8.8	11.7	6	21.8	84%	19.6
65|30|2 *	4	8.8	11.7	6	22.2	90%	18.6
65|43|1.5	4	6.5	10.0	6	16.5	68%	18.5
65|30|1.5	4	6.5	11.0	7	17.7	80%	16.6
65|30|1	4	4.3	8.3	6	12.0	56%	16.7
50|43|2 *	5.5	12.6	11.7	7	17.6	85%	17.1
50|30|2 *	5.5	12.6	11.7	7	16.7	92%	15.7
50|43|1.5	5.5	9.4	11.8	8	16.3	78%	15.5
50|30|1.5 *	5.5	9.5	11.6	8	16.3	90%	13.8
50|30|1	5.6	6.2	10.9	7	12.6	75%	12.2

* The * added to the scenario code indicates that the HT-ATES can deliver 100% of the heat to the multi-energy system within the first five years.

4.3.4 Overall Performance: An Integral View on Heat Delivery, System Efficiency and Costs

In this study, we considered several scenarios with varying heat pump designs and storage temperature levels and assessed how these variations impact the fulfilment of the neighborhood heat demand, the performance of the HT-ATES system, and the costs of heat production including storage (LCOE). The overall performance of the varied scenarios is assessed here by combining all assessment criteria, as shown in Figure 4.10. Here, the arrows indicate the influence of the HT-ATES feeds heat pump mode compared to the normal operation mode. The most optimal system would have: 1. a large amount of delivered heat (y-axis); 2. a high HT-ATES system efficiency (x-axis); and 3. low LCOE (colour). The following observations stand out:

- At a small heat pump size and a high storage temperature (65|30|1), a relatively small amount of the total heat demand can be delivered to the multi-energy system (0.56) and LCOE does not decrease compared to a 1.5 MW_{el} heat pump scenario (both around 16.6 €/GJ). However, decreasing the storage temperature to 50 °C has a large positive effect for this small heat pump scenario (50|30|1); the LCOE strongly decreases (16.7 to 12.2 €/GJ) and the delivered amount of heat increases to 75%.
- Overall, the 50 °C storage temperature ensures lower costs and higher fulfilment of heat demand to the neighborhood. This is probably caused because the heat pump is cheaper and more effective, which results in larger amounts of stored heat. This has a stronger effect than the increase in costs due to the needed number of wells.
- For all scenarios, the HT-ATES system feeds heat pump mode (43 °C vs. 30 °C shut-off temperature) has a strong positive effect on all assessment criteria: the LCOE decreases, the fulfilment of heat demand increases, and the MES efficiency increases. Hence, this mode of operation has a high potential to be integrated into future HT-ATES systems. With only a small amount of electricity use in winter (not more than 2–6% of the total electricity use), the amount of heat delivered from the HT-ATES increases by 6–12%.
- The most optimal scenario for this neighborhood, based on all assessment criteria, is the 50|30|1.5 MW scenario. This scenario can provide 100% of the heat demand year-round to the neighborhood within the first five years, while the LCOE is 13.8 €/GJ, the second cheapest system.

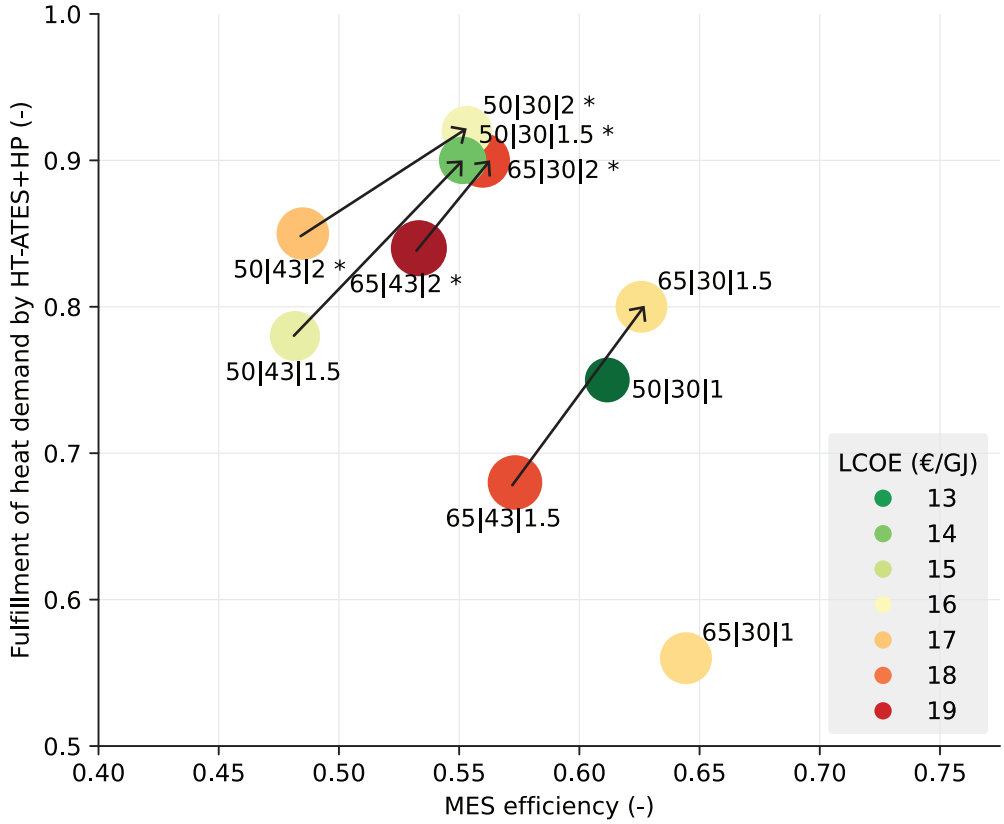

Figure 4.10 The relationships between the three main aspects investigated in this study; the fulfilment of heat demand by HT-ATES + heat pump to the MES (10-year average), the 10y MES efficiency and the costs of heat production and storage (LCOE). The * added to the scenario code indicates that the HT-ATES can deliver 100% of the heat to the multi-energy system within the first five years.

4.4 Discussion

4.4.1 The Functioning of a HT-ATES within a Multi-Energy System

We have shown that seasonal heat storage, HT-ATES, is crucial to be able to increase the amount of locally provided sustainable energy in a multi-energy system. Hence, HT-ATES is probably a better option for seasonal heat storage instead of the hot water storage tanks that are usually applied in a multi-energy [67], [69], [73], [77]. However, HT-ATES is not applicable everywhere, as it requires the presence of an aquifer.

The use of HT-ATES including the heat pump booster mode enables better utilization of the stored heat, and with that, increases HT-ATES performance. We showed that this mode of operation has a

high potential to be integrated into future HT-ATES systems, because the costs strongly decrease and HT-ATES performance increases, leading to an increase in local sustainable heat delivery.

The performance of the HT-ATES system is assessed via the recovery efficiency of heat from the HT-ATES system. The HT-ATES system recovery is determined by the recovery efficiency of heat from the hot and the warm well, which are strongly related to the volume (im)balance between the two wells. When the volume imbalance is negative (net extraction from the hot well), the recovery efficiency of the hot well increases and decreases at the warm well. However, the total amount of energy that can be provided to the MES can be larger than expected based on a simulation with a volume balance. For example, this could have a significant improvement for the recovery efficiency of HT-ATES wells that experience high heat losses during storage. Previous studies [220], [238], [254] evaluated the effect of several HT-ATES storage conditions on the recovery efficiency at Vin = Vout, and showed that energy losses can vary significantly. Therefore, it is recommended to analyze the combined effect of both varying storage conditions and the effect of volume (im)balance on recovery efficiency to get insight in the optimal combination of both factors for a given scenario.

In this study, we separately simulated the hot and warm wells of the HT-ATES systems. In reality, the wells will be placed next to each other, in such a way that positive interaction from the hot and warm wells is optimal. Previous studies showed that this leads to increased HT-ATES system performance [243].

4.4.2 The Impact of HT-ATES in a Multi-Energy System

In a multi-energy system with power-to-heat but without a HT-ATES, the heat pump size would be determined by the maximum peak in heat demand. By including a HT-ATES system in the multi-energy system, the heat demand and supply are mostly decoupled and the (peak) heat demand is delivered from the HT-ATES system during winter. The heat pump is employed in an optimal way by producing most of the heat in summer, the most likely time of abundance of (local) solar energy, but is also, to a small extent, employed in winter for the HT-ATES feeds heat pump mode when necessary.

Figure 4.11 shows the maximum capacity delivered to the heat users and the condenser capacity of the applied heat pump. The scenarios which end up in 100% heat delivery by the HT-ATES in the multi-energy system (*) indicate that the peak heating demand is 11.8 MW_{th}. For these scenarios, the ratio of the maximum demand and the applied condenser capacity shows how much smaller heat pump capacity can be installed to optimally utilize heat produced by power surplus. The 50|43|2 and 50|30|2 scenarios have a positive ratio, indicating the heat pump is over-dimensioned. From the 65|43|2, 65|30|2, 50|43|1.5 and the 50|30|1.5 scenario results, it is concluded that the heat pump can have a 21–25% smaller capacity than the actual peak heating demand. The other scenarios (not leading to 100% heat delivery) have ratios of 0.6–0.7, indicating that 25% lower heat pump capacity is the maximum. Besides a smaller capacity, the heat pump is employed both in summer to store the heat and in winter to provide additional heat when the HT-ATES heat pro-

duction is not sufficient. This fosters year-round heat pump utilization, although the energy use in winter is a fraction (< 6%) of the total energy use of the HT-ATES system (see Figure 4.5). Thus, most energy demand is still during summer, with a likely oversupply of sustainable local electricity from PV.

The addition of HT-ATES in a power-to-heat MES affects the total yearly electricity use, and, the yearly distribution of electricity use, as energy demand and availability are decoupled. For a multi-energy system with power-to-heat without HT-ATES, all heat needs to be produced directly by the heat pump on demand, which can become a problem in winter because (a) the temperature of the heat source (canal) becomes too low to use, and (b) sustainable power to run the heat pump is not available. This results in the need for larger heat exchangers and the need for other sources of heat and associated costs, as well as a reduction in the use of local sustainable energy.

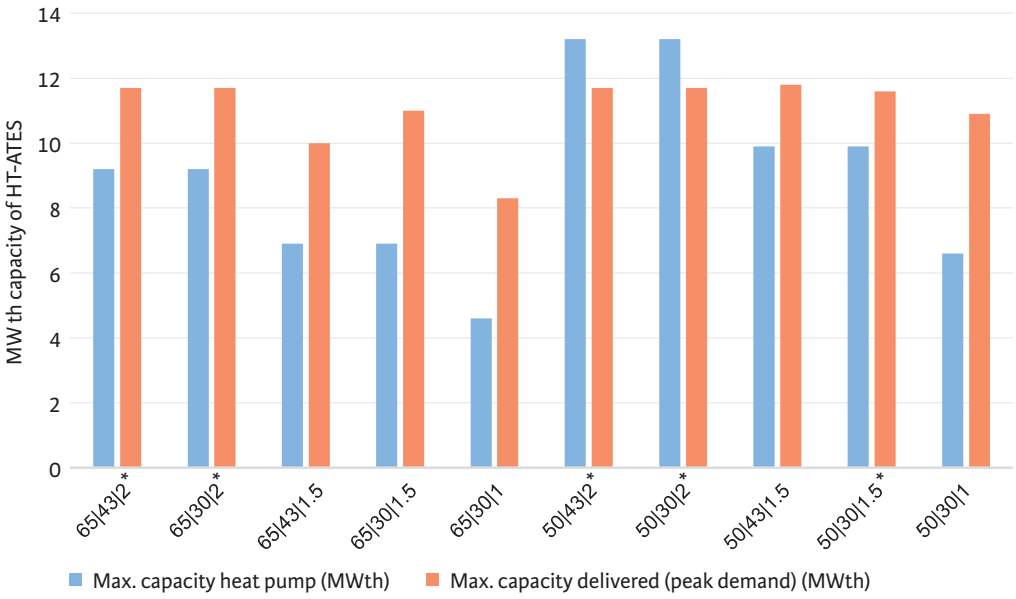

Figure 4.11 The maximum heat pump capacity vs. the heat delivery at the peak demand is shown for all scenarios. Because of the addition of the HT-ATES system, it is possible to deliver the peak demand from the HT-ATES, which explains why the maximum thermal heat pump capacity is lower than the maximum capacity delivered. The * sign shows which scenarios reach 100% heat delivery by the HT-ATES to the MES (within the first five years of operation).

Following the basic heat pump dynamics, a simplified calculation for a multi-energy system with only direct heat production will result in a total average electricity use of 12.8 TJ/year with a 3.1 MW_{el} heat pump (assuming an average heat pump evaporator temperature of 8 °C, and 50 °C condenser temperature), with an electricity demand as shown in Figure 4.12. In the first 10 years of operation, a MES with HT-ATES will consume around 16–17 TJ/year of electricity and a maximum of 90% of the heat demand will be fulfilled. Yet, after the first two to four years of operation, the heat demand can be provided completely from the HT-ATES and the electricity demand of the system decreases. For example, in the case of the most optimal 50|30|1.5 scenario, the electricity

demand in the 10th year of operation is 13.6 TJ. This is about 6% higher than a MES with direct heat production. The total electricity use thus slightly increases when HT-ATES is included. The total electricity use by the HT-ATES + HP system is influenced in two ways. Firstly, the source of heat (canal) is mainly harvested when its temperature is relatively high. This is favorable for the heat pump COP and results in relatively less electricity use. Secondly, more heat needs to be produced than the total yearly heat demand because a part of the produced heat will be lost during storage. Hence, the second effect is of slightly more influence on the total electricity demand in this study, for the first 10 years of operation. However, as pointed out in the previous section, the energy losses of HT-ATES systems, and thus their electricity use, may vary strongly for different HT-ATES storage conditions (e.g., storage volume, hydrogeological conditions). Consequently, under more favorable storage conditions, yearly electricity use of the MES may be lower compared to direct heat production.

More importantly, the integration of HT-ATES has a strong effect on the distribution of electricity use over the year. The electricity use is decoupled by the integration of HT-ATES, and the electricity use peak switches from winter to summer, following the availability of sustainable electricity by solar energy (Figure 4.12). Here, we compare the electricity use of a MES with and without HT-ATES. The electricity use of scenario 50|30|1.5 is compared to a reference system that uses a HP for direct heat production only. Thus, the HT-ATES system enables the use of more sustainable and local electricity when available (in summer) and reduces the size of the heat pump compared to systems with direct heat production. The yearly electricity use slightly increases for the modelled scenarios in this study; however, this may change under more favorable HT-ATES storage conditions.

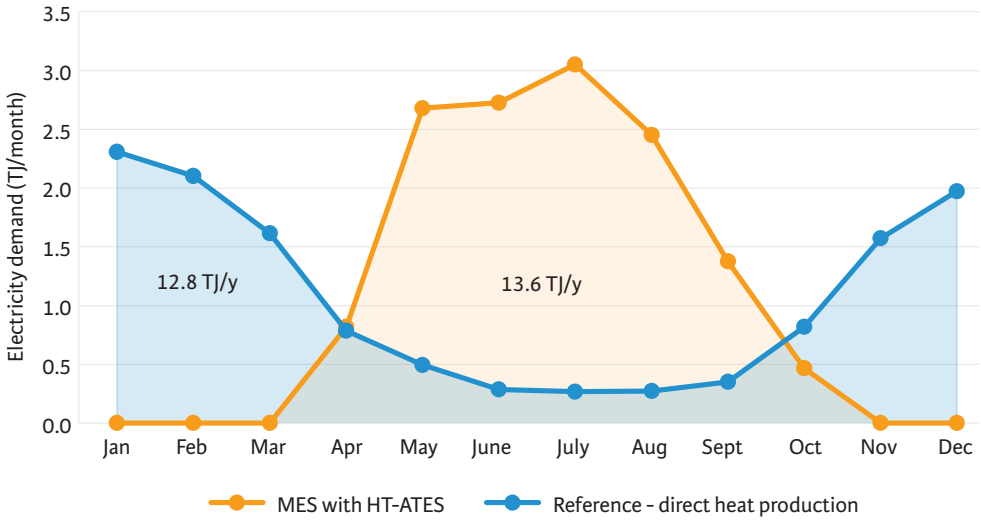

Figure 4.12 Comparison of the monthly electricity demand of a reference scenario with direct heat production by a heat pump with 8 °C evaporator temperature and the 50|30|1.5 scenario with HT-ATES. The areas under the graph show the total electricity demand over the year, in this case the year 2019.

4.4.3 The LCOE Placed in Perspective

The LCOE for the different scenarios of heat pump size, condenser temperature and threshold temperature varies between 16.6–19.6 €/GJ for 65 °C heat pump condenser temperature, and between 12.2–17.1 €/GJ for 50 °C condenser temperature. Choosing a lower condenser temperature (50 °C instead of 65 °C) leads to lower costs as the COP of the heat pump is higher and the costs of the heat pump are assumed to be lower. However, exact cost curves of (large scale) heat pumps are not available, so the cost difference is not known exactly and needs further investigation. Additionally, at 50 °C condenser temperature, the total stored volume in the HT-ATES is approximately twice as large as at 65 °C, and therefore requires more hydraulic pumping for the injection and abstraction. Lastly, a higher condenser temperature could lead to lower investments for household installations as heat is delivered at higher temperature, possibly counteracting the higher heat delivery costs.

The costs of the assessed scenarios in this chapter are comparable to the costs (20.5 €/GJ) that were determined by Wesselink et al. [75], who considered a HT-ATES system in combination with geothermal energy. In an overview of different HT-ATES feasibility studies, the LCOE of heat varied between 14.7–29.3 €/GJ, with larger systems (> 350,000 m^3) resulting in a LCOE below 20 €/GJ [255]. The LCOE calculated in this chapter thus fits within the price range known for HT-ATES systems. Heat delivered by a gas boiler costs on average 10–12 €/GJ [49]. For the scenarios considered in this study, calculated prices are higher with a minimum difference of 0.2–2.2 €/GJ (50|30|1). This gap could be bridged by an increase in the CO_2 price or subsidies on the installation or heat price of 100% renewable power-to-heat systems with HT-ATES. With a CO_2-price of 55.6 €/ton CO_2 and CO_2-emission factor of 35.97 kg CO_2/GJ of heat [150], the LCOE of a gas boiler would rise to 12–14 €/GJ, which would then fall in the same range as the 50|30|1 and 50|30|1.5 scenarios. At a CO_2-price of 100 €/tonne CO_2, the price range of heat from a natural gas boiler would rise to 13.6–15.6 €/GJ, increasing the feasibility of a HT-ATES system with power-to-heat further.

4.4.4 Prolonged Lifetime of the Multi-Energy System with HT-ATES

In this study, only the first ten years of operation of the HT-ATES have been simulated. The lifetime of the multi-energy system and HT-ATES is longer than ten years, and the results show that most scenarios can reach a 100% heat delivery within the first ten years of operation (see Figure 4.6 and Figure 4.7). After this time, the electricity demand is more representative compared to the first few years of operation as the system is still stabilizing and not able to provide the total heat demand. Hence, we performed an extra financial analysis assuming the electricity demand of the 10th year of operation would stay constant for the next 30 years of operation. This is a conservative estimation because the systems will most likely continue to improve in performance and system recovery efficiency over the years. On the other hand, we assumed that all systems would be able to provide the total heat demand of the neighborhood after 10 years of operation, although we are not completely sure about this for i.e., scenario 65|43|1.5, 65|30|1.5, 65|30|1, and 50|30|1. The results can thus not be used to reliably compare the scenarios with each other, but give an idea of how the LCOE would develop over time.

The results are shown in Table 4.7 and show a reduction of 1.2–5.6 €/GJ, which is a reduction in LCOE of 4–28% and 13% on average. The LCOE presented in this study are thus a conservative estimation and will be significantly lower when considering a lifetime of 30 years, which would be further enhanced when a reduction in electricity consumption is taken into account as well.

Table 4.7 LCOE analysis with 30 years of operation of the heat pump/HT-ATES system.

	Heat Production Costs (LCOE) in €/GJ—10 Years	Heat Production Costs (LCOE) in €/GJ—30 Years
65|43|2	19.6	17.4
65|30|2	18.6	17.4
65|43|1.5	18.5	14.3
65|30|1.5	16.6	14.3
65|30|1	16.7	11.1
50|43|2	17.1	14.6
50|30|2	15.7	14.2
50|43|1.5	15.5	13.0
50|30|1.5	13.8	12.3
50|30|1	12.2	10.1

4.5 Conclusions

In this study, it is shown that with the novel integration of a HT-ATES system to a multi-energy system, it is possible to provide > 90% of the heat demand during the first ten years of operation, and supply the full heat demand after 3–5 years. The system recovery efficiency of the HT-ATES system was 50–70% depending on the system design chosen. By including a HT-ATES system in a multi-energy system, the size of the heat pump could be reduced by maximally 25% as the peak in heat demand can be delivered from the HT-ATES system, which reduces both the impact on the surface level (smaller installation) and costs. The integration of HT-ATES allows for the decoupling of energy demand and availability, meaning that the yearly distribution of electricity use is shifted completely from mainly in winter to mainly in summer, to match the availability of sustainable electricity by e.g., solar PV.

Choosing a condenser temperature of 50 °C led to a 11–18% lower LCOE than a system with 65 °C condenser temperature at the same heat pump size and threshold temperature. Overall, a heat pump condenser temperature of 50 °C with a 1 MW_{el} heat pump and a threshold temperature of 30 °C led to the lowest LCOE (12.2 €/GJ). Yet, with this heat pump size, only 75% of the heat demand was fulfilled and 25% of the heat demand had to be fulfilled by another source (in the first ten years

of operation). The scenario with a 50 °C condenser temperature, 1.5 MW_{el} heat pump size and 30 °C threshold temperature is seen as the most optimal regarding the combination of LCOE (13.8 €/GJ), fulfilment of heat demand (90% in the first 10 years of operation) and MES efficiency (55%).

The extra mode of operation of the heat pump is a booster mode during recovery from the HT-ATES system and allowed to lower the acceptable temperature threshold value of the hot well below the actual delivery temperature of the DHN. We have shown that this innovative "HT-ATES feeds heat pump mode" is able to prolong heat delivery from the HT-ATES, and therefore the amount of heat delivered increases, as well as the system recovery efficiency and MES efficiency. The effect of the HT-ATES feeds heat pump mode is most pronounced in situations where the size of the heat pump is becoming a limiting factor for a well-functioning system. In these cases, the HT-ATES feeds heat pump mode allows the installation of a smaller heat pump without compromising on the efficiency of the HT-ATES, which eventually leads to lower costs of heat within the multi-energy system.

Supplementary information

The Supplementary Information containing schemes for a heat pump condenser temperature of 65 °C can be found via: *https://www.mdpi.com/article/10.3390/en14237958/s1*

Data

The modeling data presented in this study are openly available via 4TU: *http://doi.org/10.4121/16964773*.

Funding

This research was co-financed with PPS-funding from the Topconsortia for Knowledge and Innovation (TKI's) of the Ministry of Economic Affairs and Climate. The authors would like to thank the TKI Watertechnology (2016KWR019 or RVO5289) and TKI Urban Energy (TEUE117059) in the Netherlands for their financial contribution to the research projects that lay at the foundation of this publication.

5 Utilization of waste heat from PEM electrolyzers – Unlocking local optimization

" Don't ask whether you can do something, but how to do it "

Adele Goldberg

Abstract: Recovery of heat from electrolyzers is potentially interesting to increase the total system efficiency, reduce CO_2 emissions, and increase the economic feasibility of both hydrogen and heat production. This study examines different designs for the utilization of (waste) heat from a 2.5 MW_{el} polymer electrolyte membrane (PEM) electrolyzer. Redundancy is important in the design, to ensure safe operation regardless of the heat demand of the heat consumer. We analyzed cases with local heat consumption (with/without a heat pump) and coupling with a district heating network (DHN). Overall, 14-15% of the electricity input to the stack can be utilized by a heat consumer, increasing the total system efficiency to 90% (HHV) with CO_2-savings of 0.08 (DHN)-0.28 (direct use) tonne $CO_2/MWh_{heat,used}$. We performed a first-order techno-economic analysis showing that the levelized costs of the electrolyzer heat (8.4-36.9 €/MWh) fall within the range of other industrial heat sources and below lower-temperature heat sources.

This chapter is based on the publication:

E. van der Roest, R. Bol, T. Fens, and A. van Wijk, "Utilisation of waste heat from PEM electrolysers – Unlocking local optimisation," Int. J. Hydrogen Energy, vol. 48, no.72, p. 27872, 2023, https://doi.org/10.1016/j.ijhydene.2023.03.374.

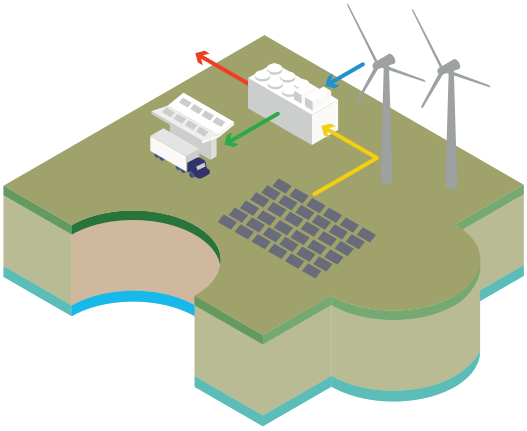

5.1 Introduction

Our future energy system needs to be reliable, affordable and clean. To reach that goal, an integrated energy system needs to be created has smart combinations of technologies so energy supply and demand are matched in both time and space. In this future integrated energy system, green hydrogen is increasingly seen as an essential energy carrier [18], [256]. Hydrogen is a feedstock for industry as well as a zero-carbon energy carrier, that can transport and store renewable energy cost-efficiently and de-carbonize energy use in industry, transport and buildings [40], [193], [256]. As (green) hydrogen is an energy carrier, and not an energy source, it needs to be produced first by water electrolysis with renewable electricity. The European Commission has raised the ambition of renewable hydrogen production with the REPowerEU action plan from 5.6 Mton to 10 Mton domestic EU production and 10 Mton of hydrogen imports [8]. Production of hydrogen can take place both at local hydrogen clusters ('Hydrogen valleys') as well as at or near large RES production sites in less inhabited areas (oceans, deserts) [38]. At these remote locations with high wind speeds or high solar irradiation, hydrogen can be produced, if necessary converted, and transported to areas with high demand for either hydrogen or electricity. To connect areas of supply (i.e. Africa, Iceland) with areas of hydrogen demand (i.e. Europe) [257], [258] infrastructure has to be installed, which is reflected in the plans for a European hydrogen backbone [199], [259].

In this chapter, we focus on local hydrogen clusters, as these clusters give more possibilities for the integration of hydrogen production with other sectors and services. Because the electrolysis process is not 100% efficient, (waste) heat is produced as a by-product and could be utilized by other sectors. The new generation electrolyzers have a system efficiency of 74-79% [256], [260] and a balance of stack efficiency of 77-80% (higher heating value – HHV) [261]. For most of the balance of plant processes (i.e. electricity transformation or demineralized water production) no heat can be recovered, so the technical potential of heat recovery can only be based on the balance of stack efficiency. Conventionally, the heat (at 50-80°C) from the stacks is dissipated by dry coolers on top of the electrolyzer containers. When electrolyzers are installed at short distances of heat demand, the heat produced by the electrolyzer can potentially be used resulting in a higher overall system efficiency. Eventually, the utilization of waste heat can lead to a reduction in CO_2 emissions, when the electrolyzer heat is exchanged with heat from natural gas or other fossil energy sources. Besides CO_2 emission reduction, it will also reduce the dependence on fossil sources and could lower the hydrogen production cost.

Utilizing waste heat from electrolyzer installations is mentioned by Buttler & Spliethoff as a way of increasing the system (stack + balance of plant) efficiency from 75-80% to 86-95% (HHV based) [129]. They mention three concrete projects where heat integration was part of the activities. Firstly, the BioCat project deployed a 1 MW installation to produce hydrogen via electrolysis and converted it to methane with the help of biological methanation. The intention was to reuse both the heat from the electrolyzer and methanation process in the waste water treatment plant or a renewable heat grid. Eventually, the utilization of heat from the electrolyzer was not realized in the project (p. 6 final report) [262]. Secondly, Stromlückenfuller is a project where waste heat from a 200 kW electrolyzer is used in a heating network [263]. A similar project with a 1 MW electrolyzer and reuse in a

district heating grid is Green Hydrogen Esslingen [264]. Lastly, RWE uses heat from electrolysis (150 kW) in a gas pressure regulation station [265], but no further publications are found on how these systems work and how much heat is recovered. It is thus hard to find concrete examples of the realization of waste heat recovery, but new plans for heat utilization are created. In Hamburg, a 100 MW electrolysis system is proposed with waste heat utilization in the district heating network and thermal treatment of municipal waste, that should be operational in 2025 [266]. The 2050 scenario for the district heating network of Aalborg, the utilization waste heat from a 330 MW electrolyzer is mentioned as an additional heat source [267]. The Institute of Process Technology has worked out a design for a 1 GW electrolysis plant, which should be heat integration ready [268].

The scientific literature on heat utilization of electrolyzers is limited. Bilbao [269] worked out a case study in Chile for an alkaline electrolyzer, with as goal to provide the electrolyzer with pre-heated water to have a higher overall efficiency. The overall efficiency increase was marginal (< 1%). The reason for the small overall efficiency increase is not the amount of available waste heat, but the relatively small amount of water consumption, which is 30 times lower than the mass flow of waste heat water. This means that the waste heat it not used to its full potential. Bilbao states that when it would be possible to utilize the full potential, it could lead to a total increase in efficiency of 13%, comparable to Buttler & Spliethoff [129], but they do not mention how this heat could be used [269]. A modelling and experimental study on an alkaline electrolyzer of 46.5 kW showed that the efficiency of the electrolyzer system can be increased to >90% if heat recovery is included [270]. Frank et al. [271] notice an 18% increase in efficiency if all waste heat from their 1 MW_{el} electrolyzer would be used. Huang et al. [272] consider a model predictive control strategy including the waste heat of the electrolyzer and conclude that it leads to more cross-sectoral flexibility of their system, but does not quantify the amount of heat recovered. Hückebrink & Bertsch introduce a concept for a neighborhood where both a fuel cell and electrolyzer are installed in a building and their heat is used, reducing the need for a heat pump [273]. No quantification of the amount of heat from the fuel cell and electrolyzer is given in this study. Böhm et al. [274] give a conceptual overview of the use of electrolyzer waste heat from low temperature and high-temperature electrolysis in district heating systems. Based on literature research and expert consultation, they conclude that there is possible synergy between power-to-hydrogen and district heating systems and a significant potential for electrolyzer waste heat of temperature levels below 100°C. They state that there is a need for more quantitative research. Overall, we conclude that both the scientific community and industry recognize the potential of electrolyzer waste heat, yet both publications and practical examples are scarce. Moreover, there is a lack of detailed system design and analysis for the utilization of waste heat from electrolysis.

5.1.1 Research goal

Based on the scarce availability of literature and concrete examples of waste heat utilization from electrolysis, our research question is:

What is the potential of waste heat from electrolyzers and how could it be utilized?

To answer this question, we will elaborate on different designs for the utilization of electrolyzer waste heat based on a 2.5 MW_{el} Polymer Electrolyte Membrane electrolysis (PEM) electrolyzer (stack size) in Nieuwegein, the Netherlands. The electrolyzer is part of the H-Flex project, which investigates multiple ways in which the electrolyzer can be utilized next to hydrogen production, by offering flexibility to the electricity grid as well as waste heat utilization [275]. The theoretical heat utilization potential can be 500 kW_{th} of heat at 100% load at the start of the lifetime, based on 80% efficiency (HHV) of the electrolyzer stack. How heat can be utilized will differ per use case. We will work out three different use cases that represent possible situations for local system integration. In an ideal case, there is a heat consumer that uses heat at the output temperature level of the electrolyzer. As a second case, we include a heat pump for higher-temperature heat. The third use case is the delivery of heat to a local district heating system. We will perform a first-order techno-economic analysis on these three use cases including calculations on how much heat can be utilized and what the combined system efficiency will be. Furthermore, the potential CO_2 reduction is calculated when electrolyzer heat replaces heat from fossil sources. Finally, the costs of heat recovery and transportation are calculated to get a first idea of the feasibility of heat recovery in general and specifically for these three cases.

5.2 Methodology

5.2.1 Design of a PEM electrolyzer with heat utilization

In this chapter, we focus on a 2.5 MW PEM electrolyzer installation in Nieuwegein [275], although our method could potentially be applied to other electrolyzer capacities as well. In water electrolysis, water is converted via an electrochemical process with two electrodes into hydrogen and oxygen. The chemical reactions in a PEM electrolyzer are given in equations 5.1-5.3, with a change in enthalpy ΔH of 285.84 kJ/mol, which is the energy required to drive the reaction.

Cathode: $2H^+ + 2e^- \rightarrow H_2$ (5.1)

Anode: $H_2O \rightarrow \frac{1}{2}\, O_2 + 2\, H^+ + 2e^-$ (5.2)

Overall: $H_2O(l) \rightarrow H_2(g) + \frac{1}{2}\, O_{2(g)} \quad \Delta H = 285.84\ kJ/mol$ (5.3)

5.2.1.1 Heat sources in an electrolyzer

Heat is produced in the electrolyzer stack due to the irreversibility of the chemical reactions happening and the ohmic resistance of the cell. The electrolysis reaction can occur without consumption or production of heat, at the so-called thermoneutral voltage. However, at this potential, the reaction rate is too low, so there is almost no hydrogen production. Therefore, an overvoltage is applied to the cells, which increases the reaction rate and makes the electrolysis reaction exothermic, thus heat is released. The total amount of heat produced ($Q_{produced}$,, in Watt) is the cell current ($Q_{produced} = I \cdot (U_{operating} - U_{thermoneutral})$ in ampere) times the difference between the operating voltage ($U_{operating}$ in Volt) and the thermoneutral voltage ($U_{thermoneutral}$, in Volt) is given in equation 5.4.

$$Q_{produced} = I \cdot (U_{operating} - U_{thermoneutral}) \tag{5.4}$$

In some cases, the released heat is in balance with the heat consumption for the evaporation of water in the stack, but otherwise, this heat needs to be removed from the electrolysis stack to maintain the cell temperature and prevent overheating. Heat can be extracted from the stack from three different sources in a PEM electrolyzer [276], [277]; from the oxygen stream, the hydrogen stream and the water recirculation loop. Both the oxygen and hydrogen flow contain some water vapor after leaving the stack from which heat can be extracted.

Based on the design of Mancera et al. [276], the one GigaWatt electrolyzer project [268] and information from electrolyzer manufacturers, Figure 5.1 shows a simplified cooling system of an electrolyzer. Heat is extracted from the recirculating water that is separated from the hydrogen/water stream by the gas-liquid separator. The oxygen/water stream flows to an oxygen separation tank which is combined with the deionized (ultra-pure) water recirculation stream, with a heat exchanger on the stream between the oxygen separation tank and the recirculation pump. Excess heat is removed to limit the inlet temperature to the stack if the condensing heat from the oxygen flow exceeds the heat needed to raise the temperature of the demineralized water inlet. Temperature levels for PEM electrolyzers are mostly reported in the 50-80°C range [129], [268], [277]. We have considered here an average working temperature of the electrolyzer of 65°C, and a cooling circuit with a maximum inlet temperature of 57°C and a ΔT of 3°C over the heat exchangers [277].

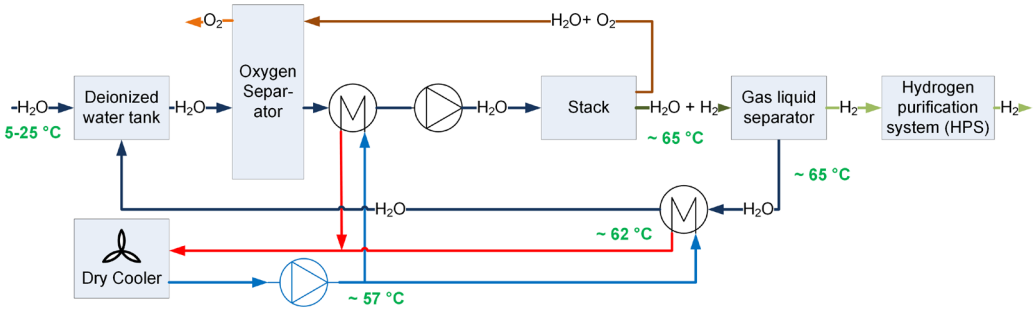

Figure 5.1 Cooling system of an electrolyzer stack. In orange/brown the oxygen flow is shown, in (dark)green the hydrogen flow and in dark blue the water flow. The cooling water flow is shown in red and blue.

This is an efficient design where heat is extracted from both the oxygen and (indirectly) the hydrogen stream and directly used to heat the deionized water stream to the electrolyzer. If the temperature of the stack is known, then one can calculate the amount of heat necessary to heat the incoming water based on the hydrogen production. According to the thesis of Tiktak [277], this amounts to approximately 5-8% of the total available heat. The excess heat is removed by a dry cooler. In case the excess heat would be used by a third party, the design has to be adapted to make this possible with an extra tie-in on the cooling system. Choosing for and extra tie-in on the cooling system instead of replacing the dry cooler makes the system redundant.

5.2.1.2 *Variance in heat production*

Two factors lead to variation in heat production; the efficiency load curve of the electrolyzer stack and the degradation process. Firstly, the efficiency is negatively correlated with the load, therefore we use an efficiency curve (equation 5.5, visualized in Figure 5.2) that varies with the load based on empirical statistics analysis [278], but with efficiency values adapted to recent developments. Equation 5.5 gives an electricity consumption of about 49.25 kWh/kg at 75% load or an expected balance of stack efficiency of 80%which is the expected stack efficiency of the PEM electrolyzers that are currently available [135], [260].

$$E_{electrolyser\ stack,eff}(>10\%\ load) = \frac{HHV_{H_2}}{7.8455\frac{kWh}{kg} * Load_{electrolyser} + \frac{43.409kWh}{kg}} \cdot 100 \tag{5.5}$$

With $E_{electrolyser\ stack,eff}$ the electrolyzer stack efficiency in %, $Load_{electrolyser}$ represented as a fraction of full load (i.e. 0.8) and the HHV_{H_2} being 39.4 kWh/kg. Equation 5.5 is only valid above 10% load. Below 10% load, the efficiency sharply decreases. In this study, we will only consider electrolyzer capacities above 10% load.

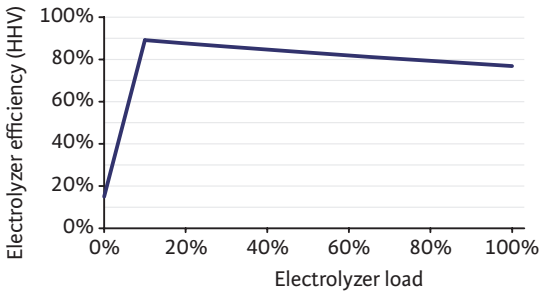

Figure 5.2 Electrolyzer balance of stack efficiency in relation to the load, based on equation 5.5, [135], [260], [278].

Secondly, the ageing and degradation of the electrolyzer stack lead to a lower hydrogen production efficiency. Mainly due to the degradation of the stacks, the resistance over the membranes increases and therefore requires a higher overpotential over time. This linear voltage degradation can result in a cell voltage increase. With an 80,000-hour lifetime, this would result in a voltage degradation of 1.9V to 2.06-2.22 V [129]. Therefore, the amount of heat production will increase over the lifetime of the project if the hydrogen production rate is kept constant. An evaluation of

several electrolyzer projects in the EU [279] shows that these PEM electrolyzers have a degradation of 0.12%/1000 hours, which is the FCHJU target for 2030. The final reported value for PEM degradation is 0.19% per 1000 hours, which means after a year of full production (8000 hours) 1.5% extra energy consumption and 15% extra energy consumption after 10 years [279]. Suppliers on the other hand report <1.0% efficiency degradation [261]. We will adopt the lower-end values for newer generation electrolyzers, thus assuming a 1.0% annual efficiency degradation which will lead to a 10% increase in energy consumption after 10 years.

5.2.2 HHV vs LHV

The chemical energy content of a fuel is expressed as the HHV (higher heating value). For hydrogen, this is 39.4 kWh/kg or 141.8 MJ/kg. In addition, there is also a lower heating value (LHV, 33.3 kWh/kg or 120 MJ/kg), which is only relevant when a substance is burned and no heat is recovered from flue gases. When the latent heat from flue gases is recovered, there is no burning process involved, or hydrogen is used as feedstock, it is misleading to use the LHV as it leads to an overestimation of the waste heat potential.

Let's illustrate this with an example of electrolysis (electrochemical conversion, so no burning process is involved), where the LHV would lead to an overestimation of the available heat from electrolysis. If we would assume 80% electrolyzer stack efficiency on HHV, this amounts to an electricity consumption of 49.25 kWh/kg hydrogen by the electrolyzer. The LHV value of hydrogen is 33.3 kWh/kg or 121 MJ. The LHV stack efficiency would then be 33.3/49.25 * 100 = 68.2%. Using the LHV for the calculation of the heat recovery potential of electrolysis would lead to a perceived heat recovery of 31.8%. While at HHV, a stack efficiency of 80% means there is a theoretical heat recovery potential of 20% . By using the LHV, one would thus overestimate the heat recovery potential by more than 50%. So, calculating with the HHV is required to arrive at a univocal energy balance in the electrolyzer/fuel cell application. It provides more information on the actual energy content of hydrogen, as well as how much waste heat is available. In this dissertation, we will therefore consistently use the HHV.

5.2.3 Case studies

The waste heat utilization of the electrolyzer was analyzed by three relevant use cases. For all cases, the electrolyzer details as presented in Table 5.1, based on the 2.5 MW (stack size) installation in Nieuwegein. The hydrogen production pattern was based on the yearly production target, scaled down to a hourly production target. The electrolyzer is stimulated to run at 75% of its capacity, on local solar PV as much as possible (based on weather data) or during hours of low electricity prices (based on day-ahead prices). In case the production capacity stayed behind the target (based on the sum of the production), the capacity target was increased to 90%. In hours where no renewable capacity is available, the capacity was limited to 75%. In our analysis, we only considered the stack size for heat recovery, as no heat will be recovered from the auxiliary equipment. The

efficiency of the total electrolysis installation is thus lower. The electrolyzer worked on average at a 75% load and 80% efficiency (HHV), so the theoretical waste heat potential of the electrolyzer stack would be 20% of the energy input. The technical potential for heat recovery was set at 80%, which means 16% of the electrolyzer waste heat was recovered. Tiktok found a recovery percentage of 92% [277] with internal cooling in the stack inside the bipolar plates. Our design has cooling outside of the stack, with multiple heat exchangers (see Figure 5.1) and more heat losses, therefore we have chosen a value of 80%. Over time, the heat potential increased (see 5.2.1.2) which at 75% load (1.875 kW) meant 300 kW_{th} of heat in the first year of operation which increased to 330 kW_{th} in year 10. Heat losses during heat transport are based on calculations of a DN80 pipe (90/162mm) with insulation (class 1) based on heat loss norms for heat pipes [280]. For pump energy, a pump efficiency of 60% is assumed.

Table 5.1 Electrolyzer parameters.

	Electrolyzer parameters
Size of electrolyzer stack	2.5 MW_{el}
Auxiliary equipment – outside of scope	Energy use is ca. 5% of stack capacity
Production target	300 tonnes/year (capacity factor 0.71)
Hydrogen production efficiency (HHV)	80% at 75% load, see further equation 5.5
Minimum load	10%
Waste heat recovery efficiency [277]	80%
Available heat at 75% load	Year 1: 300 kW_{th} Year 10: 330 kW_{th}
Heat for water flow to stack	0.571 kWh/kg H_2 produced ($\Delta T = 55°C$)
Electrolyzer working temperature	65°C
Full load hours of the electrolyzer	6250
Cooling water inlet temperature [277]	57°C
Cooling water outlet temperature [277]	62°C
Loss over heat exchanger	3°C
Annual efficiency degradation [129], [268], [279]	1.0%

5.2.3.1 Case 1 - Local use of heat

If the electrolyzer is placed in an area with more industrial applications, there may be a direct consumer for the available electrolyzer heat. In the case of Nieuwegein, this is an industrial-scale laundry washing company, but it could be a different user as well. We considered two options, either the heat was directly utilized at the right temperature, or the temperature was raised by a (high-temperature) heat pump, see Figure 5.3. High temperature heat pumps with temperature levels of up to 100°C are proven technology [185], [281]. In Table 5.2 the chosen parameters for case 1 are shown. The maximum heat production of the 2.5 MW electrolyzer (at 100% load) would be 580

kW_{th} up to 640 kW_{th} after 10 years. Yet, most of the time the electrolyzer will work at a lower load (i.e. 75%) and not all heat can be recovered, hence the heat exchanger size was chosen to be 400 kW_{th}. The heat consumer has a larger heat load than the electrolyzer offers and has a heat buffer available which means the electrolyzer heat can be stored there outside of the working hours of the company. The heat load of the consumer is therefore not modelled in detail, but it is assumed that in general the electrolyzer will be able to deliver its heat to the consumer. Yet, the buffer could be full at a certain point, therefore it is not likely that all electrolyzer heat can always be utilized. We have assumed that 80% of the available heat can be used by a heat consumer.

Table 5.2 Case 1 - Direct heat consumer parameters.

Parameter	Value
Preferred temperature level – low (1a)	54°C
Preferred temperature level – high (1b)	100°C
Distance between production and use	200 m
Heat exchanger capacity	400 kW_{th}
% of overlapping working hours of electrolyzer and heat consumer (including buffer)	80%
High-temperature heat pump capacity (1b)	520 kW_{th}
Average COP heat pump (1b, see SI.1)	4.3

5.2.3.2 Case 2 - Low-temperature district heating network

The electrolyzer heat could also be used in district heating systems. The temperature level fits best for low-temperature heating systems (4^{th} or 5^{th} Generation [282]), with a temperature level of 40-50°C/25°C (supply/return temperature). In **Chapter 3**, a case of 2000 houses in a neighborhood was analyzed at a distance of about 3 km from the electrolyzer. In the 'Power-to-X' scenario, the heating system consisted of a district heating network (DHN), heat extraction from surface water with a heat pump, seasonal heat storage in a high-temperature aquifer thermal energy storage (HT-ATES) system and a day buffer [235] (**Chapter 3**). Space heating was supplied directly via the DHN, for domestic hot water (tap water) additional booster heat pumps are installed in buildings or houses to provide safe tap water of at least 60°C to households. Heat demand was varied based on house type and hourly weather data via the degree-day method [283]. We have considered the use of waste heat from an electrolyzer there as well, but with a strict assumption that the waste heat could only be delivered to the DHN if it would fulfil the total heat demand in that hour. Then, only 1.5% of the waste heat could be utilized [235] (**Chapter 3**). In the current chapter, we took a more flexible approach. Instead of delivering heat directly to the DNH, the electrolyzer heat was delivered to the day buffer of the DHN, see Figure 5.3 and Table 5.3 for details. The buffer adds the necessary flexibility so the electrolyzer heat could be combined with heat from other sources. We assumed that the electrolyzer heat can be added without limitations to the day buffer of the DHN. The day buffer of the DHN was estimated at 600 m^3 (21 MWh_{th}) to accommodate 12 hours of average heat demand (1.750 kWh_{th}), while the electrolyzer delivers a maximum of 400 kWh_{th} of heat to

the buffer in one hour. In case the buffer is full and there is low heat demand, heat could be stored in the HT-ATES system. Moreover, in the calculation, we took into account the ageing effects of the electrolyzer leading to an increase in heat availability over time.

Table 5.3 Case 2 - Parameters for heat delivery to a district heating network.

Parameter	Value
Preferred temperature level - low	45-60°C
Total neighborhood heat demand	55 TJ/y
Distance between production and use	3 km
Distance between waste heat production and day-buffer/HT-ATES	200 m
Size heat exchanger between electrolyzer and day buffer	400 kW_{th}
Heat source	Surface water + heat storage (HT-ATES)
Average COP large-scale heat pump [284], [285]	5
Day buffer charging/discharging efficiency [286]	90%/100%
Day buffer heat loss per week[a] [287]	2%

[a] Data are given for 500 m^3 with 2.1% heat loss, as we need a smaller tank here, we increased the heat loss to 3%.

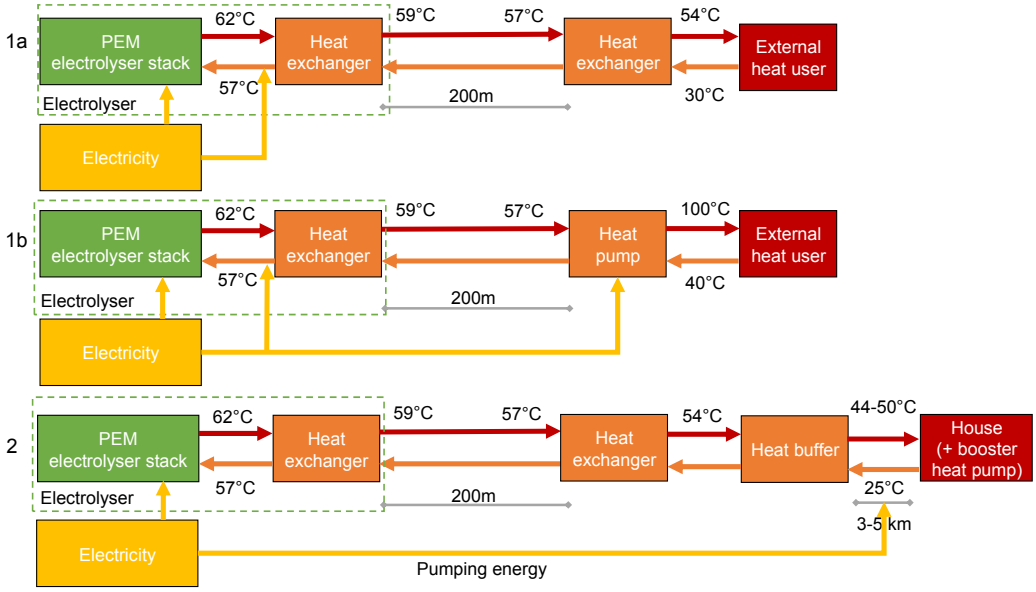

Figure 5.3 Schematic overview of the different cases; 1a – Local use of waste heat at low temperature, 1b – Local use of waste heat at high temperature, 2 – Delivery of waste heat to a low-temperature district heating network. The yellow arrows show which electricity demands are taken into consideration (pumping energy is included). Heat losses during heat transport are based on calculations of a DN80 pipe (90/162mm) with insulation (class 1) based on heat loss norms for heat pipes [280].

5.2.4 Efficiency & energy balance

The amount of heat utilization was calculated on an hourly basis with the Power-to-X techno-economic simulation model based on the Power-to-H3 concept introduced in earlier publications [171], [235] (**Chapter 2 & 3**). Based on varying hourly demand profiles, hourly weather data, and data about conversion and storage technologies (batteries, power-to-heat, power-to-hydrogen, long-term heat storage and hydrogen storage), an hourly energy balance was calculated for multiple years. Because the electrolyzer degrades over time while the hydrogen production target is constant, the electricity demand increased over time, as well as the heat production. Both a yearly and 10-year average efficiency of the electrolyzer stack (η_{EL} in %) were calculated according to equation 5.6.

$$\eta_{EL} = \frac{\sum_i^{nN_t} H_{2,produced,i} \cdot HHV_{H_2} + \sum_i^{N_t} E_{heat,used,i}}{\sum_i^{N_t} E_{Elec,i}} \cdot 100\% \quad (5.6)$$

With $H_{2,produced}$ the amount of hydrogen produced in a year (when i.e. i =1 and the number of time steps in hours N_t =8760) or over the total period (i =1 and n=87600) in kg, $HHV_{H_2}$the higher heating value of hydrogen (39.4 kWh/kg), $E_{heat,used}$ the amount of useful heat from the electrolyzer in kWh over the period i to N_t, and $\sum_i^n E_{Elec}$ the electricity consumption of the electrolyzer in kWh over the period i to N_t in hours.

5.2.5 CO_2 emission reduction

If the heat from the electrolyzer replaces heat from fossil sources, there is a CO_2 reduction potential. The amount of CO_2 reduction depends on the use case. For case 1, the local use of heat by a third party, we assume that this heat was otherwise produced by natural gas. For the gas boilers, we assumed an HHV efficiency of 90% (η_{boiler}) for the industrial boiler. The CO_2 emission reduction potential in kg for heat $CO_{2,reduction,heat}$ is calculated by eq 5.7 for case 1a, and by eq 5.8 for case 1b, including the heat pump electricity consumption. We assumed that the electricity for the heat pump is not certified renewable electricity, and therefore a CO_2 emission factor is added. The reference situation for case 2 (DHN) is a heat pump. For the heat pumps, we calculated the maximum potential for CO_2 emission reduction by using the CO_2 emission factor for the average grid electricity mix in the Netherlands, see equation 5.9. In all cases, the pumping energy necessary for transporting the heat to the heat consumer E_{pump} (in kWh) is taken into account.

$$CO_{2,reduction,heat,case\ 1a} = CO_{2,emissionfactor,gas} \cdot \frac{E_{heat,used}}{\eta_{boiler}} - E_{pump} \quad (5.7)$$

$$CO_{2,reduction,heat,case\ 1b} = CO_{2,emissionfactor,gas} \cdot \frac{E_{heat,used}}{\eta_{boiler}} + CO_{2,emissionfactor,electricity} \cdot \left(\frac{E_{heat,used}}{COP_{average,heat\ pump}} - E_{pump}\right) \quad (5.8)$$

$$CO_{2,reduction,heat,case\ 2} = CO_{2,emissionfactor,electricity} \cdot \left(\frac{E_{heat,used}}{COP_{average,heat\ pump}} - E_{pump}\right) \quad (5.9)$$

With $COP_{average,heat\ pump}$ the average COP of the heat pump over the period analyzed. The emission factors ($CO_{2,emissionfactor}$) in kg/kWh are given in Table 5.4.

Table 5.4 CO_2 emission factors for natural gas and renewable electricity, from a CO_2 emission factors database for the Netherlands [150].

Well-to-wheel CO_2 emissions	
Natural gas – case 1 & case 2	2.085 kg/Nm³ or 25.7 g/kWh (HHV)
Grid electricity (grid mix The Netherlands)	42.7 g/kWh

5.2.6 Cost calculation

The levelized yearly costs for the heat recovery installation (LC_{total} in €/year) including delivery at the consumer were calculated by equation 5.10 by summing over the number of units N_u. The calculation was made from the perspective of the electrolyzer owner delivering heat to a heat consumer. General cost parameters used in the calculations are given in Table 5.5.

$$LC_{total} = \sum_{i}^{N_u} LC_i \ with \quad (5.10)$$

$$LC_i = \alpha \cdot CAPEX_i + OM_i + Ecost_i \quad (5.11)$$

Where LC_i represents the annual levelized costs for a certain system component in (€/unit/year). The $CAPEX_i$ (€/unit) are the capital expenditures for a particular system component i such as the pumps, the pipes or the tie-in, see Table 5.6 for an overview of components. More information on the specific components and their costs is given in SI.1. The calculations included the necessary costs for heat recovery at the electrolyzer, transportation costs and control technology. It did not include an installation on the consumer side as it is not known how the heat will exactly be integrated into the process of the heat consumer.

The OM_i (€/unit/year) represent the operational expenditures for a particular system component, which are a percentage of the CAPEX costs. $Ecost_i$ (€/unit/year) are the electricity costs for a system component i., such as the electricity costs for pumps. The capital recovery factor (α, no unit) is a fraction of the total CAPEX cost. It represents a constant yearly value of depreciation and is calculated based on the project lifetime (L, in years) and the discount rate (r, as a fraction of 1) (eq 5.12). In the cost calculations, we allocated the investments of the heat recovery installation completely to the costs of waste heat. The costs of the electrolyzer were however excluded from the costs calculation of the waste heat as the investments for the electrolyzer installation are done regardless of the waste heat consumption. Yet, if there is a positive business case for waste heat utilization, this could lead to a lower hydrogen price.

$$\alpha = \frac{r}{1 - (1+r)^{-L}} \tag{5.12}$$

Based on the yearly costs, the levelized costs of heat ($LCOE_{heat}$) in €/MWh were calculated according to eq 5.13, with $E_{heat,used}$ the amount of heat utilized by the heat consumer in MWh_{th}/year.

$$LCOE_{heat} = \frac{LC_{total}}{E_{heat,used}} \tag{5.13}$$

To know if the business case is positive, we calculated the cost savings for the consumer. Then, we calculated the margin between yearly costs and savings. If the margin is positive, it means there is a possibility for a business case as the saved cost for the consumer are higher than the costs for heat delivery. The costs savings for the consumer ($C_{savings}$) in €/year were calculated in euros by using heat from the electrolyzer instead of gas (case 1) or electricity (case 2). The costs savings are based on the average amount of $E_{heat,used}$ over the total project lifetime (in kWh/year), see equation 5.14-5.15.

$$C_{savings,case1} = c_{gas} \cdot \frac{E_{heat,used}}{\eta_{boiler}} \tag{5.14}$$

$$C_{savings,case2} = c_{electricity} \cdot \frac{E_{heat,used}}{COP_{average,heat\ pump}} \tag{5.15}$$

With c_{gas} the costs of natural gas in €/kWh, η_{boiler} the gas boiler efficiency (presented as a decimal value) of the heat consumer and $c_{electricity}$ the costs of electricity in €/kWh. In case 2 (DHN), the heat would otherwise have been produced by an industrial-scale heat pump. In this case, the amount of heat from the electrolyzer was divided by the average COP of the heat pump $COP_{average,heat\ pump}$ over the same time period.

Finally, the margin per case ($C_{Margin,case-j}$ in €/year) between potential savings and cost for the heat, recovery installation was calculated as an outcome according to equation 5.16.

$$C_{Margin,case-j} = C_{savings,case-j} - LC_{total,case-j} \quad (5.16)$$

Yet, these calculations are highly sensitive to the costs assumptions of gas and electricity prices. Therefore, a sensitivity analysis was done (see section 5.2.7) to investigate the effects of energy prices on the business case.

Lastly, the effect of CO_2 pricing has been taken into account for every case j as optional cost savings with equation 5.17, with $CO_{2\ savings,case-j}$the saved costs by CO_2-pricing of CO_2 emission reduction in €/year. c_{CO_2} is the CO_2 price in €/tonne.

$$CO_{2\ savings,case-j} = c_{CO_2} \cdot \frac{CO_{2,reduction,heat,case-j}}{1000\ (\frac{kg}{tonne})} \quad (5.17)$$

The CO_2 cost savings are taken into account in the LCOE as a reduction of the yearly costs according to eq 5.18.

$$LCOE_{heat} = \frac{LC_{total} - CO_{2\ savings}}{E_{heat,used}} \quad (5.18)$$

In the margin, they are added to the other cost savings (eq 5.19).

$$C_{Margin\ with\ CO_2,case-j} = C_{savings,case-j} + CO_{2\ savings,case-j} - LC_{total,case-j} \quad (5.19)$$

Table 5.5 General cost parameters.

Parameter	Value
OM	2% of CAPEX
Discount rate (r)	5%
Installation factor pipes	1.2
Installation factor for pump, heat exchanger, tie in & electronics	1.4
Electricity costs (for pumps/heat pumps)[a] ($c_{electricity}$)	0.0834 €/kWh
Gas price industrial users[a] (c_{gas})	0.0341 €/kWh
CO_2 price[b] (c_{CO_2})	60 €/tonne

[a] Price of gas and electricity for industrial users in the 10-1000 TJ (gas) or 2,000-20,000 MWh (electricity) range, including taxes, excluding VAT, average price 2016-2020. Prices are converted from GJ to kWh [288]
[b] The CO_2 price is based on the middle value of the carbon pricing benchmark of the OECD [289], which is a conservative number compared to recent developments [290].

Table 5.6 Individual component costs parameters. In SI.1, more information is given on the cost calculations for specific system components.

Component	CAPEX	Lifetime (L, in years)
Tie-in electrolyzer	10 k€	15
Electronics, controls & monitoring	40 k€	10
Pumps	see SI.1	15
Pipes[a]	230 €/m (2019)	40
Heat exchanger	$1500 * \sqrt{P_{HE}}$ (2017)	20
Heat pump (including installation)[b] – case 1b	600 €/kW_{th}	20

[a] Based on the Polytherm pricelist (2019) [291]
[b] The investment is including installation, approx. 50% of costs [183]

5.2.7 Sensitivity analysis

To assess the effect of changes in variables that are still uncertain, or from which a large effect is expected, a local sensitivity analysis was performed. In Table 5.7 the parameters chosen for the sensitivity analysis are shown, including the ranges over which the parameters were varied and in which cases they are applied. The annual efficiency degradation, tie-in costs and costs for electronics are relevant and these numbers are hard to verify as there are no installations yet in place. Therefore, we assessed their influence on the LCOE to know how a change in value would affect the LCOE. The overlapping working hours, discount rate, heat pump temperature, the distance between production and use and the electricity price are likely to have a significant influence on the LCOE. Moreover, these values are likely to vary for other use cases, so the sensitivity analysis gives more general insights as well. High-temperature heat pumps with temperature levels above 100°C are not yet standard products, but there are suppliers available with a technology-readiness level (TLR) of 7-9 for temperatures up to 200°C [292]. Here we have chosen a maximum of 150°C, so as to not overestimate the possible temperature lift at the heat consumer side.

The gas price is not taken into account in the LCOE but only in the saved costs by the heat consumer, therefore, we will assess this variable for the margin. As gas prices have recently been shown to be highly sensitive to geopolitical circumstances, we have taken extremely high prices into account. The range for the CO_2 price is chosen to be 0 (no CO_2 pricing) to 120 €/tonne based on the high range of the carbon pricing benchmark of OECD [289].

Table 5.7 Ranges for sensitivity analysis.

	Number	Range	Case
Annual efficiency degradation electrolyzer [129], [268], [279]	1.0%	0.5 – 2%	1,2
Overlapping working hours	80%	20-100%	1,2
Discount rate	5%	2-10%	1,2
Tie-in costs	10.000 €	+/- 30%	1,2
Electronics	40.000 €	+/- 30%	1,2
Heat pump temperature	100°C	80-150°C	1b
Distance between production and use/storage	200 m	100-5000m	1,2
Electricity price	0.0834 €/kWh	-50/+500%	1,2
Gas price	0.0341 €/kWh	-25/+500%	1
CO_2 price	60 €/tonne	0-120 €/tonne	1,2

5.3 Results & Discussion

5.3.1 Design for heat recovery from a PEM electrolyzer

To utilize the electrolyzer heat, we propose a tie-in on the cooling system as shown in Figure 5.4. The tie-in is an add-on to the cooling system to create a redundant design independent of the heat consumer. The electrolyzer can thus either be cooled through heat consumption by an external heat consumer or by the dry cooler when there is no external heat consumption. We choose deliberately for a tie-in on the cooling system instead of replacing the dry cooler, as this makes the system redundant. Both the hydrogen producer as well as the heat consumer should continue their processes regardless of the delivery or demand of the other to give them the most flexibility.

Table 5.8 shows the simulation results for all cases, starting with the reference case. The amount of available heat increases over time (Figure 5.7) due to the degradation of the electrolyzer stack (for specs see Table 5.1). The electric resistance increases and thereby the electricity consumption. This extra electricity consumption is not converted to hydrogen, but to heat instead. At the start, about 20% of the electricity input to the stack is converted to heat. After ten years, the total electricity consumption has raised by 10%, so now 30% of the electricity input to the stack is converted to heat, which means the heat production increased by 50%. In the reference case, this heat is not recovered leading to an average (HHV) efficiency of 76% for the electrolyzer stack.

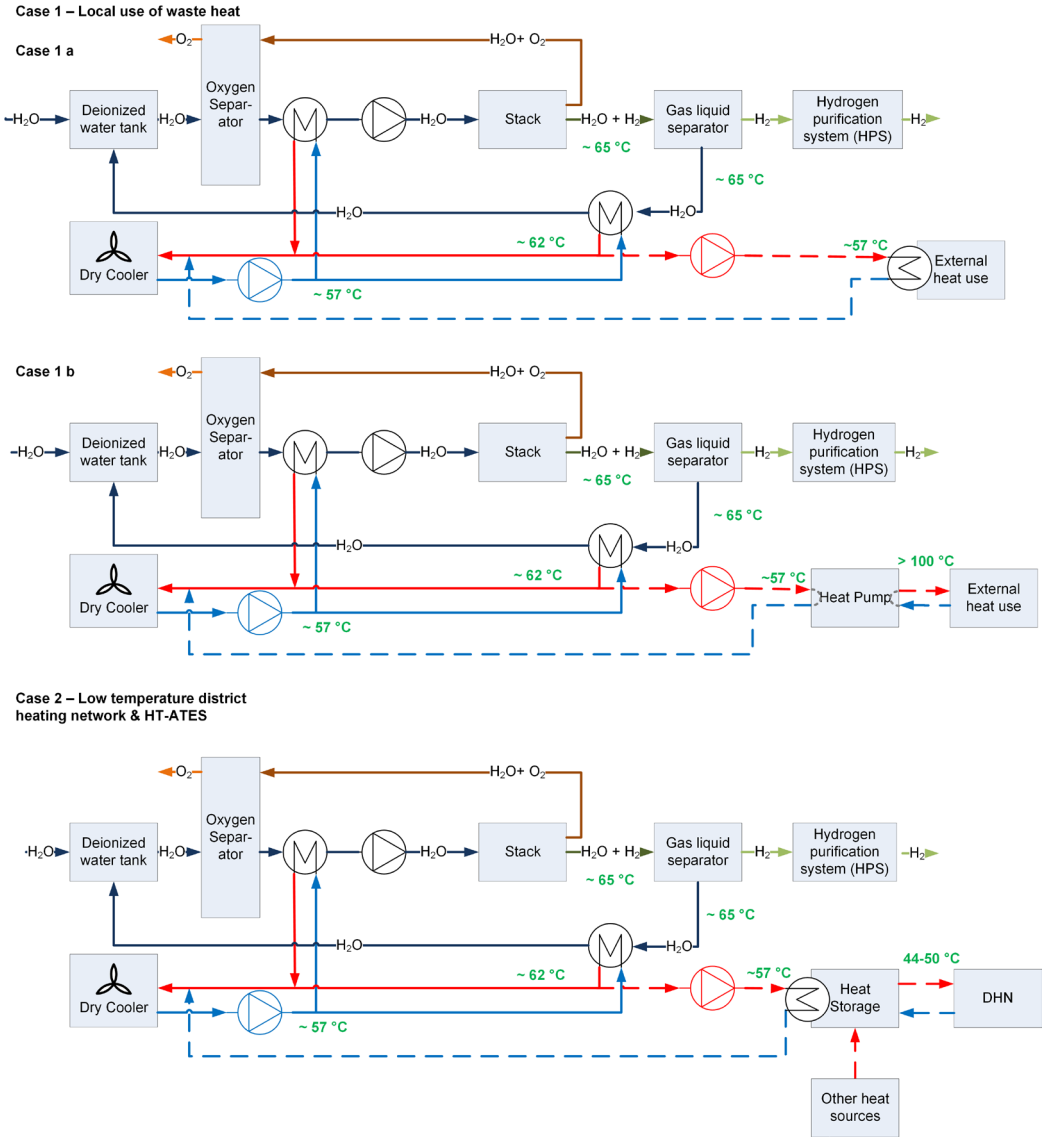

Figure 5.4 Redundant designs for heat recovery from a PEM electrolyzer.

Table 5.8 Results overview table. Case 1a and 1b have the same total (stack) efficiency, thus these values are only presented once.

			Reference case		Case 1 a			Case 1b			Case 2				
Year	Electricity consumption electrolyzer (MWh)	H_2 production (tonne)	Heat production (MWh)	Base efficiency (HHV)	Heat utilized (MWh)	Total efficiency (stack +heat)	CO_2 savings (tonne/year)	Electricity consumption heat pump (MWh)	Heat utilized (Electrolyzer & heat pump) (MWh)	CO_2 savings (tonne/year)	Heat utilized (MWh)	Total efficiency (stack +heat)	Heat demand neighbourhood (MWh)	% electrolyzer heat of total heat demand	CO_2 savings (tonne/year)
Y1	14,840	299	2,270	79%	1,820	92%	510	540	2,360	430	1,900	92%	19,060	10%	150
Y2	15,040	300	2,400	79%	1,920	91%	540	580	2,490	450	2,020	92%	14,420	14%	160
Y3	15,240	301	2,540	78%	2,020	91%	560	610	2,630	480	2,130	92%	15,730	14%	170
Y4	15,350	301	2,660	77%	2,100	91%	590	630	2,740	500	2,230	91%	17,080	13%	180
Y5	15,510	300	2,780	76%	2,190	90%	610	650	2,840	510	2,330	91%	12,860	18%	190
Y6	15,670	300	2,910	75%	2,270	90%	630	680	2,950	530	2,440	91%	14,040	17%	200
Y7	15,880	301	3,050	75%	2,360	90%	660	710	3,060	560	2,530	90%	15,760	16%	205
Y8	16,010	300	3,180	74%	2,440	89%	680	730	3,170	570	2,610	90%	14,750	18%	210
Y9	16,170	300	3,310	73%	2,520	89%	700	760	3,280	590	2,690	90%	15,270	18%	220
Y10	16,340	300	3,450	72%	2,600	88%	730	780	3,380	610	2,780	89%	14,450	19%	225
Avg	15,605	300	2,855	76%	2,220	90%	620	665	2,890	525	2,365	91%	15,340	16%	190

5.3.2 Efficiency & Energy balance

The reference situation without heat utilization can be compared to three cases where the electrolyzer heat is utilized, overall results are shown in Table 5.8. The first case has a heat consumer that utilizes the electrolyzer heat directly with an 80% overlap in electrolyzer heat production and heat consumption, thereby reducing gas consumption by a gas boiler. On average 2,220 MWh/year of heat can be utilized by the heat consumer in case 1a, which leads to a total system efficiency of 90% (stack + waste heat, HHV based). In the Sankey diagram, all different energy flows are shown including the heat losses and amount of unused heat (see Figure 5.5) based on a ten-year average. Pumping energy is about 7 MWh/year, rounded off to 5 MWh and too small to be visible in the Sankey diagram. The increase in heat production and consumption over time and the overall

efficiency are shown in Figure 5.7. Eventually, almost 59% of the heat that is formed in the electrolyzer is utilized by the consumer. Similarly, we find that 14% of the electricity input in the electrolyzer is used as heat by a heat consumer. Compared to the base scenario without heat utilization, the average 10-year efficiency increases by 14% from 76% to 90%. In case 1b, with a heat pump to raise the temperature of the electrolyzer heat, 2,890 MWh/y of heat is available on average. The amount of heat delivered by the electrolyzer stays equal, but electricity has been used to increase the temperature, thereby increasing the ΔT and thus the amount of heat available at the consumer. The efficiency of the electrolysis system in case 1b is thus equal to case 1a and therefore not shown separately.

In case 2, the electrolyzer heat is reused in a low-temperature district heating grid (Figure 5.6), and the heat from the electrolyzer is supplied to the heat buffer of the DHN. The total system efficiency raises to 91% when the heat from the electrolyzer is used in a low-temperature DHN. The amount of heat provided increased over the years and accounts on average for 16% of the total heat demand of the neighborhood (2000 houses) supplied by the DHN. The variation in the percentage of fulfilled heat demand by the electrolyzer is caused by a difference in heat demand over the years due to varying climate data (the years considered are 2010-2019). About 15% of the electricity input of the electrolyzer is finally used as heat in the DHN. Interesting to note is that the electrolyzer waste heat is not used to fill the seasonal heat buffer, but only the day buffer. Thus, the daily heat demand in summer is still high enough to take up the daily heat produced by the electrolyzer.

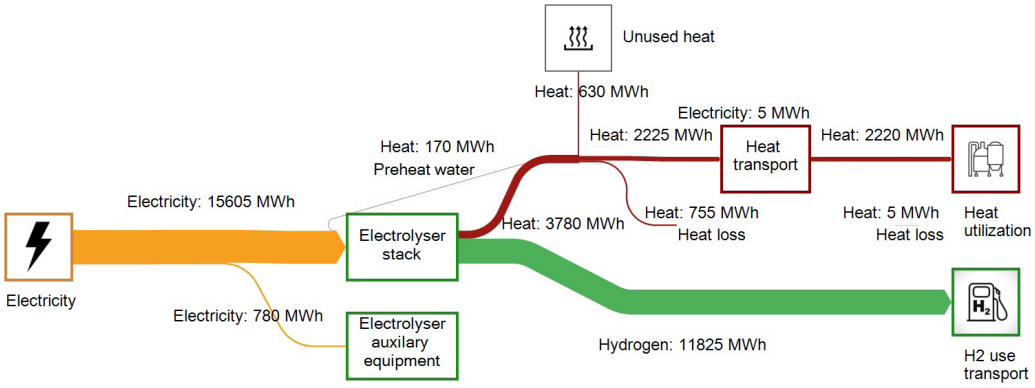

Figure 5.5 Sankey diagram for the energy balance of an electrolyzer system with an industrial (local) heat consumer (1a). The 10-year average energy flows are shown.

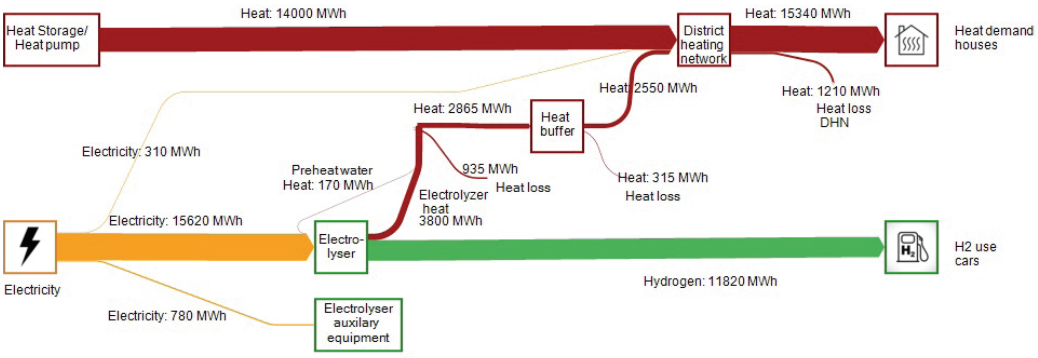

Figure 5.6 Sankey diagram with an average yearly energy balance when electrolyzer heat is provided to a DHN (case 2), 10-year average flows are shown.

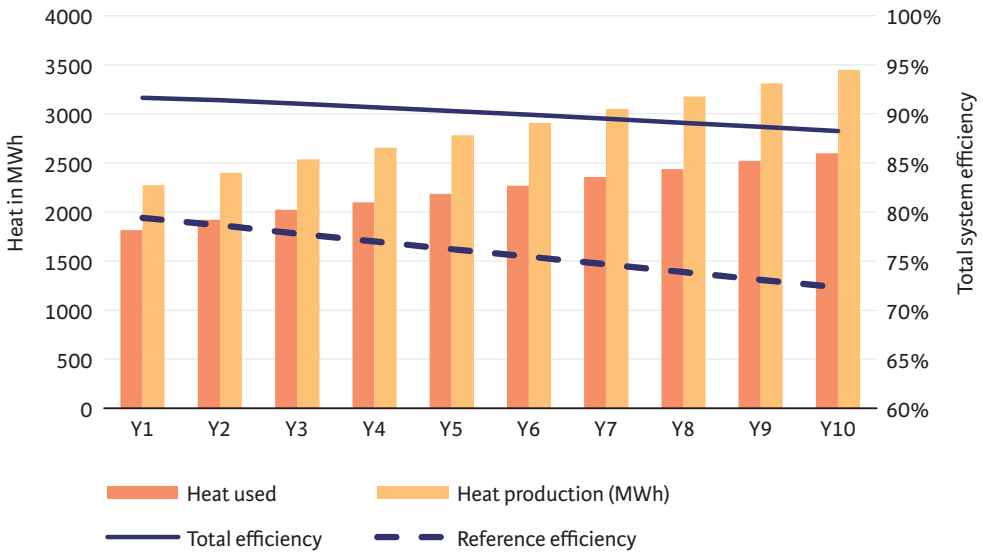

Figure 5.7 Heat production by the electrolyzer and heat used by the heat consumer shown over 10 years for case a1 (local heat consumer), including the reference case of the electrolyzer (without heat recovery) and the efficiency including heat recovery (total efficiency of stack + waste heat utilization). Efficiency (HHV) is shown on a secondary axis.

5.3.3 CO_2 reduction potential

The current energy source of the heat consumer is natural gas. When part of its heat demand is fulfilled by the electrolyzer heat, on average 620 tonnes of CO_2 are mitigated each year, or 270,000 m^3 of natural gas (0.845 kg/Nm^3 [293] and a boiler efficiency of 90%). In more general terms, this means 0.28 tonne CO_2 per MWh of waste heat used ($MWh_{heat,used}$). For the case with a heat pump (1b), the CO_2 emission reduction is 525 tonnes per year or 0.18 tonne $CO_2/MWh_{heat,used}$. We assumed

that the electricity for the heat pump is not certified renewable electricity, which results in more CO_2 emissions for the use of electricity by the heat pump than the savings by switching from natural gas to electricity. Yet, the amount of saved natural gas is higher in this case, about 350.000 m^3. If the heat consumer would buy or produce renewable electricity, the CO_2 emission reduction would be higher than in case 1a.

For the DHN network (case 2), the CO_2 emission reduction is on average 190 tonnes/year or 0.08 tonne $CO_2/MWh_{heat,used}$, compared to when the electricity would have been produced with a heat pump working on an average grid-electricity mix. The heat pump has an average COP of around 5, so only $1/5^{th}$ of the heat demand is reflected in electricity demand. On the other hand, the CO_2 emission factor for electricity is higher than for gas (due to conversion losses). In summary, the CO_2 CO_2 reduction will be the highest when the electrolyzer heat would be used directly without a heat pump (1a), as long as the heat pump at the heat consumer is not running on green electricity.

5.3.4 Economic results

The results of the economic analysis are shown in Table 5.9 for all three scenarios. A detailed breakdown of the costs per component including OM costs and energy costs is given in table S2-S5 of the ***supplementary information*** (SI). The yearly costs are similar for cases 1a and 2, but case 1b has factor 5 higher yearly costs, because of the investments in the heat pump. This effect is reflected in the LCOE, which is 36.9€/MWh_{heat}, while case 1a has an LCOE of 8.9 €/MWh_{heat}. In case 2, the LCOE is slightly lower than for 1a with 8.4 €/MWh_{heat}, because more heat can be utilized in this scenario due to the larger heat buffer.

When taking the saved yearly costs into account, we note that all scenarios have a positive margin, so a possible business case. Although in the current analysis, only a heat exchanger (or heat pump) has been taken into account at the heat consumer, so there are possible other costs for adaptations at the heat consumer to use the heat that have been neglected. Thus, a margin just above zero for case 1b, makes it uncertain if a business case can be realized. For the heat delivery without a heat pump, the margin is almost 65 k€/year. For case 2 (DHN) the margin is also positive (18.5 k€/year), although it is a factor 3 less than for the industrial heat consumer, while more heat is delivered. Our reference case for the DHN was heat produced with a heat pump that has a COP of 5, and not gas boilers. Therefore, just as with the CO_2 calculations, here we see again the effect of the high COP of the heat pump. The heat pump produces heat with only 0.2 units of electricity for one unit of heat. Hence, the savings in electricity costs in case 2 are less than the gas savings in cases 1a and 1b. How the margin is divided among the stakeholders (electrolyzer owner, heat user and possibly others) will finally determine the effect on the heat costs for the heat consumer as well as the hydrogen production costs. If CO_2 pricing is taken into account (Table 5.10), the LCOE decreases substantially while the margin increases. All margins are now at least 30 k€/year, pointing towards a high possibility for a business case. For direct heat use (case 1a) the LCOE becomes negative. In practice, this means that a company can save more money on CO_2 costs than it would cost to replace natural gas with waste heat, not even including the saved costs of the natural gas itself. Upgrading the heat with a heat pump to 100°C could also be economically feasible if CO_2 costs are taken into account.

Table 5.9 Costs without CO_2-pricing - results for the cases.

	Case 1a	Case 1b	Case 2
Total yearly costs (k€/y)	19.7	106.5	19.7
$LCOE_{heat}$ (heat production costs in euro/MWh)	8.9	36.9	8.4
Saved yearly costs (k€/y)	84.2	109.4	38.3
Margin (k€/y)	64.5	2.9	18.6

Table 5.10 Costs with CO_2 pricing - results for the cases.

	Case 1a	Case 1b	Case 2
Total yearly costs (k€/y)	19.7	106.5	19.7
CO_2 emissions reduction cost savings (k€/year)	37.2	31.4	11.5
$LCOE_{heat}$ (heat production costs in euro/MWh)	-7.9	26.0	3.5
Saved yearly costs (k€/y)	84.2	109.4	38.3
Margin including CO_2 emissions reduction cost savings (k€/y)	101.8	34.3	30.0

5.3.5 Sensitivity analysis

We have investigated the impact of a change in certain input parameters on the LCOE, in Figure 5.8 the results of the sensitivity analysis are presented. Although in the case of Nieuwegein, the distance is known, in other cases of heat utilization the distance between the electrolyzer and heat consumer could deviate considerably. The sensitivity analysis clearly shows that the distance has a large influence on the LCOE, especially with direct heat delivery (case 1a, Figure 5.8a) and delivery to a low-temperature DHN (case 2, Figure 5.8c). Delivering waste heat over long distances will thus not be feasible. The CO_2 price is the second most important factor in case 1a and 2 that influences the LCOE, yet the adoption of a CO_2 price would positively influence the business case. When a heat pump is installed (case 1b, Figure 5.8b), the electricity prices are the most important factor in determining the LCOE. Long-term contracts for electricity prices will give more certainty in the business case. Another option would be to have dedicated renewable production capacity for the heat pump electricity demand. In cases 1a and 2 (a&c), the electricity price is not such a major factor as electricity is only used for pumping the heat around. Besides the distance, the percentage of overlapping working hours shows to be sensitive as well in the case of delivery to a heat consumer (a&b). For case 1b (b), the LCOE furthermore proves to be sensitive to the heat pump temperature and to the CO_2 price as well. Of slightly less importance in all cases is the discount rate chosen.

The exact percentage of annual efficiency degradation, costs for electronics and tie-in in the electrolyzer for heat recovery have a high degree of uncertainty still. Yet, the sensitivity analysis

shows that their impact on the LCOE remains small. So, although we need more exact information about these parameters, they are not the most essential while developing a business case for heat recovery from electrolysis. Of these three parameters, the annual efficiency degradation has the largest impact on the LCOE.

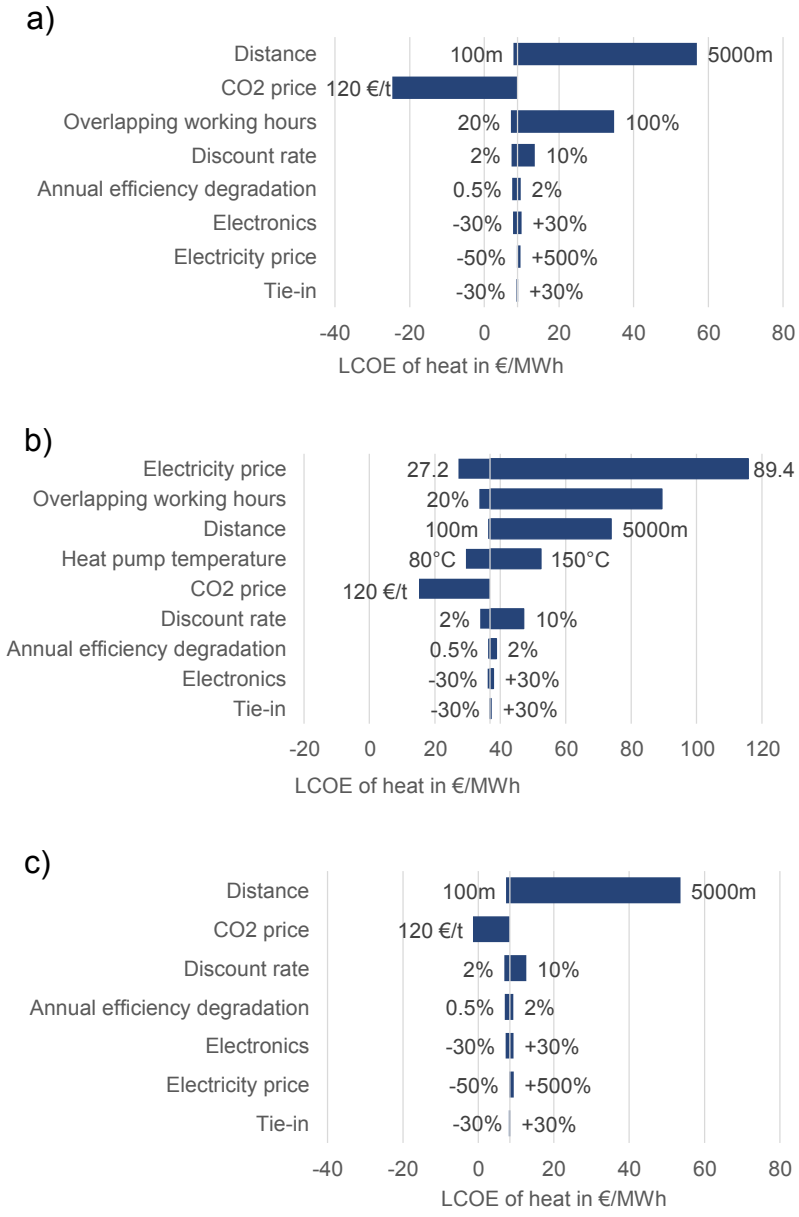

Figure 5.8 Results of the sensitivity analysis with tornado diagrams of case 1a (a), case 1b (b) and case 2 (c).

As the distance shows to be an important factor in the business case of electrolyzer heat, Figure 5.9a shows more precisely how the distance influences the margin between costs and benefits (saved costs) for the consumer. If heat is delivered directly to the consumer (1a) the maximum feasible distance is around 3 km. For heat delivery to the DHN (2), this distance is 1 km. For heat delivery with the heat pump (1b), the margin is too small resulting in a negative business case above 200 m distance. These values are valid for an electrolyzer size of 2.5 MW_{el}, with larger installations, the more heat is transported, the lower the investment costs per unit of heat will be, as well as smaller heat losses [294], [295].

The sensitivity of the gas price is shown with respect to the margin in Figure 5.9b. We have assumed a relatively low gas price in the analysis based on historical data, but the war in Ukraine has caused a tremendous increase in gas prices. It is uncertain how the gas price will develop in the coming years, yet it is more likely to stay high. As expected, high gas prices will have a (highly) positive influence on the margin. In the analysis, the gas price and electricity price are changed by the same percentage, as the gas price will influence the electricity price. Because of the electricity consumption of the heat pump in case 1b, it has a lower margin than case 1a over the total range.

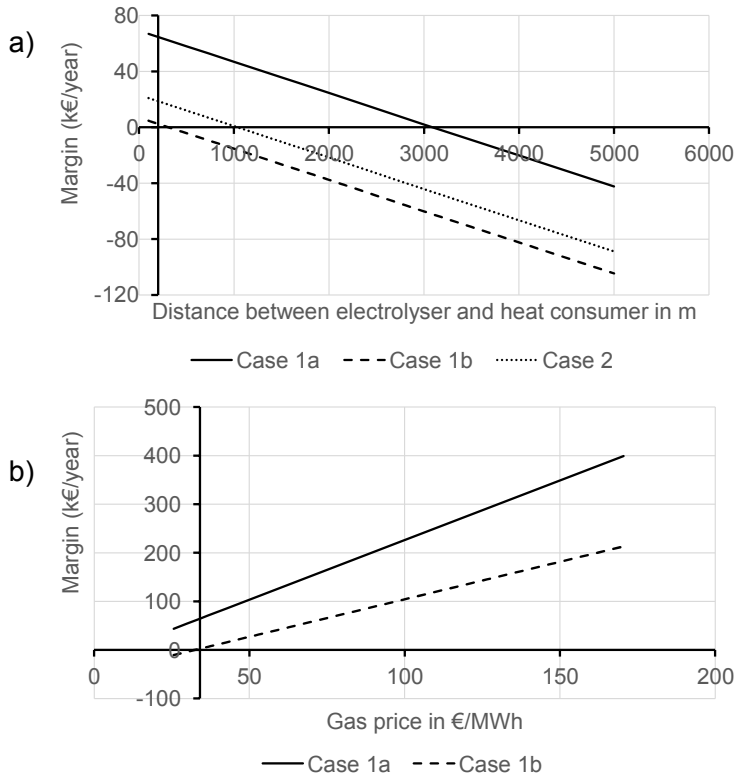

Figure 5.9 Sensitivity of a) distance between electrolyzer and heat consumer and b) gas price on the margin between costs and saved costs at the heat consumer. The y-axis crossing shows the currently chosen value in the analysis. In b) the gas price is shown on the x-axis, but in this analysis, the electricity price is changed simultaneously with the same percentage for a fair comparison.

5.4 Discussion

5.4.1 General reflections and limitations of the study

The results presented in this study are subjected to certain limitations. The lack of literature and concrete examples of heat recovery from electrolysis, as mentioned in the introduction as a reason to perform this study, is also its limitation. We have given insight into the feasibility of using electrolyzer waste heat, but we have had to make assumptions as there is no available data. Therefore, we have included a sensitivity analysis (see also 5.3.5), which has shown that uncertain parameters such as the actual efficiency degradation and exact prices for the tie-in and electronics have a limited influence on the business case. Thus, the results obtained are reliable enough regardless of the uncertainties in these parameters.

Another general comment is that every case will have its specific circumstances. The BOP will be different per supplier and will also depend on the engineering. Yet, the design we propose gives both possibilities to reuse heat within the electrolyzer as well as supply heat to an external consumer, and could thus be helpful as a starting point for other studies. Regarding the economics, we should note that we have worked with a stable hydrogen production rate for over ten years. New electrolyzer projects are not likely to start producing at full capacity from year one. Over time the production capacity will increase, building up to full capacity, thus in the first circa five years probably less heat will be delivered (and less CO_2 reduced). More precise calculations for specific cases should be done to determine the exact effect on the business case. For the cases presented in this chapter, it means that the LCOE and margins presented should be seen as a first-order approximation. A highly feasible case (1a) will probably stay feasible even with these start-up effects taken into account. Furthermore, the decision for a heat consumer to replace natural gas with waste heat does not have to be of a purely economic nature, or more indirectly. A 'green' profile can enhance the reputation of a company, leading to a better position in the market and eventually to higher financial performance [296].

Furthermore, in this study, we only considered the costs to extract and deliver waste heat, independent from the hydrogen production costs. Eventually, both 'products' (hydrogen and heat) are connected for the owner of the electrolyzer, and thus the hydrogen production costs could play a role in the business case of the waste heat. For example, in the results (see 5.3.5), we have shown that high gas prices will increase the margin between the costs of waste heat delivery and saved costs for the consumer. But, high gas and (therefore) electricity prices will affect the business case for green hydrogen and may lead to the hydrogen producer asking a higher price for the waste heat to compensate for higher electricity costs. This is even the case for green hydrogen produced with a solar or wind-based power purchase agreement (PPA), as those PPA prices are affected by the wholesale market including fossil-based electricity sources [297].

5.4.2 Ancillary services and hot standby mode

Electrolyzers can fulfil ancillary services [298], [299]. This would mean that the electrolyzer would quickly (within seconds) reduce or increase its capacity [300]. We have not considered the impact of this mode of operation in this study. Yet, although the ancillary services can have a positive impact on the business case of the electrolyzer [301], the total amount of hydrogen (and thus heat) produced will not vary significantly when production targets have to be met. We thus expect that the influence on the amount of heat produced will not deviate more than a few per cent.

When ancillary services are part of the business case for an electrolyzer, it either has to operate at the time when it is bidding in for the balancing markets, or it has to stay in hot standby mode so it can react quickly [300]. In the hot standby mode, the electrolyzer will consume electricity, about 3% of its nominal power [300], [302]. Part of the electricity consumption for the hot standby mode is used to keep the electrolyzer warm and could maybe be supplied by its own waste heat. With the assumption of 50% of the hot standby energy use being fulfilled by waste heat, we calculated that about 28 MWh/year of heat could be used within the electrolyzer itself (for case 1a). This is a small potential but could be interesting in combination with other waste heat uses, so the costs for a heat buffer could be shared.

5.4.3 Efficiency raise of electrolyzer stack

We have seen an efficiency raise of the total PEM electrolyzer stack from 76% to 90/91% (HHV based) when the electrolyzer heat is taken into account, thus a 14-15% efficiency increase in total. Bilbao mentions a 13 % potential efficiency increase for an alkaline electrolyzer if heat would be recovered [269]. In Buttler & Spliethoff two projects are mentioned that increase their efficiency including heat utilization to 95% and 86%. Frank et al. [271] show a range of options for a 1 MW Power-to-Gas plant with an alkaline electrolyzer including different parts of the electrolyzer design to recover heat from. With the stack, electrolyte circuit, product gas treatment and water supply taken into account, they calculated an efficiency gain of external heat use from circa 78% to 97% with a 60°C operating temperature. For the overall electrolysis system, the efficiency gain would be 17.6% (from 72.8-90.4%). Jonsson & Miljanovic found an overall system efficiency for a PEM electrolyzer including heat recovery of 94.7%, an 18% increase from their reference scenario if all waste heat can be utilized (at 80°C working temperature) [303]. So although most available data are for alkaline electrolysis, our findings for the efficiency raise are comparable with the literature. Moreover, we have not yet considered the possible reduction in energy use of the dry coolers of the electrolyzer system, which could lead to lower energy use of the electrolysis process. The heat utilization from the electrolyzer can thus clearly increase the overall system efficiency of the electrolysis process. When applied, the electrolyzer will be a hydrogen as well as heat producer and will help to make even better use of available renewable energy.

5.4.4 Comparison to other (waste) heat costs

We have calculated the LCOE of waste heat from the electrolyzer for different temperature levels and applications. We have concluded that there is a high possibility for a positive business case for direct heat delivery to a heat consumer and heat delivery to a low-temperature DHN (40-60°C). Moreover, it is relevant to compare our results with other sources of (waste) heat, especially for district heating networks. Table 5.11 shows a comparison of heat production costs per MWh, without the distribution costs. For low-temperature waste-heat sources below 40°C, a heat pump is necessary to increase the temperature, which is reflected in the LCOE. The LCOE of electrolyzer heat without a heat pump including a short transport distance (8.4-8.9 €/MWh_{heat}) is well below this range (36-73.4 €/MWh_{heat}). Even with a heat pump to increase the temperature, the costs for electrolyzer heat are at the lower end of the range with 36.9 €/MWh_{heat}, while the temperature is higher (100°C). Electrolyzer heat could compete as well with higher temperature waste heat sources, but only at a lower temperature level (at 54°C), so without a heat pump. Overall, these data show that the waste heat from the electrolyzer may compete with other industrial waste heat sources depending on the necessary temperature level, and is likely to be cheaper than lower-temperature heat sources.

Other sources that specifically discuss the business case of heat from electrolyzers are scarce. Jonsson & Miljanovic found costs of 20 €/MWh_{th} for waste heat utilization from a PEM electrolyzer of 100MW, with a heat pump raising the temperature to 120°C [303]. Without the heat pump (so only a heat exchanger), they calculated 1.65 €/MWh_{th}, yet costs for a tie-in and controls have not been taken into account here so these values seem to be an underestimation. Our results show higher costs because more cost components have been taken into account, but Jonsson & Miljanovic [303] show that with larger electrolyzer installations, the costs will probably decrease.

Table 5.11 Heat source cost (LCOE) comparison.

Heat source	Costs (LCOE) in €/MWh_{heat}
Waste heat electrolyzer to DHN – this study without heat pump (54°C)	8.4-8.9
Waste heat electrolyzer to DHN – this study with heat pump (100°C)	36.9
Heat from surface water with a heat pump (45°C)	55.4-73.4
Industrial waste heat sources (<35°C, with heat pump to 75°C) [304]	36-46
Industrial waste heat sources (75-100°C) [304]	6-10
Geothermal energy at low temperature (50°C, depth 500-1000m, including heat pump) [305]	54-65

5.4.5 Theoretical potential of electrolyzer heat

In our case study, we have considered a 2.5 MW electrolyzer that could part of a local hydrogen cluster. Local green hydrogen production is expected to grow exponentially in the coming years and decades, within the current plans of for example the EU and its RePowerEU programme [8]. The waste heat from the electrolyzer could thus potentially become a waste heat source for district heating. Yet, there are many other possible waste heat sources available, so what would be the share of heat from hydrogen production compared to the total available waste heat potential? We will focus on Europe to answer this question. Fleiter et al. [103] calculated that there is a potential of 425 PJ (118 TWh_{th}) of heat at 95°C available within Europe, 503 PJ (140 TWh_{th}) at 55°C and 960 PJ (267 TWh_{th}) with a temperature of 25°C. Of this 425 PJ at 95°C, 151 PJ could be utilized within a 10km range from the heat source in existing district heating grids and almost all of the heat (415 PJ – 115 TWh_{th}) would be usable considering the expected increase of district heating grids.

How does the amount of heat from electrolyzer installations relate to this? The EU target is 10 million tonnes of domestic hydrogen production in 2030 [8]. According to van Wijk et al. [182], about 5% of this hydrogen production capacity will be decentral capacity, and 15% will be produced directly at the industry/point of use itself (captive market). The other 80% of green hydrogen production will be large centralized production, at places with good solar and wind resources, probably further away from (heat) consumers. For the captive market and decentral capacity, it is most likely that there is a useful purpose for the waste heat. Thus, if we assume that about 20% of the expected hydrogen production capacity could lead to useful heat production, this corresponds to 2 million tonnes of hydrogen production. With 80% efficiency of the electrolysis (HHV based), this amounts to 98.5 TWh of electricity input. We have calculated that 14% of the electricity input will be used as heat (see section 5.3.2), so around 13.8 TWh_{th} of electrolyzer heat could be added to the total waste heat potential within the EU. This is about 10% of the waste heat potential at 55°C, a modest, but not insignificant amount of heat. Böhm et al. calculated a 56-84 TWh_{th} (theoretical) potential of thermal energy from hydrogen supply based on the European hydrogen strategy [274], but haven't corrected for hydrogen production in proximity of heat demand. Our calculations are thus probably closer to the technical potential of hydrogen waste heat.

5.4.6 Recommendations for future research

We have obtained insights on how heat from electrolyzers could (technically) be recovered as well as an energetic, environmental (CO_2-reduction) and economic potential. Yet, the adoption of heat utilization from electrolyzers is still small so there is a lack of real data from actual projects. Validation of results is now merely done with other theoretical studies, so for future research, validation with practical data would be very valuable. These data could also give more insight into a stepwise increasing hydrogen (and thus heat) production pattern during the first period of operation. Furthermore, other use cases can be evaluated. Some interesting other use cases could be a wastewater treatment plant with local hydrogen production (where oxygen could be utilized in aeration) or a hydrogen fuelling station with local hydrogen production and use of the waste

heat for car washing. Another possibility is to use the waste heat for thermal desalination, thereby producing deionized water at lower costs than with reversed osmosis technology [306].

If a heat pump is necessary to increase the waste heat temperature, more research could be done on how local renewable capacity would influence the business case in terms of electricity prices. Lastly, the results could be further refined by taking into account the business case of hydrogen as well, including different modes of operation of the electrolyzer as well as ancillary services. Furthermore, there is the possibility to use part of the waste heat for the hot standby mode of the electrolyzer, combined with another heat consumer.

5.5 Conclusions

We have shown that it is possible to make a redundant system design to utilize heat from an electrolyzer without compromising on the hydrogen production process. The utilization and valorization of heat from electrolyzers could lead to:

- *Higher system efficiency* - An increase in combined electrolyzer system (stack + waste heat) efficiency from 76% to to 90-91%, based on HHV. Furthermore, 14-15% of the electricity input to the electrolyzer stack can be utilized as heat by a heat consumer, depending on the use case. For the district heating system (case 2), we have shown that the electrolyzer (waste) heat can fulfil around 16% of the total heat demand of the neighborhood.
- *CO_2 savings* - Direct heat use (case 1a) leads to 0.28 tonne CO_2/$MWh_{heat,used}$. With a heat pump (case 1b) to increase the heat temperature, the savings would be 0.18 tonne CO_2/$MWh_{heat,used}$ if the heat pump works on an average electricity grid mix. Delivery of heat to a low-temperature DHN leads to 0.08 tonne CO_2/$MWh_{heat,used}$, compared to heat produced directly by a heat pump working on an average electricity grid mix.
- *Economic feasibility* - When a heat pump is necessary to increase the waste heat temperature, it will be harder to realize a business case (LCOE 36.9 €/$MWh_{heat,used}$) than without a heat pump (8.9 €/$MWh_{heat,used}$). If CO_2-pricing of 60 €/tonne would be taken into account, the business case is likely to be positive in all cases (LCOE of -7.9 - 26 €/$MWh_{heat,used}$). The sensitivity analysis has shown that the transport distance of heat is an important factor in determining the feasibility of electrolyzer heat utilization. The feasible distance varies per use case between 1-3 km. Compared to other waste heat sources, the LCOE of the electrolyzer heat (8.4-36.9 €/$MWh_{heat,used}$) falls within or below the range of lower-temperature heat sources. Without a heat pump, the LCOE (8.4-8.9 €/$MWh_{heat,used}$) also falls within the range of other high-temperature industrial heat sources.

Overall, we show that electrolyzer heat can both from an environmental and economic point of view be a valuable addition to a local integrated energy system, and further enhance local system optimization by integrating both hydrogen and heat production.

Supplementary Information

Supplementary information containing a detailed breakdown of the costs per component including OM costs and energy costs is available via:
https://ars.els-cdn.com/content/image/1-s2.0-S0360319923015410-mmc1.docx

Data

Raw data of the modelling results from the cases described in this chapter can be accessed via *http://doi.org/10.4121/21666152*.

Acknowledgements

The authors would like to thank Hysolar for their collaboration in the project and for providing information about the electrolyzer. The authors would like to thank Hans Huiting from Hans Huiting Onderzoek & Advies for his help on the initial design of the balance of plant of the electrolyzer with a tie-in. The authors would also like to thank Daniël Bakker from KWR Water for his contributions to the economic model for the waste heat calculations.

Funding

The H-Flex project is funded by the Dutch National Chamber of Commerce (RVO) via the DEI programme (Demonstration Energy Innovation) with project number DEI4891013.

The electrolyzer in the H-Flex project is operated by Hysolar (*https://www.hysolar.nl/en*) and co-funded by the EU LIFE programme via the LIFE NEW HYTS project (LIFE20 CCM/NL/001664).

6 Increasing solar panel output with blue-green roofs in water-circular and nature inclusive urban development

" If you want to go fast, go alone;
but if you want to go far, go together "

African proverb

Abstract: With an increasing demand for climate resiliency, water sensitivity, nature inclusiveness and energy efficiency in dense urban environments, the call for layered and multifunctional use of rooftops is rising. Vegetated roofs combined with Photo-Voltaic (PV) installations are an example of multifunctional and more effective use of available space, and well-irrigated systems could have an enhanced cooling effect. This research investigated a blue-green capillary irrigated solar roof with grey (shower) water suppletion, with a constructed wetroof for grey water purification. Two full-scale commercial PV systems on twin rental apartment blocks in Amsterdam were analyzed, on a blue-green roof (BGR) versus a bitumen roof (BiR). The energy output, PV panel temperature, relative humidity and air temperature under the panels were monitored during 5 warmer months (June-October 2022). On average, a solar panel on the BGR is expected to produce 4.4% more energy than a solar panel on the BiR at similar irradiation. A clear difference in panel temperature on the roofs is only seen when the surface temperature of the roofs differs by at least 4.64°C. Otherwise, other factors such as wind or albedo have probably more influence on the PV panel temperature and thus on PV power output.

This chapter is based on the publication:
E. van der Roest, J. G. W. F. Voeten, D. G. Cirkel, "Increasing Solar Panel output with Blue-Green Roofs in Water-Circular and Nature Inclusive Urban Development", Building & Environment, vol. 244, p.110704, May 2023, https://doi.org/10.1016/j.buildenv.2023.110704.

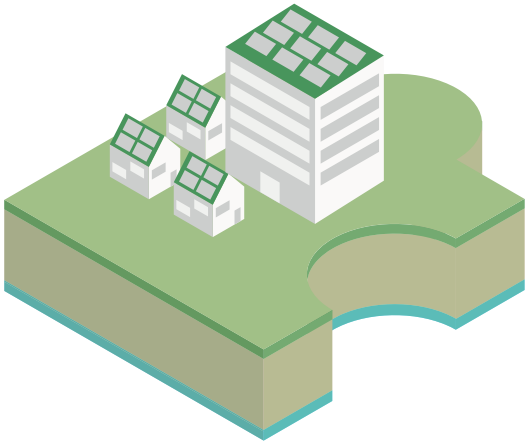

6.1 Introduction

Expectations of multifunctionality and functional-layered urban design are rising. Urban environments need to reduce air pollution, adapt to climate change-induced drought, flooding and heat stress, and play a key role in the energy transition. At the same time, urban space is often scarce, and choices have to be made on how to utilize space effectively. Roofs are in general seen as an ideal location for local renewable energy production and on new buildings, PV panels are becoming indispensable to meet energy performance requirements. At the same time, greening roofs is seen as a promising solution for urban heat island mitigation, and stormwater runoff reduction [221], [307] as well as reducing energy consumption for cooling, noise- and air pollution, while enhancing biodiversity [308], [309]. Would this mean that we have to choose between energy production or the beneficial effects of vegetated roofs?

It is well known that the performance of PV modules decreases with increasing temperature, with a temperature coefficient of 0.2-0.4%/°C depending on the type of solar cell [310]. There is a clear correlation found between the average daily air temperature under the PV module and the temperature of PV modules [311], [312]. Over the last few years, it has been shown that green roofs and PV are not necessarily in conflict over the same space, but can be combined on the same surface with possible positive effects for the energy production of solar panels.

Green roofs namely have transpiring plants cool the air in their surroundings by shifting the distribution of energy from warming up air (sensible heat, H in J m^{-2}) to using energy for the evaporation of water (latent heat, LE in J m^{-2}). If water is abundantly available LE on green roofs can become as high as 95% of net incoming radiation, Rn (J m^{-2}) on a long-term annual basis [221]. On a green roof, the evapotranspiration of the plants can thus lead to cooling of the air under the panels, which in turn positively affects the PV efficiency [313], [314]. As mentioned, water availability is crucial for evapotranspiration. When water becomes scarce, rooftop plants stop transpiring and the ratio H / LE can change from below 0.1 to more than 10 [221] resulting in strong heating of air. In this respect, so-called blue-green roofs are an interesting option. These roof systems capture and store rainwater under the vegetation layer, reducing stormwater runoff and provide the vegetation with water, ideally through sub-surface capillary irrigation, for longer periods of time. It is interesting to note that Schindler et al. (2018) [315] suggested that regular irrigation of green roofs in Mediterranean climates could enhance the power output of PV-green roofs, and El Helow found water stress of the plants in Toronto causing them to evaporate less [316]. Osma-Pinto & Ordóñez-Plata [317] state that a green roof will only give a thermal benefit as long as it has a satisfactory moisture level (in tropical climates).

Although still limited, the number of studies on the effect of green roofs on energy production of solar panels is increasing and the results so far are summarized in Table 6.1. The available studies show a positive effect of green roofs on PV performance with between 0.5-6% increase in power output. Yet, many studies have a small set-up [313], [315], [317]–[319] of only one or a few panels. Moreover, the set-ups of PV systems on green and bitumen roofs are often not comparable in height [315], [317], [320], [321], although the height is indicated as a factor that influences solar

panel performance [322], [323]. Therefore, there is a need for more large-scale systematic research on green roofs with PV systems whereby the height of the panels above the roof is comparable between set-ups [322], [323]. Also, the application of a blue-green roof could lead to continuous evapotranspiration of the vegetation during dry (and warm) periods and thus positively affect the PV panel efficiency. Thus, our research question is:

Is there an increased performance of solar PV above a capillary irrigated, blue-green roof vs a bitumen roof in a temperate maritime climate?

To answer this question, research is performed on two identical rental apartment buildings in Amsterdam (The Netherlands), providing a unique setting for a large scale field study. The novel system set-up combines a blue-green roof with PV, and has additional water supply by transforming grey water from showers to irrigation water with a shallow rooftop version of a horizontal flow constructed wetland, a so-called constructed wetroof [324]. This way a local source of irrigation water is available for the vegetated roof, even during dry spells, reducing the sewer loading and the use of drinking water for irrigation. This way we opt to demonstrate the win-win-win situation for future buildings, contributing to energy production, local water reuse, reduction of urban drought and increasing biodiversity while reducing heat stress and flooding as a result of heavy rainfall.

(Table 6.1 is presented on p.202-203)

Table 6.1 Literature overview of studies focusing on green roofs with PV.

Study	Measured parameters	Location	Measurement design	Minimum panel height above the roof	Angle	Measurement duration/period	Increase in PV power output
Köhler et al. (2007)[320]	PV power output, infrared temperature measurements	Berlin, Germany	Many different designs.	Green: 50cm Bitumen: 0 cm	8-30°	5 years	6% for panels above green roof compared to bitumen.
Perez et al. (2012)[318]	Internal building temperature, near surface roof temperature, back-of-module temperature, PV power production	New York City, USA	Very small setup with miniature 'houses' (about 0.5 m high).	Unknown	45°	8 months (May-January)	2.42% for PV above a green roof vs. a gravel roof
Nagengast et al. (2013)[321]	Panel temperature on panel, PV output. Solar irradiance, measured parallel to the PV panel. Weather station on the roof with wind speed, direction, solar radiation, rain, ambient temperature	Pittsburg, USA	Large roof with different solar setups. 60 PV panels on moss green roof, 90 PV panels on black roof.	Black roof: 13 cm Green roof: 51 cm	15°	One year	Max. 0.5%
Chemisana & Lamnatou (2014)[319]	Module temperature on panel, on the surface beneath the panel, in the surface and the air above panel, PV output.	Lleida, Spain	Tiny panels (36.5 x 19.5 cm) in wooden trays (0.9 x 1.30 m^2) on a gravel roof with Sedum and Gazania.	2 cm (because of very small panels).	33°	2 months (June-July)	1.29-3.33% increase in maximum power output on a green vs gravel roof.
Ogaili (2015) [323]	Temperature of back surface of panel, heat flux, air temperature, and windspeed under panel, surface temperature, DC voltage, DC current, AC power.	Portland, USA	Roof with PV rack with 0.3 m distance between panels, both with white, black and green (Dianthus) surface. Sensors were placed at two panels at the same time and conditions (surface/height) were changed over time	18cm and 24 cm above roof surface	30°	At least 3 sunny days per condition, experiments lasted from July to September.	At 18cm: 1.2% PV-green roof vs black roof, 0.8% more above a PV-green roof vs white roof. At 24 cm: 1.0% PV-green roof vs. black roof, 0.7% for a PV-green roof vs. white roof.

Alshayeb & Chang (2018) [311]	Under panel air temperature, roof surface temperature, relative humidity, PV panel temperature, PV output. Weatherstation; wind speed + direction, solar radiation, ambient temperature, relative humidity.	Kansas, USA	9 panels with black roof surface, 9 panels with green roof (sedum) surface.	20 cm	10°	One year	3.3 – 5.3 % extra PV power output with warm weather. Year round 1.4%.
Osma et al. (2016) [325]	PV output	Bucaramanga, Colombia	3 panels installed on a green (sedum, 7 cm substrate) roof, vegetation could be removed under a panel to obtain a black surface (black)	50 cm and 75cm m above the roof surface	10°	3 weeks	Lower height increases PV output by 2%, a green roof increases the PV output by ca 1%.
El Helow (2017) [326]	Temperature of back surface of panel, PV output, biomass data, ambient temperature	Toronto, Canada	40 panels on a white roof, in four rows with green beds (grasses and wildflower species) underneath at different heights.	61cm and 122 cm above the roof surface	-	About 7 weeks	Larger height increases cooling effect. More biomass growth (18%) with higher distance. WR vs GR – 1.1% higher on GR. GR 122 cm 2.2% higher output than at 61 cm.
Osma-Pinto & Ordonez-plata (2019)[317]	Solar irradiation, air temperature, air velocity, DC, AC power	Buramanga, Colombia	Green and black plots constructed on one roof.	25/50/75/100 cm Vegetation decreases space between panel/ surface with ca. 20 cm	10°		1-1.3%
Schindler et al. (2018) [315]	Substrate temperature, air temperature in front of the panel and at under the panel, panel temperature, PV output.	Haifa,Israel	Experimental plots on 4 x 3.8 m wooden frames.	Black: 50 cm Green: 30 cm	20°	18 months	No difference measured

6.2 Material and methods

6.2.1 General experimental setup

PV panels were placed on the rooftops of two identical six-story, 34.4 m high apartment buildings in Amsterdam (latitude 52.35°N, longitude 4.84°E). One building was equipped with a blue-green roof (BGR) and the other with standard bitumen roofing (BiR) (Figure 6.1). The climate of the research site is temperate maritime, with an average maximum day temperature of 22.5 °C in July, average global radiation of 393 MJ $cm^{-2}yr^{-1}$, average precipitation of 880 mm yr^{-1} and an average Makkink reference crop evapotranspiration [327] of 627 mm yr^{-1} (period 1992 until 2022, from weather station Schiphol, located 7 km from the research site). On the roof of the western building, we installed a blue-green roof equipped with a Permavoid 85s rainwater retention and capillary irrigation system [328] and a substrate layer of 6 cm. The rainwater storage level in the Permavoid units was set to 60 mm. An added advantage of the full field surface capillary irrigation system is the fact that water availability for plants underneath and in between the rows of panels is equal. The constructed wetroof [324] was integrated into a waterproof-lined section (ca 30 m^2) of the substrate layer in the blue-green roof, to receive and treat grey water (shower only), coming from a collection, pre-treatment and pump tank in the basement of the building, with an overflow of the treated water into the Permavoid rainwater retention units underneath the substrate layer. The initial vegetation consisted of sedum mix blankets from the company Sempergreen. After placement of the sedum mix blankets, 26 plant species native to the Netherlands were sown on the blankets.

The installed Jinko 405 Wp PV panels (see Table 6.2 for specifications) are facing south (180°) and are fixed at a 20° angle and have a size of 1.03 x 1.86 m in landscape position. The total system capacity on each roof is 23.78 kWp (62 panels per roof) of which 6 panels per roof were chosen for more detailed monitoring (see Figure 6.2 and next section). The panels for detailed monitoring were chosen such that the panels on the blue-green and bitumen roofs are as close together as possible, yet the panels closest to the roof edge are excluded from the study as they will be influenced more by i.e. wind effects and less by vegetation. A sunlight study (Figure 6.2) has shown that due to adjacent tall buildings, the eastern roof (the black roof) receives quite a lot of shade in the morning hours in spring and autumn. In summer the effect is less pronounced, and in winter shade has a similar impact on both buildings. To be able to correct for shade effects, we installed a pyranometer on both roofs (see next section).

The lower side of the panels were positioned 32 cm above the surface, being either the soil surface or the rooftop surface on both roofs (see Figure 6.3). Rows are spaced at 73 cm between the high end of a panel in one row and the low end of the panel in the next row. The reduction in electric efficiency due to the warming up of the panels compared to the efficiency at standard test conditions can be calculated as follows:

$$\eta_{\mathrm{mp}} = \eta_{\mathrm{mp,STC}}\left[1 + \alpha_{\mathrm{P}}\left(T_{\mathrm{p}} - T_{\mathrm{p,STC}}\right)\right] \tag{6.1}$$

With η_{mp} (%) the efficiency of the solar cell, $\eta_{\mathrm{mp,STC}}$ the efficiency (%) at standard test conditions (STC), α_{P} the temperature coefficient of power (Pmax) in %/°C, T_p the panel temperature and $T_{p,STC}$ the cell temperature at standard test conditions (25°C). Characteristic values for $\eta_{\mathrm{mp,STC}}$ and α_{P} are given in Table 6.2.

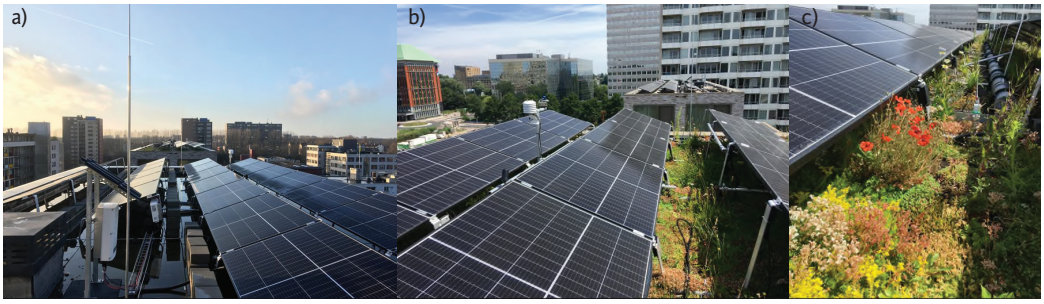

Figure 6.1 Overview of (a) the BiR, (b) the BGR (c) the blooming BGR with the integrated constructed wetroof in the background (grey PVC water inlet distribution pipe).

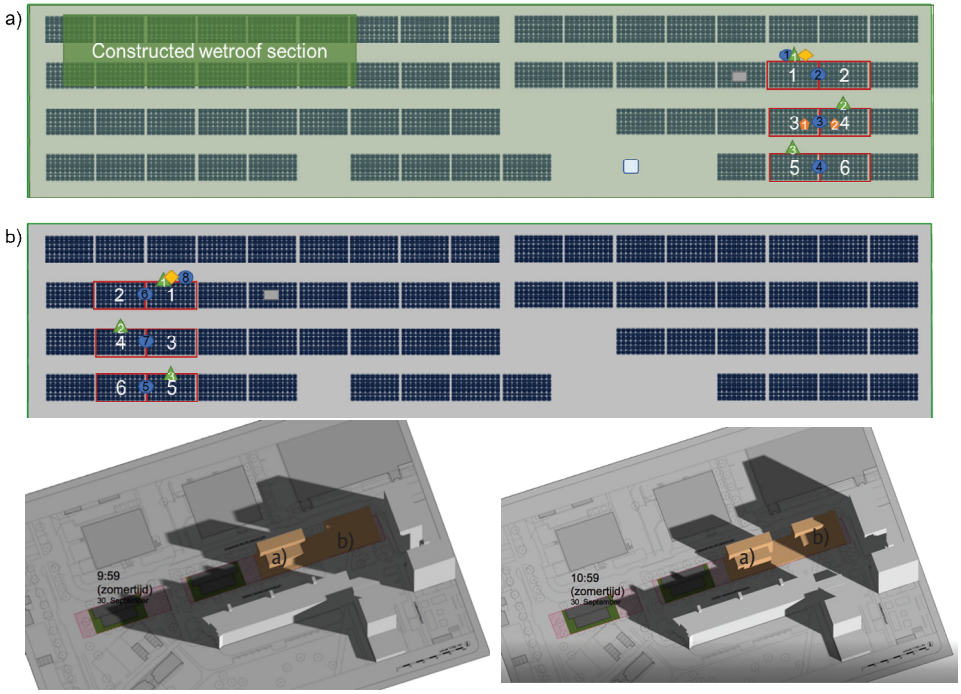

Figure 6.2 Schematic overview of the chosen panels for monitoring on the western blue- green roof (a), and the eastern bitumen roof (b). The panels for detailed monitoring are chosen in such a way that the differences in shading are kept to a minimum. The symbols represent sensors and are explained in Figure 6.3 The shade situation is given for 30 September 9:59 (bitumen roof is still in the shade) and 10:59 (half of the bitumen roof is in the sun).

Table 6.2 PV panel characteristics of the Jinko Solar 405Wp panels.

Panel characteristic	Unit	Value
Maximum Power Output at STC	W	385
Module efficiency ($\eta_{mp,STC}$)	%	20.17
Nominal Operating Cell Temperature (NOCT)	°C	45 ±2
Temperature coefficient of P_{max} (α_P)	%/°C	-0.35
Temperature coefficient of Voc	%/°C	-0.28
Temperature coefficient of Isc	%/°C	-0.048

6.2.2 Data acquisition

On each roof, a section of six panels was equipped with sensors to measure incoming short wave radiation Rs (J m^{-2}), ambient air temperature T_{amb} (°C), air temperature below the PV panels T_a (°C), relative humidity RH (%), surface temperature T_S (°C), substrate temperature T_{sub} (°C) and back of panel temperature T_p (°C) (Figure 6.3 & Table 6.3). Precipitation P (mm) was measured with a rain gauge (ARG314, EML Ltd.) on the blue-green roof. Incoming shortwave radiation (R_s) was measured at 1.25 cm above the roof surface using pyranometers (CS320, Campbell Scientific Inc.). Air temperature (T_{amb} &T_a) and relative humidity (RH) were measured using a combined element (HygroVUE5, Campbell Scientific Inc.) placed in a radiation shield next to the pyranometer and below each pair of solar panels at a height of 25 cm. The surface temperature (T_s) of the vegetation and bitumen was measured, in the shade, below three panels on each roof using infrared radiometers (SI-431-SS, Apogee Instruments). The substrate temperature (T_{sub}) was measured at two locations below the panels on the blue-green roof using a temperature sensor string (CS225, Campbell Scientific Inc.). PV panel temperature (T_p) was measured at the back of each of the six panels on each roof using back-of-module temperature sensors (CS241, Campbell Scientific Inc.). Measurements were collected at 10 min intervals, aggregated to hourly values, and logged on a datalogger (CR380, Campbell Scientific Inc.). Wind data was obtained from the nearby Schiphol weather station. Besides the detailed measurements the energy output of each panel on the two roofs is logged on an hourly basis. The PV panels are installed with microinverters to avoid string effects, enabling us to measure PV output of each panel at hourly intervals via the SolarEdge data platform.

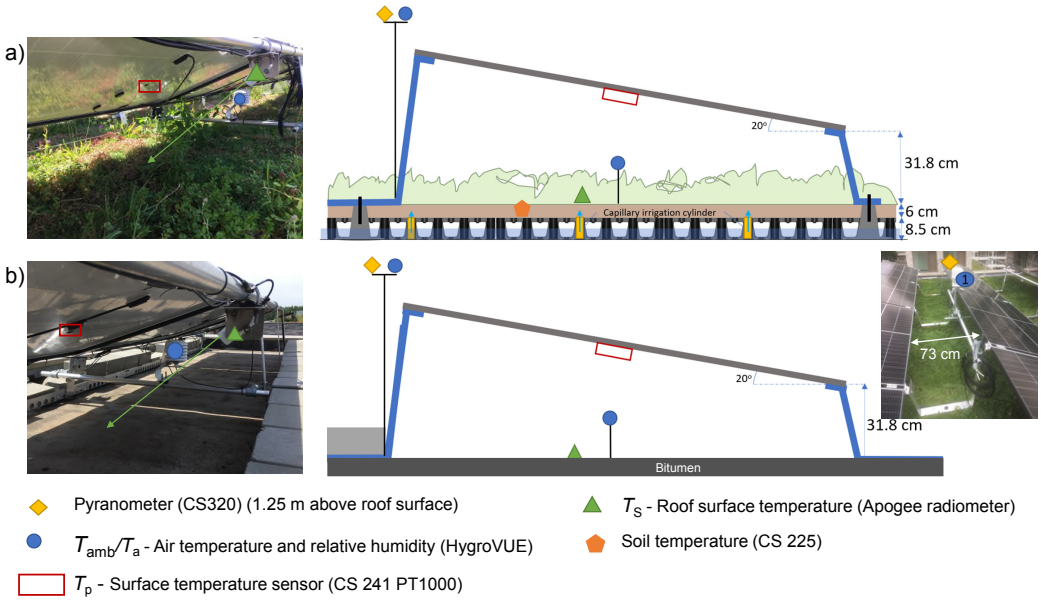

Figure 6.3 Overview of sensor types and locations on both roofs. The Apogee sensor is pointed towards the roof surface and thus measures the roof surface temperature below the panels.

Table 6.3 Overview of sensor type, characteristics and location.

Sensor	Accuracy	Operating temperature	Amount	Location
HygroVUE5 air temperature and relative humidity (RH)	± 0.3-0.4°C ± 1.8-3% (RH)	-40°C to 70°C	3 per roof/ 1 per roof	Under panel/ 1.25m above panel
CS320 pyranometer	± 2.6%	-50°C to 60°C	1 per roof	1.25m above panel
Apogee radiometer SI-431-SS	± 0.2°C	-30°C to 65°C	3 per roof	Mounted in the middle of the panel
CS 241 PT1000	±(0.15 + 0.002t)°C	-40°C to 150°C	6 per roof	Placed on the back side of the panel (in the middle)
ARG314 Raingauge	99% up to 120 mm/hr	+1°C to 70°C	1 (on blue-green roof)	Open location on the roof
CS225 Temperature sensor	± 0.2°C	-55°C to 85°C	2 (on blue-green roof)	In soil under panel (3 cm depth)

6.2.3 Data analysis methods

The presented data are from the measurement period of June up until October 2022. We have only used daytime values (Irradiation > 4 Wm^{-2}) and removed outliers of PV output. If the average energy output of 6 measured panels was higher than their maximum capacity (385 Wh) or the energy production was very low (< 3 Wh) while the irradiation was > 100 Wm^{-2}, the data were not considered.

On this combined dataset of sensor data and PV output, different methods were applied. First, we calculated the differences in PV output for both roofs, whereby the data were divided into bins of both temperatures (per 5°C) as well as irradiation (per 100 Wm^{-2}). Secondly, we performed a linear regression analysis (OLS method) on the daytime dataset for both roofs, to find a relationship between irradiance and solar PV output, with the intercept at 0 (at zero irradiation, there will be no PV output).

Thirdly a multilinear regression analysis was performed on the combined day-time dataset of both roofs. In the combined dataset, all measurements from both roofs were merged, whereby roof type was added as a parameter (integer, BGR=1, BiR=0). A correlation table was obtained for the correlation values between PV performance and roof type, irradiation, relative humidity, PV back panel temperature T_p, roof surface temperature T_S, air temperature under PV panel T_a , the ambient air temperature above the roof (1.25 m) T_{amb}, and wind (nearby Schiphol weather station).

6.2.4 Calculation of sensible heat flux densities

The sensible heat flux QH (Wm^{-2}) is proportional to the difference between surface temperature and air temperature measured at a certain level times a convective heat transfer coefficient [329]. QH was calculated according to:

$$Q_H = h_c \cdot (T_S - T_a) \tag{6.2}$$

With h_c the convective heat transfer coefficient ($Wm^{-2}K^{-1}$). h_c can be approximated using the empirical Jürges formula which is used in urban canopy models [329]–[331]:

$$h_c = 5.9 + 4.1v \cdot \left(\frac{511 + 294}{511 + T_a}\right) \tag{6.3}$$

With v the wind velocity (ms^{-1}). Given the complexity of urban surfaces, it is questionable whether the application of an empirical heat transfer coefficient will provide exact values for QH. Xu & Asawa [331] mention an uncertainty of ±15-20% associated with the use of Jürges formula. Calculated values are, however, valuable for comparison between the two roofs and to other applications.

6.3 Results & Discussion

6.3.1 PV performance

To assess the effect of roof type on PV performance, we present the average difference in PV power output and categorized the data based on both ambient temperature and solar irradiance. Due to the differences in shade on both roofs, we have chosen to not compare the roofs at similar moments in time, but at similar irradiance. This was possible because we have placed two irradiance sensors at both measurement locations.

Overall, the BGR is constantly performing better than the BiR in all solar irradiance categories (see Table 6.4). The absolute difference is increasing as well, which is expected as the absolute solar output also increases with higher irradiance. A similar trend is seen for all temperature categories, although there is a significant outlier at the 5-10 °C/100-200 Wm^{-2} category (with only 1.2% of the data). The data thus suggest that for temperatures above 10°C, regardless of the amount of irradiation, the PV system on the BGR produces more power than the BiR.

Table 6.4 Average difference in solar PV output of 6 panels on each roof presented as solar output BGR– solar output BiR in kW (kWh/hr) is shown. The data are categorized according to solar irradiance and ambient temperature. Table layout inspired by Nagengast et al. (2013) [321].

Solar Irradiance (Wm^{-2}) - Irr	Ambient temperature (°C) - T_{amb}										Weighted average BGR – BiR per panel (kW)	% of data
	< -5	-5 - 0	0 - 5	5 - 10	10 -15	15 -20	20 -25	25-30	30- 35	>35		
0-100				0.2	2.0	0.1	-0.7	-1.0			0.6	23.9
100-200				-6.3[a]	4.8	3.3	-0.8	-1.0			1.7	16.7
200-300					8.9	2.0	1.3	0.9	7.3a	-4.7[a]	2.5	14.0
300-400					14.5	4.8	6.8	-4.1	4.7a	-1.8[a]	5.2	11.9
400-500					-1.8	9.4	3.8	17.2	19.6[a]		3.1	11.1
500-600					6.7[a]	-0.7	11.2	6.4	15.1	10.4[a]	6.1	7.7
600-700					4.8[a]	16.7	9.8	2.1	19.0	5.6[a]	6.1	7.6
700-800						13.2	13.0	16.3	12.3[a]	-3.5[a]	9.8	4.9
800-900						19.0[a]	14.2	10.0			9.0	2.1
900-1000						8.1[a]					4.1[a]	0.1
>1000												
Weighted average BGR – BiR (kW)	0	0.0	0.0	-1.1	4.6	5.5	6.0	5.6	13.6	1.2		
% of Data	0	0.0	0.0	1.2	16.7	49.4	24.4	6.8	1.2	0.2		

[a] Value is based on 1-3 datapoints

To quantify this effect further, we have done a linear regression analysis with all daytime data for both roofs with irradiation versus PV output. The 95% confidence interval is shown in Figure 6.4, and the confidence intervals of both regression lines do not overlap, which means the difference in PV output between the two roofs is significant. Based on the regression values (see Table 6.5), the BGR roof would on average produce 4.4% more electrical energy at similar irradiance.

This result is on the higher side of the range based on available studies (see Table 6.1), for which we discuss two possible explanations. Firstly, different studies [322], [323] pointed out that differences in enhanced solar panel performance between studies are influenced by the height of the panels above the roof. The higher the panels are placed, the larger the cooling effect of the airflow is. This could have influenced the almost insignificant results of Nagengast et al. [321] who conclude that only if the temperature is > 25 °C/irradiance > 800 Wm^{-2} a green roof would make a difference on PV panel output, otherwise it would not. However, the height of the panels above the green

roof was 53 cm, and for the black roof 13 cm, so this could explain the small difference. The study of Alshayeb & Chang [311] could have been influenced by the different heights as well. Here, the sedum is placed under already installed panels which results in less height between the surface and panel on a green roof than with a black surface. The same seems to be true for Schindler et al. [315], although the windy climate could have influenced the results here as well, combined with the low evaporation of plants on the green roof. Our study is one of the few studies with a long-term large-scale set-up that paid attention to comparable heights between PV systems on both roof types. Secondly, our BGR has a continuous water supply, thus evapotranspiration doesn't decline during dry and warm periods, as in other studies [315]. An inconvenience of our setup was the difference in shadow effects between the BGR and BiR. Therefore, the BGR is longer exposed to sunlight than the BiR, so even at similar irradiation, the BGR is already receiving sunlight for a longer period and thus the solar panels could already have warmed up a bit, this could have influenced our results. That means that our results could be on the conservative side, so with similar shadow effects, the BGR could possibly perform even better than measured here.

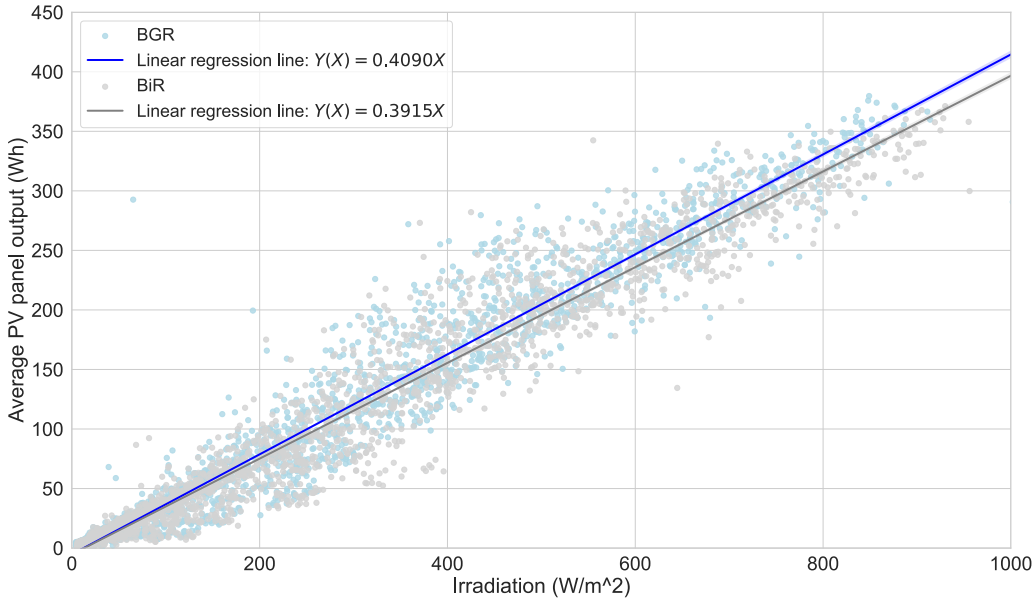

Figure 6.4 Linear regression results including a 95% confidence interval for the average PV panel output versus irradiation in Wm^{-2} for both the BiR) and BiR based on all hourly daytime data, outliers removed.

Table 6.5 Linear regression results (OLS method) for irradiation vs PV panel output for both roof types.

	Number of observations	Coefficient (irradiation/ PV panel output)	t-statistic	P-value	R^2
BiR	2048	0.3915	291.7	0.000	0.977
BGR	2048	0.4090	294.1	0.000	0.977

6.3.2 Multi-regression analysis

We have performed a multi-linear regression analysis on the combined dataset of the two roofs to determine if the roof type has a significant effect on the PV panel output, roof type was added to the dataset as a parameter (BGR = 1, BiR = 0).

First, the correlation coefficients of all measured parameters were analyzed (Table 6.6) to check which parameters influence each other. The roof type has only a small negative correlation with T_S, meaning that the BGR tends to result in a lower roof surface temperature. On the other parameters, no effect is visible, which means as well that there is no risk of multicollinearity with other parameters. Moreover, we see that T_S and T_{amb} are highly correlated and thus shouldn't both be included in the multilinear regression equation. The same line of reasoning is valid for the T_S and T_p, and for T_{amb} and T_p. Therefore, we have chosen to include the air temperature T_{amb}, and not T_S and T_p in the regression analysis. Furthermore, irradiance (Irr) was included as we know it highly affects PV output. To assess the effect of roof type, two analyses were done.

First, we have taken only the irradiation and air temperature into account and evaluated how these two parameters explain the variance PV power output. With an $R^2 = 0.943$ the coefficients were significant ($P < 0.05$) at a 95% confidence interval (Table 6.7). Secondly, we have added the roof type as a factor in the regression analysis. The roof type proves to be significant as well ($P < 0.05$) and the R^2 for the combined analysis of irradiation, solar panel temperature and roof type was 0.944 (Table 6.8). Thus, the roof type proves to be a significant factor, although it does not explain the variance in the data significantly more than without the roof type included as a factor.

Table 6.6 Correlation coefficients for roof type (here interpreted as BG=1) , air temperature above the roof (Tair), irradiation (Irr), relative humidity (RH), PV panel back temperature (T_p), roof surface temperature under the panel (T_s) and air temperature under a PV panel ($T_{a,p}$) for the combined dataset of the two roofs (day values).

	Roof type	T_{amb}	Irr	RH	T_p	T_S	T_a
Roof type (1 is BG, 0 is BiR)	1						
Tair	-0.02	1					
Irr	-0.03	0.47	1				
RH	0.02	-0.74	-0.65	1			
T_p	-0.02	0.79	0.87	-0.78	1		
T_S	-0.21	0.90	0.61	-0.76	0.87	1	
T_a	-0.03	0.99	0.53	-0.76	0.84	0.93	1

Table 6.7 Multi-regression analysis results for PV panel output variance explained by air temperature and irradiation.

	Coefficient	Standard Deviation	t-statistic	P-value
Intercept	4.86	1.665	2.93	0.003
Irr	0.415	0.002	237	0.000
Tair	-0.599	0.096	-6.25	0.000
R^2		0.943		
No. of observations		4210		

Table 6.8 Multi-regression analysis results for PV panel output variance explained by air temperature, irradiation and roof type.

	Coefficient	Standard Deviation	t-statistic	P-value
Intercept	1.943	1.69	1.15	0.25
Irr	0.415	0.002	237	0.000
Tair	-0.598	0.095	-6.27	0.000
Roof type	5.50	0.74	7.44	0.000
R^2		0.944		
No. of observations		4210		

6.3.3 Differences in surface temperature T_S, Air temperature below panels T_a and back of panel temperature T_p

The daytime roof surface temperature T_S measured underneath the PV panels was lower on the BGR compared to the BiR. ΔT_S (BiR – BGR) increases with higher irradiation and can become as high as 12 °C on a clear summer day (Figure 6.5). Mean daytime T_S were lower on the blue-green roof with a statistically significant difference of 2.39 °C. Although less pronounced, the BiR indicates a measurable, positive effect on the daytime near-roof air temperature T_a measured below the PV panels. During the measurement period, T_a was on average 0.19 °C higher on the BiR, this difference was however statistically non-significant. A maximum ΔT_a of 2.63 °C was reached on August 14 2022 at 14:00 PM. Mean T_p was almost equal on the BiR and BGR (mean ΔT_p = -0.05). There were several periods where positive ΔT_p's were measured, reaching a maximum ΔT_p of 6.63 °C on September 2 2022.

However, as is also visible in Figure 6.5, there are negative spikes in the ΔT_S, ΔT_a and especially ΔT_p data, indicating a higher T_p on the BGR compared to the BiR. This is caused by shade from a nearby tall building on the BiR in the morning before 11 am (Figure 6.2). Even with the sun at its highest azimuth (around the 21st of June) we still see these shadow effects causing discrepancies in the amount of irradiance on both roofs, resulting in lower temperatures on the BiR. Besides these shade effects, there are also periods with negative ΔT_p, ΔT_a (Figure 6.5) and sometimes even negative ΔT_S. So, although the mean surface temperature of the BGR is significantly cooler than the BiR and we saw in Figure 6.5 that there seemed to be a smaller but similar effect on ΔT_a as well as ΔT_p, there are also periods where temperatures measured at the BiR are lower than at the BGR.

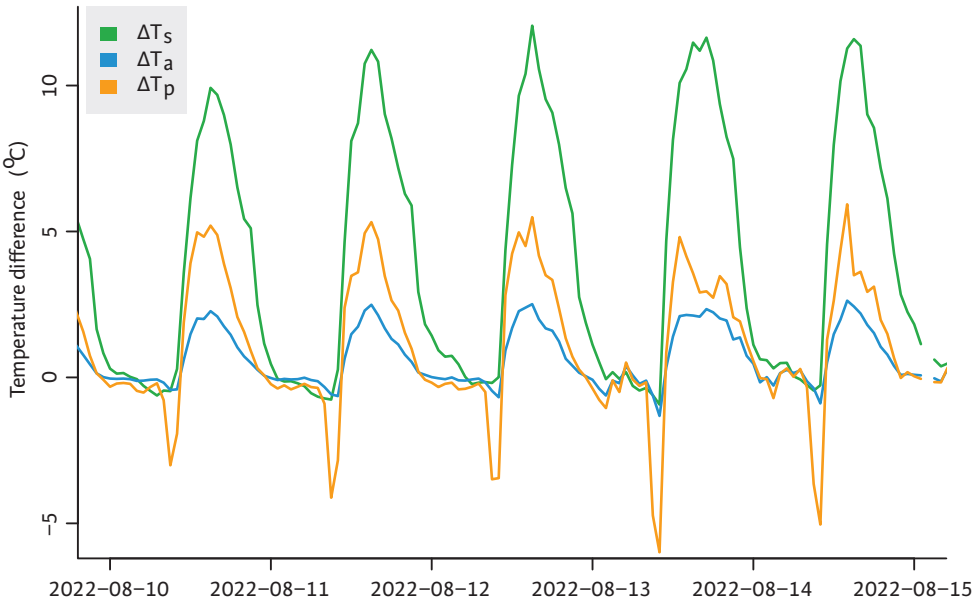

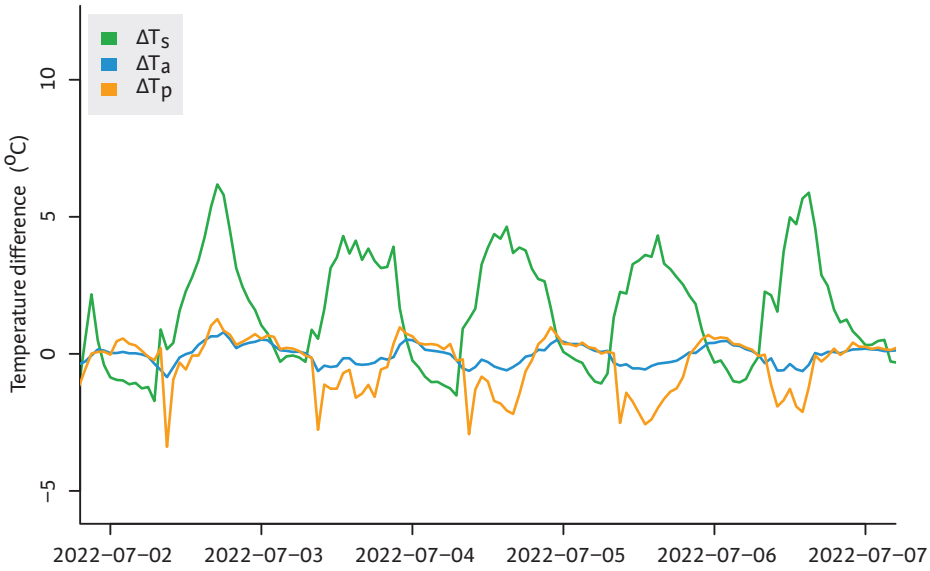

Figure 6.5 Hourly differences in temperature (ΔT_s, ΔT_a and ΔT_p) between the BiR and the BGR during the periods 10-15 August and 2-7 July. A positive value means that the temperature measured at the bitumen roof is higher than at the blue-green roof.

6.3.4 Differences in estimated sensible heat flux

Sensible heat flux estimates QH, below the PV panels, were higher at the BiR compared to the BGR with a significant mean difference of 52.5 Wm^{-2}. During our measuring period estimated QH at the BGR stayed below 60.0 Wm^{-2} and were often very small, or even negative during daytime (Figure 6.6). At the BiR estimated QH was much higher with a mean value of 50.2 Wm^{-2} and peaks reaching 291.1 Wm^{-2}. Negative sensible heat flux estimates point to a so-called oasis effect, where energy is transferred from the surrounding air to the plants and used for evapotranspiration. The observed negative daytime QH estimates on the BGR coincide with cooler T_a and T_p on the BGR (Figure 6.5). Note that above QH estimates are based on temperature measurements in the shade of PV panels, resulting in relatively low sensible heat flux densities. In literature values for QH reaching up to 280 and 750 Wm^{-2} were found for respectively green and bitumen roofs without the shade of PV panels in a similar climatic setting [329].

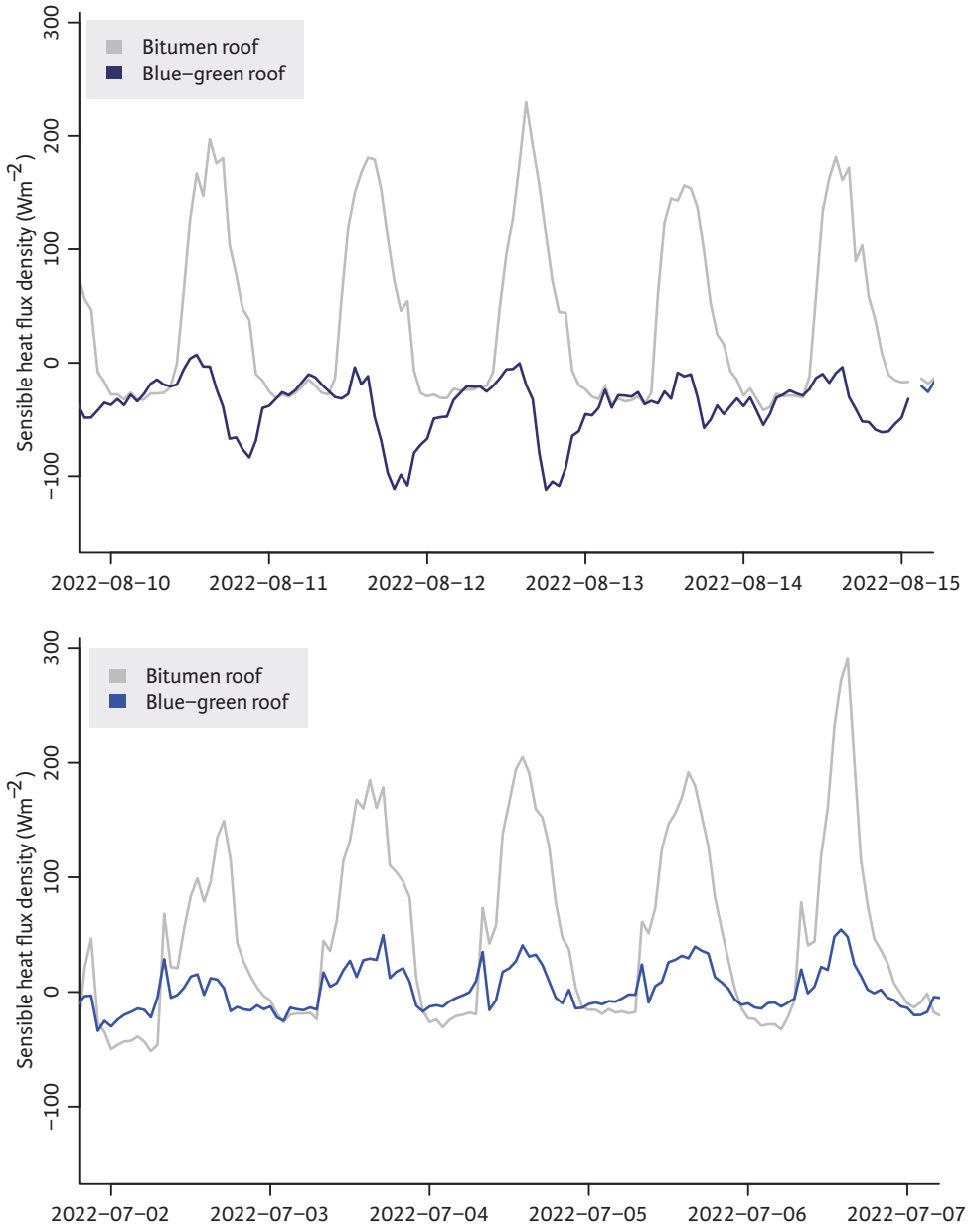

Figure 6.6 Estimated sensible heat flux densities QH on both roofs for two periods: 10-15 August and 2-7 July.

6.3.5 Nonlinear relation between T_s, T_a and T_p

From earlier studies, we know that a clear temperature effect of green-solar roofs [311], [313] versus bitumen roofs is expected. There are several explanations for our more ambiguous results. On the BGR energy is stored in the substrate and water storage layer, buffering temperature fluctuations at the surface. As a result, the cooling rate of the bitumen roof is higher over the course of the night resulting in lower nocturnal T_S than the green roof [329]. Note that in our setup T_S is measured in the shade of the solar panels on both roofs, which delays the warming effect of irradiation in the morning. Another explanation can be found in rainfall. After rainfall events, not all rainfall is drained from the BiR immediately and the roof surface stays wet for several hours or even days until the remaining water is evaporated, cooling down the BiR surface during that proces. Wind effects can also play a role, mainly in the sense that the cooling effect of wind can overrule the effects of roof temperature. For example, Osma-Pinto & Ordóñez-Plata [317] conclude that the air velocity is more influential than the roof type, at least in warm and tropical climates. Lastly, positive effects of the BGR besides the roof temperature could be the difference in albedo between both roofs [332].

Additional analysis was done to further understand the temperature effects. We found that there is a significant positive non-linear relationship between ΔT_s and ΔT_a (R^2: 0.69) and between ΔT_s and ΔT_p (R^2: 0.43) (Figure 6.7). Fitting segmented linear regression models [333] on the data results in two linear sections with different slopes for each relation with an estimated significant breakpoint at ΔT_s = 4.64 °C (st err. 0.14 and 0.31). Below this temperature difference there is almost no measurable relation between ΔT_s and ΔT_a or ΔT_p. The cooling effect of the BGR thus has to result in an at least 4.64°C lower surface temperature compared to the BiR, before an effect on ΔT_a and T_p becomes measurable.

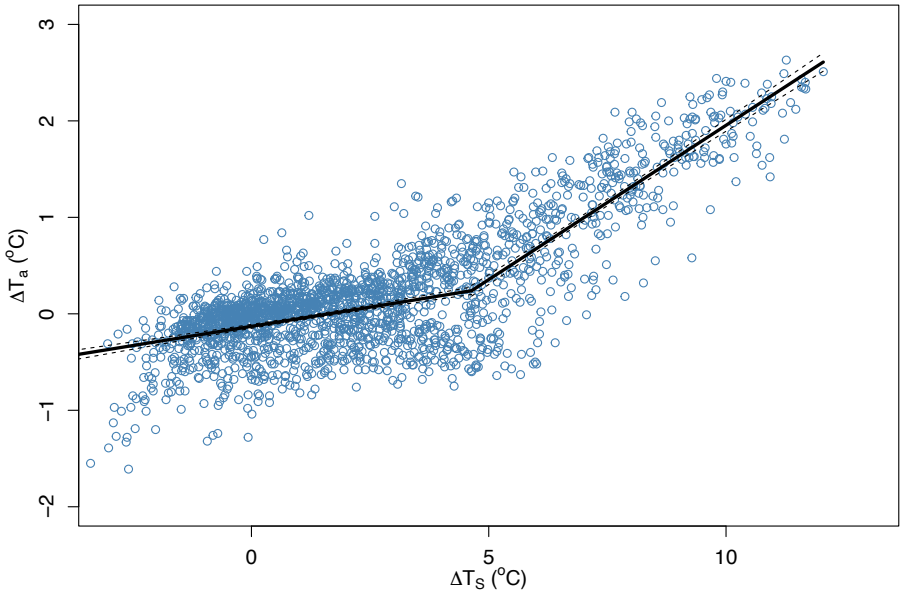

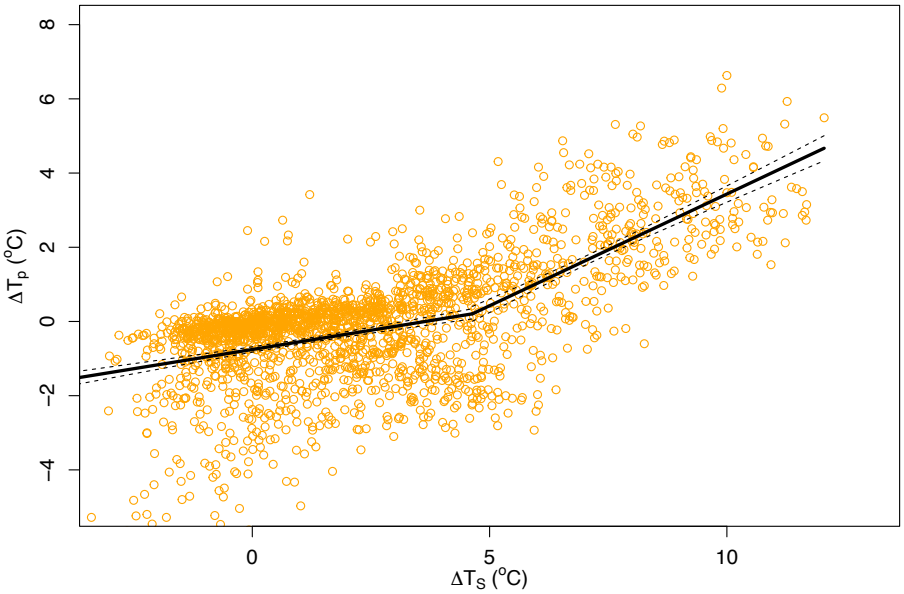

Figure 6.7 Relation between ΔT_s and ΔT_a and ΔT_s and ΔT_p and fitted segmented linear regression lines with 95% confidence intervals.

6.3.6 Vegetation-PV interaction

From the literature we know there is also an effect of PV on the vegetation; PV systems on green roofs lead to lower evapotranspiration due to the shade effect of the PV panels [334]. In warm climates, the shading of the PV panels can even lead to faster growth of vegetation and 50% lower pigment levels [317]. The type of plant chosen also affects the power output performance [322]. During our measurements, relatively low sedum species still dominated the vegetation, but (taller) native herbs started to slowly overtake the vegetation and gradients in plant growth became visible between shaded and sunny areas (Figure 6.8). Below the panels, plants remained relatively low. In the sunny paths between the panel rows plant growth was more abundant. If succession proceeds to a grass/herbs-dominated vegetation with taller plants, this might also affect air circulation underneath the PV panels. As we discussed in the previous section air velocity can be an important factor in cooling PV panels [317]. Taller vegetation might therefore result in a less positive effect on PV output than observed during our measurement period.

Figure 6.8 Impression of the vegetation in between the PV panels (sunnier area) and under the PV panels (shaded area).

6.3.7 Grey water system

The grey water system in the building provided a more continuous water supply for the vegetation and therefore prevented drought stress. As a result, transpiration and the cooling effect of the plants can be considered optimal for the meteorological conditions during the measurement period. However, the abundant supply of water comes at a price. Energy is needed to pump the collected shower water from the basement to the roof. We have calculated that the (multi-05) pump which has to overcome 34m of height difference can pump about 1m^3/hour at full capacity (900 W). Depending on if the water supply to the roof is only functioning during spring and summer, or during the whole year, this means that between 65-160 kWh per year is needed for pumping. The expected extra production of the BGR versus the BiR with 62 panels is about 970 kWh/year (405 Wp panels, based on the 4.4% higher power production). Thus, 7-17% of the expected extra power production is needed for the water supply on the roof, which is significant, yet manageable. Moreover, the water supply is not only influencing (indirectly) the solar panel output, but is used for the vegetation on the balconies and lower roofs as well. Overall, the extra solar power output is expected to more than compensate the pump energy, the water system meanwhile is also enhancing other positive effects of the building such as reducing heat stress, increased urban plant coverage, increased biodiversity and better stormwater management [319], [322].

6.3.8 Development of water- and energy-sensitive buildings

Design and construction of the twin buildings, where we performed our research, required a lot of extra effort from all parties involved because of the non-conventional water system in the building and multifunctional use of the rooftops for energy, vegetation and water management. The most important lessons learned are:

- Sustainability goals like water circularity, stormwater management, biodiversity, energy production and improved liveability for the tenants have to be considered and included in the designs from the start of the process because these goals affect architecture, structural design, rooftop waterproofing systems and water- and power infrastructure from the basement all the way up to the roof.

- Where in the past the roof was considered lost space where for example HVAC, ventilation and other technical infrastructure could be placed where convenient, with the multifunctional approach it now becomes important to minimise the amount of space used for this infrastructure and cluster it in limited and specific areas on the roof.

- Normally the roof is the 'final' stage of waterproofing the building, yet to create a multifunctional rooftop landscape, specialists from different fields (ventilation and HVAC, power, water management, landscaping, solar PV) should be involved in design and construction. This requires understanding, extra cooperation and design, and smart building planning between these specialists, to construct the roof in an efficient manner.

- When creating buildings with novel and innovative water management systems, it will take at least one year after construction (covering all seasons) to optimize the systems and get experience in actual required maintenance to be incorporated in the final maintenance manual. Clearly appoint responsibility and budget time and money for these tasks.

6.4 Conclusion

We have investigated the performance of a full-scale solar PV system on a bitumen roof and a blue-green capillary irrigated roof on twin buildings in Amsterdam. Based on a 5-month data collection period (June-October 2022) we see a clear positive effect of the BGR on the PV performance. On average, a solar panel on the BGR is expected to produce 4.4% more energy than a solar panel on the BiR at similar irradiation, in a North-West European climate. The positive effect is seen at air temperatures above 10°C, regardless of irradiation. A clear difference in panel temperature on the roofs is only seen when the surface temperature of the roofs differs by at least 4.64°C. Otherwise, other factors such as wind or albedo have probably more influence on the PV panel temperature and thus on PV power output. Overall, we have shown that a blue-green PV roof creates a win-

win-win situation both for PV production, the local water balance as well as biodiversity. Future research could better investigate wind and albedo effects, different heights of solar panels above the roof and development of the vegetation and the effects of this changing vegetation on PV output.

Data

The dataset of the sensors and PV output of the measured panels on both roofs that was used for this publication can be accessed via:
http://doi.org/10.4121/679c03a2-bcae-46b9-a4f0-91c230708ca5

Acknowledgements

The authors would like to thank Aedes Care BV/Plan 8 Vastgoedontwikkeling BV for facilitating this research by making it possible to perform this full-scale research on their water-sensitive and green building and facilitating the research in all possible ways. We furthermore thank the technical project partners for the fruitful collaboration and technical base underneath the project: Permavoid B.V., ECOFYT, Techniplan Adviseurs BV, and SDR Elektrotechniek BV. We would like to thank Solnet for letting us monitor the solar panels and install sensors on them.

Also, we thank the municipality of Amsterdam for the cooperation on the research concerning the tenants and the outreach/communication. Lastly, Pim Post and Diederik van Hasselt (deceased) are thanked for their help with the statistical analysis.

Funding

This study is a result of the TKI project Urban Photosynthesis and is co-financed with PPS funding from the Topconsortia for Knowledge & Innovation (TKI's) of the Ministry of Economic Affairs and Climate.

7 Concluding remarks and recommendations

"We have such a long way to go", sighed the boy.
"Yes, but look how far we've come", said the horse.

The Boy, the Mole, the Fox and the Horse - Charlie Mckay

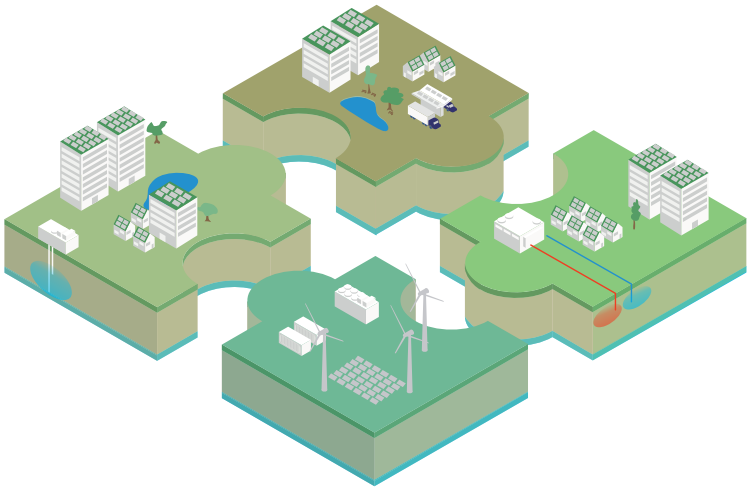

7.1 Research context

The transition from a fossil-based energy system to one that is primarily based on renewable energy sources has significant implications for the energy system. While the cost of renewable energy production is decreasing, the availability of materials may emerge as a limiting factor. Furthermore, the transition necessitates the development of innovative solutions to balance supply and demand in space and time in a hybrid energy system that combines centralized and decentralized energy sources and relies for an important part on electricity production from intermittent resources. In this dissertation, system integration and sector coupling are proposed as a strategy that supports a transition to a reliable, affordable and clean energy system.

Yet, most policies and plans to guide the energy transition are divided in different sectors and there is an expectation to solve challenges within those sectors as well. The climate agreement ('Klimaatakkoord') from the Dutch government is a good example of this sectoral thinking [3]. With the growth of solar and wind parks and increased electrification at end users, limited grid capacity is a particularly acute issue in the Netherlands. During the period in which this dissertation was written, installing new grid connections for both generation and consumption has become difficult or even impossible [335]. In the last four years, various solutions are proposed at both at institutional (different rules for regulators) as well as technical levels:

- Grid reinforcement; expanding the grid, or increasing existing capacity, yet there are limitations on workforce and materials [21].
- Cable pooling; connecting solar and wind capacity to the same cable as they have complementary production profiles [21], [336].
- More flexible contracts (such as a non-firm ATO), grid congestion management, shared connections, and tariff structures [21].
- Batteries for peak shaving and grid balancing next to a solar park [336], or at a combined solar and wind park [337].

Yet, these solutions lack a broader system perspective, while this could help to more effectively solve the problem of grid congestion and the design of a sustainable energy system as a whole. When looking at the energy system of the Netherlands, it is good to realize that historically The Netherlands has an extensive gas infrastructure, and 93% of the households have a connection to the gas grid (in 2020) [338]. This is also reflected in the infrastructure design. The distribution system operators (DSOs) work with average household grid capacities on a neighborhood level to determine the capacity (and amount) of their gas and electricity substations. These average connection capacities are around 30 kW per household for gas connections, yet for electricity the average capacity that grid operators work with is 1.5-3 kW per household [205], thus 10-20 times lower than for gas. From the perspective of infrastructure, it thus seems logical to see how different infrastructures (such as electricity, gas and heat) can be integrated in such a way that grid congestion is solved in a manner that it contributes to a clean, reliable and affordable energy system. From this broader system perspective, some additional examples can be given of developments and ideas that were introduced during the course of this dissertation and can assist in reducing grid congestion:

- Mainly at business parks with offices and small industries, the concept of smart energy hubs or renewable energy communities is investigated whereby (local) electricity, heat and storage in the form of batteries or hydrogen production are shared to reduce grid congestion [21], [339].
- Specifically at wastewater treatment plants, the energy hub concept is receiving more attention as a way to combine local energy production with hydrogen production and the use of both waste heat and oxygen within the wastewater treatment plant [340], [341], leading to a further reduction of energy use and nitrous oxide emissions [342].
- Municipalities in the Netherlands had to prepare a heat transition vision for their cities and chose neighborhoods that will start the transition before 2030. In 62% of these neighborhoods, a district heating grid is considered, whereby innovative solutions such as thermal energy from water (wastewater, drinking water, or surface water) are taken into account [343].
- More research and demonstration projects have been performed such as WarmingUP [344] and HEATSTORE [345] on high-temperature ATES systems, both for district heating networks and greenhouses [346]. HT-ATES systems can directly fulfill heat demand in winter and thus reduce electricity demand peaks and can be combined with power-to-heat in summer to reduce grid congestion.
- New policy supports the installation of hybrid heat pumps, which will from 2026 onwards become the standard when replacing a gas boiler in The Netherlands [347], [348]. In larger Dutch houses, the hybrid heat pump electrifies about 60% of the energy demand, and the gas grid fulfills the winter peak and the production of hot water [349]. This policy supports a quick (partly) decarbonization of heat demand, without too much pressure on the electricity grid.

From these examples, it is clear that system integration, whereby multiple energy carriers, infrastructures and sectors are combined, is an essential part of the solution, which is also recognized on the EU level [23], [339] and recently on the Dutch level as well in the roadmap for energy storage [350]. On the neighborhood scale, the urgency to come up with (integrated) solutions is rising too. Here again, electrification poses challenges to the low voltage grid with the increase of electric vehicles, heat pumps, and decentralized PV production [351], and different directions of solutions could be explored (i.e. batteries, fuel cells, FCEV, power-to-x etc).

In this dissertation, it was studied how locally integrated energy and water systems for neighborhoods can contribute to a balanced and robust energy and water system. The Power-to-H3 concept was proposed as an example of an integrated system that includes different technologies for the production, storage and supply of electricity, heat, hydrogen and water (**Chapter 2**). A techno-economic approach was taken including dynamic simulations to assess the cleanliness, affordability and reliability of the system (**Chapter 3**). **Chapters 4-6** zoomed in on specific aspects of the concept, namely heat (storage), hydrogen and energy and water in buildings, thereby contributing to the four knowledge gaps as defined in the introduction. The main findings are synthesized below in the form of design principles, followed by the contributions to the knowledge gaps and future directions for research. Finally, policy recommendations are given based on practical experience gained during this research.

7.2 Answering the research question – Design Principles

This dissertation aimed to answer the research question:

How can an integrated renewable energy and water system on the urban level be designed in order to provide energy and water in a clean, affordable and reliable way?

It was found that an integrated system design is possible and valuable, as it contributes to a clean, affordable and reliable energy and water system for a neighborhood. Integrated designs can include sector coupling via power-to-heat and/or power-to-hydrogen, and have the potential to be 100% clean while offering a continuous supply of energy and water with lower system costs than all-electric. Both heat and hydrogen were found to add to the reliability and affordability of the system. Local conversion and storage will thus contribute to ensure the continuous availability (reliability) of all neighborhood system services (energy, transport and water). Yet, for existing neighborhoods, a connection to the larger energy and water system is inevitable. Combining energy and water within one design makes it possible to make design choices in a way that allows both sectors to mutually enhance each other.

From these main conclusions and based on the findings from the different chapters in this dissertation, five design principles for integrated energy and water systems for neighborhoods are derived that together constitute an answer to the 'how' part of the research question. The neighborhood modeled in this research was based on an actual case in Nieuwegein, but the number of houses and heat demand are chosen such that they resemble an average European neighborhood in accordance with other research [59]. The investigated techniques for energy production, storage and supply are not specific for the Netherlands but could be applied in most North-West European countries. In the design principles, the obtained results can therefore be generalized to the broader North-West European context. More specifically, they are valid for neighborhoods in European countries with a temperate to cold climate, and mainly for villages and small to medium cities. The first two design principles are most useful for the Netherlands as grid congestion is an issue here. These design principles are targeted for both policymakers, researchers as well as (local) government officials and city planners:

1. ***Keep the connection with the centralized system, but stay as a neighborhood as much as possible within the boundaries of the current infrastructure connections***
   Finding the balance between centralized and decentralized infrastructure is one of the challenges of a completely renewable energy system. In this research, an existing neighborhood with a fixed electricity grid capacity was the focus of the study. In **Chapter 2**, a neighborhood was investigated with 900 houses (20.4 TJ/year of heat demand), with an 8.7 MWp solar park, a 2.5 MW_{el} heat pump and 2.5 MW electrolyzer, as well as 150,000 m^3 of underground heat storage and 40,000 m^3 of rainwater storage. It was demonstrated that this system design could fulfill the demands for heat, transport, and (pure) water every hour

of the year (electricity was not taken into account), thereby establishing the reliability of the system. Additionally, an integrated system approach was found to decrease the costs for heat, transport and water by 17% and with 15% lower CO_2 emissions compared to a scenario when all renewable energy capacity would be sold to the electricity grid. In **Chapter 3** the neighborhood size was expanded to 2000 houses to represent an average European neighborhood with different insulation levels (49-67 TJ/year heat demand). Local PV production on roofs and household electricity demand (19.4 TJ/year) were included and different system designs were compared. Again, the integrated system designs, including local hydrogen production and/or a low-temperature district heating network and heat storage were found to reduce costs by 145-300 €/household/year (6-13 %) compared to an all-electric, non-integrated system. Furthermore, these integrated systems were better equipped to handle supply and demand peaks by converting surplus electricity to heat and/or hydrogen, thereby avoiding full electrification of energy use in winter. In the selected case study, the current grid capacity was not exceeded (on an hourly basis), and only 5-10% of locally produced electricity was exported to the grid. Yet, the local electricity supply fulfills at most 25-35% of the total demand, which makes clear that energy autarky hard to reach for an existing neighborhood. As such, existing neighborhoods will most probably continue to rely on the electricity grid in the future. Nonetheless, with an integrated approach that applies conversion and storage techniques, supply and demand peaks could be reduced to a level where the current grid capacity is sufficient or requires only limited extension.

2. ***In existing neighborhoods, explicitly include hybrid options (combinations of energy carriers) in the energy system***

There is a tendency to focus on only one energy carrier (electricity, heat or gas) in the transition of neighborhood heating systems, for example in the Netherlands [352]. However, **Chapter 3** of this research demonstrated that a narrow focus on a single energy carrier (i.e. electricity in an all-electric design) does not necessarily lead to the most affordable and reliable system. In fact, hybrid heat pumps in combination with hydrogen or booster heat pumps combined with a district heating network have been found to be less expensive (11%) than the all-electric alternative.

In the cost consideration, one might expect the costs of extending the electricity grid to be most decisive. Yet, **Chapter 3** included both the costs for grid extension, retrofitting, and installing new infrastructure (i.e. a DHN) as well as yearly energy costs. It was found that the costs for extensive retrofitting measures are most decisive (24% in an all-electric scenario), while grid reinforcement costs comprise only 2% of the total yearly costs per household.

It is important to recognize that a transition asks for transition solutions on the way to the final destination. For example, installing hybrid heat pumps combined with natural gas can electrify two-thirds of the heating demand cost-effectively, as demonstrated in **Chapter 3**. This is in line with findings from other research for larger households, where 60% of the energy demand could be electrified [349]. Additionally, this approach is likely to be less drastic for residents than extensive insulation measures. The next step in the transition could be converting from natural gas to biogas or hydrogen. Over time, more insulation measures could be taken (that have become cheaper and/or easier to apply), to further

reduce the heating demand. This principle aligns with recent policy in the Netherlands, which mandates the installation of hybrid heat pumps when replacing a gas boiler from 2026 onwards [347], [348].

3. *Include the subsurface as an essential part of the neighborhood design*

Chapters 2, 3 and 4 of this dissertation underscore the crucial role of subsurface utilization in balancing energy demand and supply while reducing pressure on the electricity grid. **Chapter 2** gave a first impression of the way in which the subsurface is able to store heat at 40-60°C in a high-temperature aquifer thermal storage system (HT-ATES) during summer to fulfill heat demand in winter. Additionally, rainwater collection from solar parks and roofs, along with storage in the subsurface, leads to a continuous supply of water for hydrogen production, toilets, dishwashers, washing machines and irrigation purposes. In **Chapter 3**, more extensive subsurface modeling was done which showed that a system design with local seasonal heat storage reached the most distributed energy imports over the year compared to the other scenarios. **Chapter 4** compared different heat storage temperatures (50°C and 65°C) and heat pump sizes (1-2 MW_{el}) and demonstrated that a HT-ATES can reduce the size of a collective heat pump up to 25% by lowering winter heat demand peaks. This also results in reduced surface-level installation size and costs. Integrating HT-ATES models in MES modeling will thus help to find more optimal solutions in lowering pressure on the electricity grid and improves the balance between supply and demand. Especially at higher storage temperatures, the pressure on the grid is both reduced in summer (power-to-heat) as well as winter (higher temperature delivered to houses, so lower electricity demand peaks). The subsurface can thus contribute to a more reliable energy and water system, and should be considered more often in studies and concepts for integrated energy systems. The applicability of either heat or water storage will depend on the location, as the subsurface characteristics and thus the geohydrological suitability will vary as well, yet large parts of mainly North-West and Eastern Europe (as well as parts of North America, Russia and Asia) have potential for ATES systems, representing 15% of the world's urban population [353].

When integrated energy and water concepts are applied to neighborhoods, multi-purpose use of the subsurface will become increasingly important. Utilizing the subsurface for storage reduces the impact of conversion and storage elements on street level, yet the subsurface is already in use for many other purposes such as infrastructure, as a groundwater source and in the near future also for geothermal energy. It is thus important to collaborate with different stakeholders to make the best and safest use of the subsurface, which is also stated in the Dutch vision on the subsurface, with as goal "sustainable, safe and efficient utilization of soil and subsoil, where utilization and protection are balanced" [354].

4. *Look for multiple values from both an energy- as well as a water perspective*

This dissertation presents a novel approach that combines technologies from both energy and water perspectives to demonstrate how multiple value creation can be achieved. In **Chapters 3 and 4** it was shown that the integration of power-to-heat and HT-ATES creates added value by reducing pressure on the electricity grid during both summer and winter.

Chapter 5 demonstrated how waste heat from electrolyzers can create value when it replaces natural gas or other heat sources at a heat consumer or in a district heating network. Thereby, the total efficiency of the electrolyzer was increased from 76 to 90% (HHV), and CO_2-savings of 0.08 (DHN)-0.28 (direct use) tonne $CO_2/MWh_{heat,used}$ could be obtained, thus contributing to a cleaner energy system while being affordable. Similarly, the heat from fuel cells, either in a neighborhood (**Chapter 3**) or within houses could be recovered as well. Additionally, the multifunctional building introduced in **Chapter 6** combines energy production, (rain) water storage, vegetation and greywater recovery within one building. This chapter shows that these different functions amplify each other, with as a tangible result 4.4% higher PV production on the green-blue roof versus the bitumen roof at similar irradiation. Furthermore, the building enhances biodiversity, reduces the risk of flooding during heavy precipitation, cools the building and the environment and in general improves the livability of a neighborhood by its appearance. These examples show that in the design of an integrated neighborhood system, one should always try to zoom out and assess which options there are to combine functions and create extra value from an environmental, economic, architectural or social perspective.

5. ***Begin as early as possible with co-designing of both the energy as well as the water system in the neighborhood***

The benefits of integrated system design were the focus of this dissertation. However, to bridge the gap from science to practice, it is essential to start as early as possible bringing the water and energy sector together to create a shared design perspective. Both systems need infrastructure, and there can be conflicting interests. A neighborhood energy and water system could include both (HT)-ATES as well as rainwater storage, as demonstrated in **Chapter 2**. However, both systems need space in the subsurface and early coordination is necessary to avoid conflicts regarding space utilization. It is possible to achieve sustainable co-existence of these systems by maintaining adequate distances [355], which should be considered during the design stage. Similarly, infrastructure installation should be planned to minimize the impact of heat exchange on the drinking water network [356], [357]. In **Chapter 6** the design of a multifunctional blue-green-PV roof and greywater system was investigated, highlighting the importance of early design choices to enable greywater recovery from showers, such as creating space to pump water to the roof and connecting shower drains to the greywater system. In the end, not all showers were connected to the system due to miscommunication, but by then, the design was literally 'set in stone'. Therefore, early communication and stakeholder involvement are essential, and a collaborative approach should be adopted rather than a competitive one.

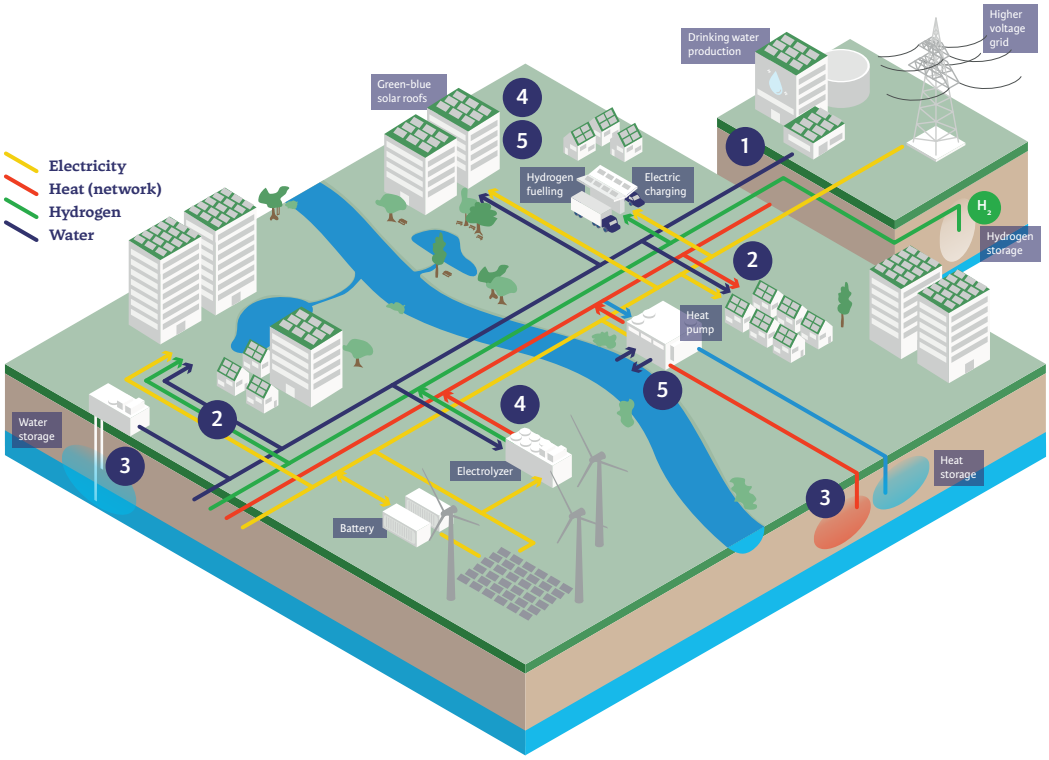

1. Keep the connection with the centralized system, but stay as a neighborhood as much as possible within the boundaries of the current infrastructure connections

2. In existing neighborhoods, explicitly include hybrid options (combinations of energy carriers) in the energy system

3. Include the subsurface as an essential part of the neighborhood design

4. Look for multiple values from both an energy- as well as a water perspective

5. Begin as early as possible with co-designing of both the energy as well as the water system in the neighborhood

7.3 Contributions to the knowledge gaps and future directions for research

At the outset of this research, four main knowledge gaps were defined, and the different chapters have made contributions to fill these gaps. This section addresses the identified knowledge gaps, summarizes how the different chapters contributed to them and presents directions for future research that emerge from this work or have not yet been touched upon.

- *Knowledge gap 1: A lack of focus on 100% renewable systems*
  Many studies on MES include natural gas in their system design, which makes them not completely carbon-free [51], [63]–[67]. In **Chapters 2 and 3**, it was shown that it is possible to design neighborhood systems with local production of renewable energy, collection of rainwater, and conversion and storage of heat and hydrogen without the need for fossil fuels, that are reliable and affordable. Yet, in **Chapter 3** it was demonstrated that an existing neighborhood will still depend on the larger electricity grid for 65-75% of its total energy demand, meaning that imported electricity must be 100% renewable to achieve a completely carbon-free system. Therefore, full sustainability should be attained at other levels in the energy system. How these local energy systems can be combined with national, regional or Mondial levels of the energy system on both a temporal as well as a spatial scale is an interesting subject for further research, especially because the possibilities of 100% renewable energy systems are underestimated by both the IEA as well as the IPCC [358]. In the book 'Green Energy for All' [10] suggestions are done for the energy system in 2100, with a division between the energy carriers electricity (50%), hydrogen (40%) and heat (10%). Hydrogen production will take place on a Mondial level, while electricity is produced on a regional or local level. This dissertation has primarily focused on the energy system goals clean, affordable and reliable, yet safety, security of supply, fairness, circularity and security of materials should be included in future research as well. This would for example include a further analysis of the material use in (local) integrated energy systems, as materials might become critical within the energy transition [13], [358]–[360]. One way to assess the broader impact would be the use of life-cycle analysis methods (LCA) to better understand the sustainability of these systems besides the costs and energy balance. To avoid or mitigate material shortages, strategies as rethink, reduce, reuse and recycle can be applied [361].

- *Knowledge gap 2: Seasonal heat storage in MES is unexamined*
  This dissertation has contributed to the application of seasonal heat storage in MES modeling, particularly focusing on HT-ATES systems (40-60°C) in both **Chapters 2,3** and especially **Chapter 4**. **Chapter 4** describes that incorporating an extra mode of operation of the heat pump in booster mode prolongs heat delivery and allows for a lower threshold temperature for the HT-ATES system (30°C instead of 43°C in this case). This prolongation of heat delivery results in improved system recovery efficiency, eventually leading to reduced costs for the heat pump due to the smaller size. Overall, the research suggests that HT-ATES systems have the potential to play a valuable role in MES by ena-

bling the temporal decoupling of heat supply and demand. The lack of attention for heat storage in models for future energy systems is highlighted as well by the roadmap for energy storage in the Netherlands [350]. Therefore, it is recommended to adopt seasonal storage in MES modeling, and hopefully, the methodologies and modeling techniques explained mainly in **Chapter 4** will assist with that. However, further studies are required to gain more insights into the working mechanisms and conditions of HT-ATES to enhance its applicability, both by research and demonstrations [362]. Additionally, a regulatory framework is still in development and should be accelerated to support the transition from pilot to demonstration/commercial scale [234]. On top of that, a future direction for research would be a triplet system with three temperature levels to deliver both (higher temperature) heat as well as cooling from the same system [124].

- ***Knowledge gap 3: Limited attention for a combination of multiple energy carriers (electricity, heat, gas) in one neighborhood design***
  The Power-to-H3 concept combines three energy carriers (electricity, heat -carried in the form of water- and hydrogen) in one concept and model for a multi-energy system (MES) as shown in **Chapter 2**, with Nieuwegein in the Netherlands as a case study.
  In **Chapter 3** different configurations of the concept were compared. However, this was just one case, and although the neighborhood could be generalized for European countries with a temperate to cold climate, the most suitable system design will depend largely on the exact location and the associated climate. Thus, it would be interesting to extend the analysis to other types of neighborhoods and add more utility functions (offices, schools, supermarkets etc). Furthermore, in **Chapter 5** a concrete example of the integration of electricity, gas and heat was demonstrated by utilizing the waste heat from electrolysis (power-to-gas) to further enhance system integration. In the case whereby waste heat would replace natural gas at a heat consumer without the need for a heat pump, the heat price would be 8.9 €/MWh_{heat}. This is lower than when the heat would be produced with natural gas (using the average price for 2016-2020), thus contributing to both a cleaner as well as a more affordable energy system. In future research, more waste heat potentials could be included.
  In the modeling work on MES, different storage options were included for electricity (batteries), heat (underground heat storage), and hydrogen (tanks or salt cavern storage). Not yet included was vehicle-to-grid as a storage option. Vehicle-to-grid from either battery electric vehicles [350], [363] or fuel cell electric vehicles [364] is a promising technology that could replace collective batteries and could be considered in further research. Additionally, the use of a collective fuel cell was considered in **Chapter 3**, but individual fuel cells in houses are an option as well [10], [365] which would avoid the construction of district heating infrastructure when not yet in place.
  The time scale of the modeling work was hourly, which allowed for variations in supply and demand. Still, even smaller timescales (minutes or 15-minute blocks) are relevant as well to gain more insight in peak demands, such as electric vehicle charging or electric cooking as well as peak supply of PV output. Finally, the need for practical examples

of integrated energy and water systems for neighborhoods is crucial to validate the concept and apply methods and algorithms from research [366].

- *Knowledge gap 4: Lack of an integrated approach to water and energy*
  A knowledge gap was defined in the combined analysis of both energy and water in neighborhood systems. This research has taken some initial steps towards integrating water and energy elements in the neighborhood design, mainly in **Chapters 2 and 6**. **Chapter 2** has shown how rainwater from solar panels and roofs could be stored and used for hydrogen production, irrigation and some household water uses (toilet, washing machine, dishwasher). **Chapter 6** illustrated how water, biodiversity and energy functions can be combined and even enhance each other within a building by combining solar PV with a green roof, water storage, shower water reuse and purification. Nonetheless, more research is needed to foster further integration and cooperation between the energy and water sector, both from an institutional as well as a practical perspective. Water companies could play a role in the operation of low-temperature district heating and cooling networks. Knowledge about network design could be shared and utilized among the sectors to achieve better performance of infrastructure. Additionally, the co-existence of ATES and water storage (ASR) systems requires further investigation, to know how and under which conditions both technologies could be installed [355].

7.4 Bridging science to practice - policy recommendations

In most chapters (**Chapters 2,3,4,5**) of this dissertation, a solar park and neighborhood in Nieuwegein were used as a case study. The process of developing this dissertation mirrored the journey from concept to realization of the Power-to-H3 concept in Nieuwegein. This paragraph provides an overview of the main developments and lessons learned from bridging science to practice.

The Power-to-H3 concept, as introduced in **Chapter 2**, captured the attention of the local municipality, and via a book [105] and subsequent research projects [134], [217], the first techno-economic results paved the way for closer collaboration between the municipality and water research institute KWR. With the involvement of a growing number of stakeholders, steps were taken toward the realization of the heat storage and distribution and hydrogen aspects of the concept. Meanwhile, the ambition for the number of houses in the (partly retrofitted) neighborhood was expanded from 900 to 2500. The stakeholder engagement during the process included the municipality, province, drinking water company, water utility, energy company, hydrogen fueling company, project developers in the neighborhood and local parties interested in using hydrogen (from public transport to contractors and a laundry company). Despite intensive collaboration between stakeholders involved in the heat production, heat storage and district heating network (DHN) between 2018-2020, further development was ultimately halted. The permitting and construction process of the over 20 different project developers that owned parcels in the neighborhood did not align with the development of the heating system by the energy company and the municipality.

Additionally, as the municipality did not own the parcels or buildings in the neighborhood, they were unable to force a decision. The energy company involved in the district heating network deemed the investment risk too high, given that there was not yet a DHN in place, and with more than 20 different project developers in the neighborhood, it proved to be difficult to jointly decide to adopt district heating.

On the hydrogen front, progress has been relatively smooth. In 2019 a new company (Hysolar) was established that is dedicated to the production and distribution of green hydrogen [367]. As a result of this initiative, a temporary slow-fill hydrogen fueling station was installed between 2019 and 2022, followed by a full-scale hydrogen fueling station at the site of a contractor in 2021 [368]. The company will start its own local hydrogen production in 2024 with the installation of an on-site PEM electrolyzer with a capacity of 2.5 MW. The collaboration between research and practice has contributed to the further development of the decoupling of heat from the electrolyzer, which was discussed in **Chapter 5**.

However, during the implementation of new technologies such as an electrolyzer or a hydrogen fueling station, it has become apparent that innovation, by definition, runs ahead of, and can therefore be delayed by, regulation (legislation, permitting etc). The realization of these new technologies takes considerable time and effort due to relative unfamiliarity among the authorities. Often, there is no regulation in place yet that fits the technology (i.e. an electrolyzer for green hydrogen production), and sometimes existing procedures for other types of technology are used that are not (fully) applicable, which can lead to miscommunications, delays in permitting and increase in costs. One example is the installation of a liquid-tight floor under a hydrogen tank (a requirement for i.e. liquid natural gas), while hydrogen is a gas that would disappear to the air and not a liquid that would leak out of the tank on the floor. Based on the experiences during the process from idea to realization, the following recommendations for policymakers are obtained. The recommendations are based on experience in the Netherlands, but apply to all countries where energy innovation is happening, and are thus generalizable to other (EU) countries as well:

1. ***Create more low-regulation zones for testing and demonstrating new technologies***
   The climate crisis and energy transition asks to move swiftly with new developments. It is important to create more space for testing and demonstrating new technologies, methods and system designs that do not comply with the current rules and regulations. An example of such an environment is the Green Village in Delft in The Netherlands [369], where testing and demonstration at the building and small neighborhood level takes place. More of these kinds of low-regulation zones or regulatory sandboxes are needed, also for larger innovations. So far, Great Britain, Italy and the Netherlands are the pioneer countries for regulatory sandboxes, but the focus has been mostly on electricity at the lower voltage level, while power-to-x technologies are also important [370]. Still, even in these low-regulation zones permitting processes can take a long time. Another option would be to let an expert committee grant a permit or permission based on their knowledge about the safety of the innovation, while monitoring is carried out. Ultimately, new standards can then be formulated based on practical experience [10].

2. ***Acknowledge that a transition is not incremental, and sometimes a step back is necessary to leap forward later on***

Some developments within a transition will technically speaking be a step back instead of a step forward, regarding for example CO_2 emissions. As a society, we have to accept that this is an inevitable part of a transition and put these 'in-between' steps in perspective. For example, in the case of Nieuwegein, the hydrogen fueling station was installed before the electrolyzer could produce local green hydrogen. This meant that in the first period, there was no 100% renewable local hydrogen, but (certified green) hydrogen had to be purchased and transported to Nieuwegein on short-term contracts, which increased the price. Yet, the 'chicken-egg' problem was solved and on the demand side, investments in hydrogen vehicles (i.e. tractors) could be made. Similarly, but on a larger scale, low-carbon (or blue) hydrogen might be necessary to start developing infrastructure and support the future uptake of green hydrogen, as long as renewable capacity and costs for green hydrogen are not yet on track [38], [199], [371]. This way of thinking is comparable to the developments in our electricity grid, with a current fossil share of 60% and renewable share of 40% (including biomass), in both the Netherlands and on average in the EU [7], [372], but striving to become 100% renewable over time.

3. ***The societal business case should be leading in decision-making, not the individual business cases of stakeholders***

When designing an integrated energy and water system for a neighborhood, its impacts extend beyond reduced (greenhouse gas) emissions, reliability and costs. In **Chapter 2**, it was demonstrated that if avoided costs for CO_2 and grid reinforcement were included in the business case of the Power-to-H3 system, the heat production cost would decrease by 26%, while hydrogen production costs decreased by 20%. **Chapter 4** illustrated that taking CO_2 emission costs into account for the replacement of natural gas by electrolyzer waste heat would increase the margin between total yearly costs and saved costs by a factor of 1.6 – 12. Finally, the multifunctional building introduced in **Chapter 6** not only produces energy but enhances biodiversity, reduces the risk of flooding during heavy precipitation, cools the building and the environment and in general improves the livability of a neighborhood by its appearance. These aspects should be included in a societal business case, as opposed to business cases for individual stakeholders reasoning from their own perspectives and interests. One way to do so is through a societal cost-benefit analysis or multi-criteria analysis in order to include aspects that are harder to monetize (i.e. biodiversity) as well. The outcomes of such a societal cost-benefit analysis will probably make the broader impacts of an integrated concept even stronger and more convincing. Institutional interventions, such as legal measures like fiscal arrangements, changes in policy and legislation, and financial compensation schemes, could help address the suboptimal allocation of costs and benefits within an integrated energy and water system.

7.5 Epilogue

Sometimes it seems that we as a society still do not fully comprehend the current and future impacts of the climate crisis. At least, we do not act like it. Although progress has been made, it is not nearly enough and certainly not fast enough [373]. We need to collaborate with scientists from many different disciplines, policymakers, (world) leaders and citizens to limit global warming. With this research, I have tried to give conceptual and concrete examples of how our neighborhood system services could be supplied without or with highly reduced greenhouse gas emissions, and at the same time stay reliable and affordable. I hope it provides inspiration and motivation to keep progressing toward a truly sustainable built environment. Thereby I would argue that research should not stop with a report or paper. Although there are still many uncertainties, what we need right now is the implementation of all the research, plans and visions published already, as we have no time to lose. Scientists have a responsibility here as well, to contribute to the realization process by following it closely and trying to mitigate the hurdles encountered on the way. Yet, technological solutions are just one part of the puzzle. As a scientist, I will keep contributing, but as a citizen, I will also play my part. We all have a possibility to change our behavior and raise our voices to keep this planet livable for generations to come.

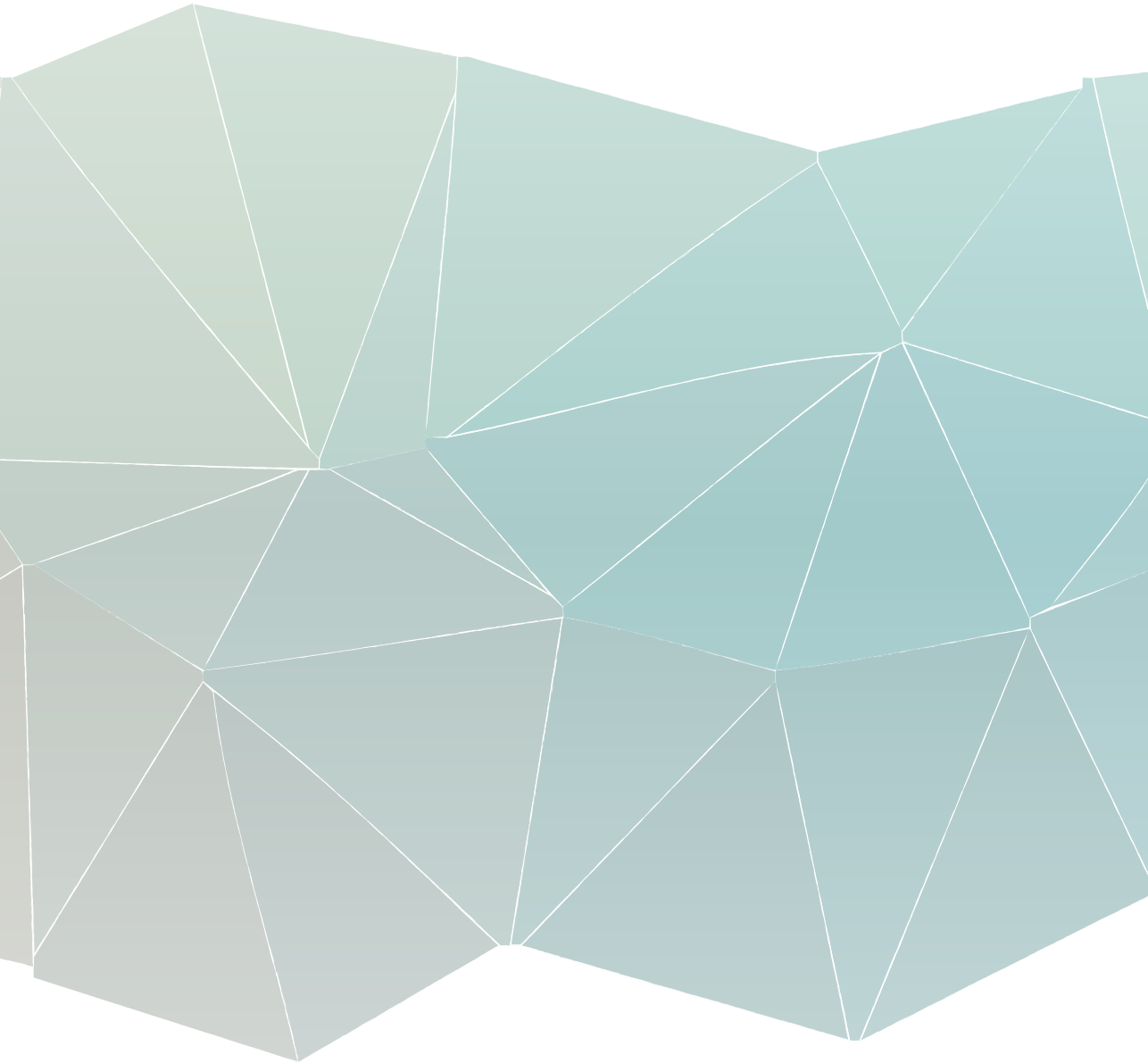

Bibliography

[1] United Nations, "Adoption of the Paris Agreement," in Conference of the Parties on its twenty-first session, 2015, no. December, p. 32 [Online]. Available: http://unfccc.int/resource/docs/2015/cop21/eng/l09r01.pdf

[2] European Commission, "The European Green Deal," Eur. Comm., vol. 53, no. 9, p. 24, 2019, doi: 10.1017/CBO9781107415324.004. [Online]. Available: https://eur-lex.europa.eu/legal-content/EN/TXT/PDF/?uri=CELEX:52019DC0640&from=EN

[3] Klimaatberaad, "Klimaatakkoord." Den Haag, 2019 [Online]. Available: https://www.klimaatakkoord.nl/documenten/publicaties/2019/06/28/klimaatakkoord

[4] Ministerie van Economische Zaken en Klimaat, "Klimaatplan 2021 - 2030," 2020 [Online]. Available: https://www.rijksoverheid.nl/Onderwerpen/Klimaatverandering/Documenten/Beleidsnotas/2020/04/24/Klimaatplan-2021-2030

[5] Nationaal Programma Regionale Energie Strategie, "RES 1.0 per regio," 2021. [Online]. Available: https://www.regionale-energiestrategie.nl/bibliotheek/res++media/1643638.aspx?t=RES-10-per-regio. [Accessed: Feb. 01, 2023]

[6] J. Osička and F. Černoch, "European energy politics after Ukraine: The road ahead," Energy Res. Soc. Sci., vol. 91, no. August, p. 102757, 2022, doi: 10.1016/j.erss.2022.102757.

[7] D. Jones, "European Electricity Review," 2023 [Online]. Available: https://ember-climate.org/app/uploads/2023/01/Report-European-Electricity-Review-2023.pdf

[8] EU Commission, "REPowerEU: Joint European Action for more affordable, secure and sustainable energy." 2022 [Online]. Available: https://eur-lex.europa.eu/legal-content/EN/TXT/?uri=COM:2022:108:FIN

[9] European Commission, "European Green Deal: EU agrees stronger legislation to accelerate the rollout of renewable energy," 2023. [Online]. Available: https://ec.europa.eu/commission/presscorner/detail/en/IP_23_2061. [Accessed: May 01, 2023]

[10] A. J. M. van Wijk, E. van der Roest, and J. Boere, Green Energy for all [In press]. 2023.

[11] IRENA, Renewable Power Generation Costs in 2021. Abu Dhabi: International Renewable Energy Agency, 2022 [Online]. Available: https://www.irena.org/-/media/Files/IRENA/Agency/Publication/2018/Jan/IRENA_2017_Power_Costs_2018.pdf

[12] DNV, "Energy Transition Outlook 2022," 2022 [Online]. Available: https://www.dnv.com/energy-transition-outlook/download.html

[13] IEA, "The Role of Critical Minerals in Clean Energy Transitions," Paris, 2022 [Online]. Available: https://www.iea.org/reports/the-role-of-critical-minerals-in-clean-energy-transitions

[14] European Commission, "Questions and Answers on the new EU rules on gas storage," 2022. [Online]. Available: https://ec.europa.eu/commission/presscorner/detail/en/qanda_22_1937. [Accessed: Jun. 22, 2023]

[15] Navigant, "Gas for Climate. The optimal role for gas in a net-zero emissions energy system," 2019 [Online]. Available: https://gasforclimate2050.eu/wp-content/uploads/2020/03/Navigant-Gas-for-Climate-The-optimal-role-for-gas-in-a-net-zero-emissions-energy-system-March-2019.pdf

[16] M. Stork, J. de Beer, N. Lintmeijer, and B. den Ouden, "Chemistry for Climate : Acting on the need for speed Roadmap for the Dutch Chemical Industry towards 2050," Utrecht, 2018.

[17] B. Zakeri et al., "Pandemic, War, and Global Energy Transitions," Energies, vol. 15, no. 17, pp. 1–23, 2022, doi: 10.3390/en15176114.

[18] IRENA, Global Renewables Outlook: Energy transformation 2050. 2020 [Online]. Available: https://www.irena.org/publications/2020/Apr/Global-Renewables-Outlook-2020

[19] IEA, "Unlocking the Potential of Distributed Energy Resources - Power system opportunities and best practices," 2022 [Online]. Available: https://www.iea.org/reports/unlocking-the-potential-of-distributed-energy-resources

[20] German National Academy of Sciences Leopoldina, National Academy of Science and Engineering acatech, and Union of the German Academies of Sciences and Humanities, "Grid Congestion as a Challenge for the Electricity System Options for a Future Market Design," no. April, pp. 1–72, 2021 [Online]. Available: https://energiesysteme-zukunft.de/fileadmin/user_upload/Publikationen/PDFs/ESYS_Position_Paper_Grid_congestion.pdf

[21] Netbeheer Nederland, "Landelijk Actieprogramma Netcongestie," 2022 [Online]. Available: https://www.netbeheernederland.nl/_upload/Files/Actieplan_voor_meer_ruimte_op_het_net__sneller_bouwen__slimmer_gebruiken_en_flexibeler_afnemen__261.pdf

[22] PWC, "De energietransitie en de financiele impact voor netbeheerders," no. april, 2021 [Online]. Available: https://www.netbeheernederland.nl/_upload/Files/PwC_De_energietransitie_en_de_financiele_impact_voor_netbeheerders_15_04_2021_193.pdf

[23] European Commission, "Powering a climate-neutral economy: An EU Strategy for Energy System Integration," European Commission, Brussels, 2020 [Online]. Available: https://ec.europa.eu/energy/sites/ener/files/energy_system_integration_strategy_.pdf

[24] IEA, Water Energy Nexus. Paris: OECD/IEA, 2017 [Online]. Available: https://www.iea.org/reports/water-energy-nexus

[25] European Commission, "Jrc Science for Policy Report Water Energy Nexus in Europe," 2019 [Online]. Available: https://publications.jrc.ec.europa.eu/repository/handle/JRC115853

[26] D. J. Rodriguez, A. Delgado, P. Delaquil, and A. Sohns, "Thirsty Energy. Water Papers," Washington, DC, 2013 [Online]. Available: https://openknowledge.worldbank.org/entities/publication/4573ce-aa-3a43-5e7e-8804-57f856fe3e0d

[27] IEA, "Buildings," Paris, 2022 [Online]. Available: https://www.iea.org/reports/buildings

[28] European Commission, "Energy performance of buildings directive," 2021. [Online]. Available: https://energy.ec.europa.eu/topics/energy-efficiency/energy-efficient-buildings/energy-performance-buildings-directive_en#facts-and-figures. [Accessed: Jan. 18, 2023]

[29] H. E. Beck, N. E. Zimmermann, T. R. McVicar, N. Vergopolan, A. Berg, and E. F. Wood, "Present and future Köppen-Geiger climate classification maps at 1-km resolution," Sci. Data, vol. 5, pp. 1–12, 2018, doi: 10.1038/sdata.2018.214.

[30] IEA, "Solar PV," Paris, 2022 [Online]. Available: https://www.iea.org/reports/solar-pv

[31] O. Gandhi, D. S. Kumar, C. D. Rodríguez-Gallegos, and D. Srinivasan, "Review of power system impacts at high PV penetration Part I: Factors limiting PV penetration," Sol. Energy, vol. 210, no. May, pp. 181–201, 2020, doi: 10.1016/j.solener.2020.06.097.

[32] T. Aziz and N. Ketjoy, "PV Penetration Limits in Low Voltage Networks and Voltage Variations," IEEE Access, vol. 5, pp. 16784–16792, 2017, doi: 10.1109/ACCESS.2017.2747086.

[33] J. G. Kirkerud, T. F. Bolkesjø, and E. Trømborg, "Power-to-heat as a flexibility measure for integration of renewable energy," Energy, vol. 128, pp. 776–784, 2017, doi: 10.1016/j.energy.2017.03.153.

[34] A. Bloess, W. P. Schill, and A. Zerrahn, "Power-to-heat for renewable energy integration: A review of technologies, modeling approaches, and flexibility potentials," Appl. Energy, vol. 212, pp. 1611–1626, 2018, doi: 10.1016/j.apenergy.2017.12.073.

[35] M. N. I. Maruf, G. Morales-España, J. Sijm, N. Helistö, and J. Kiviluoma, "Classification, potential role, and modeling of power-to-heat and thermal energy storage in energy systems: A review," Sustain. Energy Technol. Assessments, vol. 53, no. July, 2022, doi: 10.1016/j.seta.2022.102553.

[36] H. Ümitcan Yilmaz, D. Keles, A. Chiodi, R. Hartel, and M. Mikuli, "Analysis of the power-to-heat potential in the European energy system," vol. 20, pp. 6–19, 2018, doi: 10.1016/j.esr.2017.12.009.

[37] Eurostat, "Energy consumption in households," 2022. [Online]. Available: https://ec.europa.eu/eurostat/statistics-explained/index.php?title=Energy_consumption_in_households#Energy_consumption_in_households_by_type_of_end-use. [Accessed: Jan. 13, 2023]

[38] European Commission, "A hydrogen strategy for a climate-neutral Europe." Brussels, pp. 1–23, 2020 [Online]. Available: https://eur-lex.europa.eu/legal-content/EN/TXT/?uri=CELEX:52020DC0301

[39] A. Z. Arsad et al., "Hydrogen energy storage integrated hybrid renewable energy systems: A review analysis for future research directions," Int. J. Hydrogen Energy, vol. 47, no. 39, pp. 17285–17312, 2022, doi: 10.1016/j.ijhydene.2022.03.208. [Online]. Available: https://doi.org/10.1016/j.ijhydene.2022.03.208

[40] Hydrogen Council, "How hydrogen empowers the energy transition," 2017 [Online]. Available: https://hydrogencouncil.com/wp-content/uploads/2017/06/Hydrogen-Council-Vision-Document.pdf

[41] IRENA, "World energy transitions outlook: 1.5 degrees pathway," 2021 [Online]. Available: https://irena.org/publications/2021/March/World-Energy-Transitions-Outlook

[42] Frontier Economics, CE Delft, and THEMA Consulting Group, "Potentials of sector coupling for decarbonisation - Assessing regulatory barriers in linking the gas and electricity sectors in the EU," 2019 [Online]. Available: https://energy.ec.europa.eu/publications/potentials-sector-coupling-decarbonisation-assessing-regulatory-barriers-linking-gas-and-electricity_en

[43] European Commission et al., "Study on energy storage-Contribution to the security of the electricity supply in Europe," European Commission, 2020 [Online]. Available: https://op.europa.eu/en/publication-detail/-/publication/a6eba083-932e-11ea-aac4-01aa75ed71a1/language-en?WT.mc_id=Searchresult&WT.ria_c=37085&WT.ria_f=3608&WT.ria_ev=search

[44] DNV, "Energy Transition Outlook 2021: A global and regional forecast to 2050.," 2021 [Online]. Available: https://eto.dnv.com/2021

[45] S. Madeddu et al., "The CO_2 reduction potential for the European industry via direct electrification of heat supply (power-to-heat)," Environ. Res. Lett., vol. 15, no. 12, 2020, doi: 10.1088/1748-9326/abbd02.

[46] P. Mancarella, "MES (multi-energy systems): An overview of concepts and evaluation models," Energy, vol. 65, pp. 1–17, 2014, doi: 10.1016/j.energy.2013.10.041. [Online]. Available: http://dx.doi.org/10.1016/j.energy.2013.10.041

[47] M. Robinius et al., "Linking the Power and Transport Sectors—Part 1: The Principle of Sector Coupling," Energies, vol. 10, no. 7, p. 956, Jul. 2017, doi: 10.3390/en10070956. [Online]. Available: http://www.mdpi.com/1996-1073/10/7/956

[48] B. V. Mathiesen et al., "Smart Energy Systems for coherent 100% renewable energy and transport solutions," Appl. Energy, vol. 145, pp. 139–154, 2015, doi: 10.1016/j.apenergy.2015.01.075. [Online]. Available: http://dx.doi.org/10.1016/j.apenergy.2015.01.075

[49] J. Z. Thellufsen and H. Lund, "Cross-border versus cross-sector interconnectivity in renewable energy systems," Energy, vol. 124, pp. 492–501, 2017, doi: 10.1016/j.energy.2017.02.112. [Online]. Available: http://dx.doi.org/10.1016/j.energy.2017.02.112

[50] J. Gea-Bermúdez et al., "The role of sector coupling in the green transition: A least-cost energy system development in Northern-central Europe towards 2050," Appl. Energy, vol. 289, no. September 2020, p. 116685, 2021, doi: 10.1016/j.apenergy.2021.116685. [Online]. Available: https://doi.org/10.1016/j.apenergy.2021.116685

[51] A. Bartolini, F. Carducci, C. B. Muñoz, and G. Comodi, "Energy storage and multi energy systems in local energy communities with high renewable energy penetration," Renew. Energy, vol. 159, pp. 595–609, 2020, doi: 10.1016/j.renene.2020.05.131.

[52] H. Lund and D. Connolly, "Energy Storage and Smart Energy Systems," Int. J. Sustain. Energy Plan. Manag., vol. 11, pp. 2016–3, 2016, doi: 10.5278/ijsepm.2016.11.2.

[53] Eurostat, "Supply, transformation and consumption of gas - monthly data," 2023. [Online]. Available: https://ec.europa.eu/eurostat/databrowser/view/NRG_CB_GASM__custom_6236595/default/table. [Accessed: May 17, 2023]

[54] E. Barbour, D. Parra, Z. Awwad, and M. C. González, "Community energy storage: A smart choice for the smart grid?," Appl. Energy, vol. 212, no. June 2017, pp. 489–497, 2018, doi: 10.1016/j.apenergy.2017.12.056. [Online]. Available: https://doi.org/10.1016/j.apenergy.2017.12.056

[55] P. Lubello, M. Pasqui, A. Mati, and C. Carcasci, "Assessment of hydrogen-based long term electrical energy storage in residential energy systems," Smart Energy, vol. 8, no. October, p. 100088, 2022, doi: 10.1016/j.segy.2022.100088. [Online]. Available: https://doi.org/10.1016/j.segy.2022.100088

[56] D. Grosspietsch, P. Thömmes, B. Girod, and V. H. Hoffmann, "How, When, and Where? Assessing Renewable Energy Self-Sufficiency at the Neighborhood Level," Environ. Sci. Technol., vol. 52, no. 4, pp. 2339–2348, 2018, doi: 10.1021/acs.est.7b02686.

[57] M. Robinius et al., "Linking the Power and Transport Sectors—Part 2: Modelling a Sector Coupling Scenario for Germany," Energies, vol. 10, no. 7, p. 957, Jul. 2017, doi: 10.3390/en10070957. [Online]. Available: http://www.mdpi.com/1996-1073/10/7/957

[58] X. Xu et al., "Optimal operational strategy for a future electricity and hydrogen supply system in a residential area," Int. J. Hydrogen Energy, vol. 47, no. 7, pp. 4426–4440, 2022, doi: 10.1016/j.ijhydene.2021.11.085. [Online]. Available: https://doi.org/10.1016/j.ijhydene.2021.11.085

[59] V. Oldenbroek, L. A. Verhoef, and A. J. M. van Wijk, "Fuel cell electric vehicle as a power plant : Fully renewable integrated transport and energy system design and analysis for smart city areas," Int. J. Hydrogen Energy, vol. 42, no. 12, pp. 8166–8196, 2017, doi: 10.1016/j.ijhydene.2017.01.155. [Online]. Available: http://dx.doi.org/10.1016/j.ijhydene.2017.01.155

[60] C. B. Robledo, V. Oldenbroek, F. Abbruzzese, and A. J. M. van Wijk, "Integrating a hydrogen fuel cell electric vehicle with vehicle-to-grid technology, photovoltaic power and a residential building," Appl. Energy, vol. 215, no. February, pp. 615–629, 2018, doi: 10.1016/j.apenergy.2018.02.038. [Online]. Available: https://doi.org/10.1016/j.apenergy.2018.02.038

[61] V. Oldenbroek, G. Smink, T. Salet, and A. J. M. van Wijk, "Fuel cell electric vehicle as a power plant: Techno-economic scenario analysis of a renewable integrated transportation and energy system for smart cities in two climates," Appl. Sci., vol. 10, no. 1, 2020, doi: 10.3390/app10010143.

[62] V. Oldenbroek, S. Wijtzes, K. Blok, and A. J. M. van Wijk, "Fuel cell electric vehicles and hydrogen balancing 100 percent renewable and integrated national transportation and energy systems," Energy Convers. Manag. X, vol. 9, no. January, p. 100077, 2021, doi: 10.1016/j.ecmx.2021.100077. [Online]. Available: https://doi.org/10.1016/j.ecmx.2021.100077

[63] K. Orehounig, R. Evins, and V. Dorer, "Integration of decentralized energy systems in neighbourhoods using the energy hub approach," Appl. Energy, vol. 154, pp. 277–289, 2015, doi: 10.1016/j.apenergy.2015.04.114. [Online]. Available: http://dx.doi.org/10.1016/j.apenergy.2015.04.114

[64] C. Wouters, E. S. Fraga, and A. M. James, "An energy integrated, multi-microgrid, MILP (mixed-integer linear programming) approach for residential distributed energy system planning - A South Australian case-study," Energy, vol. 85, pp. 30–44, 2015, doi: 10.1016/j.energy.2015.03.051. [Online]. Available: http://dx.doi.org/10.1016/j.energy.2015.03.051

[65] K. Siraganyan, A. T. Dasun Perera, J. L. Scartezzini, and D. Mauree, "Eco-SiM: A parametric tool to evaluate the environmental and economic feasibility of decentralized energy systems," Energies, vol. 12, no. 5, pp. 1–22, 2019, doi: 10.3390/en12050776.

[66] G. Mavromatidis and I. Petkov, "MANGO: A novel optimization model for the long-term, multi-stage planning of decentralized multi-energy systems," Appl. Energy, vol. 288, no. December 2020, p. 116585, 2021, doi: 10.1016/j.apenergy.2021.116585. [Online]. Available: https://doi.org/10.1016/j.apenergy.2021.116585

[67] P. Gabrielli, M. Gazzani, E. Martelli, and M. Mazzotti, "Optimal design of multi-energy systems with seasonal storage," Appl. Energy, vol. 219, no. July 2017, pp. 408–424, 2018, doi: 10.1016/j.apenergy.2017.07.142. [Online]. Available: https://doi.org/10.1016/j.apenergy.2017.07.142

[68] I. Petkov, P. Gabrielli, and M. Spokaite, "The impact of urban district composition on storage technology reliance: trade-offs between thermal storage, batteries, and power-to-hydrogen," Energy, vol. 224, p. 120102, Jun. 2021, doi: 10.1016/j.energy.2021.120102. [Online]. Available: https://linkinghub.elsevier.com/retrieve/pii/S0360544221003510

[69] P. Murray, K. Orehounig, D. Grosspietsch, and J. Carmeliet, "A comparison of storage systems in neighbourhood decentralized energy system applications from 2015 to 2050," Appl. Energy, vol. 231, no. May 2018, pp. 1285–1306, 2018, doi: 10.1016/j.apenergy.2018.08.106. [Online]. Available: https://doi.org/10.1016/j.apenergy.2018.08.106

[70] I. Petkov and P. Gabrielli, "Power-to-hydrogen as seasonal energy storage: an uncertainty analysis for optimal design of low-carbon multi-energy systems," Appl. Energy, vol. 274, no. June, p. 115197, 2020, doi: 10.1016/j.apenergy.2020.115197. [Online]. Available: https://doi.org/10.1016/j.apenergy.2020.115197

[71] P. Murray, J. Carmeliet, and K. Orehounig, "Multi-Objective Optimisation of Power-to-Mobility in Decentralised Multi-Energy Systems," Energy, vol. 205, p. 117792, 2020, doi: 10.1016/j.energy.2020.117792. [Online]. Available: https://doi.org/10.1016/j.energy.2020.117792

[72] M. Mittelviefhaus, G. Pareschi, J. Allan, G. Georges, and K. Boulouchos, "Optimal investment and scheduling of residential multi-energy systems including electric mobility: A cost-effective approach to climate change mitigation," Appl. Energy, vol. 301, no. June, p. 117445, 2021, doi: 10.1016/j.apenergy.2021.117445. [Online]. Available: https://doi.org/10.1016/j.apenergy.2021.117445

[73] A. Maroufmashat, M. Fowler, S. Sattari Khavas, A. Elkamel, R. Roshandel, and A. Hajimiragha, "Mixed integer linear programing based approach for optimal planning and operation of a smart urban energy network to support the hydrogen economy," Int. J. Hydrogen Energy, vol. 41, no. 19, pp. 7700–7716, 2016, doi: 10.1016/j.ijhydene.2015.08.038. [Online]. Available: http://dx.doi.org/10.1016/j.ijhydene.2015.08.038

[74] B. Drijver, M. Van Aarssen, and B. De Zwart, "High-temperature aquifer thermal energy storage (HT-ATES): sustainable and multi-usable," in Innostock 2012 - 12th International Conference on Energy Storage, 2012, vol. 1, no. 16-18 May, pp. 1–10 [Online]. Available: https://www.iftechnology.com/wp-content/uploads/2018/05/Drijver-et-al-2012-High-temperature-aquifer-thermal-energy-storage-HT-ATES-sustainable-and-multi-usable-1.pdf

[75] M. Wesselink, W. Liu, J. Koornneef, and M. van den Broek, "Conceptual market potential framework of high temperature aquifer thermal energy storage - A case study in the Netherlands," Energy, vol. 147, pp. 477–489, 2018, doi: 10.1016/j.energy.2018.01.072. [Online]. Available: https://doi.org/10.1016/j.energy.2018.01.072

[76] N. Hartog, M. Bloemendal, E. Slingerland, and A. van Wijk, "Duurzame warmte gaat ondergronds," Nieuwegein, 2016 [Online]. Available: https://library.kwrwater.nl/publication/54683679/

[77] T. Brown, D. Schlachtberger, A. Kies, S. Schramm, and M. Greiner, "Synergies of sector coupling and transmission reinforcement in a cost-optimised, highly renewable European energy system," Energy, vol. 160, pp. 720–739, 2018, doi: 10.1016/j.energy.2018.06.222. [Online]. Available: https://doi.org/10.1016/j.energy.2018.06.222

[78] R. McKenna, D. Fehrenbach, and E. Merkel, "The role of seasonal thermal energy storage in increasing renewable heating shares: A techno-economic analysis for a typical residential district," Energy Build., vol. 187, pp. 38–49, 2019, doi: 10.1016/j.enbuild.2019.01.044. [Online]. Available: https://doi.org/10.1016/j.enbuild.2019.01.044

[79] I. Sarbu and C. Sebarchievici, "A comprehensive review of thermal energy storage," Sustain., vol. 10, no. 1, 2018, doi: 10.3390/su10010191.

[80] T. Yang, W. Liu, G. J. Kramer, and Q. Sun, "Seasonal thermal energy storage: A techno-economic literature review," Renew. Sustain. Energy Rev., vol. 139, no. January, p. 110732, 2021, doi: 10.1016/j.rser.2021.110732. [Online]. Available: https://doi.org/10.1016/j.rser.2021.110732

[81] PBL Netherlands Environmental Assessment Agency, "The Geography of Future Water Challenges - Bending the Trend," 2023 [Online]. Available: https://www.pbl.nl/en/publications/geography-of-future-water-challenges

[82] IEA, "Introduction to the water-energy nexus." IEA, Paris, 2020 [Online]. Available: https://www.iea.org/articles/introduction-to-the-water-energy-nexus

[83] Directorate-General for Environment, "Proposal for a directive concerning urban wastewater treatment (recast)." European Commission, Brussels, 2022 [Online]. Available: https://environment.ec.europa.eu/publications/proposal-revised-urban-wastewater-treatment-directive_en

[84] IEA, "Clean energy can help to ease the water crisis." IEA, Paris, 2023 [Online]. Available: https://www.iea.org/commentaries/clean-energy-can-help-to-ease-the-water-crisis. [Accessed: Mar. 27, 2023]

[85] S. Werner, "International review of district heating and cooling," Energy, vol. 137, pp. 617–631, 2017, doi: 10.1016/j.energy.2017.04.045.

[86] Hydrogen Council, "Hydrogen decarbonization pathways A life-cycle assessment," no. January, 2021 [Online]. Available: https://hydrogencouncil.com/en/hydrogen-decarbonization-pathways/

[87] C. Kaandorp, N. van de Giesen, and E. Abraham, "The water use of heating pathways to 2050: Analysis of national and urban energy scenarios," Environ. Res. Lett., vol. 16, no. 5, 2021, doi: 10.1088/1748-9326/abede7.

[88] T. M. I. Mahlia, T. J. Saktisahdan, A. Jannifar, M. H. Hasan, and H. S. C. Matseelar, "A review of available methods and development on energy storage; Technology update," Renew. Sustain. Energy Rev., vol. 33, pp. 532–545, 2014, doi: 10.1016/j.rser.2014.01.068. [Online]. Available: http://dx.doi.org/10.1016/j.rser.2014.01.068

[89] I. Sarbu and E. S. Valea, "Energy savings potential for pumping water in district heating stations," Sustain., vol. 7, no. 5, pp. 5705–5719, 2015, doi: 10.3390/su7055705.

[90] J. I. Ahmad, S. Giorgi, L. Zlatanovic, G. Liu, and J. P. van der Hoek, "Maximizing thermal energy recovery from drinking water for cooling purpose," Energies, vol. 14, no. 9, pp. 1–14, 2021, doi: 10.3390/en14092413.

[91] J. P. Van Der Hoek, "Climate change mitigation by recovery of energy from the water cycle: A new challenge for water management," Water Sci. Technol., vol. 65, no. 1, pp. 135–141, 2012, doi: 10.2166/wst.2011.820.

[92] K. L. Lam and J. P. van der Hoek, "Low-Carbon Urban Water Systems: Opportunities beyond Water and Wastewater Utilities?," Environ. Sci. Technol., vol. 54, no. 23, pp. 14854–14861, Dec. 2020, doi: 10.1021/acs.est.0c05385. [Online]. Available: https://pubs.acs.org/doi/10.1021/acs.est.0c05385

[93] Z. Deng, S. Mol, and J. P. Van Der Hoek, "Shower heat exchanger: Reuse of energy from heated drinking water for CO_2 reduction," Drink. Water Eng. Sci., vol. 9, no. 1, pp. 1–8, 2016, doi: 10.5194/dwes-9-1-2016.

[94] G. T. Daigger, N. Voutchkov, U. Lall, and W. Sarni, "The Future of Water," Water and Sanitation Division. Inter-American Development Bank, 2019 [Online]. Available: https://publications.iadb.org/publications/english/document/The_Future_of_Water_A_Collection_of_Essays_on_"Disruptive"_Technologies_that_may_Transform_the_Water_Sector_in_the_Next_10_Years.pdf

[95] J. A. Elías-Maxil, J. P. Van Der Hoek, J. Hofman, and L. Rietveld, "Energy in the urban water cycle: Actions to reduce the total expenditure of fossil fuels with emphasis on heat reclamation from urban water," Renew. Sustain. Energy Rev., vol. 30, pp. 808–820, 2014, doi: 10.1016/j.rser.2013.10.007.

[96] IPCC, "Summary for policymakers," in Climate Change 2021: The Physical Science Basis. Contribution of Working Group I to the Sixth Assessment Report of the Intergovernmental Panel on Climate Change, V. Masson-Delmotte, P. Zhai, A. Pirani, S. L. Connors, C. Péan, S. Berger, N. Caud, Y. Chen, L. Goldfarb, M. I. Gomis, M. Huang, K. Leitzell, E. Lonnoy, J. B. R. Matthews, T. K. Maycock, T. Waterfield, O. Yelekçi, R. Yu, and B. Zhou, Eds. Cambridge, United Kingdom and New York, NY, USA: Cambridge University Press, 2021 [Online]. Available: https://www.ipcc.ch/report/ar6/wg1/

[97] K. G. Zuurbier, "Increasing Freshwater Recovery Upon Aquifer Storage," Technische Universiteit Delft, 2016 [Online]. Available: http://www.subsol.org/uploads/deliverables/LR-Thesis_KoenZuurbier.pdf

[98] K. G. Zuurbier, M. Bakker, W. J. Zaadnoordijk, and P. J. Stuyfzand, "Identification of potential sites for aquifer storage and recovery (ASR) in coastal areas using ASR performance estimation methods," Hydrogeol. J., vol. 21, no. 6, pp. 1373–1383, 2013, doi: 10.1007/s10040-013-1003-2.

[99] Knowledge for Climate, "Climate Proof Cities," 2014 [Online]. Available: http://knowledgeforclimate.climateresearchnetherlands.nl/%5Cnhttp://knowledgeforclimate.climateresearchnetherlands.nl/climateproofcities

[100] van Duuren, van Alphen, Koop, and de Bruin, "Potential Transformative Changes in Water Provision Systems: Impact of Decentralised Water Systems on Centralised Water Supply Regime," Water, vol. 11, no. 8, p. 1709, Aug. 2019, doi: 10.3390/w11081709. [Online]. Available: https://www.mdpi.com/2073-4441/11/8/1709

[101] G. Mavromatidis et al., "Ten questions concerning modeling of distributed multi-energy systems," Build. Environ., vol. 165, no. June, p. 106372, 2019, doi: 10.1016/j.buildenv.2019.106372. [Online]. Available: https://doi.org/10.1016/j.buildenv.2019.106372

[102] M. Papapetrou, G. Kosmadakis, A. Cipollina, U. La Commare, and G. Micale, "Industrial waste heat: Estimation of the technically available resource in the EU per industrial sector, temperature level and country," Appl. Therm. Eng., vol. 138, no. February, pp. 207–216, 2018, doi: 10.1016/j.applthermaleng.2018.04.043. [Online]. Available: https://doi.org/10.1016/j.applthermaleng.2018.04.043

[103] T. Fleiter et al., "Excess heat potentials of industrial sites in Europe, Documentation of excess heat potentials of industrial sites including open data file with selected potentials," pp. 1–76, 2020 [Online]. Available: https://www.seenergies.eu/wp-content/uploads/sites/25/2020/04/sEEnergies-WP5_D5.1-Excess_heat_potentials_of_industrial_sites_in_Europe.pdf

[104] IPCC, "IPCC special report on the impacts of global warming of 1.5 °C - Summary for policy makers," no. October 2018, 2018 [Online]. Available: http://www.ipcc.ch/report/sr15/

[105] A. van Wijk, E. van der Roest, and J. Boere, Solar power to the people (ENG). Amsterdam: Allied Waters/IOS Press BV, 2017 [Online]. Available: https://www.alliedwaters.com/wp-content/uploads/2017/11/19-12-ENG-Solar-Power-to-the-people.pdf

[106] IRENA, "Renewable Power Generation Costs in 2017," 2018 [Online]. Available: https://www.irena.org/-/media/Files/IRENA/Agency/Publication/2018/Jan/IRENA_2017_Power_Costs_2018.pdf

[107] IEA, "The Future of Hydrogen," Paris, 2019 [Online]. Available: https://www.iea.org/publications/reports/thefutureofhydrogen/

[108] OECD/IEA, "Global EV Outlook 2018 - Towards cross-modal electrification," 2018 [Online]. Available: https://www.iea.org/gevo2018/

[109] IRENA, "Electricity storage and renewables: Costs and markets to 2030," 2017 [Online]. Available: https://www.irena.org/publications/2017/Oct/Electricity-storage-and-renewables-costs-and-markets

[110] Climate Policy Initiative, Copenhagen Economics, and Energy Transitions Commission, "A new electricity era : How to decarbonize energy systems through electrification," no. January. 2017 [Online]. Available: https://www.energy-transitions.org/publications/a-new-electricity-era/

[111] J. L. Moraga and M. Mulder, "Electrification of Heating and transport - a scenario analysis for the Netherlands up to 2050," CEER Policy Papers 2 - University of Groningen, Groningen, 2018 [Online]. Available: https://www.rug.nl/ceer/blog/electrification-report.pdf

[112] R. Baetens et al., "Assessing electrical bottlenecks at feeder level for residential net zero-energy buildings by integrated system simulation," Appl. Energy, vol. 96, pp. 74–83, 2012, doi: 10.1016/j.apenergy.2011.12.098. [Online]. Available: http://dx.doi.org/10.1016/j.apenergy.2011.12.098

[113] R. J. Nicholls and A. Cazenave, "Sea-Level Rise and Its Impact on Coastal Zones," Science (80-.)., vol. 328, no. 5985, pp. 1517–1520, Jun. 2010, doi: 10.1126/science.1185782. [Online]. Available: http://www.sciencemag.org/cgi/doi/10.1126/science.1185782

[114] H. Lund, P. A. Østergaard, D. Connolly, and B. V. Mathiesen, "Smart energy and smart energy systems," Energy, vol. 137, pp. 556–565, 2017, doi: 10.1016/j.energy.2017.05.123. [Online]. Available: https://doi.org/10.1016/j.energy.2017.05.123

[115] J. Keirstead, M. Jennings, and A. Sivakumar, "A review of urban energy system models: Approaches, challenges and opportunities," Renew. Sustain. Energy Rev., vol. 16, no. 6, pp. 3847–3866, 2012, doi: 10.1016/j.rser.2012.02.047. [Online]. Available: http://dx.doi.org/10.1016/j.rser.2012.02.047

[116] R. Niemi, J. Mikkola, and P. D. Lund, "Urban energy systems with smart multi-carrier energy networks and renewable energy generation," Renew. Energy, vol. 48, pp. 524–536, 2012, doi: 10.1016/j.renene.2012.05.017. [Online]. Available: http://dx.doi.org/10.1016/j.renene.2012.05.017

[117] B. Morvaj, R. Evins, and J. Carmeliet, "Optimising urban energy systems: Simultaneous system sizing, operation and district heating network layout," Energy, vol. 116, pp. 619–636, 2016, doi: 10.1016/j.energy.2016.09.139. [Online]. Available: http://dx.doi.org/10.1016/j.energy.2016.09.139

[118] G. De Luca, S. Fabozzi, N. Massarotti, and L. Vanoli, "A renewable energy system for a nearly zero greenhouse city: Case study of a small city in southern Italy," Energy, vol. 143, pp. 347–362, 2018, doi: 10.1016/j.energy.2017.07.004. [Online]. Available: https://doi.org/10.1016/j.energy.2017.07.004

[119] S. Haehnlein, P. Bayer, and P. Blum, "International legal status of the use of shallow geothermal energy," Renew. Sustain. Energy Rev., vol. 14, no. 9, pp. 2611–2625, 2010, doi: 10.1016/j.rser.2010.07.069. [Online]. Available: http://dx.doi.org/10.1016/j.rser.2010.07.069

[120] L. F. Cabeza et al., "CO_2 mitigation accounting for Thermal Energy Storage (TES) case studies," Appl. Energy, vol. 155, pp. 365–377, 2015, doi: 10.1016/j.apenergy.2015.05.121. [Online]. Available: http://dx.doi.org/10.1016/j.apenergy.2015.05.121

[121] P. Fleuchaus, B. Godschalk, I. Stober, and P. Blum, "Worldwide application of aquifer thermal energy storage – A review," Renew. Sustain. Energy Rev., vol. 94, no. November 2017, pp. 861–876, 2018, doi: 10.1016/j.rser.2018.06.057. [Online]. Available: https://doi.org/10.1016/j.rser.2018.06.057

[122] B. Ciapała, J. Jurasz, and M. Janowski, "Ultra-low-temperature district heating systems – a way to maximise the ecological and economical effect of an investment?," in 10th Conference on Interdisciplinary Problems in Environmental Protection and Engineering EKO-DOK 2018, 2018, vol. 00018, pp. 1–5.

[123] R. Lund, D. S. Østergaard, X. Yang, and B. V. Mathiesen, "Comparison of Low-temperature District Heating Concepts in a Long-Term Energy System Perspective," Int. J. Sustain. Energy Plan. Manag., vol. 12, no. 0, pp. 5–18, 2017, doi: 10.5278/ijsepm.2017.17.x. [Online]. Available: https://journals.aau.dk/index.php/sepm/article/view/1661/1421

[124] M. Bloemendal and N. Hartog, "Thermal Energy Storage with geothermal triplet for space heating and cooling," in EGU General Assembly 2017, 2017 [Online]. Available: http://meetingorganizer.copernicus.org/EGU2017/EGU2017-3626.pdf

[125] M. Bloemendal and N. Hartog, "Analysis of the impact of storage conditions on the thermal recovery efficiency of low-temperature ATES systems," Geothermics, vol. 71, no. June 2017, pp. 306–319, 2018, doi: 10.1016/j.geothermics.2017.10.009. [Online]. Available: http://dx.doi.org/10.1016/j.geothermics.2017.10.009

[126] J. H. van Lopik, N. Hartog, and W. J. Zaadnoordijk, "The use of salinity contrast for density difference compensation to improve the thermal recovery efficiency in high-temperature aquifer thermal energy storage systems," Hydrogeol. J., pp. 1255–1271, 2016, doi: 10.1007/s10040-016-1366-2. [Online]. Available: http://link.springer.com/article/10.1007/s10040-016-1366-2/fulltext.html

[127] A. Réveillère, V. Hamm, H. Lesueur, E. Cordier, and P. Goblet, "Geothermal contribution to the energy mix of a heating network when using aquifer thermal energy storage: Modeling and application to the paris basin," Geothermics, vol. 47, pp. 69–79, 2013, doi: 10.1016/j.geothermics.2013.02.005.

[128] KPMG Automotive Institute, "KPMG's 20th Global Automotive Executive Survey 2019," 2019 [Online]. Available: https://automotive-institute.kpmg.de/GAES2019/

[129] A. Buttler and H. Spliethoff, "Current status of water electrolysis for energy storage, grid balancing and sector coupling via power-to-gas and power-to-liquids: A review," Renew. Sustain. Energy Rev., vol. 82, no. September 2017, pp. 2440–2454, 2018, doi: 10.1016/j.rser.2017.09.003.

[130] W. van Sark, "Opbrengst van zonnestroomsystemen in Nederland," 2014 [Online]. Available: https://www.rvo.nl/sites/default/files/2019/02/Opbrengst van zonnestroomsystemen in NL.pdf

[131] CBS, PBL, RIVM, and WUR, "Jaarlijkse hoeveelheid neerslag in Nederland, 1910-2015," 2016. [Online]. Available: https://www.clo.nl/indicatoren/nl050806-jaarlijkse-hoeveelheid-neerslag-in-nederland. [Accessed: Aug. 02, 2019]

[132] J. Wood, J. Gifford, J. Arba, and M. Shaw, "Production of ultrapure water by continuous electrodeionization," Desalination, vol. 250, no. 3, pp. 973–976, 2010, doi: 10.1016/j.desal.2009.09.084. [Online]. Available: http://dx.doi.org/10.1016/j.desal.2009.09.084

[133] Dorin, "Dorin software." 2018 [Online]. Available: http://www.dorin.com/en/Software/

[134] E. van der Roest, L. Snip, M. Bloemendal, and A. van Wijk, "Power-to-X," Nieuwegein, KWR 2018.032, 2018 [Online]. Available: https://library.kwrwater.nl/publication/56051448/

[135] Thyssenkrupp, "Hydrogen from large-scale electrolysis." 2018 [Online]. Available: https://www.thyssenkrupp-uhde-chlorine-engineers.com/en/products/water-electrolysis-hydrogen-production/power-to-gas/

[136] Hydrogenics, "Hydrogenics' HyLYZER® 600." p. 1350, 2017 [Online]. Available: http://www.hydrogenics.com/wp-content/uploads/HyLYZER_600_3MW.pdf

[137] ACM, "Warmtetarieven," 2019. [Online]. Available: https://www.acm.nl/nl/warmtetarieven. [Accessed: Jan. 25, 2019]

[138] DGMR, "Referentie gebouwen BENG," p. 101, 2015 [Online]. Available: https://www.rvo.nl/sites/default/files/2017/02/Referentiegebouwen BENG.pdf

[139] CBS, "Energieverbruik woningen naar bewonersklasse 2016," 2017. [Online]. Available: https://www.cbs.nl/nl-nl/maatwerk/2017/36/energieverbruik-woningen-naar-bewonersklasse-2016. [Accessed: Apr. 17, 2019]

[140] P. J. J. G. Geudens, "Tarievenoverzicht drinkwater per 1 januari 2019." Vewin, Den Haag, 2019 [Online]. Available: http://www.vewin.nl/SiteCollectionDocuments/Publicaties/Cijfers/Tarievenoverzicht-drinkwater-2019.pdf

[141] Energinet.dk and The Danish Energy Agency, "Technology data for energy plants." p. 212, 2012 [Online]. Available: https://www.osti.gov/etdeweb/servlets/purl/1045519

[142] IEA ETSAP, "District Heating," no. January. IEA ETSAP, 2013 [Online]. Available: https://iea-etsap.org/E-TechDS/PDF/E16_DistrHeat_EA_Final_Jan2013_GSOK.pdf

[143] M. Blom and S. Ahdour, "Socialiseren van netkosten van warmtenetten," Delft, 2017.

[144] L. Beurskens and J. Lemmens, "Conceptadvies SDE+ 2019 Zonne-energie." PBL, Den Haag, 2018.

[145] A. Isenstadt and N. Lutsey, "Developing hydrogen fueling infrastructure for fuel cell vehicles: A status update," 2017 [Online]. Available: https://www.theicct.org/publications/developing-hydrogen-fueling-infrastructure-fuel-cell-vehicles-status-update

[146] M. Bloemendal et al., "Innovatieve oplossingen waterketen Lelystad Airport en Lelystad Airport Businesspark," 2016 [Online]. Available: http://www.tkiwatertechnologie.nl/wp-content/uploads/2015/08/KWR-2016_033-Sustainable-Airport-Lelystad.pdf

[147] Werkgroep Discontovoet, "Rapport werkgroep discontovoet 2015," Den Haag, 2015 [Online]. Available: https://zoek.officielebekendmakingen.nl/blg-619458

[148] Onderzoeksraad voor Veiligheid, "Koolmonoxide: Onderschat en onbegrepen gevaar," Den Haag, 2015 [Online]. Available: https://www.onderzoeksraad.nl/nl/onderzoek/2040/koolmonoxide-onderschat-en-onbegrepen-gevaar/publicatie?s=9FA1D8006A6B5C26B2C24A233E7A4D128A26210E#fasen

[149] K. Sircar, J. Clower, M. K. Shin, C. Bailey, M. King, and F. Yip, "Carbon monoxide poisoning deaths in the United States, 1999 to 2012," Am. J. Emerg. Med., vol. 33, no. 9, pp. 1140–1145, 2015, doi: 10.1016/j.ajem.2015.05.002. [Online]. Available: http://dx.doi.org/10.1016/j.ajem.2015.05.002

[150] SKAO, Stimular, Connekt, Milieu Centraal, and Ministerie van Infrastructuur en Milieu, "CO_2 emissiefactoren," 2022. [Online]. Available: https://CO_2emissiefactoren.nl/. [Accessed: Nov. 16, 2022]

[151] J. Stiglitz et al., "Report of the High-Level Commission on Carbon Prices," 2017 [Online]. Available: https://www.carbonpricingleadership.org/report-of-the-highlevel-commission-on-carbon-prices

[152] Agora Energiewende, "The Integration Costs of Wind and Solar Power," 2015 [Online]. Available: https://www.agora-energiewende.de/en/events/the-integration-costs-of-wind-and-solar-power-2/

[153] K. Bruninx, E. Delarue, H. Ergun, K. May, K. Van Den Bergh, and D. Van Hertem, "Determining the impact of renewable energy on balancing costs, back up costs, grid costs and subsidies," 2016 [Online]. Available: http://www.creg.info/pdf/ARCC/161019-KULeuven.pdf

[154] J. Warnaars, A. Kooiman, and B. den Ouden, "Systeemconsequenties van Ecovat," 2018 [Online]. Available: https://www.berenschot.nl/actueel/2018/juli/berenschot-berekent-vergeten/

[155] K. van Kranenburg, R. de Kler, N. Jansen, A. van der Veen, C. de Vos, and H. Gelevert, "Waterstof uit elektrolyse voor maatschappelijk verantwoord netbeheer - Business model en business case," Den Haag, 2018 [Online]. Available: https://www.enpuls.nl/media/2350/eindrapport-module-3-_-businessmodel-en-businesscase-_-enpuls.pdf

[156] T. v. Melle, L. Ramaekers, and W. Terlouw, "Waarde van slimme netten," 2014 [Online]. Available: https://www.netbeheernederland.nl/_upload/Files/Waarde_van_slimme_netten_141.pdf

[157] ACM, "Warmtetarieven," 2018. [Online]. Available: https://www.acm.nl/nl/onderwerpen/energie/energiebedrijven/warmte/warmtetarieven. [Accessed: Jan. 31, 2018]

[158] CBS, "Energieverbruik particuliere woningen; woningtype en regio's," 2018. [Online]. Available: https://opendata.cbs.nl/statline/#/CBS/nl/dataset/81528NED/table?dl=3FC71. [Accessed: Oct. 15, 2020]

[159] O. Schmidt, A. Hawkes, A. Gambhir, and I. Staffell, "The future cost of electrical energy storage based on experience rates," Nat. Energy, vol. 6, no. July, p. 17110, 2017, doi: 10.1038/nenergy.2017.110. [Online]. Available: http://www.nature.com/articles/nenergy2017110

[160] O. Schmidt, A. Gambhir, I. Staffell, A. Hawkes, J. Nelson, and S. Few, "Future cost and performance of water electrolysis: An expert elicitation study," Int. J. Hydrogen Energy, vol. 42, no. 52, pp. 30470–30492, 2017, doi: 10.1016/j.ijhydene.2017.10.045. [Online]. Available: https://doi.org/10.1016/j.ijhydene.2017.10.045

[161] S. M. Saba, M. Müller, M. Robinius, and D. Stolten, "The investment costs of electrolysis – A comparison of cost studies from the past 30 years," Int. J. Hydrogen Energy, vol. 43, no. 3, pp. 1209–1223, Jan. 2018, doi: 10.1016/j.ijhydene.2017.11.115. [Online]. Available: https://linkinghub.elsevier.com/retrieve/pii/S0360319917344956

[162] M. Weiss, M. Junginger, and M. K. Patel, Learning energy efficiency - Experience curves for household appliances and space heating , cooling , and lighting technologies. Utrecht: Copernicus Institute – Research Institute for Sustainable Development and Innovation, 2008 [Online]. Available: http://reflex-project.eu/wp-content/uploads/2018/12/REFLEX_policy_brief_Experience_curves_12_2018.pdf

[163] A. Louwen, M. Junginger, and A. Krishnan, "Reflex policy brief - Technological Learning in Energy Modelling : Experience Curves," 2018 [Online]. Available: http://reflex-project.eu/wp-content/uploads/2018/12/REFLEX_policy_brief_Experience_curves_12_2018.pdf

[164] EHPA, "European Heat Pump Market and Statistics Report," 2014.

[165] IEA, "The Future of Cooling," Futur. Cool., 2018, doi: 10.1787/9789264301993-en.

[166] REN21, Renewables 2020 Global Status Report. Paris: REN21 Secretariat, 2020 [Online]. Available: https://www.ren21.net/wp-content/uploads/2019/05/gsr_2020_full_report_en.pdf

[167] European Energy Agency, Trends and projections in Europe 2019, no. 15. Luxembourg: Publications Office of the European Union, 2019 [Online]. Available: https://www.eea.europa.eu/publications/trends-and-projections-in-europe-1

[168] IEA, "Power systems in transition," Paris, 2020 [Online]. Available: https://www.iea.org/reports/power-systems-in-transition

[169] REN21, Renewables Global Futures Report. Paris: REN21, 2017 [Online]. Available: https://www.ren21.net/2017-renewables-global-futures-report/

[170] Y. Parag and B. K. Sovacool, "Electricity market design for the prosumer era," Nat. Energy, vol. 1, no. 4, p. 16032, Apr. 2016, doi: 10.1038/nenergy.2016.32. [Online]. Available: http://www.nature.com/articles/nenergy201632

[171] E. van der Roest, L. Snip, T. Fens, and A. van Wijk, "Introducing Power-to-H3: Combining renewable electricity with heat, water and hydrogen production and storage in a neighbourhood," Appl. Energy, vol. 257, 2020, doi: 10.1016/j.apenergy.2019.114024.

[172] M. Bloemendal, A. Van Wijk, and N. Hartog, "Verwarming en koeling zonder warmtepomp met WKO-triplet," H_2O, no. december 2017, pp. 1–9 [Online]. Available: https://www.h2owaternetwerk.nl/vakartikelen/verwarming-en-koeling-zonder-warmtepomp-met-wko-triplet

[173] HOMER Energy, "How HOMER Calculates the PV Array Power Output." [Online]. Available: https://www.homerenergy.com/products/grid/docs/1.5/how_homer_calculates_the_pv_array_power_output.html. [Accessed: Nov. 21, 2020]

[174] O. Ruhnau, L. Hirth, and A. Praktiknjo, "Time series of heat demand and heat pump efficiency for energy system modeling," Sci. data, vol. 6, no. 1, p. 189, 2019, doi: 10.1038/s41597-019-0199-y. [Online]. Available: http://dx.doi.org/10.1038/s41597-019-0199-y

[175] K. Zuurbier and T. van Dooren, “Urban Waterbuffer Spangen: Resultaten,” Nieuwegein, KWR 2019.111, 2019 [Online]. Available: http://api.kwrwater.nl/uploads/2020/01/KWR-2019.111-Urban-Waterbuffer-Spangen-Resultaten.-Deelrapport-TKI-project-Urban-Waterbuffer.pdf

[176] K. Mongird et al., “Energy Storage Technology and Cost Characterization Report | Department of Energy,” 2019 [Online]. Available: https://www.energy.gov/eere/water/downloads/energy-storage-technology-and-cost-characterization-report

[177] S. S. Farahani, C. Bleeker, A. van Wijk, and Z. Lukszo, “Hydrogen-based integrated energy and mobility system for a real-life office environment,” Appl. Energy, vol. 264, no. March, p. 114695, 2020, doi: 10.1016/j.apenergy.2020.114695. [Online]. Available: https://doi.org/10.1016/j.apenergy.2020.114695

[178] Fraunhofer ISE, “Current and Future Cost of Photovoltaics: Long-term Scenarios for Market Development.,” 2015 [Online]. Available: https://www.ise.fraunhofer.de/content/dam/ise/de/documents/publications/studies/AgoraEnergiewende_Current_and_Future_Cost_of_PV_Feb2015_web.pdf

[179] E. Vartiainen, G. Masson, and C. Breyer, “PV LCOE in Europe 2014-2030, final report, 23 June 2015,” 2015 [Online]. Available: http://www.etip-pv.eu/fileadmin/Documents/FactSheets/English2015/PV_LCOE_Report_July_2015.pdf

[180] Goldman Sachs, “NextGen Power: Solar to transform Europe’ s energy mix,” 2018 [Online]. Available: https://www.goldmansachs.com/insights/pages/gs-research/nextgen-power/report.pdf

[181] Hydrogen Europe, “Technology Roadmaps Full Pack,” 2018 [Online]. Available: https://hydrogeneurope.eu/sites/default/files/2018-10/Public_HE Tech Roadmaps_full pack_0.pdf

[182] A. Van Wijk and J. Chatzimarkakis, “Hydrogen Europe sets out 2×40 GW green hydrogen initiative,” Fuel Cells Bull., no. 5, pp. 10–11, May 2020, doi: 10.1016/S1464-2859(20)30204-2. [Online]. Available: http://www.magonlinelibrary.com/doi/10.1016/S1464-2859%2820%2930204-2

[183] EnergiNet and The Danish Energy Agency, “Technology Data - Generation of Electricity and District Heating,” 2020 [Online]. Available: https://ens.dk/en/our-services/projections-and-models/technology-data/technology-data-generation-electricity-and

[184] Fuel Cells and Hydrogen Joint Undertaking (FCHJU), “State-of-the-art and future targets (KPIs) - Large scale FC installations, converting hydrogen and renewable methane into power in various applications (0.4 - 30 MW),” 2020. [Online]. Available: https://www.clean-hydrogen.europa.eu/large-scale-fc-installations-converting-hydrogen-and-renewable-methane-power-various-applications-04_en. [Accessed: Nov. 30, 2020]

[185] C. Arpagaus, F. Bless, M. Uhlmann, J. Schiffmann, and S. S. Bertsch, “High temperature heat pumps: Market overview, state of the art, research status, refrigerants, and application potentials,” Energy, vol. 152, pp. 985–1010, 2018, doi: 10.1016/j.energy.2018.03.166.

[186] TNO and ISPT, “Cost reduction industrial heat pumps (CRUISE),” Amersfoort, 2019 [Online]. Available: https://ispt.eu/projects/cruise/

[187] O. Gudmundsson, J. E. Thorsen, and L. Zhang, “Cost analysis of district heating compared to its competing technologies,” in WIT Transactions on Ecology and the Environment, 2013, vol. 176, no. June 2013, pp. 107–118, doi: 10.2495/ESUS130091.

[188] N. Naber, B. Schepers, M. Schuurbiers, and F. Rooijers, “Een klimaatneutrale warmtevoorziening voor de gebouwde omgeving – update 2016,” 2016 [Online]. Available: https://www.ce.nl/publicatie/een_klimaatneutrale_warmtevoorziening_voor_de_gebouwde_omgeving_-_update_2016/1838

[189] E. van Vliet, J. de Keijzer, E. Slingerland, J. van Tilburg, W. Hofsteenge, and V. Haaksma, “Collectieve warmte naar lage temperatuur - Een verkenning van mogelijkheden,” 2016 [Online]. Available: https://www.ecofys.com/files/files/collectieve-warmte-naar-lage-temperatuur.pdf

[190] N. Hoogervorst, "Waterstof voor de gebouwde omgeving; operationalisering in de Startanalyse 2020," 2020 [Online]. Available: https://www.pbl.nl/sites/default/files/downloads/pbl-2020-waterstof-voor-de-gebouwde-omgeving-operationalisering-in-de-startanalyse-2020_4250.pdf

[191] Milieu Centraal, "Energierekening," 2020. [Online]. Available: https://www.milieucentraal.nl/energie-besparen/snel-besparen/grip-op-je-energierekening/energierekening/. [Accessed: Nov. 30, 2020]

[192] M. Weeda and R. Niessink, "Waterstof als optie voor een klimaatneutrale warmtevoorziening in de bestaande bouw," 2020 [Online]. Available: https://energy.nl/publication/waterstof-als-optie-voor-een-klimaatneutrale-warmtevoorziening-in-de-bestaande-bouw/

[193] Fuel Cells and Hydrogen Joint Undertaking (FCH), "Hydrogen Roadmap Europe," 2019 [Online]. Available: https://www.fch.europa.eu/sites/default/files/Hydrogen Roadmap Europe_Report.pdf

[194] CBS, "Gemiddelde aardgas- en elektriciteitslevering woningen, 2018," 2019. [Online]. Available: https://www.cbs.nl/-/media/_excel/2019/22/gemiddelde-aardgas-enelektriciteitslevering-woningen-2018.xls. [Accessed: Jul. 07, 2020]

[195] B. Schepers et al., "Functioneel ontwerp Vesta 4.0," 2019 [Online]. Available: https://www.pbl.nl/sites/default/files/downloads/pbl-2019-ce-delft-functioneel-ontwerp-vesta-4.0_4085.pdf

[196] D. D'Agostino and L. Mazzarella, "What is a Nearly zero energy building? Overview, implementation and comparison of definitions," J. Build. Eng., vol. 21, no. September 2018, pp. 200–212, 2019, doi: 10.1016/j.jobe.2018.10.019. [Online]. Available: https://doi.org/10.1016/j.jobe.2018.10.019

[197] N. Hoogervorst, "Kosten van klimaatneutrale elektriciteit in 2030," 2020 [Online]. Available: https://www.pbl.nl/sites/default/files/downloads/pbl-2020-kosten-van-klimaatneutrale-elektriciteit-in-2030-4252.pdf

[198] Planbureau voor de Leefomgeving, "Klimaat en Energieverkenning 2019," 2019 [Online]. Available: www.pbl.nl/kev

[199] A. Wang, K. van der Leun, D. Peters, and M. Buseman, "European Hydrogen Backbone - How a dedicated hydrogen infrastructure can be created," 2020 [Online]. Available: https://guidehouse.com/insights/energy/2020/developing-europes-hydrogen-infrastructure-plan

[200] R. E. Roobeek, "Shipping Sunshine," TU Delft, 2020 [Online]. Available: https://repository.tudelft.nl/islandora/object/uuid%3A9d1225b7-65ed-44d2-b9c9-d60cfce64a5f

[201] Renewable Energy Policy Network, Renewables 2018 · Global Status Report. Paris, 2018 [Online]. Available: www.ren21.net

[202] CBS, "Kerncijfers wijken en buurten 2018," 2018. [Online]. Available: https://www.cbs.nl/nl-nl/maatwerk/2018/30/kerncijfers-wijken-en-buurten-2018. [Accessed: Nov. 20, 2020]

[203] Netbeheer Nederland, "Basisinformatie over energie-infrastructuur," 2019 [Online]. Available: https://www.regionale-energiestrategie.nl/Nieuws/1305967.aspx

[204] NEDU, "Verbruiksprofielen - User profiles electricity 2018," 2018. [Online]. Available: https://www.nedu.nl/documenten/verbruiksprofielen/. [Accessed: Nov. 26, 2020]

[205] P. M. van Oirsouw, Netten voor distributie van elektriciteit. Arhem: Phase to Phase, 2011 [Online]. Available: https://www.phasetophase.nl/boek/

[206] Milieu Centraal, "Inductie kookplaat: elektrisch koken," 2020. [Online]. Available: https://www.milieucentraal.nl/energie-besparen/apparaten-en-verlichting/huishoudelijke-apparaten/inductie-kookplaat/. [Accessed: Nov. 06, 2020]

[207] CBS, "Personenauto's rijden gemiddeld 37 kilometer per dag," 2012. [Online]. Available: https://www.cbs.nl/nl-nl/nieuws/2012/10/personenauto-s-rijden-gemiddeld-37-kilometer-per-dag. [Accessed: Sep. 06, 2020]

[208] L. Canals Casals, E. Martinez-Laserna, B. Amante García, and N. Nieto, "Sustainability analysis of the electric vehicle use in Europe for CO_2 emissions reduction," J. Clean. Prod., vol. 127, pp. 425–437, 2016, doi: 10.1016/j.jclepro.2016.03.120. [Online]. Available: http://dx.doi.org/10.1016/j.jclepro.2016.03.120

[209] Movares, "Laadstrategie Elektrisch Wegvervoer," 2013 [Online]. Available: https://www.netbeheernederland.nl/_upload/Files/Elektrisch_vervoer_11_ccede3d2ae.pdf

[210] M. Cuijpers, M. Staats, W. Bakker, and A. Hoekstra, "Eindrapport - Toekomstverkenning elektrisch vervoer," 2016 [Online]. Available: http://www.ecofys.com/files/files/ecofys-2016-eindrapport-toekomstverkenning-elektrisch-vervoer.pdf

[211] KNMI, "Klimatologie - Uurgegevens van het weer in Nederland." [Online]. Available: http://projects.knmi.nl/klimatologie/uurgegevens/selectie.cgi. [Accessed: Feb. 21, 2020]

[212] Rijkswaterstaat, "Waterinfo," 2017. [Online]. Available: https://waterinfo.rws.nl/#!/nav/index/. [Accessed: Feb. 12, 2020]

[213] R. Hermkens, S. Jansma, M. van der Laan, H. de Laat, B. Pilzer, and K. Pulles, "Toekomstbestendige gasdistributienetten," 2018 [Online]. Available: https://www.netbeheernederland.nl/nieuws/huidige-gas-net-geschikt-te-maken-voor-waterstof-1240

[214] O. Kleefkens, "Legionella and Heat Pump Water Heaters," 2020 [Online]. Available: https://heatpumpingtechnologies.org/annex46/wp-content/uploads/sites/53/2020/10/hpt-an46-03-task-1-legionella-and-heat-pumps-1.pdf

[215] O. Kleefkens, J. Van Berkel, C. Geelen, and M. Bos, "Booster Heat Pump, development of test procedure and calculation methodology in order to estimate the energy performance in various domestic applications," in 12th IEA Heat Pump Conference, 2017, p. 12 [Online]. Available: http://hpc2017.org/wp-content/uploads/2017/05/P.1.7.5-Booster-Heat-Pump-development-of-test-procedure-and-calculation-methodology.pdf

[216] S. Jansen, S. Mohammadi, and R. Bokel, "Developing a locally balanced energy system for an existing neighbourhood, using the 'Smart Urban Isle' approach," Sustain. Cities Soc., vol. 64, no. August 2019, p. 102496, 2021, doi: 10.1016/j.scs.2020.102496. [Online]. Available: https://doi.org/10.1016/j.scs.2020.102496

[217] E. van der Roest, "Systeemontwerp Power to X," Nieuwegein, KWR 2020.004, 2020 [Online]. Available: https://library.kwrwater.nl/publication/61141429/

[218] C. Wenzlaff, G. Winterleitner, and F. Schütz, "Controlling parameters of a mono-well high-temperature aquifer thermal energy storage in porous media, Northern Oman," Pet. Geosci., vol. 25, no. 3, pp. 337–349, 2018, doi: 10.1144/petgeo2018-104.

[219] K. S. Marif, "Counteraction of buoyancy flow in high temperature aquifer thermal energy storage systems by applying multiple partially penetrating wells," TU Delft, 2019 [Online]. Available: https://repository.tudelft.nl/islandora/object/uuid%3A9e19d52e-ec21-4e4a-a2b7-be28b8b9b66c

[220] M. Collignon et al., "Evaluating thermal losses and storage capacity in high-temperature aquifer thermal energy storage (HT-ATES) systems with well operating limits: insights from a study-case in the Greater Geneva Basin, Switzerland," Geothermics, vol. 85, no. June 2019, p. 101773, 2020, doi: 10.1016/j.geothermics.2019.101773. [Online]. Available: https://doi.org/10.1016/j.geothermics.2019.101773

[221] D. G. Cirkel, B. R. Voortman, T. van Veen, and R. P. Bartholomeus, "Evaporation from (Blue-)Green Roofs: Assessing the Benefits of a Storage and Capillary Irrigation System Based on Measurements and Modeling," Water, vol. 10, no. 9, p. 1253, Sep. 2018, doi: 10.3390/w10091253. [Online]. Available: http://www.mdpi.com/2073-4441/10/9/1253

[222] Drinkwaterplatform, "Verzilting: een bedreiging voor ons drinkwater?," 2020. [Online]. Available: https://www.drinkwaterplatform.nl/verzilting-drinkwater/. [Accessed: Nov. 19, 2020]

[223] P. J. J. . Geudens and J. Grootveld, “Dutch Drinking Water Statistics 2017,” 2017 [Online]. Available: https://www.vewin.nl/SiteCollectionDocuments/Publicaties/Cijfers/Drinkwaterstatistieken-2017-EN.pdf

[224] R. Hofman-Caris et al., “Rainwater Harvesting for Drinking Water Production: A Sustainable and Cost-Effective Solution in The Netherlands?,” Water, vol. 11, no. 3, p. 511, Mar. 2019, doi: 10.3390/w11030511. [Online]. Available: https://www.mdpi.com/2073-4441/11/3/511

[225] S. Pilpola and P. D. Lund, “Different flexibility options for better system integration of wind power,” Energy Strateg. Rev., vol. 26, no. April, p. 100368, 2019, doi: 10.1016/j.esr.2019.100368. [Online]. Available: https://doi.org/10.1016/j.esr.2019.100368

[226] IEA, “Global EV Outlook 2020,” Glob. EV Outlook 2020, 2020, doi: 10.1787/d394399e-en. [Online]. Available: https://www.iea.org/reports/global-ev-outlook-2020

[227] FHP project, “Flexible Heat and Power, Connecting heat and power networks by harnessing the complexity in distributed thermal flexibility,” 2017 [Online]. Available: http://cordis.europa.eu/project/rcn/206238_en.html

[228] S. Kær, Søren Knudsen; Al Shakhshir, “Power2Hydrogen WP1 Potential of hydrogen in energy systems,” 2016 [Online]. Available: http://hybalance.eu/wp-content/uploads/2017/01/Power2Hydrogen-WP1-report-Potential-of-hydrogen-in-energy-systems.pdf

[229] F. Schilder and M. van der Stark, “Woonlastenneutraal koopwoningen verduurzamen,” 2020 [Online]. Available: https://www.pbl.nl/sites/default/files/downloads/pbl-2020-woonlastenneutraal-koopwoningen-verduurzamen-4152.pdf

[230] European Commission and Fuel Cell and Hydrogen Joint Undertaking, “Commercialisation of Energy Storage,” 2015 [Online]. Available: https://www.fch.europa.eu/publications/commercialisation-energy-storage-europe

[231] IEA, “Technology Roadmap: Energy Storage,” 2014 [Online]. Available: https://www.iea.org/reports/technology-roadmap-energy-storage

[232] B. Böckl, M. Greiml, L. Leitner, P. Pichler, L. Kriechbaum, and T. Kienberger, “HyFloW—A hybrid load flow-modelling framework to evaluate the effects of energy storage and sector coupling on the electrical load flows,” Energies, vol. 12, no. 5, 2019, doi: 10.3390/en12050956.

[233] A. David, B. V. Mathiesen, H. Averfalk, S. Werner, and H. Lund, “Heat Roadmap Europe: Large-scale electric heat pumps in district heating systems,” Energies, vol. 10, no. 4, pp. 1–18, 2017, doi: 10.3390/en10040578.

[234] A. J. Kallesøe and T. Vangilde-Pedersen, Eds., HEATSTORE Underground Thermal Energy Storage (UTES) - state-of-the-art, example cases and lessons learned. GEOTHERMICA - ERA NET Cofund Geothermal, 2019 [Online]. Available: https://www.heatstore.eu/documents/HEATSTORE_UTES State of the Art_WP1_D1.1_Final_2019.04.26.pdf

[235] E. van der Roest, T. Fens, M. Bloemendal, S. Beernink, J. P. van der Hoek, and A. J. M. van Wijk, “The Impact of System Integration on System Costs of a Neighborhood Energy and Water System,” Energies, vol. 14, no. 9, p. 2616, May 2021, doi: 10.3390/en14092616. [Online]. Available: https://www.mdpi.com/1996-1073/14/9/2616

[236] M. Bloemendal, “The hidden side of cities: Methods for governance, planning and design for optimal use of subsurface space with ATES,” TU Delft, 2018 [Online]. Available: https://doi.org/10.4233/uuid:0c6bcdac-6bf7-46c3-a4d3-53119c1a8606

[237] P. Fleuchaus, S. Schüppler, M. Bloemendal, L. Guglielmetti, O. Opel, and P. Blum, “Risk analysis of High-Temperature Aquifer Thermal Energy Storage (HT-ATES),” Renew. Sustain. Energy Rev., vol. 133, no. August, p. 110153, 2020, doi: 10.1016/j.rser.2020.110153. [Online]. Available: https://doi.org/10.1016/j.rser.2020.110153

[238] G. Schout, B. Drijver, M. Gutierrez-Neri, and R. Schotting, "Analysis of recovery efficiency in high-temperature aquifer thermal energy storage: a Rayleigh-based method," Hydrogeol. J., vol. 22, no. 1, pp. 281–291, Feb. 2014, doi: 10.1007/s10040-013-1050-8. [Online]. Available: http://link.springer.com/10.1007/s10040-013-1050-8

[239] C. D. Langevin, W. B. Shoemaker, and W. Guo, "MODFLOW-2000, the USGS modular groundwater model - Documentation of the SEAWAT-2000 version with variable density flow process and integrated MT3DMS transport process," 2003.

[240] C. Zheng and P. P. Wang, MT3DMS: A Modular Three-Dimensional Multispecies Transport Model for Simulation of Advection, Dispersion, and Chemical Reactions of Contaminants in Groundwater Systems; Documentation and User's Guide. US Army Corps of Engineers, 1999.

[241] C. D. Langevin, D. T. Thorne, A. M. Dausman, M. C. Sukop, and W. Guo, "SEAWAT Version 4: A computer program for simulation of multi-Species Solute and heat transport," 2008.

[242] M. Bakker et al., "Scripting MODFLOW Model Development Using Python and FloPy," Groundwater, vol. 54, no. 5, pp. 733–739, 2016, doi: 10.1111/gwat.12413.

[243] S. Beernink, M. Bloemendal, and N. Hartog, "Prestaties en thermische effecten van ondergrondse warmteopslagsystemen. WINDOW fase 1 (C2).," Nieuwegein, KWR 2020.146, 2020 [Online]. Available: https://www.warmingup.info/documenten/window-fase-1---c2---prestaties-en-thermische-effecten.pdf

[244] C. D. Langevin, "Modeling axisymmetric flow and transport," Ground Water, vol. 46, no. 4, pp. 579–590, 2008, doi: 10.1111/j.1745-6584.2008.00445.x. [Online]. Available: https://www.ncbi.nlm.nih.gov/pubmed/18384599

[245] J. Hecht-Mendez, N. Molina-Giraldo, P. Blum, and P. Bayer, "Evaluating MT3DMS for Heat Transport Simulation of Closed Geothermal Systems," Ground Water, vol. 48, no. 5, pp. 741–756, 2010.

[246] C. Voss, "A Finite-Element Simulation Model for Saturated-Unsaturated, Fluid-Density-Dependent Groundwater Flow with Energy Transport or Chemically-Reactive Single-Species Solute Transport," U.S. Geological Survey. p. 409, 1984.

[247] R. M. Zeghici, G. H. P. Oude Essink, N. Hartog, and W. Sommer, "Integrated assessment of variable density-viscosity groundwater flow for a high temperature mono-well aquifer thermal energy storage (HT-ATES) system in a geothermal reservoir," Geothermics, vol. 55, pp. 58–68, 2015, doi: 10.1016/j.geothermics.2014.12.006.

[248] "Calculating Degree Days," 2021. [Online]. Available: https://www.degreedays.net/calculation. [Accessed: Mar. 09, 2021]

[249] KNMI, "Database - Daggegevens van het weer in Nederland," 2017. [Online]. Available: https://www.knmi.nl/nederland-nu/klimatologie/daggegevens. [Accessed: Jul. 04, 2020]

[250] Warmtepompinfo, "Graaddagen," 2017. [Online]. Available: https://www.warmtepomp-info.nl/tapwaterkosten/graaddagen/. [Accessed: Apr. 12, 2017]

[251] S. Beernink, N. Hartog, M. Bloemendal, and M. van der Meer, "ATES systems performance in practice: analysis of operational data from ATES systems in the province of Utrecht, The Netherlands.," Proc. Eur. Geotherm. Congr. 2019 Den Haag, Netherlands, 11-14 June 2019, no. June, 2019.

[252] CBS, "Aardgas en elektriciteit, gemiddelde prijzen van eindverbruikers," 2020. [Online]. Available: https://opendata.cbs.nl/#/CBS/nl/dataset/81309NED/table?dl=59C6. [Accessed: Jan. 19, 2021]

[253] M. Zwamborn, "Berekening onrendabele top voor bodemenergiesystemen," Amersfoort, 2018.

[254] J. S. Jeon, S. R. Lee, L. Pasquinelli, and I. L. Fabricius, "Sensitivity analysis of recovery efficiency in high-temperature aquifer thermal energy storage with single well," Energy, vol. 90, pp. 1349–1359, 2015, doi: 10.1016/j.energy.2015.06.079.

[255] M. Zwamborn and R. Kleinlugenbelt, "Window fase 1 - A1. Notitie vergelijking en selectie locaties voor ondergrondse warmteopslag," Nieuwegein, KWR 2020.148, 2020 [Online]. Available: https://www.warmingup.info/documenten/window-fase-1---a1---notitie-vergelijking-en-selectie-locaties.pdf

[256] DNV, "Hydrogen forecast to 2050 - Energy Transition Outlook 2022," 2022 [Online]. Available: https://www.dnv.com/focus-areas/hydrogen/forecast-to-2050.html

[257] B. van der Zwaan, S. Lamboo, and F. Dalla Longa, "Timmermans' dream: An electricity and hydrogen partnership between Europe and North Africa," Energy Policy, vol. 159, no. August, p. 112613, 2021, doi: 10.1016/j.enpol.2021.112613. [Online]. Available: https://doi.org/10.1016/j.enpol.2021.112613

[258] A. van Wijk and F. Wouters, "Hydrogen - The bridge between Africa and Europe," in Shaping an Inclusive Energy Transition, 1st ed., M. C. P. Weijnen, Z. Lukszo, and S. Farahani, Eds. Springer Cham, 2021, pp. 91–120 [Online]. Available: https://link.springer.com/chapter/10.1007/978-3-030-74586-8_5

[259] A. van Wijk, K. Westphal, and J. F. Braun, "How to deliver on the EU Hydrogen Accelerator" [Online]. Available: https://hydrogeneurope.eu/wp-content/uploads/2022/05/How-to-deliver-on-the-EU-Hydrogen-Accelerator_Final.pdf

[260] Siemens Energy, "Silyzer PEM electrolysers, an overview." 2020 [Online]. Available: https://4echile-datastore.s3.eu-central-1.amazonaws.com/wp-content/uploads/2020/10/10132733/20200930-SE-NEB-PEM-Electrolyzer-and-Applications_EW.pdf

[261] Cummins, "HyLYZER® WATER ELECTROLYZERS," Cummings Product Specification Sheets. pp. 30–31, 2021 [Online]. Available: https://www.cummins.com/sites/default/files/2021-08/cummins-hylyzer-1000-specsheet.pdf

[262] "Power-to-Gas via Biological Catalysis - Final report," 2014 [Online]. Available: https://energiforskning.dk/en/node/15072

[263] T. Weber, "Let's see, what tomorrow brings," Erneuerbare Energien, 2016. [Online]. Available: https://www.erneuerbareenergien.de/technik/windtechnik/lets-see-what-tomorrow-brings. [Accessed: Mar. 03, 2022]

[264] G. H. E. Gmbh, "Green Hydrogen Esslingen." [Online]. Available: https://green-hydrogen-esslingen.de/. [Accessed: Mar. 01, 2023]

[265] "RWE starts up P2G plant with ITM electrolyser," Fuel Cells Bull., vol. 2015, no. 8, p. 1, 2015, doi: 10.1016/S1464-2859(15)30205-4.

[266] "Shell, Mitsubishi Heavy Industries, Vattenfall and Wärme Hamburg sign Letter of Intent for 100MW Hydrogen Project in Hamburg," 2021. [Online]. Available: https://www.hghh.eu/news/shell-mitsubishi-heavy-industries-vattenfall-and-warme-hamburg-sign-letter-of-intent-for-100mw-hydrogen-project-in-hamburg

[267] M. Yuan, J. Z. Thellufsen, P. Sorknæs, H. Lund, and Y. Liang, "District heating in 100% renewable energy systems: Combining industrial excess heat and heat pumps," Energy Convers. Manag., vol. 244, no. 18, p. 114527, 2021, doi: 10.1016/j.enconman.2021.114527. [Online]. Available: https://doi.org/10.1016/j.enconman.2021.114527

[268] H. van 't Noordende and P. Ripson, "A One-GigaWatt Green-Hydrogen Plant - Advanced Design and total Installed-Capital Costs," 2022 [Online]. Available: https://ispt.eu/media/ISPT-public-report-gigawatt-green-hydrogen-plant.pdf

[269] D. Contreras Bilbao, "Valorization of the waste heat given off in a system alkaline electrolyzer-photovoltaic array to improve hydrogen production performance: Case study Antofagasta, Chile," Int. J. Hydrogen Energy, vol. 46, no. 61, pp. 31108–31121, 2021, doi: 10.1016/j.ijhydene.2021.07.016. [Online]. Available: https://doi.org/10.1016/j.ijhydene.2021.07.016

[270] Q. Hu, J. Lin, Q. Zeng, C. Fu, and J. Li, "Optimal control of a hydrogen microgrid based on an experiment validated P2HH model," IET Renew. Power Gener., vol. 14, no. 3, pp. 364–371, 2020, doi: 10.1049/iet-rpg.2019.0544.

[271] E. Frank, J. Gorre, F. Ruoss, and M. J. Friedl, "Calculation and analysis of efficiencies and annual performances of Power-to-Gas systems," Appl. Energy, vol. 218, no. February, pp. 217–231, 2018, doi: 10.1016/j.apenergy.2018.02.105. [Online]. Available: https://doi.org/10.1016/j.apenergy.2018.02.105

[272] C. Huang, Y. Zong, S. You, and C. Træholt, "Economic model predictive control for multi-energy system considering hydrogen-thermal-electric dynamics and waste heat recovery of MW-level alkaline electrolyzer," Energy Convers. Manag., vol. 265, no. May, p. 115697, 2022, doi: 10.1016/j.enconman.2022.115697. [Online]. Available: https://doi.org/10.1016/j.enconman.2022.115697

[273] D. Huckebrink and V. Bertsch, "Decarbonising the residential heating sector: A techno-economic assessment of selected technologies," Energy, vol. 257, p. 124605, 2022, doi: 10.1016/j.energy.2022.124605. [Online]. Available: https://doi.org/10.1016/j.energy.2022.124605

[274] H. Böhm, S. Moser, S. Puschnigg, and A. Zauner, "Power-to-hydrogen & district heating: Technology-based and infrastructure-oriented analysis of (future) sector coupling potentials," Int. J. Hydrogen Energy, vol. 46, no. 63, pp. 31938–31951, 2021, doi: 10.1016/j.ijhydene.2021.06.233.

[275] E. van der Roest, D. Vries, and A. J. M. van Wijk, "H-Flex: green hydrogen in a flexible electricity system," KWR Water, 2020. [Online]. Available: https://www.kwrwater.nl/en/projecten/h-flex-green-hydrogen-in-a-flexible-electricity-system/. [Accessed: Mar. 16, 2022]

[276] J. J. C. Mancera, F. S. Manzano, J. M. Andújar, F. J. Vivas, and A. J. Calderón, "An optimized balance of plant for a medium-size PEM electrolyzer. Design, control and physical implementation," Electron., vol. 9, no. 5, 2020, doi: 10.3390/electronics9050871.

[277] W. J. Tiktak, "Heat Management of PEM Electrolysis," 2019 [Online]. Available: http://resolver.tudelft.nl/uuid:c046820a-72bc-4f05-b72d-e60a3ecb8c89

[278] M. Kopp, D. Coleman, C. Stiller, K. Scheffer, J. Aichinger, and B. Scheppat, "Energiepark Mainz: Technical and economic analysis of the worldwide largest Power-to-Gas plant with PEM electrolysis," Int. J. Hydrogen Energy, vol. 42, no. 19, pp. 13311–13320, 2017, doi: 10.1016/j.ijhydene.2016.12.145. [Online]. Available: http://dx.doi.org/10.1016/j.ijhydene.2016.12.145

[279] J. Davies, F. Dolci, and E. Weidner, Historical Analysis of FCH 2 JU Electrolyser Projects: evaluation of contributions towards advancing the state of the art, EUR 30648. Luxembourg: Publications Office of the European Union, 2021 [Online]. Available: https://publications.jrc.ec.europa.eu/repository/bitstream/JRC121704/electrolyser_hist._analysis_public_20200323final_identifiers_1.pdf

[280] Nederlands Normalisatie-Instituut, "NEN-EN 13941-1 - District heating pipes - Design and installation of thermal insulated bonded single and twin pipe systems for directly buried hot water networks." 2016 [Online]. Available: https://www.nen.nl/nen-en-13941-1-2019-en-258340

[281] European Heat Pump Association, "Large scale Heat Pumps in Europe," vol. 2. 2020 [Online]. Available: https://www.ehpa.org/wp-content/uploads/2022/11/Large-heat-pumps-in-Europe-and-industrial-uses_2020.pdf

[282] H. Lund et al., "Perspectives on fourth and fifth generation district heating," Energy, vol. 227, p. 120520, 2021, doi: 10.1016/j.energy.2021.120520. [Online]. Available: https://doi.org/10.1016/j.energy.2021.120520

[283] E. van der Roest, S. Beernink, N. Hartog, J. P. van der Hoek, and M. Bloemendal, "Towards Sustainable Heat Supply with Decentralized Multi-Energy Systems by Integration of Subsurface Seasonal Heat Storage," Energies, vol. 14, no. 23, p. 7958, Nov. 2021, doi: 10.3390/en14237958. [Online]. Available: https://www.mdpi.com/1996-1073/14/23/7958

[284] J. Schilling, F. van de Poll, and P. van Berkel, "CO_2-effecten van de Transitievisie Warmte: Gemeente Amsterdam." Delft, pp. 1–23, 2020 [Online]. Available: https://ce.nl/wp-content/uploads/2021/03/CE_Delft_200154_-CO_2-effecten_Transitievisie_Warmte_Amsterdam_DEF.pdf

[285] IF Technology, "Thermische Energie uit Oppervlaktewater - Business case 'Genderdal' Eindhoven," 2018 [Online]. Available: https://edepot.wur.nl/460776

[286] M. Stadler, H. Aki, R. Firestone, J. Lai, and A. Siddiqui, "Distributed energy resources on-site optimization for commercial buildings with electric and thermal storage technologies," 2008 ACEEE Summer Study Energy Effic. Build. Scaling Up Build. Tomorrow's Solut., vol. 8, no. May 2008, pp. 1–12, 2008 [Online]. Available: https://escholarship.org/uc/item/8nv7m8sx.pdf

[287] EnergiNet and T. D. E. Agency, "Technology Data Energy Storage," 2020 [Online]. Available: https://ens.dk/en/our-services/projections-and-models/technology-data/technology-data-energy-storage

[288] CBS, "Aardgas en elektriciteit, gemiddelde prijzen van eindverbruikers," 2021. [Online]. Available: https://opendata.cbs.nl/#/CBS/nl/dataset/81309NED/table?dl=6ABB2. [Accessed: Jun. 29, 2022]

[289] OECD, "Effective Carbon Rates 2021." pp. 1–12, 2021 [Online]. Available: https://www.oecd.org/tax/tax-policy/effective-carbon-rates-2021-brochure.pdf

[290] Ember, "Carbon Price Tracker - The latest data on EU and UK ETS carbon prices [Graph]," 2023. [Online]. Available: https://ember-climate.org/data/data-tools/carbon-price-viewer/. [Accessed: Mar. 01, 2023]

[291] Polytherm, "Complete Price List March 2019." 2019 [Online]. Available: http://www.polytherm.ie/v4/0940aa0c-5421-4a9b-840d-c9a2ae5d95bb/uploads/PolythermCompletePricelist.pdf

[292] IEA HPT TCP, "Task 1: Technologies – State of the art and ongoing developments for systems and components," Annex 58 about HTHP, 2022. [Online]. Available: https://heatpumpingtechnologies.org/annex58/task1/. [Accessed: Feb. 24, 2023]

[293] H. Croezen, M. Doe, and N. Jorna, "Broeikasgasemissies aardgasketens," 2022 [Online]. Available: https://www.CO_2emissiefactoren.nl/wp-content/uploads/2022/01/35-RHDHV-Broeikasgasemissies-aardgasketens-2022.pdf

[294] A. Colmenar-Santos, E. Rosales-Asensio, D. Borge-Diez, and J.-J. Blanes-Peiró, "District heating and cogeneration in the EU-28: Current situation, potential and proposed energy strategy for its generalisation," Renew. Sustain. Energy Rev., vol. 62, pp. 621–639, 2016, doi: 10.1016/j.rser.2016.05.004. [Online]. Available: http://dx.doi.org/10.1016/j.rser.2016.05.004

[295] K. C. Kavvadias and S. Quoilin, "Exploiting waste heat potential by long distance heat transmission: Design considerations and techno-economic assessment," Appl. Energy, vol. 216, no. February, pp. 452–465, 2018, doi: 10.1016/j.apenergy.2018.02.080. [Online]. Available: https://doi.org/10.1016/j.apenergy.2018.02.080

[296] C. Baah et al., "Examining the correlations between stakeholder pressures, green production practices, firm reputation, environmental and financial performance: Evidence from manufacturing SMEs," Sustain. Prod. Consum., vol. 27, pp. 100–114, 2021, doi: 10.1016/j.spc.2020.10.015. [Online]. Available: https://doi.org/10.1016/j.spc.2020.10.015

[297] J. Stones and J. Hamilton, "ICIS WHITEPAPER: Renewable PPAs and a review of the commodity price spike on renewable hydrogen production costs." ICIS, pp. 1–6, 2022 [Online]. Available: https://www.icis.com/explore/resources/news/2022/10/11/10813598/icis-whitepaper-renewable-ppas-and-a-review-of-the-commodity-price-spike-on-renewable-hydrogen-production-costs/

[298] International Renewable Energy Agency (IRENA), "Demand-side flexibility for power sector transformation," Abu Dhabi, 2019 [Online]. Available: https://www.irena.org/-/media/Files/IRENA/Agency/Publication/2019/Dec/IRENA_Demand-side_flexibility_2019.pdf

[299] V. G. Suárez, J. L. Rueda Torres, B. W. Tuinema Arcadio, P. Guerra, and M. Van Der Meijden, "Integration of Power-to-Gas Conversion into Dutch Electricity Ancillary Services Markets," in 12th Conference on Energy Economics and Technology, 2018, pp. 1–7 [Online]. Available: http://resolver.tudelft.nl/uuid:d63402bb-2e26-477c-b3d7-e3c6583242ff

[300] G. Matute, J. M. Yusta, and L. C. Correas, "Techno-economic modelling of water electrolysers in the range of several MW to provide grid services while generating hydrogen for different applications: A case study in Spain applied to mobility with FCEVs," Int. J. Hydrogen Energy, vol. 44, no. 33, pp. 17431–17442, 2019, doi: 10.1016/j.ijhydene.2019.05.092. [Online]. Available: https://doi.org/10.1016/j.ijhydene.2019.05.092

[301] HyBalance, "Final report with strategic learnings from performance reporting, business case analysis," 2021 [Online]. Available: https://cordis.europa.eu/project/id/671384/results

[302] G. Matute, J. M. Yusta, J. Beyza, and L. C. Correas, "Multi-state techno-economic model for optimal dispatch of grid connected hydrogen electrolysis systems operating under dynamic conditions," Int. J. Hydrogen Energy, vol. 46, no. 2, pp. 1449–1460, 2021, doi: 10.1016/j.ijhydene.2020.10.019. [Online]. Available: https://doi.org/10.1016/j.ijhydene.2020.10.019

[303] F. Jonsson and A. Miljanovic, "Utilization of Waste Heat From Hydrogen Production," Mälardalen University, 2022 [Online]. Available: https://www.diva-portal.org/smash/get/diva2:1670187/FULLTEXT01.pdf

[304] M. Muller and S. Lensink, "Conceptadvies SDE++ CO_2-Reducerende Opties," 2019 [Online]. Available: https://www.pbl.nl/sites/default/files/downloads/pbl-2019-conceptadvies-SDE-plus-plus-industriele-rest-warmte_3745.pdf

[305] B. Schepers, T. Scholten, G. Willemsen, M. Koenders, and B. de Zwart, "Weg van gas - Kansen voor de nieuwe concepten LageTemperatuurAardwarmte en Mijnwater," 2018 [Online]. Available: https://ce.nl/wp-content/uploads/2021/03/CE_Delft_3K61_Weg_van_gas_DEF.pdf

[306] M. Ginsberg, Z. Zhang, A. A. Atia, M. Venkatraman, D. V. Esposito, and V. M. Fthenakis, "Integrating Solar Energy, Desalination, and Electrolysis," Sol. RRL, vol. 6, no. 5, pp. 1–13, 2022, doi: 10.1002/solr.202100732.

[307] A. Scherba, D. J. Sailor, T. N. Rosenstiel, and C. C. Wamser, "Modeling impacts of roof reflectivity, integrated photovoltaic panels and green roof systems on sensible heat flux into the urban environment," Build. Environ., vol. 46, no. 12, pp. 2542–2551, 2011, doi: 10.1016/j.buildenv.2011.06.012. [Online]. Available: http://dx.doi.org/10.1016/j.buildenv.2011.06.012

[308] D. B. Rowe and K. L. Getter, "The role of extensive green roofs in sustainable development," HortScience, vol. 41, no. 5, pp. 1276–1285, 2006.

[309] M. Shafique, R. Kim, and M. Rafiq, "Green roof benefits, opportunities and challenges – A review," Renew. Sustain. Energy Rev., vol. 90, no. April, pp. 757–773, 2018, doi: 10.1016/j.rser.2018.04.006.

[310] B. R. Paudyal and A. G. Imenes, "Investigation of temperature coefficients of PV modules through field measured data," Sol. Energy, vol. 224, no. February, pp. 425–439, 2021, doi: 10.1016/j.solener.2021.06.013. [Online]. Available: https://doi.org/10.1016/j.solener.2021.06.013

[311] M. Alshayeb and J. Chang, "Variations of PV Panel Performance Installed over a Vegetated Roof and a Conventional Black Roof," Energies, vol. 11, no. 5, p. 1110, May 2018, doi: 10.3390/en11051110. [Online]. Available: http://www.mdpi.com/1996-1073/11/5/1110

[312] R. Ciriminna, F. Meneguzzo, M. Pecoraino, and M. Pagliaro, "Solar Green Roofs: A Unified Outlook 20 Years On," Energy Technol., vol. 7, no. 6, pp. 1–7, 2019, doi: 10.1002/ente.201900128.

[313] H. H. K. Ogaili, "Measuring the Effect of Vegetated Roofs on the Performance of Photovoltaic Panels in Combined Systems," Portland University, 2015 [Online]. Available: https://pdfs.semanticscholar.org/5dcf/fec3a8c3a99179ab934cb4569182d3885095.pdf

[314] C. Catalano and N. Baumann, "Biosolar Roofs: A Symbiosis between Biodiverse Green Roofs and Renewable Energy," City Green, no. 15, pp. 42–49, 2017 [Online]. Available: https://www.nparks.gov.sg/-/media/cuge/ebook/citygreen/cg15/cg15_05.pdf?la=en&hash=742D039957FCA9CB7640F52498428F81CAAF42A9

[315] B. Y. Schindler, L. Blaustein, R. Lotan, H. Shalom, and G. J. Kadas, "Green roof and photovoltaic panel integration : Effects on plant and arthropod diversity and electricity production," J. Environ. Manage., vol. 225, no. March, pp. 288–299, 2018, doi: 10.1016/j.jenvman.2018.08.017. [Online]. Available: https://doi.org/10.1016/j.jenvman.2018.08.017

[316] D. El Helow, "Performance of Green Roof Integrated Solar Photovoltaics in Toronto," University of Toronto, 2018 [Online]. Available: https://hdl.handle.net/1807/89540

[317] G. Osma-Pinto and G. Ordóñez-Plata, "Measuring factors influencing performance of rooftop PV panels in warm tropical climates," Sol. Energy, vol. 185, no. April, pp. 112–123, 2019, doi: 10.1016/j.solener.2019.04.053. [Online]. Available: https://doi.org/10.1016/j.solener.2019.04.053

[318] M. J. R. Perez, N. T. Wight, V. M. Fthenakis, and C. Ho, "Green-roof integrated pv canopies-an empirical study and teaching tool for low income students in the South Bronx," World Renew. Energy Forum, WREF 2012, Incl. World Renew. Energy Congr. XII Color. Renew. Energy Soc. Annu. Conf., vol. 5, no. 1, pp. 4046–4052, 2012.

[319] D. Chemisana and C. Lamnatou, "Photovoltaic-green roofs : An experimental evaluation of system performance," Appl. Energy, vol. 119, pp. 246–256, 2014, doi: 10.1016/j.apenergy.2013.12.027. [Online]. Available: http://dx.doi.org/10.1016/j.apenergy.2013.12.027

[320] M. Köhler, W. Wiartalla, and R. Feige, "Interaction between PV-systems and extensive green roofs," in Greening rooftops for sustainable communities, 2007, pp. 1–16 [Online]. Available: http://www.worldgreenroof.org/files/pdf/Manfred-KoehlerMinneapolisPV.pdf

[321] A. Nagengast, C. Hendrickson, H. Scott Matthews, and H. S. Matthews, "Variations in photovoltaic performance due to climate and low-slope roof choice," Energy Build., vol. 64, pp. 493–502, 2013, doi: 10.1016/j.enbuild.2013.05.009. [Online]. Available: http://dx.doi.org/10.1016/j.enbuild.2013.05.009

[322] M. Shafique, X. Luo, and J. Zuo, "Photovoltaic-green roofs: A review of benefits, limitations, and trends," Sol. Energy, vol. 202, no. October 2019, pp. 485–497, 2020, doi: 10.1016/j.solener.2020.02.101. [Online]. Available: https://doi.org/10.1016/j.solener.2020.02.101

[323] H. Ogaili and D. J. Sailor, "Measuring the Effect of Vegetated Roofs on the Performance of Photovoltaic Panels in a Combined System," J. Sol. Energy Eng., vol. 138, no. 6, pp. 1–8, Dec. 2016, doi: 10.1115/1.4034743. [Online]. Available: https://asmedigitalcollection.asme.org/solarenergyengineering/article/doi/10.1115/1.4034743/380622/Measuring-the-Effect-of-Vegetated-Roofs-on-the

[324] M. Zapater-Pereyra, S. Lavrnić, F. van Dien, J. J. A. van Bruggen, and P. N. L. Lens, "Constructed wetroofs: A novel approach for the treatment and reuse of domestic wastewater," Ecol. Eng., vol. 94, pp. 545–554, 2016, doi: 10.1016/j.ecoleng.2016.05.052.

[325] G. Osma, G. Ordóñez, E. Hernández, L. Quintero, and M. Torres, "The impact of height installation on the performance of PV panels integrated into a green roof in tropical conditions," in Energy Production and Management in the 21st Century II: The Quest for Sustainable Energy, 2016, vol. 1, pp. 147–156, doi: 10.2495/eq160141.

[326] D. El Helow, J. Drake, and L. Margolis, "Testing the Potential Synergy of Green Roof-Integrated Photovoltaics at the University of Toronto Green Roof Innovation Testing (GRIT) Laboratory," in 32nd RCI International Convention and Trade Show, 2017, no. August, pp. 229–235.

[327] G. F. Makkink, "Testing the Penman Formula by Means of Lysimeters," J. Inst. Water Eng., vol. 11, pp. 277–288, 1957.

[328] J. G. W. F. Voeten, L. van de Werken, and A. P. Newman, "Demonstrating the Use of Below-Substrate Water Storage as a Means of Maintaining Green Roofs -Performance Data and a Novel Approach to Achieve Public Understanding," World Environmental and Water Resources Congress. ASCE Library, West Palm Beach, FL, USA, pp. 12–21, Feb. 02, 2016 [Online]. Available: https://doi.org/10.1061/9780784479841.002

[329] J. Heusinger and S. Weber, "Comparative microclimate and dewfall measurements at an urban green roof versus bitumen roof," Build. Environ., vol. 92, pp. 713–723, 2015, doi: 10.1016/j.buildenv.2015.06.002. [Online]. Available: http://dx.doi.org/10.1016/j.buildenv.2015.06.002

[330] F. Chen et al., "The integrated WRF/urban modelling system: Development, evaluation, and applications to urban environmental problems," Int. J. Climatol., vol. 31, no. 2, pp. 273–288, 2011, doi: 10.1002/joc.2158.

[331] X. Xu and T. Asawa, "Systematic numerical study on the effect of thermal properties of building surface on its temperature and sensible heat flux," Build. Environ., vol. 168, no. October 2019, 2020, doi: 10.1016/j.buildenv.2019.106485.

[332] M. P. Brennan, A. L. Abrahamse, R. W. Andrews, and J. M. Pearce, "Effects of spectral albedo on solar photovoltaic devices," Sol. Energy Mater. Sol. Cells, vol. 124, pp. 111–116, 2014, doi: 10.1016/j.solmat.2014.01.046. [Online]. Available: http://dx.doi.org/10.1016/j.solmat.2014.01.046

[333] V. M. R. Muggeo, "segmented: an R Package to Fit Regression Models with Broken-Line Relationships.," R news, vol. 8, no. 1, pp. 20–25, 2008 [Online]. Available: https://journal.r-project.org/articles/RN-2008-004/RN-2008-004.pdf

[334] A. Jahanfar, J. Drake, B. Gharabaghi, and B. Sleep, "An experimental and modeling study of evapotranspiration from integrated green roof photovoltaic systems," Ecol. Eng., vol. 152, no. July 2019, p. 105767, 2020, doi: 10.1016/j.ecoleng.2020.105767. [Online]. Available: https://doi.org/10.1016/j.ecoleng.2020.105767

[335] Netbeheer Nederland, "Capaciteitskaart," 2023. [Online]. Available: https://capaciteitskaart.netbeheernederland.nl/. [Accessed: Mar. 29, 2023]

[336] B. Steman, P. Nieuwesteeg, M. Plantema, and K. Friele, "Verbeteren netinpassing zonne-energieprojecten," 2021 [Online]. Available: https://www.rvo.nl/sites/default/files/2022/02/Verbeteren-netinpassing-zonne-energieprojecten-10-toepassingen-in-kaart-gebracht.pdf

[337] C. Murray, "Wind-solar-storage hybrid project with 12MWh BESS online in Netherlands," Energy Storage News, 2022. [Online]. Available: https://www.energy-storage.news/wind-solar-storage-hybrid-project-with-12mwh-bess-online-in-netherlands/. [Accessed: Mar. 30, 2023]

[338] R. Kloosterman, M. Akkermans, C. Reep, M. Wingen, H. Molnár- In 't Veld, and J. van Beuningen, "Klimaatverandering en energietransitie: opvattingen en gedrag van Nederlanders in 2020." CBS, 2021 [Online]. Available: https://www.cbs.nl/nl-nl/longread/rapportages/2021/klimaatverandering-en-energietransitie-opvattingen-en-gedrag-van-nederlanders-in-2020/4-duurzaam-wonen#:~:text=De meeste huishoudens%2C 93 procent%2C hebben in 2020,23 procent verwarmt de woning %28aanvul

[339] A. Monti, N. Hatziagyrio, and N. Souza e Silva, "Analysis of Projects - Major Achievements and R&I Gaps," 2021 [Online]. Available: https://energy.ec.europa.eu/system/files/2021-06/bridge_tf_ri_priorities_report_2020-2021_0.pdf

[340] A. de Jong and R. Bol, "Verkenning toepassing Power-to-gas concepten op RWZI's," 2018 [Online]. Available: https://www.stowa.nl/sites/default/files/assets/PUBLICATIES/Publicaties 2018/STOWA 2018-71 P2G.pdf

[341] Unie van Waterschappen and Pondera, "De rwzi als smart energie-hub," 2021 [Online]. Available: https://www.stowa.nl/sites/default/files/assets/PUBLICATIES/Publicaties 2021/UVW 2021-XX De-rwzi-als-smart-energie-hub.pdf

[342] T. Flameling, L. Nieukoop, R. van der Lans, B. Reitsma, and A. Visser, "Benutting zuivere zuurstof uit duurzame waterstofproductie in RWZI's met fijne- bellenbeluchtingssystemen." STOWA, Amersfoort, 2022 [Online]. Available: https://www.stowa.nl/sites/default/files/assets/PUBLICATIES/Publicaties 2022/STOWA 2022-51 SEH.pdf

[343] Netbeheer Nederland, "Appreciatie van de Transitievisies Warmte," 2022 [Online]. Available: https://www.netbeheernederland.nl/_upload/RadFiles/New/Documents/20220303 NBNL - TVW Rapport.pdf

[344] M. Zwamborn et al., "HT-ATES systems in district heating networks, a Dutch benchmark study," in European Geothermal Congress 2016, 2022, pp. 1–12 [Online]. Available: https://www.egec.org/wp-content/uploads/2023/02/Zwamborn-HT-ATES-systems-in-district-heating-networks-a-Dutch-benchmark-study-411_ExtAbstract.pdf

[345] HEATSTORE, Roadmap for flexible energy systems with underground thermal energy storage towards 2050. 2021.

[346] P. Oerlemans, B. Drijver, M. Koenen, J. Koornneef, D. Dinkelman, and B. Godschalk, "First field results on the technical risks and effectiveness of mitigation measures for the full scale HT-ATES demonstration project in Middenmeer," in European Geothermal Congress 2022, 2022 [Online]. Available: https://iftechnology.nl/wp-content/uploads/2022/11/Oerlemans-et-al-First-results-of-one-year-full-scale-HT-ATES-operation-in-the-Netherlands-1.pdf

[347] Rijksoverheid, "Hybride warmtepomp de nieuwe standaard vanaf 2026," 2022. [Online]. Available: https://www.rijksoverheid.nl/actueel/nieuws/2022/05/17/hybride-warmtepomp-de-nieuwe-standaard-vanaf-2026. [Accessed: Mar. 30, 2023]

[348] Directoraat-generaal Klimaat en Energie, "Kamerbrief actieplan hybride warmtepompen." [Online]. Available: https://www.rijksoverheid.nl/documenten/kamerstukken/2022/06/15/actieplan-hybride-warmtepompen

[349] M. Hommelberg, G. Janssen, and P. Friedel, "Installatiemonitor - publieke eindrapportage februari 2022," 2022 [Online]. Available: https://www.installatiemonitor.nl/wp-content/uploads/2022/02/Eindrapportage-Installatiemonitor-v2.1.pdf

[350] Ministerie van Economische Zaken en Klimaat, "Routekaart Energieopslag," Den Haag, 2023 [Online]. Available: https://open.overheid.nl/documenten/7f9ca5c1-3f11-4efc-9b0d-1ffa36aa59ed/file

[351] N. J. Kurmayer, "Growing demand puts EU electricity grid under pressure," Euractiv, 2023. [Online]. Available: https://www.euractiv.com/section/energy-environment/news/growing-demand-puts-eu-electricity-grid-under-pressure/. [Accessed: Mar. 29, 2023]

[352] Expertise Centrum Warmte, "Handreiking voor lokale analyse," 2021 [Online]. Available: https://www.expertisecentrumwarmte.nl/documenten/handlerdownloadfiles.ashx?idnv=1986159

[353] M. Bloemendal, T. Olsthoorn, and F. van de Ven, "Combining climatic and geo-hydrological preconditions as a method to determine world potential for aquifer thermal energy storage," Sci. Total Environ., vol. 538, pp. 621–633, 2015, doi: 10.1016/j.scitotenv.2015.07.084. [Online]. Available: http://dx.doi.org/10.1016/j.scitotenv.2015.07.084

[354] Ministerie van Infrastructuur en Waterstaat and Ministerie van Economische Zaken en Klimaat, "Structuurvisie Ondergrond," 2018 [Online]. Available: https://www.rijksoverheid.nl/documenten/rapporten/2018/06/11/structuurvisie-ondergrond

[355] L. P. Brokx, M. P. Bloemendal, and N. Hartog, "Handvatten voor duurzame co-existentie van ondergrondse waterberging en open bodemenergie." Nieuwegein, KWR 2022.084, 2022 [Online]. Available: https://www.kasalsenergiebron.nl/content/research/2022_KWR_Handvatten_voor_duurzame_co-existentie_van_ondergrondse_waterberging_en_open_bodemenergie-min.pdf

[356] C. Agudelo-Vera et al., "Drinking water temperature around the globe: Understanding, policies, challenges and opportunities," Water (Switzerland), vol. 12, no. 4, 2020, doi: 10.3390/W12041049.

[357] E. J. M. Blokker and Q. Pan, "Invloed warmtenetten op temperatuur drinkwater," Nieuwegein, KWR 2022.121, 2022 [Online]. Available: https://edepot.wur.nl/582457

[358] C. Breyer et al., "On the History and Future of 100% Renewable Energy Systems Research," IEEE Access, vol. 10, no. June, pp. 78176–78218, 2022, doi: 10.1109/ACCESS.2022.3193402.

[359] IEA, "Material efficiency in clean energy transitions," Paris, 2019 [Online]. Available: https://www.iea.org/reports/material-efficiency-in-clean-energy-transitions

[360] Leiden-Delft-Erasmus Centre for Sustainability Circular Industries Hub, "Critical materials, green energy and geopolitics: a complex mix," pp. 1–52, 2022 [Online]. Available: https://www.centre-for-sustainability.nl/uploads/cfs/attachments/Critical Materials_LDE White Paper_DEF20220627_0.pdf

[361] Metabolic, Copper8, Polaris, Quintel, and Universiteit Leiden, "Towards a circular energy transition," 2021 [Online]. Available: https://www.metabolic.nl/publications/towards-a-circular-energy-transition/

[362] T. Driesner (ed), HEATSTORE - Final report on tools and workflows for simulating subsurface dynamics of different types of High Temperature Underground Thermal Energy Storage. GEOTHERMICA – ERA NET Cofund Geothermal, 2021 [Online]. Available: https://www.heatstore.eu/documents/HEATSTORE_WP2_D2.1_Rev._Final_2021.12.21.pdf

[363] F. Kachirayil, J. M. Weinand, F. Scheller, and R. McKenna, "Reviewing local and integrated energy system models: insights into flexibility and robustness challenges," Appl. Energy, vol. 324, no. May, p. 119666, 2022, doi: 10.1016/j.apenergy.2022.119666. [Online]. Available: https://doi.org/10.1016/j.apenergy.2022.119666

[364] V. D. W. M. Oldenbroek, "Integrated transport and energy systems based on hydrogen and fuel cell electric vehicles," Delft University of Technology, 2021 [Online]. Available: https://doi.org/10.4233/uuid:f-8f6566e-e50a-47e2-b1f9-67503ca1d021

[365] G. Simader and P. Vidovic, "Success factors for demonstration projects of small-scale stationary fuel cells in residential buildings," E3S Web Conf., vol. 334, 2022, doi: 10.1051/e3sconf/202233404007.

[366] J. Meuer, F. Lamaro, and N. Vetterli, "Embedding energy optimization in organizations: A case study of a Swiss decentralized renewable energy system," Energy Build., vol. 235, p. 110710, 2021, doi: 10.1016/j.enbuild.2020.110710. [Online]. Available: https://doi.org/10.1016/j.enbuild.2020.110710

[367] Hysolar, "Hysolar - About us," 2023. [Online]. Available: https://www.hysolar.nl/en/about-us. [Accessed: Mar. 31, 2023]

[368] Hysolar, "Official opening of the first public hydrogen filling station in the Province of Utrecht: Hysolar/Greenpoint in Nieuwegein," 2021. [Online]. Available: https://www.hysolar.nl/en/news/official-opening-of-the-first-public-hydrogen-filling-station-in-the-province-of-utrecht-hysolar-greenpoint-in-nieuwegein. [Accessed: Mar. 31, 2023]

[369] T. G. Village, "The Green Village - About us," 2023. [Online]. Available: https://www.thegreenvillage.org/en/about-us/. [Accessed: Mar. 28, 2023]

[370] T. Schittekatte, L. Meeus, T. Jamasb, and M. Llorca, "Regulatory experimentation in energy: Three pioneer countries and lessons for the green transition," Energy Policy, vol. 156, p. 112382, Sep. 2021, doi: 10.1016/j.enpol.2021.112382. [Online]. Available: https://linkinghub.elsevier.com/retrieve/pii/S0301421521002524

[371 A. Van Wijk, "Hydrogen key to a carbon-free energy system," in Hydrogen Storage for Sustainability, M. van de Voorde, Ed. Berlin, Boston: De Gruyter, 2021, pp. 43–104 [Online]. Available: https://www.degruyter.com/document/doi/10.1515/9783110596281-005/html

[372] CBS, “Aandeel hernieuwbare elektriciteit met 20 procent gestegen in 2022,” 2023. [Online]. Available: https://www.cbs.nl/nl-nl/nieuws/2023/10/aandeel-hernieuwbare-elektriciteit-met-20-procent-gestegen-in-2022. [Accessed: May 05, 2023]

[373] IPCC, Climate Change 2022, Mitigation of Climate Change Summary for Policymakers (SPM). Cambridge, UK and New York, USA: Cambridge University Press, 2022 [Online]. Available: https://www.ipcc.ch/report/ar6/wg3/

Acknowlegdements/Dankwoord

In de afgelopen vierenhalf jaar heb ik de kans gekregen om naast en deels tijdens mijn werk aan mijn promotieonderzoek te werken, wat heeft geresulteerd in het proefschrift dat je zojuist hebt gelezen (of hebt doorgebladerd op zoek naar dit stukje ;)). Het was een intensieve, leerzame en inspirerende tijd, en ik wil graag een aantal mensen bedanken die hierin een speciale plek hebben ingenomen.

Ten eerste mijn (co)promotoren: Ad van Wijk, Jan Peter van der Hoek en Theo Fens. Ad, onze samenwerking dateert al van voor mijn promotie, en ik ben dankbaar dat ik van je heb mogen leren en met je heb mogen samenwerken de afgelopen jaren. In een wetenschappelijke omgeving waar mensen snel geneigd zijn dingen dood te redeneren alvorens eraan te beginnen, is jouw visionaire blik heel welkom, motiverend en verfrissend. 'Kan niet', bestaat niet in jouw woordenboek, en jouw gedrevenheid is bewonderingswaardig. Aan de vraag die ik je stelde in mijn sollicitatiegesprek: 'Maar waarom zou waterstof een toevoeging zijn aan het energiesysteem?' heb jij vooral, maar hebben we ook samen een overtuigend antwoord geformuleerd in onder andere twee boeken. Jan Peter, ik vraag me soms af of jij meer uren in een dag hebt dan andere mensen, ondanks je drukke agenda reageer je altijd snel, ben je vriendelijk en constructief. Jij hebt mijn promotietraject bij de TU Delft uiteindelijk mogelijk gemaakt. Dank voor het altijd weer inbrengen van het waterperspectief, je interesse in alle energie-onderwerpen en voor je pragmatische insteek. Theo, door onze samenwerking binnen de projecten bij KWR en mijn PhD hebben we heel wat afgekletst, de gesprekken met jou waren altijd inspirerend, van de door je zelf geïnstalleerde enorme thuisbatterij gekoppeld aan je zonnepanelen, een verhandeling over gelijkstroom tot de institutionele inrichting van het energiesysteem of de kleinkinderen, alles kwam voorbij. Met ook altijd de vraag, 'Hoe is het met jou?'. Ik ben dankbaar dat je mijn copromotor wilde zijn en altijd voor me klaarstond om te sparren. Dank ook aan de andere leden van de promotiecommissie voor jullie kritische blik: dr. Edo Abraham, prof. dr. ir. Zofia Lukszo, prof. dr. ir. Luuk Rietveld en prof. dr. Bob van der Zwaan. Tessa & Margot, dank dat jullie mijn paranimfen wilden zijn, fijn om bijgestaan te worden door twee andere vrouwelijke wetenschappers met nuchtere blik en regelvermogen.

Mijn promotie heb ik deels uitgevoerd tijdens of gekoppeld aan projecten bij KWR en samen met collega's. Laura, veel dank voor je morele en programmeer ondersteuning in mijn eerste jaren bij KWR. Stijn, het was heel fijn om samen met jou aan het HTO model te werken en te kunnen sparren over met name het HTO-paper (hoofdstuk 4 in dit proefschrift). Martin en Niels, dank voor jullie kritische blik en meedenken bij alle zaken rondom bodemenergie. Ron, jouw praktische kennis en insteek waren onmisbaar bij het restwarmte onderzoek uit elektrolyse. En Gijsbert en Joris, dank dat jullie deze kluns mee het dak op en de kelder in wilden nemen en hebben laten ervaren wat echt praktisch onderzoek is. Samen in de data duiken was heerlijk om te doen Gijsbert.

Also I would like to thank the early careers at KWR and especially the first Early Career board. Sharon, Alex, Nikki, Dimitrios, Karel & Janine, we have created KWR Early career which surely has had a positive impact on early careers within KWR. If people ask me about something I am proud of, founding Early Career with you comes to my mind.

Tijdens het promotietraject heb ik ook verschillende studenten mogen begeleiden. Nynke Tack, Oguzhan Kaya, Joep van der Weijden, Diederik van Hasselt (†) & Ruben van den Berg, bedankt voor jullie vertrouwen in mij, jullie verschillende persoonlijkheden hebben mij doen groeien in mijn rol als begeleider. Op de TU Delft was het contact met Rishabh Ghotge, Chelsea Kaandorp en Ben Riemersma als mede promovendi waardevol. Ook ben ik dankbaar dat ik een jaar heb mogen meedraaien in de group meetings van de groep van Rolf Künneke, waar ik veel heb geleerd over de institutionele kant van energie infrastructuur. Ook de gesprekken met Richard van Gemert hebben me daarover waardevolle inzichten opgeleverd.

Mijn collega's bij KWR hebben mij de afgelopen jaren mede gevormd. Zo hebben we een mooi team Energie & Circulaire systemen opgezet met elkaar. Andreas, Daniël, Diederik (†), Dirk, Frank, Kees, Marette, Ruben en Tessa, ik heb mazzel met jullie als collega's. We zijn harde werkers, maar er is ook ruimte voor grappen met elkaar, en we staan voor elkaar klaar als nodig, in het bijzonder ook na het verlies van Diederik. Idsart, Jos, Luc, Marette, Mariëlle en Nellie, jullie hebben allemaal op de een of andere manier bijdragen aan het mogelijk maken van mijn promotie, veel dank daarvoor. Ook Jan Vreeburg, Jan Willem Kooiman en Stef wil ik in het bijzonder noemen, voor hun formele en informele coaching en hun vertrouwen dat ik dit kon, en om me erop te wijzen niet te verzuipen in perfectie.

En Pieter, ons buddyschap dat we hebben overgehouden aan het traineeship Talent voor Transitie is zo ontzettend waardevol geweest. Elke week en later om de week een half uurtje met elkaar bellen over wat ons bezig houdt in ons werk, onze doelen en uitdagingen. Goed luisteren, open vragen stellen, en soms ook gewoon een goed advies, ik hoop dat we er nog een tijd mee doorgaan en kan het iedereen aanraden. Diana, ook jou heb ik via TvT leren kennen, jouw coaching heeft mij enorm geholpen om dichter bij mezelf te blijven en vanuit iets meer rust mijn werk te doen.

Maar er is meer in het leven dan werk, en gelukkig zijn er veel mensen in mijn omgeving die mij daaraan helpen herinneren, steun bieden en het leven leuker maken. Mijn familie, schoon- en stieffamilie is omvangrijk; dank voor de etentjes, uitjes, sinterklaas- en kerstvieringen en goede gesprekken. Papa, dankjewel voor je interesse in mijn onderzoek en het aandragen van out-of-the box duurzame ideeën, en om me te helpen herinneren dat ik niet altijd maar moet werken. Mama, dank voor je steun in de vorm van alle kaartjes, appjes en de zo bij ons horende eindeloze gesprekken, en vooral voor het zien en waarderen van mij als mens. En jullie samen voor het vertrouwen in mij en me stimuleren om mijn capaciteiten te benutten, zonder daarbij hoge verwachtingen op te leggen. Dat deed ik zelf al genoeg. Opa, we mogen het misschien niet altijd eens zijn over het nut van duurzame energie, maar je betrokkenheid bij alles wat ik doe is enorm. Al jouw sterkte-wensen zitten vast ook ergens in dit proefschrift, en ik ben dankbaar dat we het nog steeds over van alles kunnen hebben.

Mijn vrienden zijn ook belangrijk geweest om mijn gedachten te verzetten of juist even te spuien tijdens spelletjesavonden, wandelingen, zwemtrainingen, etentjes, klimaatdemonstraties, concertgebouw- of theaterbezoekjes en vakanties. In het bijzonder wil ik Ruben bedanken voor zijn werk aan de opmaak van dit proefschrift, wie had dat kunnen bedenken toen we elkaar leerden kennen achter de kassa bij Albert Heijn een half leven geleden.

Pim, het leven is gewoon veel fijner met jou. Voor dit proefschrift ben je heel belangrijk geweest, of het nou ging om meedenken over een stukje code of over data-analyse, kopjes thee brengen tijdens de dinsdagavonden dat ik zat te werken of aanhoren tegen welke moeilijkheden ik in projecten allemaal aanliep. Je was en bent er altijd voor mij. We kunnen allebei enorm in ons hoofd zitten, maar dat soms gelukkig ook loslaten en kleine en grote avonturen beleven, zoals onze fietstocht in 2021. Ik hoop dat we dat nog heel lang blijven doen.

Ik draag dit proefschrift ten slotte graag op aan mijn oma's, ze leven allebei niet meer, maar wat zouden zij gestraald hebben als ik ze dit proefschrift had overhandigd. Met hun levensverhalen in het achterhoofd voel ik me extra dankbaar dat ik in een maatschappij en een tijd leef waarin ik wel de mogelijkheden heb om mijn interesses te volgen en door te leren.

About the author

Els van der Roest was born on the 30th of June 1991 in Amsterdam, The Netherlands. After her graduation from high school (cum laude) she started her studies with the interdisciplinary bachelor Bèta-gamma at the University of Amsterdam, with a major in Chemistry (cum laude). In between her bachelor and master, she performed water quality research in a rural area in Nepal. She continued her masters at Utrecht University in Energy Science (cum laude), with a thesis on producing electricity from waste toilet paper and a thesis on iron (II) sulfide as a starting material for alkaline batteries. Since 2017, she works as a researcher at KWR Water Research in the team Energy & Circular systems, performing research on the interface of energy and water. Besides her job, from 2018-2020 she took part in the development program of the traineeship Talent voor Transitie (Talent for Transition) for young professionals in the energy sector. Since 2019, she has been a part-time PhD candidate on energy & water system integration in neighborhoods at the TU Delft.

List of publications

Journal publications

- **van der Roest, E.**, Voeten, J. G. W. F., & Cirkel, D. G. (2023). Increasing solar panel output with blue-green roofs in water-circular and nature inclusive urban development. *Building and Environment, 244(May)*, 110704. *https://doi.org/10.1016/j.buildenv.2023.110704*
- **van der Roest, E.**, Bol, R., Fens, T., & van Wijk, A. (2023). Utilisation of waste heat from PEM electrolysers – Unlocking local optimisation. *International Journal of Hydrogen Energy, 48*(72), 27872–27891. *https://doi.org/10.1016/j.ijhydene.2023.03.374*
- **van der Roest, E**., Beernink, S., Hartog, N., van der Hoek, J. P., & Bloemendal, M. (2021). Towards Sustainable Heat Supply with Decentralized Multi-Energy Systems by Integration of Subsurface Seasonal Heat Storage. *Energies, 14*(23), 7958. *https://doi.org/10.3390/en14237958*
- **van der Roest, E**., Fens, T., Bloemendal, M., Beernink, S., van der Hoek, J. P., & van Wijk, A. J. M. (2021). The Impact of System Integration on System Costs of a Neighborhood Energy and Water System. *Energies, 14*(9), 2616. *https://doi.org/10.3390/en14092616*
- **van der Roest, E**., Snip, L., Fens, T., & van Wijk, A. (2020). Introducing Power-to-H3: Combining renewable electricity with heat, water and hydrogen production and storage in a neighbourhood. *Applied Energy, 257*. *https://doi.org/10.1016/j.apenergy.2019.114024*

Books

- van Wijk, A. J. M., **van der Roest, E**., & Boere, J. (2023). *Green Energy for all.* Allied Waters.
- van Wijk, A., **van der Roest, E**., & Boere, J. (2017). *Solar power to the people.* Allied Waters/IOS Press BV. *https://doi.org/10.3233/978-1-61499-832-7-i*

Conference papers

- Kaya, O., **van der Roest, E**., Vries, D., & Keviczky, T. (2020). Hierarchical Model Predictive Control for Energy Management of Power-to-X Systems. *2020 IEEE PES Innovative Smart Grid Technologies Europe (ISGT-Europe)*, 1094–1098. *https://doi.org/10.1109/ISGT-Europe47291.2020.9248892*

Conference presentations

- **van der Roest, E**. (2022). Green-blue roofs with solar PV – A win-win-win situation. *Smart and Sustainable Planning for Cities and Regions*, Bolzano, Italy.
- **van der Roest, E**., Fens, T., Bol, R., Huiting, H., & van Wijk, A. J. M. (2022). Heat utilization from hydrogen production – an example of local energy system integration. *Smart Energy Systems Conference*, Aalborg, Denmark.[1]
- **van der Roest, E**., & van Wijk, A. J. M. (2021). Power to X - Integration of energy and water in a neighbourhood with the Power-to-X concept. *IWA Digital World Water Congress*.
- **van der Roest, E**., Snip, L., Fens, T., & van Wijk, A. (2019). Power to X - A novel, reliable, affordable and clean energy and water system for a neighbourhood. *Smart Energy Systems Conference*, Kopenhagen, Denmark.

Prizes

- [1] Best senior presentation at the Smart Energy Systems Conference 2022 in Aalborg
- TKI Project 'Urban Photosynthesis' (**Chapter 6**) has won the 'Roof of the year' prize